MACHINABILITY STUDY OF CUPOLA SLAG REINFORCED ALUMINIUM METAL MATRIX COMPOSITES

Thesis Submitted by

SOUMYABRATA CHAKRAVARTY

Doctor of Philosophy

(Engineering)

Department of Mechanical Engineering

Faculty Council of Engineering & Technology

Jadavpur University

Kolkata

2025

JADAVPUR UNIVERSITY
KOLKATA-700032, INDIA

INDEX NO. 299/22/E

REGISTRATION NUMBER: 102211001

1. Title of Thesis:

Machinability Study of Cupola Slag Reinforced Aluminium Metal Matrix Composites

2. Name, Designation & Institution of the Supervisors:

Dr. Titas Nandi

Professor, Department of Mechanical Engineering,

Jadavpur University, Kolkata-700032.

Dr. Goutam Sutradhar

Professor, Department of Mechanical Engineering,

Jadavpur University, Kolkata-700032.

[Presently on lien as Director, NIT Jamshedpur]

And

Dr. Partha Haldar

Assistant Professor, Department of Mechanical Engineering,

Government College of Engineering and Ceramic Technology, Kolkata-700010.

3. List of Publications (Journals):

I. Chakravarty, S., Sikder, R., Haldar, P., Nandi, T., & Sutradhar, G. (2025). Dry Turning Behavior of Solution Heat Treated Cupola Slag Reinforced Aluminum Matrix Composites. **Physica Scripta,** 100 (5), 055925, **SCIE, I.F: 2.6,** DOI: 10.1088/1402-4896/adc6d1.

II. Chakravarty, S., Haldar, P., Nandi, T., & Sutradhar, G. (2024). Enhancement of mechanical properties and machinability of aluminium composites by cupola slag reinforcements. **Materialwissenschaft und Werkstofftechnik (Materials Science and Engineering Technology)**, 55(9), 1250-1267, **SCIE, I.F: 1.2,** DOI: 10.1002/mawe.202300310.

III. Chakravarty, S., Sikder, R., Haldar, P., Nandi, T., & Sutradhar, G. (2024). Exploring energy aspects and tool wear on dry turning of cupola slag-reinforced aluminium metal matrix composites. **Journal of the Brazilian Society of Mechanical Sciences and Engineering,** 46(2), 59, **SCIE, I.F: 1.8,** DOI: 10.1007/s40430-023-04651-7.

IV. Chakravarty, S., Sikder, R., Haldar, P., Nandi, T., & Sutradhar, G. (2023). Machinability of cupola slag incorporated LM11 matrix composites in turning: Surface roughness and MRR analysis. **Materials Today Communications,** 37, 107414, **SCIE, I.F: 3.7,** DOI: 10.1016/j.mtcomm.2023.107414.

V. Chakravarty, S., Sikder, R., Haldar, P., Nandi, T., & Sutradhar, G. (2023). Experimental investigation on feasibility of industrial waste to resource conversion for cupola slag. **Results in Engineering,** 17, 100962. **SCOPUS, ESCI, I.F: 6,** DOI: 10.1016/j.rineng.2023.100962.

VI. Chakravarty, S., Haldar, P., Nandi, T., & Sutradhar, G. (2023). Fabrication and machinability studies on cupola slag reinforced aluminium metal matrix composites using Taguchi method. **Materials Today: Proceedings, SCOPUS,** DOI: 10.1016/j.matpr.2023.02.080.

4. Number of Chapters Contributed in Edited Volumes Published by National/ International Publishers:

I. Chakravarty, S., Haldar, P., Nandi, T., Sutradhar, G. (2025). Grey Taguchi-Based Parametric Optimization Studies on Machinability of Cupola Slag-Reinforced LM11 Matrix Composites. **Advances in Materials, Manufacturing and Design. INCOM 2024. Lecture Notes in Mechanical Engineering**. Springer, Singapore. ISSN: 2195-4356, DOI: 10.1007/978-981-97-6667-3_33.

II. Chakravarty, S., Haldar, P., Nandi, T., Sutradhar, G. (2023). Fuzzy Logic-Based Model for Predicting Material Removal Rate of Machined Cupola Slag-Reinforced Aluminum Metal Matrix Composite. **Recent Advances in Materials. ICSTE 2023. Springer Proceedings in Materials,** vol 25. Springer, Singapore. ISSN: 2662-3161, DOI: 10.1007/978-981-99-3844-5_19.

5. List of Patents: Nil

6. List of presentation in National/International Conferences/ Workshops:

I. Chakravarty, S., Haldar, P., Nandi, T., Sutradhar, G. Grey Taguchi-Based Parametric Optimization Studies on Machinability of Cupola Slag-Reinforced LM11 Matrix Composites. International Conference in Mechanical Engineering. January 2024, Jadavpur University, Kolkata, India.

II. Chakravarty, S., Haldar, P., Nandi, T., Sutradhar, G. Fuzzy Logic-Based Model for Predicting Material Removal Rate of Machined Cupola Slag-Reinforced Aluminum Metal Matrix Composite. International Conference on Science, Technology and Engineering, February 2023, NIT Manipur, Imphal, India.

III. Chakravarty, S., Haldar, P., Nandi, T., & Sutradhar, G. (2023). Fabrication and machinability studies on cupola slag reinforced aluminium metal matrix composites using Taguchi method. International Conference &Exposition on Mechanical, Material and Manufacturing Technology. October 2022. CVR College of Engineering, Hyderabad, India.

*****

"Statement of Originality"

I SOUMYABRATA CHAKRAVARTY, registered on 5th January 2022, do hereby declare that this thesis entitled "Machinability Study of Cupola Slag Reinforced Aluminium Metal Matrix Composites" contains literature survey and original research work done by the undersigned candidate as part of Doctoral studies.

All information in this thesis has been obtained and presented in accordance with existing academic rules and ethical conduct. I declare that, as required by these rules and conduct, I have fully cited and referred all materials and results that are not original to this work.

I also declare that I have checked this thesis as per the "Policy on Anti Plagiarism, Jadavpur University, 2019", and the level of similarity as checked by iThenticate software is 6%.

Signature of the Candidate: Soumyabrata Chakravarty

Date: 25.10.25

Certified by Supervisor(s):

(Signature with date, seal)

1. Nitai Nandi 03.11.2025
PROFESSOR
Mechanical Engineering Deptt.
Jadavpur University
Kolkata-700 032

2. 26.10.2025
Director
NIT Jamshedpur

3. Haldar 02.11.25
Partha Haldar
Assistant Professor in Mechanical Engineering
Govt. College of Engineering & Ceramic Technology
73, Abinash Chandra Banerjee Lane, Kol -10
Government of West Bengal

DEPARTMENT OF MECHANICAL ENGINEERING
FACULTY OF ENGINEERING & TECHNOLOGY
JADAVPUR UNIVERSITY KOLKATA, INDIA

CERTIFICATE FROM THE SUPERVISOR/S

This is to certify that the thesis entitled **"Machinability Study of Cupola Slag Reinforced Aluminium Metal Matrix Composites"**, submitted by Shri **SOUMYABRATA CHAKRAVARTY,** who got his name registered on 05.01.2022 for the award of Ph. D. (Engineering) degree of Jadavpur University is absolutely based upon his own work under supervision of Dr. Titas Nandi, Dr. Goutam Sutradhar and Dr. Partha Haldar and that neither his thesis nor any part of the thesis has been submitted for any degree/diploma or any other academic award anywhere before.

1. ---------- 03/11/25
(Dr. Titas Nandi)
Signature of the supervisor with date and official seal

PROFESSOR
Mechanical Engineering Deptt.
Jadavpur University
Kolkata-700 032

2. ---------- 16.10.2025
(Dr. Goutam Sutradhar)
Signature of the supervisor with date and official seal

Director
NIT Jamshedpur

3. ---------- 02.11.25
(Dr. Partha Haldar)
Signature of the supervisor with date and official seal

Partha Haldar
Assistant Professor in Mechanical Engineering
Govt. College of Engineering & Ceramic Technology
73, Abinash Chandra Banerjee Lane, Kol -10
Government of West Bengal

About the Author

Soumyabrata Chakravarty was born in Raghunathpur, Purulia in the year of 1993. He spent his childhood in that town and did his schooling from Ramakrishna Mission Vidyapith, Purulia. He passed Higher Secondary exam under West Bengal Council of Higher Secondary Examination in 2012. He graduated in Mechanical Engineering (B.Tech) from Maulana Abul Kalam Azad University of Technology (formerly known as West Bengal University of Technology) in 2016. He completed Master of Technology (M.Tech) degree in Laser Science and Technology from Jadavpur University in the year of 2019. He worked as research fellow in West Bengal Department of Science, Technology and Biotechnology (WBDST&BT) sponsored project titled “Resue of Cupola Slag: An Attempt for Sustainable Manufacturing” in Mechanical Engineering Department, Jadavpur University during 2020 – 2023. He has taken admission in Ph.D programme in January 2022, in Jadavapur University. He has published several research articles in international peer reviewed journals and book chapters out of his doctoral research. He has also presented research papers at international conferences.

******

Acknowledgement

This thesis is the outcome of research conducted at Mechanical Engineering Department, Jadavpur University during November 2020 to November 2023. During this time, I served as a research fellow on a project funded by Department of Science, Technology and Biotechnology, Government of West Bengal. I am deeply grateful to the funding agency for its financial support. I would also like to take this opportunity to express my heartfelt thanks to everyone who, directly or indirectly, contributed to the success of this research.

It gives me immense pleasure to express my deep sense of gratitude to my supervisors Dr. Titas Nandi, Dr. Goutam Sutradhar and Dr. Partha Haldar, for their valuable guidance, motivation, constant inspiration, and their ever-co-operating approach that enabled me to bring up this thesis in the present form. Their suggestions, advices, life and work approach are lifetime lesson for me. I am indebted to Dr. Subhas Chandra Panja and Dr. Nabendu Mandal of Mechanical Engineering Department, Jadavpur University for the continuous monitoring and shaping my PhD work.

I am deeply saddened by the loss of two remarkable individuals who played significant roles in my academic journey. I am profoundly grateful to my most respected teacher, late Prof. Asish Bandyopadhyay, Professor, Mechanical Engineering Department, Jadavpur University, whose guidance and inspiration continue to motivate me to pursue academia. I am equally indebted to late Mr. Suman Nihar, Assistant Professor in the same department, whose thoughtful conversations and encouragement helped to sustain me through the challenges of this rigorous journey. Their absence is deeply felt, and their contributions will forever be cherished.

I take this opportunity to express my heartfelt thanks to Dr. Ranjib Biswas, Dr. Suswagata Poria, Mr. Abhishek Mandal and Mr. Dipanjan Saren faculty members of Production Specialization of Mechanical Engineering Department, Jadavpur University and Dr. Sudip Banerjee for their constant academic support and encouragement. I am deeply grateful to Mr. Nitesh Kumar for his support and guidance throughout my journey. His steadfast assistance in numerous ways has been invaluable. I will always remain indebted to him for his insightful advice and crucial guidance, not only regarding my work but also about life.

I express my gratitude to all the staff members of Blue Earth Machine Shop, Jadavpur University for their continuous support throughout my journey. I also extend my thanks to the members and technicians allotted for SEM/XRD/Mechanical testing laboratory of Jadavpur University, NIT Durgapur, NITTTR Kolkata, Government College of Engineering and Ceramic Technology and VECC Kolkata for their contributions and patience. I indebted to all the past and present members of SMART Foundry Lab, Jadavpur University. I wish to further extend my gratitude to Mr. Rakesh Bhadra, Dr. Anghsuman Roy, Mr. Dipyan Chakraborty, Mr. Rupam Rakhist and Mr. Rakesh Sikder for constantly being by my side as a fellow traveller to this journey. I would also like to thank Dr. Sougata Mukherjee, for supporting and motivating in various situation.

I extend my sincere gratitude to the Head of the Department of Mechanical Engineering, as well as the Secretary and office staff of the Faculty of Engineering and Technology, Jadavpur University, for their invaluable support and cooperation throughout the program. I would also like to thank all the academic, technical, and administrative staff of the Mechanical Engineering Department, Jadavpur University, for their assistance and contributions.

I am deeply grateful to my parents for their constant encouragement in all my endeavours. I am profoundly grateful to my spouse, Mrs. Sonia Roychowdhury, for her unwavering support and encouragement throughout the most challenging phases of my academic journey. Her constant presence, understanding, and assistance in helping me navigate the highs and lows have been invaluable. She has been a pillar of strength, enabling me to remain composed and persevere through every obstacle. I would also like to acknowledge and express my gratitude to those individuals whose names I may have unintentionally missed.

Finally, but most importantly, I thank Thakur, Maa and Swamiji for giving me the strength and will power to make it this far. Jai Maa.

Place: Kolkata

Soumyabrata Chakravarty

To

All my teachers

Contents

List of tables

List of figures

Abstract

The demand for high performance innovative materials is growing day by day with the rapid advancement of aerospace, automotive, construction and automation industries. Aluminium Metal Matrix Composites (AMCs) are well known as one of the light weight, high performance new age materials with tailored properties. The large-scale production and application of AMCs are limited due to complex fabrication method and higher cost of conventional reinforcements like silicon carbide, alumina, boron carbide, tungsten carbide, zirconia etc. Meanwhile, industrial by product of cast iron smelting, cupola slag is often discarded as solid waste. This cupola slag has the potential to be used as economic reinforcement materials. This study addresses two major challenges such as, the demand for affordable high performing AMCs and need to manage industrial solid waste sustainably. This research explores the potential to enhance material properties while maintaining the environmental sustainability by investigating the reuse of cupola slag as novel reinforcement in AMCs.

The state of the art indicates a significant gap to be bridged in development of AMCs. Most of the academicians have concentrated on conventional reinforcements making the AMCs costly. The machinability degradation with increased tool wear due to presence of hard discontinuous abrasives is another challenge prominent in the literature. Limited investigations have explored the reuse of industrial solid waste as reinforcement. The introspection on potential of cupola slag as reinforcement remains severally unattended. In spite of the fact, that cupola slag has physical and chemical properties similar to hard ceramic abrasives as it contents oxides like SiO_2, Al_2O_3, and CaO. These oxides may improve the properties of composites. A few studies have focused on slag reinforced composites structural, mechanical, and machinability characteristics. However, detailed investigations on quality, machinability, heat treatment of cupola slag reinforced composites with robust analysis of enhancements and their underlying mechanisms has been observed to be scarce. This thesis addresses these gaps by systematically investigating the feasibility and performance of novel cupola slag reinforced AMCs.

The objective of this research is to introspect the key parameters in determining industrial applicability of cupola slag reinforced AMCs. The experimental investigations aim to develop, characterize, analyse machinability and heat treatment

effect on novel cupola slag reinforced composites. The composites are fabricated following economic and simple stir casting method. The reinforcement cupola slag particle with varying average size (40, 100μm) and weight percentage (3%, 5%, and 7%) has been incorporated in Al-4.5-Cu (commercially LM11) matrix. Microstructural analyses using X-ray diffraction (XRD), energy dispersive X-ray spectroscopy (EDS) equipped scanning electron microscopy (SEM) and optical microscope are performed to evaluate particle distribution, bonding, and grain refinement. Mechanical testing focused on properties like microhardness, density, porosity, tensile properties along with fractography and specific strength has been performed. The machinability of the slag composites for dry tuning in conventional lathe has been evaluated on the basis of common indices such as cutting force, tool wear, material removal rate (MRR), power consumption, chip thickness and surface roughness. The effect of solution heat treatment on newly developed composites has been investigated in details. The potential of cupola slag to be reuse as reinforcement have been assessed along with enhancement of properties of AMCs.

The results indicates that cupola slag is an effective reinforcement for AMCs. Microstructural characterizations showed refinement of grains from 138.9 μm in the base alloy to 27.7 μm in heat-treated composites with 7 wt.% slag. SEM and EDS analyses confirmed uniform particle distribution and strong bonding with clean interfaces between the slag particles and the aluminium matrix. Mechanical properties analysis reveals an approximate increase of 47% from base LM11 in microhardness and 70% enhancement of ultimate tensile strength for heat treated composites with 7 wt.% particle content. The density of the cupola slag reinforced composites reduces by 11% demonstrating the lightweight nature. These ensures the suitability of cupola slag reinforced LM11 composites as economic, high performing, light weight material for demanding industrial applications. The machinability analysis further supports industrial applicability of these novel composites. The incorporation of cupola slag enhanced the machinability indices like low cutting force, tool wear and surface roughness. The particle debonding and participation in micro cutting along with self-lubricating nature of reinforcements contributes to better machinability especially in 7 wt.% slag reinforced composites. The heat treatment enhances these properties making composites more suitable for high precision machining.

The study also highlights the environmental benefits of industrial waste reuse. Cupola slag uses as reinforcements provides sustainable solution to waste management while reducing the dependence on expensive reinforcements for fabrication of AMCs. This dual approach addresses both material innovation and environmental sustainability, contributing to global efforts in creating eco-friendly engineering solutions. This work represents a significant step toward integrating waste-derived reinforcements into advanced materials, providing a pathway for sustainable and innovative engineering practices.

Chapter 1

Introduction

The evolution of materials over the centuries has been a cornerstone of technological and societal progress shaping the trajectory of human civilization. The 20th century marked a pivotal moment of material evolution, driven by the need for materials with enhanced performance characteristics to support the expanding demands of aerospace, automotive, and defence industries. These leads to innovation of composite material, that are engineered by combining two or more distinct components to achieve superior mechanical, thermal, and physical properties. This era of industrial innovation needs new materials with better capability at high temperature, pressure, reactivity and radiation. Composites serve all these demands as the properties of monolithic alloy can be tailored as per applications [1]. Composites consist of a matrix phase where reinforcements are suspended. Composites take the superiorities from both the matrix and reinforcement; thus, tailored properties can be achieved. The composite materials can be broadly classified according to the nature of matrix materials and the nature of reinforcement materials, as shown in Figure 1.1. Composites with ceramic as matrix where hard metals or nonmetals are suspended are called ceramic matrix composites (CMCs). These composites possessed greater refractive index resulting high temperature uses. The challenges of inherent brittleness of ceramics can be reduced by incorporating metals into the matrix [2]. The second type of composite is Polymer Matrix Composites (PMCs), which integrate polymeric matrices like epoxy or polyester with reinforcements such as fiberglass or carbon fibres, emerged as a breakthrough. PMCs offered a corrosion resistant and lightweight

alternative to metals and vastly gained popularity in aerospace and automotive applications [3]. This can be understood from the fact that the commercial aviation in 1940s enabled signification weight reduction of aircraft leading to improving fuel efficiency and operational performance, by using fibreglass reinforced composites in aircraft structure [4]. However, PMCs exhibited limitations, particularly lower mechanical strength, inability to withstand extreme temperature, restricting their applicability in high-load or high-temperature environments [5].

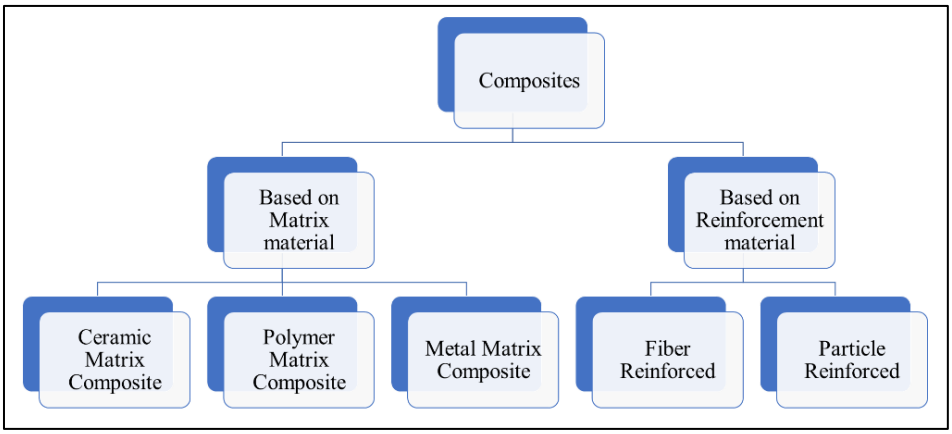

Figure 1.1 Classification of composites

These constraints catalysed the Metal Matrix Composites (MMCs) developments, combining the inherent ductility, thermal conductivity and toughness of metals with wear resistant, higher strength and other properties of reinforcements. MMCs bridged the gap between traditional metals and PMCs, offering exceptional improvement in material performance. The nature of reinforcements classifies the composites as fibre reinforced and particle reinforced one. Fiber-reinforced composites use continuous or short fibres to provide directional strength and stiffness, while particulate composites incorporate small particles to enhance properties like wear resistance and hardness [6]. MMCs opened up new possibilities for lightweight, high-performance materials with tailored properties [7]. The integration of MMCs into high-performance components, such as aircraft fuselages, engine parts, and lightweight brake systems, directly contributed to leaps in efficiency, sustainability and capability across these industries.

1.1. Metal matrix composites

MMCs distinguish themselves in terms of lightweight, higher strength, higher hardness and enhanced wear resistance properties [8]. The incorporation of second phase with extremely different properties allows these MMCs to exhibit tailored properties as per the need of application. The MMCs also exhibits higher performance

in extreme conditions like high temperature and excessively corrosive environments. The MMCs are widely used in various sectors starting from aircraft structures, automotive clutch plates, automotive engine liners etc., where the monolithic metals fail due to extreme conditions [9].

MMCs consist of two phases namely, continuous matrix of metal in which discreet phase of reinforcements is suspended. The properties of these two phases are also distinguishably different which leads to fabrication of materials with new set of properties. The continuous metal matrix can be of any metal or its alloy selected as per requirement. There are various types of reinforcements such as whisker, particulates and fibres. Among them particulate reinforcement shows better dispersion and bonding with the metal matrix [10]. These particulate reinforcements can be any material with enhanced properties which cannot be mixed with metal by the process of alloying. The most used reinforcements in material science are ceramics due do their inherent properties of withstanding extreme conditions. The ceramics like alumina, silica, zirconia and other ceramics are widely used as reinforcements of MMCs while Al, Mg, Fe etc., have been used as base matrix [9]. However, keeping sustainability and economy in mind now a days composites are being fabricated using various waste materials as reinforcements such as fly ash, steel slag, colliery slush, sanitary waste dust, marble dust, rice husk ash etc [11]. Among the various choice of matrix metals aluminium sand out as most suitable due to its properties. MMCs made with continuous phase of aluminium and its alloys is designated as Aluminium Matrix Composites (AMCs) [12].

1.2. Aluminium metal matrix composites (AMCs)

The demands of lightweight high strength materials for application in the transport and aerospace industry can be fulfilled by the MMCs with the matrix of Mg, Al, Ni, Cu, Ti or their alloys [13]. Industries, including aerospace, automotive and construction, are continuously endeavouring to attain a delicate balance between lightweight components and great mechanical performance [14]. Great strength to weight ratio along with good thermal and electric conductivity can be achieved by using Al or its alloy as matrix. Aluminium composites encompass a group of materials wherein aluminium functions as the primary matrix, along with the inclusion of other components such as ceramic or metallic particles [15]. The combination of the lightweight aluminium matrix and the

reinforcing phases results in a synergistic effect, which imparts numerous advantageous characteristics to aluminium composites.

The AMCs can be classified further based on the physical appearance of reinforcements such as continuous fibre, short fibre, particle and monofilament reinforcements [12]. Among which particle reinforcement AMCs are most widely used due to ease of fabrication and utilization. In particle reinforced AMCs various types of hard particles such as a particle of pure metals, carbides, oxides, borides and carbon nanotubes are used as reinforcements. The AMCs have better performance over monolithic alloy as improved strength, stiffness, high-temperature characteristics, hardness, wear and corrosion resistance, electrical properties and damping capacity with decreased weight and coefficient of thermal expansion [16]. Typical applications of AMCs may be seen in the production of aerospace parts, automobile parts such as piston heads, cylinder blocks, chassis, connecting rods, brake components, clutches, golf clubs, bicycles, cores for high voltage electrical cables, electronic substrates, defence weapons and safety instruments [17].

Despite the notable characteristics of AMCs, their complete potential has not been fully realized due to inherent limitations. One of the main constraints pertains to the cost of fabrication of AMCs with conventional reinforcement such as boron carbide (B_2C), silica (SiO_2), alumina (Al_2O_3), tungsten carbide (WC) etc. Moreover, aluminium possesses remarkable tensile strength, reinforcements may have diminished ductility, making them susceptible to fracture formation and breaking when subjected to specific stresses [18]. The inherent fragility of these materials has imposed constraints on their appropriateness for use in situations where components are subjected to dynamic stresses or impacts. The other challenge that hinders the wider implementation of aluminium composites is to their machinability. The machining of traditional aluminium composites poses significant difficulties, mostly attributed to the abrasive characteristics of the secondary phase. These properties contribute to increased tool wear and extended machining duration [19]. These problems can be mitigated by using non-conventional reinforcements derived from waste materials. This reduces the cost of fabrication but similar property enhancement to the conventional reinforcement can be achieved. Wastes like fly ash, rise husk ash, sanitary ware wastes, marble dust, blast furnace slag has already been demonstrated enhanced mechanical properties with

remarkably higher machinability [20 – 22]. A similar industrial waste is cupola slag which can be developed to be reused as reinforcement of AMCs.

1.2.1. Fabrication processes for AMCs

The AMCs can be manufactured using majorly three routes such as, solid phase processes, liquid phase processes and in-situ processes [23]. The suitable process is selected based on reinforcement type, desired properties and economy in fabrication. Solid state process like diffusion bonding, powder metallurgy are widely used for AMC fabrications [24]. These processes are effective for producing composites with minimal defects and superior structural integrity but are limited in scalability [25]. Liquid-state methods, including stir casting, infiltration, squeeze casting and spray casting are economic and best suited for large-scale production but faces challenges like agglomerations and interfacial reactions [26]. In situ techniques, such as centrifugal casting and chemical synthesis offer superior thermodynamic stability and homogeneous reinforcement distribution but are constrained by high costs and complex equipment requirements [27]. The AMCs have been well equipped to provide superior properties however, challenges like uniform particle dispersion, minimal interfacial reactions and reduction of cost remains significant.

1.2.2. Microstructural, physical and mechanical properties of AMCs

Academicians have been investigating AMCs reinforced with different particulates with the aim of enhanced properties that can be tailored as per application. Akbari et al. [28] investigate how stir-cast A356 alloy's mechanical characteristics are affected by Al_2O_3 nanoparticles. Compressive strength, wear resistance and hardness were evaluated with a focus on the particle dispersion in the matrix. The conclusion inferred that Al_2O_3 particle inclusion can enhance the properties significantly. The mechanical characteristics and microstructure of SiC/Al6082 AMCs have been investigated by Zhu et al. [29]. Enhanced hardness and strength have been reported to be achieved by SiC inclusion. The microstructure analysis indicates the matrix and reinforcements have clean interfacial bonding. The impact of fly ash/ B_4C hybrid reinforcements on the microstructure and mechanical behaviour of an aluminium (Al-Mg-Si-T6) hybrid metal matrix composite has been studied by Kumar et al. [30]. They came to the conclusion that the mechanical qualities, such as hardness and tensile strength, had improved with an increasing reinforcing particle content. Microstructure exhibits clean interfaces between the matrix and reinforcement as well as homogenous second phase dispersion

in the matrix. Akinwamide et al. [31] introspected the tribomechanical properties of hybrid AMCs made from ferrotitanium (TiFe) and SiC using stir casting method along with microstructural study. The microstructure shows homogeneous dispersion of particles along with refinement in grains. The investigation indicates that 5 wt.% TiFe composites showed enhanced wear resistance and elastic modulus while improved tensile properties was observed in hybrid 5wt.% TiFe/ 2wt.% SiC composites.

Attempts have been made by using various non-conventional reinforcement materials other than cupola slag by previous scholars. Sulaiman et al. [32] have reinforced quartz particles in LM6 aluminium alloy and the hardness of base alloy has been reported to improve from 36.4 HRC to 74 HRC by 30 vol.% reinforcement. The hardness of LM-0 alloyed with magnesium increased from 52 to 78 BHN by reinforcement of 20 wt.% of silica sand by stir casting in the works of Gupta et al. [33]. Umesh et al. [34] has been introspected fatigue behaviour of fly ash reinforced LM6 MMCs by varying the reinforcement composition by 0, 2.5, 5, 7.5, 10, 12.5 and 15 vol.%. The fatigue life of the composites was found to be improved by reinforcement fly ash up to 12.5 vol.%. The effect of particle size on the abrasive and mechanical behaviour of Al-fly ash composites has been discussed by Kumar et al. [35]. The study concludes a composite with coarse reinforcement particle has better mechanical and abrasive properties than composites with fine reinforcement particles. The density of aluminium alloy has been reduced by reinforcing fly ash as the second phase in AMC in the works of Bera et al. [36]. Investigations are performed by Selvam et al. [37] on fly ash particle reinforced AA6061 aluminium alloy. The fly ash reinforcements improve tensile properties and microhardness. Shanmughasundaram et al. [38] performed studies on stir casted Al-fly ash composites mechanical behaviour and surface micrographs. The density was observed to be reduced with increasing fly ash amount. Hardness and compressive strength were increased with increasing reinforcement content. The blast furnace slag inclusion effect in LM6 aluminium alloy has been observed by Kumar et al. [39]. The study observed an increase in hardness by 35.8 % with 3.5 wt.% reinforcement which is confirmed by microstructural analysis that reveal uniform distribution of the slag in the matrix. Hardness is found to improve in the works of Pankaj et al. [40]. They have fabricated composites with pure aluminium as matrix and blast furnace slag as reinforcement by stir casting. Srikanth et al. [41] attempted to reinforce the blast furnace slag in aluminium silicon alloy A356, to prepare

light weight composites. Microstructures using scanning electron microscopy show no voids and discontinuities in the composites. A good interfacial bonding between reinforcement and base phase results in increased hardness of composites. Discussions on the impact of reinforcement particle size on composite properties are uncommon. Narasaraju et al. [42] have explored rice husk ash and fly ash incorporated AMCs resulting improved mechanical properties which has been validated by microstructure analysis. Siva et al. [43] have incorporated waste colliery shale to develop novel AMCs with properties better than Al-Al_2O_3 and Al-Al_2O_3-SiC composites. Marble dust incorporated AMCs have been fabricated and investigated in the works of Muthu [44], indicating improved wear resistance. Similarly, cupola slag (CS) can be developed to be used as reinforcement of AMCs. This can be a green solution to manage the accumulated cupola slag.

Various resent studies have investigated the reinforcement of aluminium alloys with materials like fly ash, blast furnace slag, and rice husk ash, demonstrating significant improvements in mechanical properties. However, the use of cupola slag remains relatively unexplored. The detailed review of literature along with the critical findings along with chemical compositions of wastes has been presented in Table 1.1. It is evident from Table 1.1 that using industrial waste as reinforcement material generally improves the mechanical properties of AMCs with larger similarity with cupola slag composition. However, most studies have focused on materials like fly ash and blast furnace slag, with limited research dedicated to cupola slag. The available studies suggest that cupola slag has the potential to enhance the mechanical properties of AMCs at low cost, making it a promising candidate for further investigation.

Table 1.1 Property enhancement by waste reinforcing

Sl No.	Author(s)	Matrix (Al alloy)	Reinforcement	Reinforcement Composition	Findings
1	Kumar Ch et al. [39]	LM6	Blast furnace slag (3.5%)	CaO (30-50%), SiO_2 (28-38%), Al_2O_3 (8-24%), MgO (1-18%),	Hardness increased by 35.8%; uniform dispersion observed in microstructure
2	Das et al. [45]	Pure	Blast furnace slag	Fe_2O_3 (0.1-3%), MnO (0.2-2.5%), S (0.5-1.8%), TiO_2 (0.2-2%)	Enhanced hardness, wear resistance, and strength with slag particles
3	Kulkarni et al. [46]	AA6063	Rice husk ash	SiO_2 (85-95%), MgO (0.3-1.5%), Fe_2O_3 (0.1-1%), Al_2O_3 (0.2-1%), Na_2O (0.1-1%)	Significant improvement in wear resistance and hardness
4	Okokpujie et al. [47]	AA5052	Carbonized eggshell	$CaCO_3$ (94-97%), Organic matrix (1-3.5%), $MgCO_3$ (<1%),	Improved mechanical properties
5	Bhowmik et al. [48]	AA7075	Fly ash and silicon carbide	SiO_2 (45-65%), Al_2O_3 (20-35%), Fe_2O_3 (4-15%), CaO (1-12%), MgO (0.5-4%)	Enhanced tensile strength, wear resistance, and corrosion resistance

1.2.3. Machinability studies on AMCs

The successful fabrication of novel material requires detailed characterizations in terms of basic material properties as well as applicability in different secondary processes such as machining, forging, forming etc. The study of machining is significantly important in the case of AMCs as machining of AMCs is a challenging while it is inevitable post processing after casting [49]. The machining can be studied in terms of ease of machining which can be referred as machinability. There are various aspects of machinability depending on the responses considered in the analysis. Previously many researchers have explored the machinability in turning of AMCs. Studies by various authors using different metal matrix composites and alloys as tabulated in Table 1.2.

Table 1.2 Some recent works on machinability studies of composites

Sl. No	Article	Working Material	Investigated Parameter	Salient findings
1	Zakaria et al. [50]	AZ31 Magnesium Alloy	Tool wear mechanism, Cutting force, tool-work interface temperature in dry and wet turning.	The cutting force found to be reduced in wet turning.
2	Pradhan et al. [51]	Ti-6Al-4V alloy	Cutting force, Tool temperature, thermal stress and surface morphology by experiment and finite element modelling.	Cutting force found to be most important output that affects tool temperature and tool stress.
3	Gobivel et al. [52]	Mg/SiCp MMC	Cutting forces, tool morphology, chip analysis and surface quality	Cutting force found to be decreased with increasing feed and speed. Cutting force impacts other outputs such as surface roughness, tool wear.
4	Das et al. [53]	AISI D6 steel	Tool wear, cutting force, surface roughness, chip morphology, comparative study between two different coated carbide tool inserts.	Cutting force found to be decreased with increasing speed and with increasing feed rate cutting force increases.
5	Sharma et al. [54]	AISI D3 steel	Cutting force	Cutting force increased with feed and speed
6	Ruban et al. [55]	AA6061/ZrB_2-ZrC AMCs	Cutting force, chip analysis	Cutting force found to be increased with increasing feed rate but it decreases with increasing cutting speed.
7	Pugazhenthi et al. [56]	AA7075/TiB_2 AMCs	Surface integrity, cutting force	Cutting force found to be increase with increasing feed rate and with increasing weight percentage of second phase force requirement reduces.
8	Pugazhenthi et al. [57]	AA7075/TiB_2 AMCs	Cutting force, chip morphology, surface roughness and tool wear	The cutting force found to be decrease with increasing cutting speed and feed rate.
9	Shoba et al. [58]	Rice husk ash and SiC reinforced AMCs	Machinability in terms of cutting force	The result shows with increasing cutting speed the cutting force decreases. Cutting force found to be increased with increasing feed rate. Increasing of reinforcement decreases the cutting force.
10	Sujith et al. [59]	TiC reinforced Al 7079 AMCs	Cutting force, Tool wear, morphology and roughness of machined surface using a nano particle lubrication.	The cutting force found to be decreased with increasing speed and the lubrication reduces the cutting force.
11	Das et al. [60]	AISI D6	Cutting force, surface roughness, tool wear, chip analysis	The cutting force found to be important output parameter for accessing machinability. The cutting force increases with increase in feed rate and speed.

Other than these various academicians performed machinability studies on AMCs. Natraj et al. [61] fabricated and investigated machinability of hybrid Al_2O_3-MoS_2 dispersed LM6 matrix composites in turning. Authors highlighted the importance of considering cutting speed and feed as the most influencing parameters for cutting force. Machinability of Al-SiC composites in turning has been explored in the works of Muthukrishnan et al. [62]. Authors studied the impact of input parameters and different grades of polycrystalline diamond (PCD) tools on machining indices. The results show 1600 grade PCD tool performs best in terms of roughness and power consumed. Wang et al. [63] have introspected mechanism of turning of Al-SiC_p cast composites. A 3D finite element model was established to replicate the physical turning. The authors stated that small parts of reinforcement squeezed by the cutting tool can assist the machining which can be useful in improving machinability. A discussion on optimization of machining parameters of composites has been presented in the works of Suresh et al. [64]. The results show Al-10%(SiC-Gr) composite demonstrates superior machinability.

The analysis of cutting force and tool wear of AMCs with fly ash reinforcement has been presented in the experimental investigations by Dinaharan et al. [65]. The results showed that the incorporation of fly ash reduced cutting force. Amount of fly ash affects the BUE and chip size and thus improves the machinability. Sahoo et al. [66] introspected tool wear in turning of AMCs. The results show that abrasion and adhesion are the principal wear mechanisms observed from images of the tool tip, and BUE formation is noticed at low cutting speed and at high feed combination. The wear on PCD tools while machining of AMCs has been investigated by Hooper et al. [67]. They concluded that tool wear reduces with increase of reinforced SiC particles. Iuliano et al. [68] have investigated the high speed turning of alumina reinforced Al 6061 matrix composites and reported increased cutting force and tool wear along with superior surface integrity. The study provides valuable insights for optimizing machining processes for metal matrix composites. Dabade et al. [49] analysed the mechanism of chip formation in Al/SiCp composite machining. They explored the dependence of chip formation mechanisms on parameters of machining, including chip analysis and concluded that the chips changed from continuous to discontinuous with increasing feed, depth of cut and speed. Machinability in terms of surface quality, chip thickness in the turning of hybrid Al7075/SiC/Graphite composites has been discussed in the

works of Kannan et al. [69]. The investigation concluded that by incorporating reinforcement material, the surface roughness and chip thickness had been reduced. Chauhan et al. [70] conducted a study on machining hybrid AMCs with SiC and Red Mud reinforcements. The study utilized Taguchi grey relational analysis for understanding the dependency of surface texture on reinforcement parameters such as average particle size, particle volume fraction, red mud content and turning conditions. The lowest surface roughness of 0.25 μm has been observed in 6 wt.% red mud inclusions.

Machinability analysis in turning fly ash reinforced composites based on MRR, chip thickness and machined surface quality has been presented in the works of Shanmughasundaram et al. [71]. The impact of graphite content and cutting parameters on machined surfaces has been explored experimentally. They concluded that nominal surface roughness has been present in cases of higher weight percentages of fly ash. Prakash et al. [72] explored the turning of rock dust reinforced AMCs analysing the effect of process inputs on MRR and surface finish. The results revealed that cutting speed had the greatest impact on both responses, followed by depth of cut and feed rate. The study discusses selecting appropriate cutting parameters for achieving both higher MRR and improved surface quality in turning. Introspection on energy consumption along with surface integrity in the turning of Al-4032/Granite marble powder AMCs has been conducted by Saini et al. [73]. The cutting speed is indicated as most significant process input. The optimal conditions were depth of cut 0.5 mm, feed rate of 0.15 mm/rev and cutting speed of 150 m/min yielded a 31.5% reduction in surface roughness.

1.3. Cupola slag

The term sustainable application in any process is described as the system of improvement fulfilling the demand of the present without affecting future's ability to fulfil their demands [74]. Rapid growth of industrialization to meet the demand of exponential population growth leads to a large amount of industrial waste. These industrial wastes are extremely toxic to the environment, thus should be properly decomposed, reused or recycled for reaching the goal of a cleaner environment. Cast iron is very potential material that have numerous applications such as in machine tool beds, automobile components, valve bodies, soil pipe, shipbuilding, manhole cover, and sanitary castings etc. [75]. Cast iron is produced in cupola by smelting of limestone, coke, scrap and pig iron together in a proper ratio termed as the charge [76]. This process

has output of grey cast iron (of different grades) along with slag as waste product. The recent data shows that total sum of 105.5 million metric tonnes of castings is produced per annum worldwide [77]. India is producing 10 % of the global production which is about 11 million metric tonnes of castings per annum. 68 % of total castings produced in India are cast iron. There are about 5000 cupolas that are producing about 7.5 – 8 million tonnes of castings per annum [78]. Normally 5 – 6% slag is produced for every batch of melting. The quantity and properties of these slags are highly dependent on foundry location, melting technology, properties of charge and many other factors so, it varies from foundry to foundry [79]. This results in annual slag production of 0.4 – 0.5 million metric tonnes in India only [80]. The cupola slag may consist of 25 – 70wt.% SiO_2, 10 – 50 wt.% CaO, 5 – 24wt.% Al_2O_3, 2 – 25 wt.% FeO, MgO, MnO, and other oxides and with a trace of Fe_2O_3 which is more or less similar to Blast Furnace slag (BFS) [77 – 90]. This suggests there can be different uses of Cupola Slag likewise BFS.

Use of cupolas for producing grey cast iron is continuing with sufficient demand which leads to generate huge amount of slag, which is a waste product and ends up in a dump yard or landfilling that pollutes the environment [91]. Blast furnace slag which has a similar chemical composition is widely used in the cement industry maybe because production in huge quantity from a single source, rigorous research and proper implementation [92]. On the other hand, single unit of cupola produces comparatively lesser amount of slag. In general, cupolas are scattered in many places with different entrepreneurs as a result reuse of slag in an effective manner is less discussed. This is wastage of potential resource and a great hurdle for achieving sustainable development.

1.3.1. Origin, types and cupola slag properties

Cupola slag originated as a by-product of melting pig iron, coke, limestone, and scrap for producing grey cast iron in a cupola. The utilization of this waste product depends highly upon its properties as directed in various literatures [81,83,93]. Pirbulova et al. [89] described cupola slag as a non-metallic melt whose temperature dependent physical properties affects the slag's potential to be reused. The formation of slag as identified by the authors are mainly due to impurities from scrap metal such as burned silica sand, scales of iron, coke ash; SiO_2, Al_2O_3 present in furnace wall; oxides, sulphides, phosphides that generates during melting. The slag physically appeared to be vitrified, solid and dense material. The slag forming additive has a good effect on the physical property of the slag. Spontaneously formed slag (without slag forming additives) would

have high viscosity and high melting temperature, thus it creates a problem in the melting process [94]. Slag made by using slag forming additives would have optimal fluidity and low melting temperature [95,96]. Baricova et al. [88] classified cupola slag on the basis of the cooling method applied for the solidification of slag. Slow or air-cooled slag is crystalline with a grey, stony dense appearance named Cupola Slag (CS). Slag melts which cool faster by water quenching breaks into small granulated particles and solidifies as amorphous materials called Granulated Cupola Slag (GCS). CS shows a heterogeneous structure with significant pores but GCS shows a homogenous glassy structure. The relative fineness was observed to be greater in the case of GCS.

The physical property of the cupola slag is essential for its use in the building industry was investigated by Afolayan et al. [97]. Authors compared the properties with natural aggregates used for making concrete and found that cupola slag has similar properties. Thus, cupola slag can have a limitless application in concrete making. Pavlenko et al. [84] analysed some important physical properties such as absolute density, crushability, cylinder crushing strength. Aderibigbe et al. [81] indicated pozzolanic property in cupola slag and stated that it can be an artificial pozzolan. Mistry et al. [90] in their work analysed the fineness modulus, impact value, water absorption and moisture content of cupola slag. The physical properties as studied by various authors are described and tabulated in Table 1.3. The ranges are found to be specific gravity 2.5 to 2.93, bulk modulus 1210 kg/m^3 to 1650 kg/m^3, fineness modulus 3.71 to 4.6, crushability 13 to 27% as described in the existing literature. It is evident from the data that cupola slag has similar physical property when compared with blast furnace slag and typical pozzolans so there is a great possibility that similar reuse can be implemented.

1.3.2. Mineralogical and chemical properties of cupola slag

Reuse potential of cupola slag cannot be understood properly without analysing the chemical and mineralogical properties [98]. The charge material and the melting technology directly affect the chemical properties of cupola slag [88]. Slag viscosity, crystallization during cooling depends on the chemical and mineralogical composition. These affect the porosity, size of the crystal in solid slag which is a significant factor for the reusability of cupola slag [99].

The cupola slag mainly consists of SiO_2, Al_2O_3, CaO, MgO, FeO and other oxides and sulphides[77 – 86, 89, 96]. Various authors also indicate the predominant phase of

wollastonite ($CaO.SiO_2$), fayalite ($2FeO.SiO_2$), ramsdellite [81,89]. The authors analysed that cupola slag is a part of the $CaO\text{-}SiO_2\text{-}Al_2O_3$ ternary slag system which is similar to blast furnace slag which opens the door for many potential applications of cupola slag. The chemical properties of slag directly depend on the charge of the cupola. Various authors have observed the chemical and mineralogical properties in different regions of the world. A collective weight percentage range of different main components present in cupola slag are shown in Table 1.4 from the available literature. Any slag sample may have the composition within the range specified in Table 1.4. The authors have used XRD and SEM (EDX) to analyse and understand the chemical contents. The chemical compositions as tabulated in Table 1.4 suggest that maximum of the CS is made of either of three compounds namely SiO_2, Al_2O_3, and CaO. A trace of pure iron may be found in some of cupola slag composition which may be taken care of for reutilization of cupola slag. Iron particles may stick in the crusher used to break the CS for reuse and crusher life would become low which increases the operational cost many times [89]. Table 1.4 also indicates that the chemical properties of cupola slag is approximately similar to the chemical contents of other waste materials such as blast furnace slag [97 – 101], fly ash [102 – 106], rice husk ash [107 – 113] etc. This gives the indication for reuse of cupola slag in similar sectors for sustainable future.

Table 1.3 Physical properties of cupola slag from literature

Sl. No.	Sources	Colour	Type	Crystallinity	Structure	Specific Gravity	Bulk Density	Absolute Density	Crushability	Cylinder Crushing Strength	Fineness Modules	Impact Vale	Water absorption	Moisture Content
1	Pribulova et al. [89]	grey	CS	crystalline	dense and stony	ND	ND	ND	ND	ND	ND	ND	ND	ND
2	Pribulova et al. [89]	brown	GCS	amorphous	fine and glassy	ND	ND	ND	ND	ND	ND	ND	ND	ND
3	Aderibigbe et al. [81]	grey	CS	ND	ND	2.93	ND	ND	ND	ND	ND	ND	5%	ND
4	Baricova, et al. [88]	ND	CS, GCS	ND	ND	2.87	1510 kg/m^3	ND	ND	ND	ND	ND	ND	ND
5	Afolayan et al. [97]	ND	ND	ND	ND	2.87	1510 kg/m^3	ND	ND	ND	ND	ND	ND	ND
6	Pavlenko et al. [84]	grey	GCS	amorphous	coarse, various shaped	ND	1250 kg/m^3	2800 kg/m^3	13 %	2.78 MPa	3.71	ND	ND	ND
7	Mistry et al. [90]	ND	ND	ND	ND	2.5	1640 kg/m^3	ND	27 %	ND	4.6	26 %	0.4 %	0.004

*ND: Not disclosed in the source

Table 1.4 Chemical composition of cupola slag as per literature

Sl. No.	Sources	SiO_2	Al_2O_3	CaO	MgO	FeO/ Fe_2O_3	MnO	K_2O	Na_2O	TiO_2	SO_3	Fe	Others
1	Pribulova et al. [89]	45.27 to 51.12	7.45 to 9.95	24.08 to 32.64	1.04 to 5.82	3.46 to 3.56	0.5 to 1.26	ND	ND	ND	ND	2.57 to 2.68	ND
2	Aderibigbe et al. [81]	50.02	24.3	7.26	2.14	15.5	ND	0.78	0.78	ND	0.78	ND	ND
3	Agarwal et al. [83]	42	8	34	11	ND	ND	ND	ND	ND	ND	ND	3
4	Lara-Sánchez et al. [87]	38	5	49	ND	2	2	ND	ND	ND	ND	ND	4
5	Anuwattana et al. [93]	70.1	18.9	3.3	1.3	3.2	0.8	ND	2.4	ND	ND	ND	ND
6	Baricova et al. [88]	45 to 55	7 to 9.95	24.08 to 33	1.04 to 5.82	3.46 to 3.56	0.5 to 1.2	ND	ND	ND	ND	2.57 to 2.68	ND
7	Pavlenko et al. [84]	57.76	4.4	10.09	1.62	15.6	9.5	0.53	0.95	0.85	0.37	ND	ND
8	Mistry et al. [90]	45	9.5	14.25	2.35	23.5	2.9	ND	0.5	1	ND	ND	0.3
9	Balaraman et al.[85]	25 to 55	5 to 20	20 to 50	5 to 30	1 to 15	1 to 4	ND	ND	ND	ND	ND	ND
10	Stroup et al. [100]	43.87	8.5	33.3	3.38	1.93	1.1	0.3	0.1	0.34	0.3	ND	ND
11	Agarwal et al. [82]	42	8	34	11	ND	3	ND	ND	ND	ND	ND	2
12	Ladomerský et al. [86]	43.72 to 45.04	14.1to 13.8	24.49 to 25.44	10.1 to 10.6	3.35 to 3.54	ND	ND	ND	ND	ND	ND	0.37

*ND: Not disclosed in the source

1.3.3. Reuse potentials for cupola slag

The properties and composition of cupola slag shows potential to be used as recycled materials. However, due to lack of rigorous research and management of waste slag it ends up in landfills. There were some attempts of cupola slag reuse which shows great potentials. A brief account of cupola slag reuse has been presented in this section.

1.3.3.1. Utilization in construction industry

The physical, chemical, and mineralogical properties analysis has opened a vast door for reutilization of cupola slag in many sectors. The major raw materials used in construction industries specially to make concrete are cement, fine aggregates and coarse aggregate [114,115]. This industry has a very high potential to consume cupola slag for replacement of coarse aggregates, fine aggregates as well as cement for making concrete [116]. Concrete making using cupola slag draws the attention of most of the authors due to the fact that similar industrial wastes have been used for the same. The wastes such as fly ash, blast furnace slag, sanitary wear wastes, rice husk ash and other construction wastes has been in use in a commercial level for making concrete [117,118]. Concrete making has the potential to be one of the major sectors where the cupola slag may be used to reach the goal of sustainable waste management. The replacements of aggregates and cement along with the findings by various authors have been tabulated in Table 1.5.

1.3.3.2. Utilization of cupola slag in road construction

An industrial waste, cupola slag reusability should be studied based on all the sectors where utilization is possible. One of such sectors is road construction. A comparative study on the reuse of cupola slag along with Reclaimed Asphalt Pavement (RAP) and green sand in a mixture of asphalt has been accomplished by Lastra-González et al. [119]. The authors have assessed bituminous mixture made of three waste materials viz. RAP, slag and green sand in different concentration. Limestone is used as aggregates in the mix along with bitumen binders. The assessment has been followed by the Marshall method void content and cohesion loss due to water action along with plastic deformation resistance. The slag mechanical property allows only 10% use of cupola slag in the mixture. The mixture of RAP, cupola slag, and green sand along with limestone aggregate and bitumen binders gives an excellent mechanical performance as described in Spanish standards for low traffic areas. Potential use of cupola slag has been studied by Cramer et al. [120]. Authors perform two studies, in first one, cupola slag is used as filler in base coarse materials and for the second one, natural aggregate

have been substituted by 30% wt. by cupola slag for making pavement blocks. Satisfactory strength was achieved in both the studies. Though, the authors have suggested a nominal use of cupola slag in road construction but for the aim of sustainable waste management, these small steps create a huge difference.

Table 1.5 Cupola slag use in construction industry

Sl. No.	Sources	Replacement is done as			Remarks
		Fine aggregate	Coarse aggregate	Cement	
1	Sikder et al. [121]	No	Yes 0 to % to 50% by a step of 10%	No	The cast samples with up to 40 wt.% partial replacement of CFS effectively meet the requirements for the M20 grade of concrete in terms of compressive strength.
2	Pribulova et al. [89]	Yes 10, 20, 30, 100%	No	No	Significant increase in compressive strength
3	Baricova et al. [88]	Yes 10, 20, 30, 100%	No	Yes 60% by GCS	Highest of 13 MPa compressive strength when fine aggregates are substituted 30 wt.%. by cupola slag
4	Afolayan et al. [97]	No	Yes 100%	Yes 2%, 4%, 6%, 8%, and 10% by GCS	30.68 N/mm^{2}compressive strength is obtained in slag concrete while 31.33 N/mm^2 average compressive strength this obtained in controlled concrete
5	Balaraman et al. [85]	Yes 5%, 10%, 15%, 20%, 25%, 50%, 100%	Yes 5%, 10%, 15%, 20%, 25%, 50%, 100%	No	34 N/mm^2 compressive strength along with 3.2 N/mm^2 split tensile strength can be achieved by 20% replacement in fine aggregates
6	Arum et al. [122]	No	No	Yes 0%, 5%, 10% 15% by GCS	Highest of 31.9% greater compressive strength with respect to reference concrete is achieved by 15% replacement in cement
7	Ladomerský et al. [86]	Yes 25.5 %	No	No	Similar in terms of workability, strength, elasticity module, penetration of water under pressure, and suction capacity with respect to controlled concrete
8	Balaraman et al. [123]	Yes Combined replacement 20% to 40% by a step of 10%		No	Decrease of compressive strength from 5.33 MPa to 3.92 MPa due to void formation
9	Mistry et al. [90]	No		No	Significant similar strength with respect to controlled concrete along with 12.65 % cost saving per cubic meter
10	Alabi et al. [124]	Yes 0, 2, 4, 6, 10%	No	No	13 MPa compressive strength achieved without any dependency on temperature
11	Stroup et al. [100]	No	No	Yes 5 to 50% with a step of 5% by volume	Significant strength when compared to controlled concrete has been achieved
12	Rodríguez-Mendoza, et al. [125]	No	No	Yes 20, 40, 80%	Better compressive strength than fly ash concrete can be achieved
13	Pavlenko et al. [84]	No	No	Yes	Strength obtained is adequate for low and medium rise structures
14	Sosa et al. [126]	No	No	Yes 0, 10, 20, 30 vol.%	Increase in compressive strength of about 10% after 28 days when compared to other SCM's.

1.3.3.3. Utilization of cupola slag as reinforcement of AMCs

AMCs are one of the emerging classes of material but the cost of conventional reinforcements increases the production cost. Industrial waste cupola slag has various hard ceramics in its constituents and appears to be abrasive in nature if processed technically. Thus, cupola slag can be reused as reinforcement material for AMCs

reducing the cost of fabrication and sustainably mange the solid industrial waste. The cost of transportation and processing of cupola slag as reinforcement particle are nominal compared to the cost of conventional particle reinforcements. The existing academia shows reuse of waste rice husk ash, blast furnace slag, fly ash and other solid waste as reinforcement material enhancing the properties of monolithic materials [58,127,128]. However, the cupola slag utilization as reinforcement particle and subsequent property evaluation has been less discussed thus, provide a wide space of rigorous research. This work majorly delves into this specific space to study the cupola slag reinforced AMCs and build a comprehensive introspection on cupola slag reinforced composites with superior properties.

1.4. Knowledge gap

The demand of new era of rapid industrial innovation requires new age materials so development and characterization of novel materials are well documented in the pre-existing literature. AMC being one of such new edge materials with application-based properties and light weight. Despite the huge progress in the field of AMCs research, significant gaps remain in existing literature. The higher production cost due to the higher cost of conventional reinforcements like SiC, Al_2O_3, WC and B_4C etc., limits the wide scale industrial applications of AMCs. Besides, industrial waste derived reinforcements such as rice husk ash, fly ash, blast furnace slag, cupola slag holds greater potential but remain underutilized. The comparison of prior reinforcement with the cupola slag reinforcement in terms of cost, performance and environmental impact has been presented in Table 1.6. This depicts the usefulness of cupola slag as low-cost reinforcement.

Very few academicians utilized cupola slag as reinforcement and only some preliminary studies have been reported on chemical and physical properties of cupola slag. Cupola slag appears to be an appropriate substitute for expensive conventional reinforcements as it has a unique chemical composition comprising mixed oxides such as SiO_2, Al_2O_3, and CaO etc. It offers a solution for property enhancement, besides being a significant step toward sustainability. The addition of this industrial by-product in some way may reduce natural resource dependence and decrease environmental pollution. This, despite the enormous potential, points to one of the critical gaps that the research will seek to address, the structural, mechanical and microstructural properties of cupola slag-reinforced composites have been not yet studied.

Table 1.6 Comparison table of prior reinforcement with cupola slag

Reinforcement	Cost (Raw + Processing)	Performance in AMCs	Environmental Impact
SiC	High (synthetic, energy-intensive)	Excellent strength, wear resistance	High energy demand, non-waste material
Al_2O_3	Moderate	Good strength, hardness	Extracted mineral, limited sustainability benefit
Fly Ash	Low (industrial waste)	Moderate performance	Waste utilization, reduces landfill
Red Mud	Very low (hazardous waste)	Limited bonding, processing issues	Hazard mitigation, but handling challenges
Cupola Slag (this study)	Very low (abundant by-product)	Promising reinforcement: good bonding, competitive strength	Direct waste reuse, significant ecological footprint reduction

The other significant gap persists in the academia that no studies are reported that introspected the machinability of cupola slag reinforced AMCs. However, machinability is one of the most significant deciding factors for the material's industrial viability. Previous works on AMCs have investigated the machinability parameters by using conventional reinforcements such as B_4C, WC, SiC, TiO_2, and Al_2O_3 etc. These studies indicate that such reinforcements are abrasive in nature, leading to high tool wear and difficulties in getting smooth surface finishes. However, cupola slag is a new material in this regard and has not been evaluated for machinability characteristics.

The machinability studies require rigorous introspection of some the important parameters like cutting force, tool wear, MRR, and surface roughness, under different conditions. This calls for further research on industrial acceptance in terms of how the cupola slag incorporation as reinforcement influences these parameters. It would be hard to ensure the feasibility of using cupola slag reinforced AMCs in industry without detailed and comprehensive investigations. This gap is significant and calls for immediate action as machinability is a key determinant for material selection in high-performance aerospace and automotive applications.

Despite technological advancements in waste management, research into utilizing cupola slag for solid waste solutions is notably absent. While industrial waste management has recently gained attention due to environmental and regulatory pressures, cupola slag, a significant by-product of cast iron production, continues to be largely disposed of in landfills, posing environmental risks. Although materials like fly ash and blast furnace slag have found successful applications in construction and composite materials, the potential for reusing cupola slag remains unexplored.

This research addresses the novel way of waste management using cupola slag as reinforcement in AMCs to tackle two critical issues simultaneously:

- the demand for high-performance, cost-effective composite materials
- the urge for sustainable solid waste management.

The dual benefit that comes from both an environmental sustainability point of view and a materials innovation standpoint underline the relevance of this literature gap.

1.5. Scope of the research

The present work therefore systematically addresses the stated gaps by introspecting the feasibility of cupola slag reuse as reinforcement for AMCs. The focus of this research has been on material development, optimization of reinforcement parameters, and characterization with a view to establishing an all-rounded understanding of cupola slag-reinforced composites. The central hypothesis is that cupola slag can be engineered into AMCs that exhibit competitive mechanical and machinability properties while contributing to environmental sustainability. The objective of this research are as follows,

Core objectives

- To determine feasibility of cupola slag reuse as reinforcement materials with respect to their chemical and physical properties along with sustainability.
- To improve the fabrication method to have uniform particle distribution and proper bonding between slag particle and aluminium matrix.
- To perform rigorous metallurgical investigations to study the grain size, distribution of phases, bonding at interfaces and formation of any intermetallic phases.
- To evaluate the mechanical properties, such as hardness, tensile strength, density and porosity by considering the particle size and weight percentage of slag reinforcement.
- To introspect the machinability of the fabricated composites by considering parameters like MRR, surface roughness, tool wear, cutting force.
- To compare the machinability performance with conventional AMCs to understand industrial applicability.

- To look into the microstructural evolution and mechanical properties enhancement due to the influence of heat treatment on novel cupola slag reinforced composites.

Extended objectives

- To establish an outline of the environmental benefits of the recycling of cupola slag and its contribution to decreasing the ecological footprint of composite fabrication.
- To explore the possibility of using slag-based reinforced AMCs for some critical performance and durability-related applications like automotive, aerospace, and structural components.

This work bridges the gap between material innovation and sustainability engineering by offering a holistic approach towards the development of cost effective, eco-friendly composites. This integrates mechanical, microstructural studies with machinability providing a comprehensive basis for industrial acceptance of cupola slag reinforced AMCs. The results from this research may represent a new frontier in the field of metal matrix composites by offering an economically viable, high-performance, environmentally benign alternative to conventional materials. These systematic investigations will make significant contributions to knowledge advancement in materials science and sustainable engineering practices.

1.6. Thesis Organization

The present thesis has seven (7) chapters. Chapter 1 delves into an introduction and background foundational to the work. This chapter discusses the state of the art of studies on particle reinforced AMCs. The introduction to cupola slag with its properties and compositions along with reuse potential has been also provided in this chapter. Chapter 2 deals with fabrication and experimental methodology applied in this thesis. The extensive discussions on material selection, fabrication process, characterizations along with methodology for machinability investigations have been presented in this chapter. Chapter 3 present the investigation of reinforcement particle size variation on physical, microstructural and mechanical properties of novel cupola slag reinforced AMC. Chapter 4 analyses the enhancement of microstructural and physio-mechanical properties of AMCs by weight percentage variation of cupola slag particles. Chapter 5 introspected into the machinability of novel cupola slag reinforced AMCs. Chapter 6

presents insight on the influence of solution heat treatment on novel cupola slag composites, the comparisons have been based on physical, mechanical and machinability properties. The comprehensive concluding remarks along with future research scope is presented in Chapter 7. A complete bibliography has been presented at the end of the thesis.

Chapter 2

Fabrication of Composites and Experimentations

The material development study is ineffective without proper understanding of the individual materials. The properties of AMCs highly dependent on the qualities of base alloy and the reinforcing material. The properties of composites also depend on fabrication process. The quality of novel and economic composites is introspected in terms of physio-mechanical property analysis. The details of material used along with fabrication and experimentation methodology is presented in this chapter.

2.1.Raw materials

AMCs are made of continuous phase of an aluminium alloy in which particulate reinforcements are suspended. The wrought aluminium alloy Al-4.5-Cu, commercially known as LM11 has been chosen as continuous matrix in this work. LM11 exhibits excellent strength, hardness and wear resistance, making it a suitable matrix material [129]. Moreover, this particular alloy responds greatly to solution heat treatment. The copper present in the alloy improves the mechanical properties of the composite through solid solution strengthening [130]. The microstructure of LM11 alloy indicates presence of Al_2Cu intermetallic phase which strengthens the composites further [131]. The lower density of LM11 alloy allows fabrication of light weight AMCs with higher specific strength, desirable in aerospace, transportation and military equipment sectors. The LM11 has wide range of applications as aerospace hardware, aircraft construction, engine radiators, seawater piping and cryogenics due to superior mechanical and

thermal properties. The LM11 ingots used in this work has been procured from M/S Kolkata Die Cast, Liluah, Howrah, West Bengal, India. The physico-mechanical properties and chemical components of LM11 ingots have been presented in Table 2.1 and Table 2.2 respectively.

Table 2.1 Physical and mechanical properties of LM11

Properties	Values
Hardness	72 ± 3 Hv
Yield Strength	116 ± 2.4 MPa
Ultimate tensile strength	169 ± 2.5 MPa
Density	2.49 g/cm^3

Table 2.2 Chemical components of LM11

Elements	Cu	Mg	Si	Fe	Mn	Ni	Zn	Pb	Sn	Ti	Al
Weight Percentage (%wt.)	4.0 to 5.0	0.1	0.25	0.25	0.1	0.1	0.1	0.05	0.05	0.05 to 0.3	Balance

The reinforcement particles for this work have been derived from industrial waste cupola slag. Cupola slag is a byproduct of cast iron smelting in cupola furnace using a mixture of pig iron, scraps, flux and charcoal. This waste has no utilization, hence ends in landfills polluting the environment. However, cupola slag contains many hard ceramics like silica, alumina, calcium oxide etc, which indicate its use as economic reinforcement particle for enhancing the properties of base LM11. This utilization of cupola slag helps in managing a solid industrial, reduces cost of reinforcements in development of superior properties in novel slag reinforced composites. The cupola slag used in this work have been fetched from M/S Binoy Udyog Pvt. Ltd. Andul, Howrah, West Bengal, India. The as received cupola slag appeared to be stony bolder like and greenish black in colour as shown in Figure 2.1. Cupola slag needs to be processed technically for the development of low-cost reinforcement particles. The process of development has been shown in Figure 2.2. The first step in the development of low-cost reinforcement from waste materials is to collect the cupola slag from a foundry, it came in the form of a dense stony structure as shown in Figure 2.1. The slags are then ball-milled using an industrial ball milling machine. Assorted powder of cupola slag has been produced which is further sieved for categorization into different sizes. Cupola slag is a waste of cast iron melting process so it is ubiquitous that there may be a presence of small iron particles in powdered cupola slag. These iron particles may create difficulties while the fabrication of composites and hence, the iron particles are removed

by magnetic separation. Developed low-cost reinforcement powders has been shown in Figure 2.3. The final particle size analysis curve for 100 μm cupola slag particle has been presented in Figure 2.4. The particle size distribution analysis reveals characteristic size parameters of d_{10} = 79 μm, d_{50} = 100.45 μm, and d_{90} = 134.51 μm, indicating that most particles are between 79 and 134.51 μm, with median particle size of 100.45 μm. The size distribution follows a normal pattern with the highest number of particles (32%) around 105-110 μm. The particles have fairly uniform sizes, which is good for reinforcing in composites. This size range helps the particles mix well with the metal matrix and creates strong bonds, leading to better mechanical properties in the final composite material. Continuous ball milling and sieve shaking ensure size control. Developed reinforcements have been gone through various characterization techniques for getting insight into their chemical and physical properties. The chemical constituents and phases of cupola slag have been analysed by X-Ray Fluorescence (XRF) using Rigaku ED-XRF Model-NEX DE Analyzer and X-Ray Diffraction (XRD) using Ultima III, XRD, Rigaku Corporation. The morphology of developed cupola slag particle has been analysed using scanning electron microscopy (model: JEOL JSM IT500) equipped with energy dispersive spectroscopy (SEM-EDS).

Figure 2.1 Picture of received cupola slag

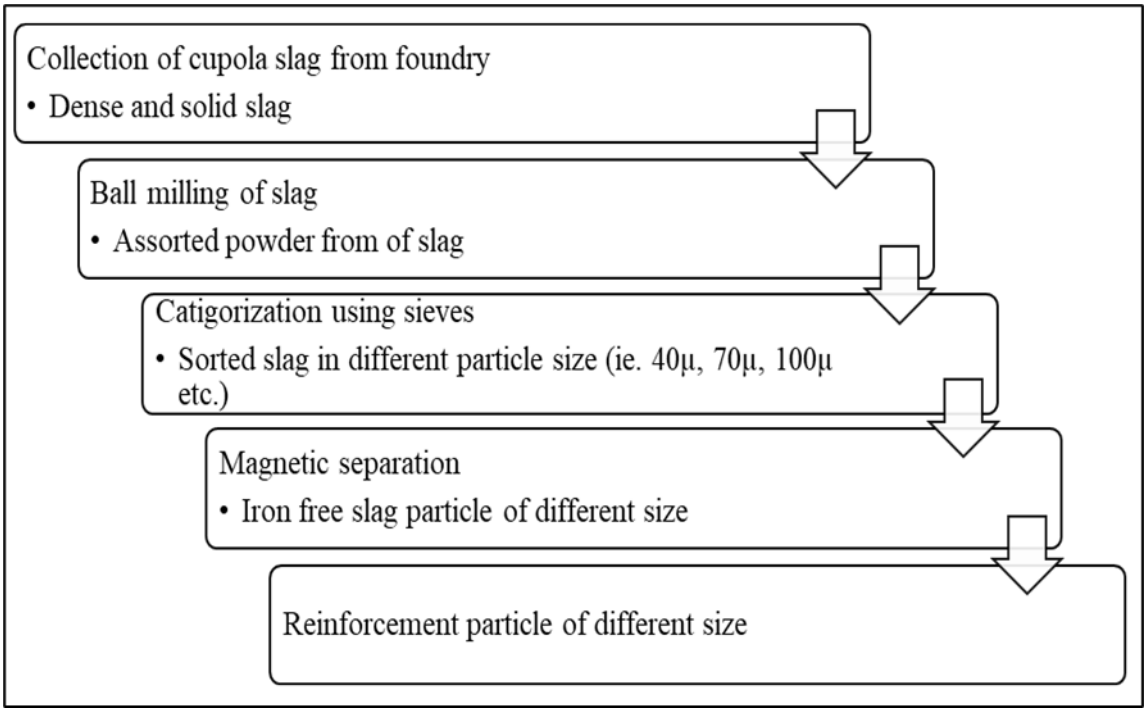

Figure 2.2 Process flow chart for developing cupola slag as reinforcement particle

Figure 2.3 (a) 40 µm and (b) 100 µm cupola slag reinforcement particles used for fabrication of AMCs

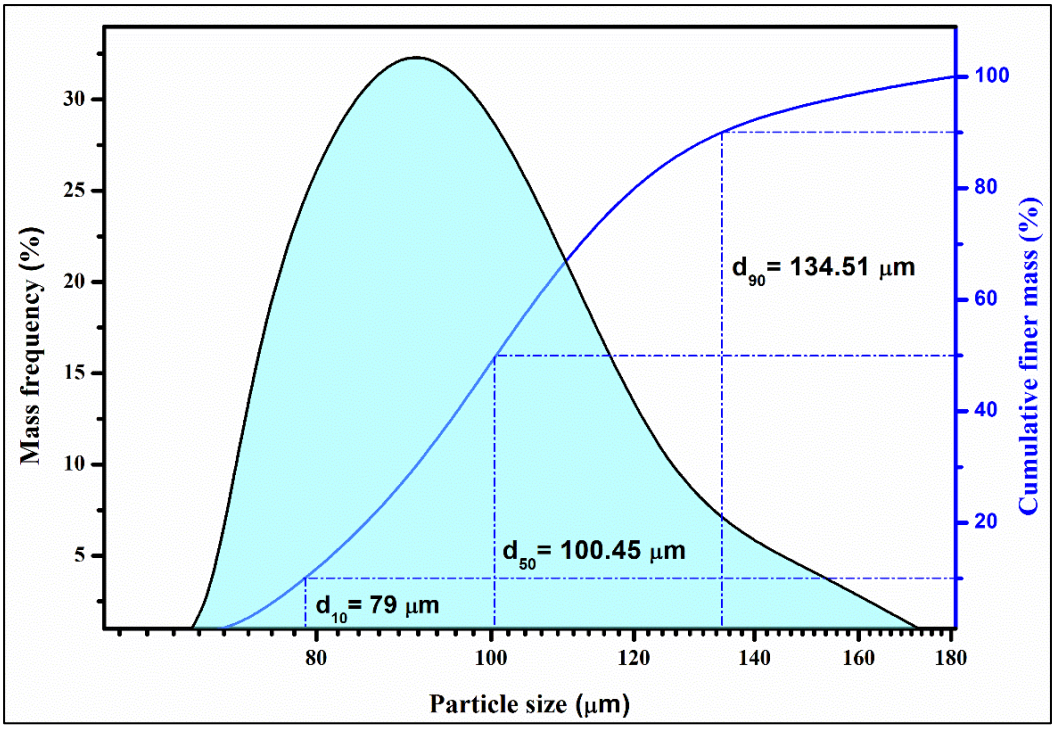

Figure 2.4 Particle size distribution curve of cupola slag (d_{50} =100 μm)

The physical properties of newly developed cupola slag powder have been presented in Table 2.3. The Table 2.4 shows the XRF outcomes indicating the chemical constituents of cupola slag used in this work. The mineralogical phase analysis using XRD has been shown in Figure 2.5. It is evident from Figure 2.5 that cupola slag is consists of predominant quartz (SiO_2) phase as the peak found in 2θ = 20.86˚ and 2θ = 26.64˚ according to reference code 00-046-1045 from International Centre for Diffraction Data (ICDD). This low angle quartz phase along with noisy XRD curve signifies the amorphous nature of cupola slag [132]. Other than quartz cupola slag contains fluorite (CaF_2), calcite ($CaCO_3$) and silicon (Si) as per the matched reference codes 00-035-0816, 00-005-0586 and 00-027-1402 respectively at 2θ values shown in Figure 2.5. Figure 2.6 shows the SEM morphology of CS particles depicting irregularly shaped particles with sharp, pointy edges beneficial for proper bonding. The EDS analysis of cupola slag particles before magnetic separation shows higher weight percentage of iron due to presence of cast iron residue in slag particles as presented in Figure 2.7. The EDS analysis of CS particles after iron removal through magnetic separation has been presented in Figure 2.8, depicts presence of Al, Ca, Si, Fe and O which indicates hard ceramics like SiO_2, Al_2O_3, CaO, Fe_2O_3 are major constituents of cupola slag. These results are well aligned with the XRF and XRD observations discussed earlier.

Table 2.3 Cupola slag physical properties

Properties	Remarks
Appearance	Greenish black, dense stony material
Crystallinity	Amorphous
Specific gravity	2.87
Bulk density	1250 kg/m^3
Water absorption	0.4 %

Table 2.4 Chemical components of cupola slag

Components	SiO_2	Fe_2O_3	Al_2O_3	CaO	MnO	MgO	TiO_2	K_2O	Other oxides
Weight Percentage (wt.%)	53.1	16.1	11.1	10.7	3.33	1.94	1.22	1.05	Remaining

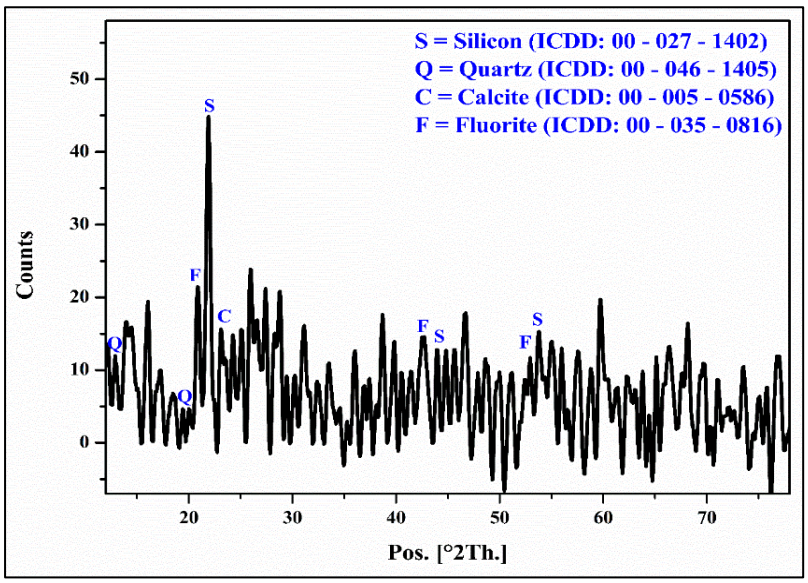

Figure 2.5 XRD plot of cupola slag

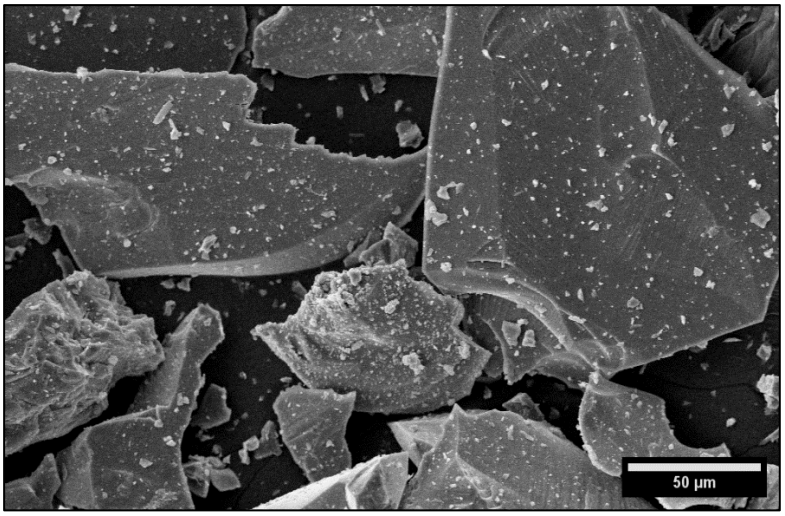

Figure 2.6 SEM morphology of cupola slag

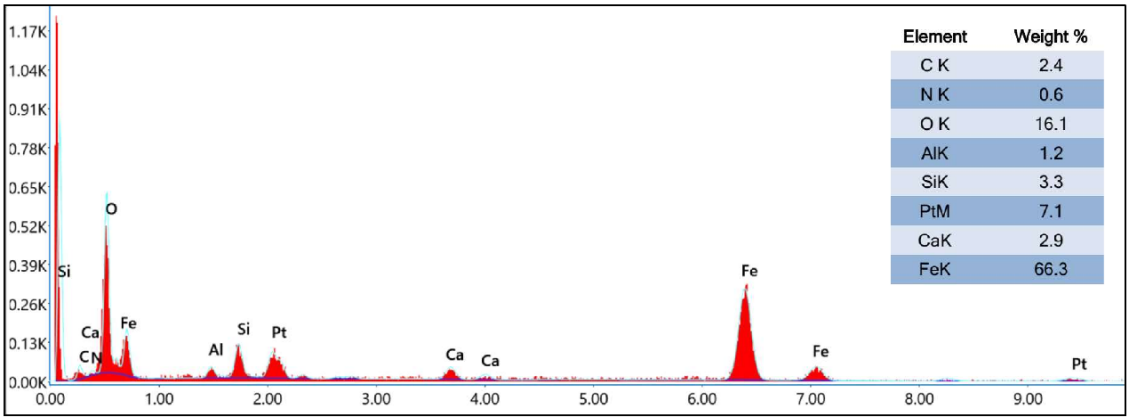

Element	Weight %
C K	2.4
N K	0.6
O K	16.1
AlK	1.2
SiK	3.3
PtM	7.1
CaK	2.9
FeK	66.3

Figure 2.7 EDS analysis of cupola slag before magnetic separation

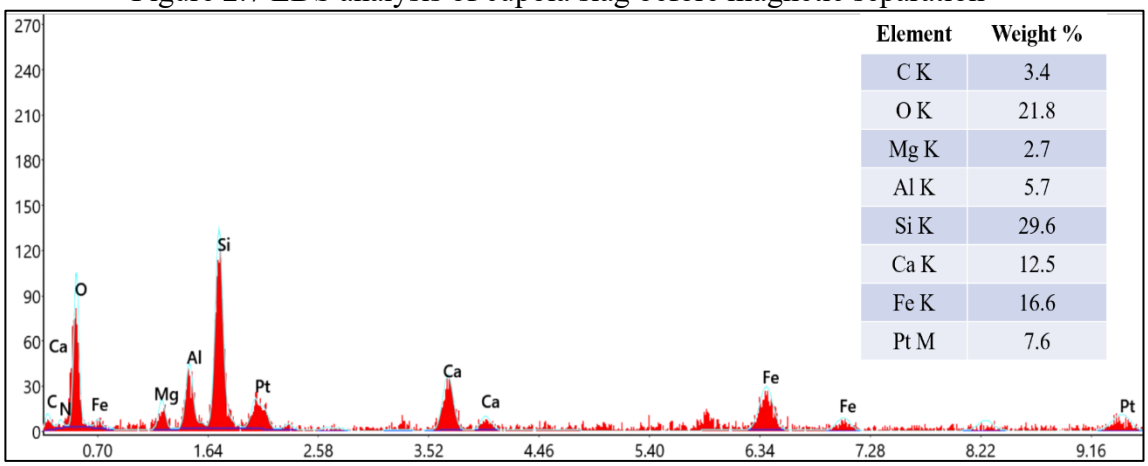

Element	Weight %
C K	3.4
O K	21.8
Mg K	2.7
Al K	5.7
Si K	29.6
Ca K	12.5
Fe K	16.6
Pt M	7.6

Figure 2.8 EDS analysis of cupola slag after magnetic separation

2.2.Fabrication of composites by stir casting

AMCs using LM11 matrix and cupola slag reinforcements have been fabricated through stir casting mode. It is the obvious choice for fabricating low-cost AMCs due to its easy operation and lower cost with respect to other fabrication techniques like powder metallurgy, in situ fabrications etc. Stir casting allows large scale production due to the simple operating process and higher economy [133]. Along with it, the stirring action facilitated the uniform particle dispersion, essential for property enhancements of composites. Stir casting is a process of melting and stirring where reinforcements are poured into molten base metal vortex formed due to stirring. This process of fabrication provides flexibility in type, size and amount of reinforcements for successfully tailoring the properties of composites [134]. The bottom pouring type vacuum stir casting machine (Make: SWAMEQUIP) has been used for this purpose. The photograph of stir casting setup has been presented in Figure 2.9. The setup indicates major components of the stir casting setup while the schematic diagram shown

in Figure 2.10 provide a detailed scientific insight about the stir casting setup. The setup has one main melting furnace along with it powder pre-heating and a mould pre-heating furnace are attached. Bottom pouring is assisted by a vacuum pump to get sound cast composites. The process parameters for stir casting have been shown in Table 2.5. Rigorous literature survey along with trial experimentations have been performed for selecting the parameters. The process of fabrication is described in Figure 2.11. According to required quantity of LM11 ingots has been melted at 750 ˚C in the main melting furnace. The melting temperature has been measured with the help of a k-type thermocouple. While melting desired quantity of cupola slag particles of predefined average particle size have been preheated at 300˚C in the powder preheating furnace. After successful melting of LM11, the mechanical stirrer has been pulled down to 3/4th depth of the crucible and rotated at a constant rpm of 500 rpm. The rotation continues till a vortex is formed in the molten LM11 alloy. A small amount (≤ 1wt.%) of 99% pure magnesium (Mg) has been added to the molten LM11 to improve wettability in the casting. Preheated particles of cupola slag have been poured from the powder preheating chamber to the main melting furnace while stirring. The rotation speed of the stirrer has been increased to 600 rpm after powder pouring and stirring continues for 8 to 10 minutes for uniform dispersion of powder particles in the mixture. Steel made split type cylindrical mould has been preheated to 400˚C to ensure flawless solidification after pouring. The mould temperature has been measured using a k-type thermocouple. Preheated mould has been placed in a chamber in alignment with the bottom pouring hole. The molten composite after uniform dispersion has been poured into the preheated mould by opening the bottom pouring valve. A vacuum pressure of 10^{-2} mbar maintained using a vacuum pump. This vacuum helps in producing defect free casting of composites. The mould has been left at room temperature for solidification for 24 hrs. The final cast composites have been obtained after the opening of the split type steel mould. A similar process has been repeated for the casting of all the composites used in this work. The composites have been fabricated firstly by varying average particle size as 40 μm and 100 μm with 5wt.% inclusion and secondly by varying weight percentage as 3, 5 and 7 wt.% with average reinforcement particle size of 100 μm.

Table 2.5 Process parameters of stir casting

Process Parameters	Values
Melting temperature	750 ˚C
Powder Preheating temperature	300 ˚C
Mould preheating temperature	400 ˚C
Mechanical stirrer material	Stainless steel
Blade angle of mechanical stirrer	45˚
Stirring speed before and while reinforcement addition	500 rpm
Stirring speed after reinforcement addition	600 rpm
Stirring time	8 to 10 minutes
Mould dimension	Φ 30 mm × 300 mm
Mould type	Split type
Vacuum pressure while pouring	10^{-2} mbar

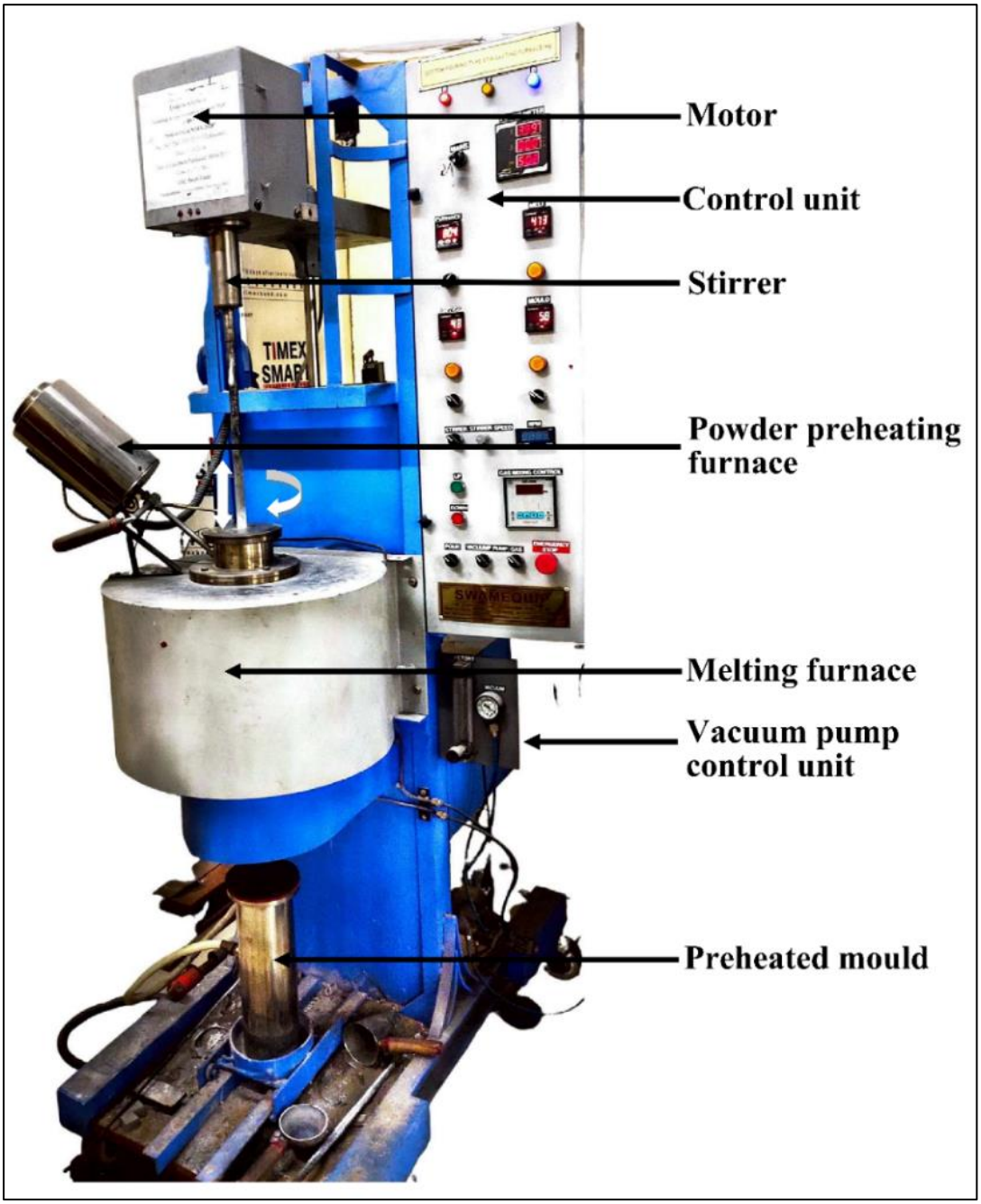

Figure 2.9 Photograph of stir casting setup

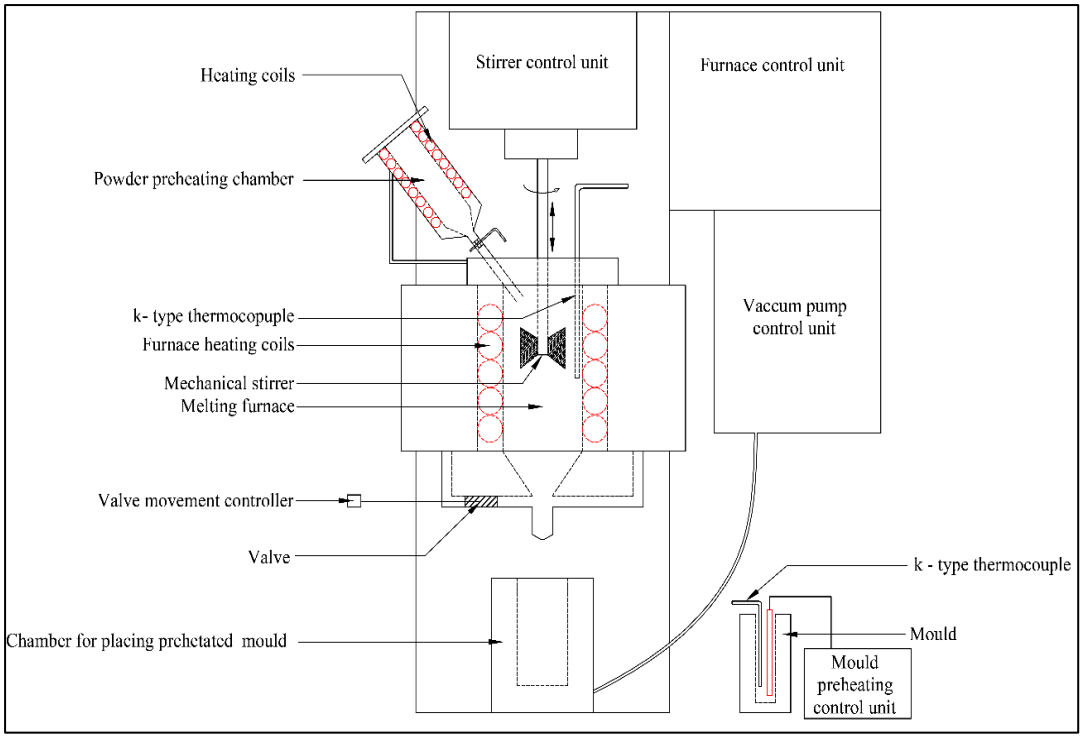

Figure 2.10 Schematic diagram of stir casting setup

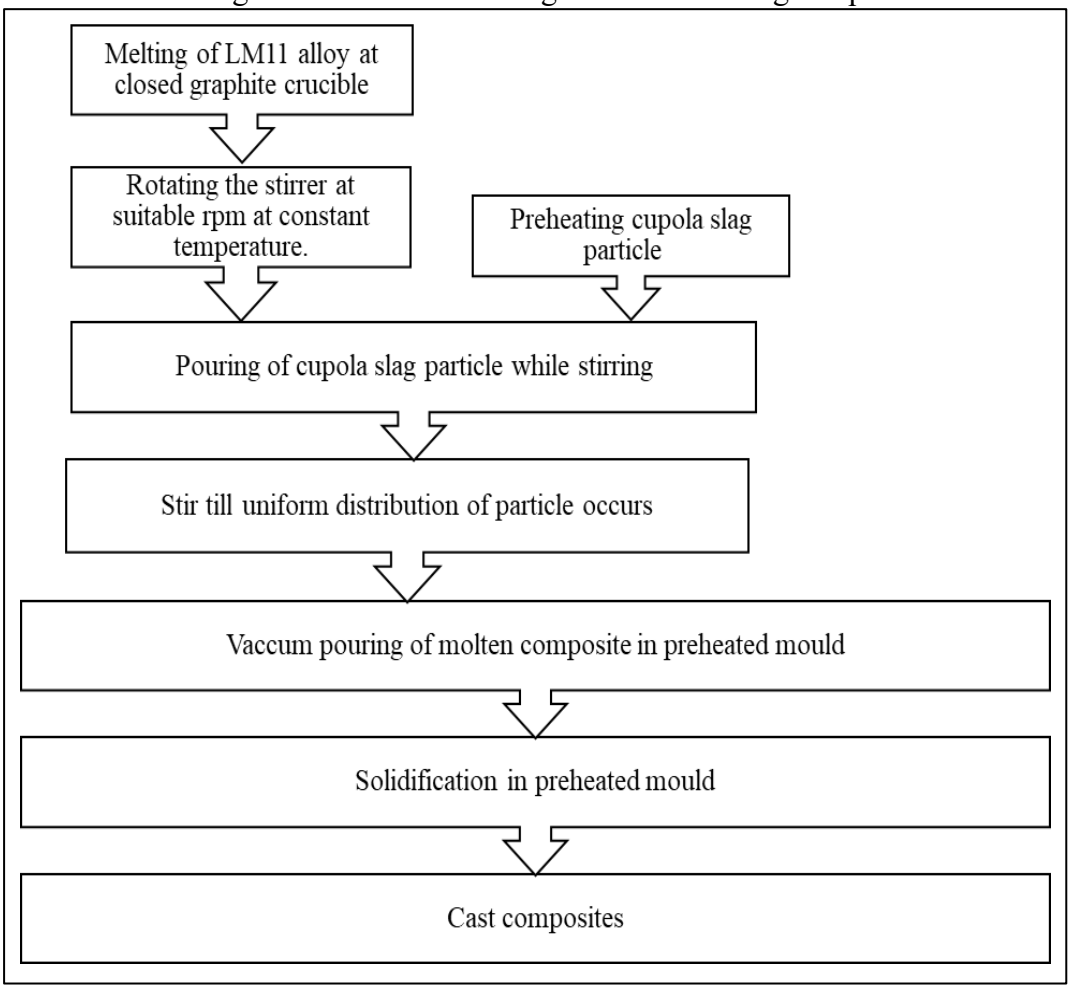

Figure 2.11 Flowchart of cupola slag reinforced composite fabrication

2.3.Measurement of density

Cupola slag reinforced LM11 matrix composites are new to the industry. Thus, it is very much necessary to understand and compare the density and porosity percentage associated with all variations cast composites. The experimental density (ρ_{exp}) of the cast composites has been measured using Archimedes' principle of volume displacement. This method reduces the errors of measurements due to presences of surface pores. Each sample has been weighted in the air (m) and then suspended in water to measure volume displacement (Δv), the density is given by Eq. 2.1. The measurements have been repeated five times and the average value has been reported.

$$\rho_{exp} = \frac{m}{\Delta v}\frac{g}{cm^3} \tag{2.1}$$

The densification behaviour or porosity percentage of the composite dependent on the theoretical density. Law of mixture has been used to calculate the theoretical density (ρ_{th}) by following Eq. 2.2, where ρ_M and $wt.\%_M$ represents density and weight percentage of matrix respectively while, ρ_R and $wt.\%_R$ represents density of reinforcement particle and weight percentage of reinforced particles respectively.

$$\rho_{th} = (\rho_M \times wt.\%_M) + (\rho_R \times wt.\%_R)\frac{g}{cm^3} \tag{2.2}$$

The porosity percentage is an important identifier of uniform reinforcement dispersion has calculated using theoretical and experimental densities. It is given by porosity percentage in Eq. 2.3, in terms of experimental and theoretical density.

$$Porosity\ percentage = \left|1 - \frac{\rho_{exp}}{\rho_{th}}\right| \times 100\ \% \tag{2.3}$$

The analysis of density and porosity can provide suggestions about the strength to weight ratio of the newly fabricated composite. Moreover, the porosity percentage provides insight about hardness and toughness of the materials.

2.4.Microstructural characterizations

Surface microstructures of novel high-performance materials can provide great amount of information which can indicate its exceptional properties. The micrographs from detailed microstructural characterizations can provide information about grain size and orientations, particle distribution, matrix reinforcement interface, homogeneity, morphology of cast composites. These investigations are vital in understanding the

properties of the composite, as it helps in explaining the operational property enhancement by cupola slag incorporation in novel cast composites. The microstructures have been analysed using optical microscopy in general. Along with it, comprehensive catheterization of morphology along with elemental chemical composition study has been introspected using scanning electron microscope equipped with energy dispersive X-ray spectroscopy (SEM-EDS). The cast composites samples need to be metallographically prepared for microstructural investigations. Cast samples have been cut to pieces of 15mm × 15mm × 10mm for characterizations The specimens have been polished by metallographic techniques. Samples have been polished using emery paper of grit size 400, 600, 800, 1200, 2000 grade respectively which is followed by cloth polishing using diamond paste (1μ) for obtaining mirror finish. Upon achieving mirror finish according to ASTM E3-01 standard, samples have been etched using Keller's reagent to improve the visibility of micrograph features. The Keller's etchant contains 2 ml HF (48 wt.%), 3 ml HCl (conc.), 5 ml HNO_3 (conc.) and 190 ml distilled water and applied fresh on the surface for 3s which enhance the clarity of grains and grain boundaries under the microscope. This work utilized an Olympus metallurgical microscope for general micrograph while high contrast higher magnification micrographs are obtained using JEOL SEM-EDS setup (model: JEOL JSM IT500). SEM uses 300 V to 30 kV accelerating voltage in high vacuum mode along with EDS of 129 eV resolution. The micrographs obtained have been further processed using standard image processing software to analyse the grain size, refinement percentages, morphological improvements. Other than these general-purpose use microscopes have been also used for insights about fractography analysis of fracture surface of tensile tests of composites.

2.5.Mechanical characterizations

The suitability of novel cupola slag reinforced composites in practical real-world application is defined by its mechanical properties. The material behaviour under different operational condition can be predicted by introspection of mechanical properties. This ensures reliability and safety in practical engineering applications. Thus, it is necessary to thoroughly introspect mechanical properties of the cupola slag reinforced LM11 matrix composite. Cast composites after subsequent sample preparation steps undergone various mechanical characterizations. These include hardness, tensile properties of composites. All the measurements have been taken

multiple times and the average has been presented to ensure of experimental accuracy. The characterization has enabled a deeper insight of the composite's mechanical properties, making it possible to optimize for specific applications.

2.5.1. Hardness

One of the wide application areas for cupola slag reinforced composites is light weight parts of automobile and aerospace equipment. These required to be resistant to wear which can be achieved by tailoring higher hardness in the cast composites. Hardness is the property of material by which resist the indentation. The micro-hardness has been measured in a Vickers hardness testing machine (VMHT-MOT) according to ASTM standard E384 – 99. A diamond indenter has been used with 50 gf force and for 10 s dwell time along with 50 µm/s loading rate for making the indentation on polished surface. The diagonals of intention mark have been measured from microscopic image as d_1 and d_2 and finally, Vickers Hardness Number (Hv) has been calculated using Eq. 2.4. The indentation has been measured across minimum of 10 different positions in the samples and the average value has been presented.

$$H_V = 1.8544 \times \frac{F}{d^2} \tag{2.4}$$

where, F is the load in kgf and d is the arithmetic mean of diagonals d_1 and d_2 in mm.

2.5.2. Tensile behaviour

The tensile properties are vital for novel AMCs as it indicates materials performance in real time applications. Many properties of material such as ultimate load bearing capacity, ultimate tensile strength, yield stress, elongation, breaking strain can be obtained by performing tensile test on newly developed slag reinforced composites. The tensile test has been done in Zwickroll universal testing machine (UTM), with rate of elongation of 1.5 mm/min. The test samples have been prepared as per ASTM E – 8 standards with a gauge length 25 mm. The load verses elongation graph has been obtained from the computer attachment of UTM and then the data has been processed to plot stress verses strain graph along with 0.2% offset strain for predicting yield stress. The specific strength which is one of the major parameters for light weight applications of composites has been calculated. The detailed fracture mechanism has been observed by fractography using SEM imaging of fractured samples. The elongation and braking strain have also been calculated from these tensile tests. Each tensile test has been conducted on three specimens of each variant of composites and the average load versus

elongation data has been accepted for further calculation of tensile properties. This understanding of tensile properties is crucial for designing AMCs for high-performance applications in fields like aerospace, automotive and structural engineering, where materials need to be strong yet lightweight.

2.6.Introspection of machinability indices

Analysis of machining behaviour is very much essential for the novel cupola slag reinforced composites. Ease of machining or machinability studies are particularly important, firstly, as slag reinforced composites are practically more difficult to machine and secondly, machining is an essential secondary process that any material should go through to be developed as product. The understanding of chip formation mechanisms, tool ware assessments, surface integrity enhancements are very important in determining the applications and life services of these economic composites. The machinability studies can give a feasibility of adding cupola slag as reinforcement in AMCs after appraising machinability characteristics in the composites. This information is vital for identifying applications and commercial viability of these materials. Hence, in this section details of machinability studies have been presented.

2.6.1. Experimental setup

The machinability studies have been conducted on turning operation as it has the ability to from widest variety of surface generation via machining. The turning has been conducted on a conventional lathe without any cutting fluid to introspect the true machinability of novel cupola slag reinforced composites. The composites are hard material due to presence of hard ceramic particles. Hence, it is recommended to use carbide coated cutting tool for turning. This work uses CNMG120408 carbide coated tool inserts along with DCLNR2020K12 tool holder has been used as cutting tool. The tool geometry along with photographs of tool insert and the tool holder have been presented in Figure 2.12 (a) and (b) respectively. The Figure 2.12 depicts that insert has a nose radius of 0.80 mm and tool holder is a right-hand cutting tool with a relief angle of 95º. The machinability of cast composites has been assessed following ISO 3685-1977 and BS 5623: 1979 standards. Turning of cast composites has been performed in a conventional centre lathe with a machining length of 50 mm on constant diameter specimen of 50 mm diameter for each experiment. The experimental set up used for this work has been presented in Figure 2.13, while a close-up view of tool workpiece interface has been presented in Figure 2.14. The setup shows robust conventional lathe

which minimizes the error in measurement due to machine vibration. The cutting force has only been measured in-situ while the other responses has been measured post experimentation.

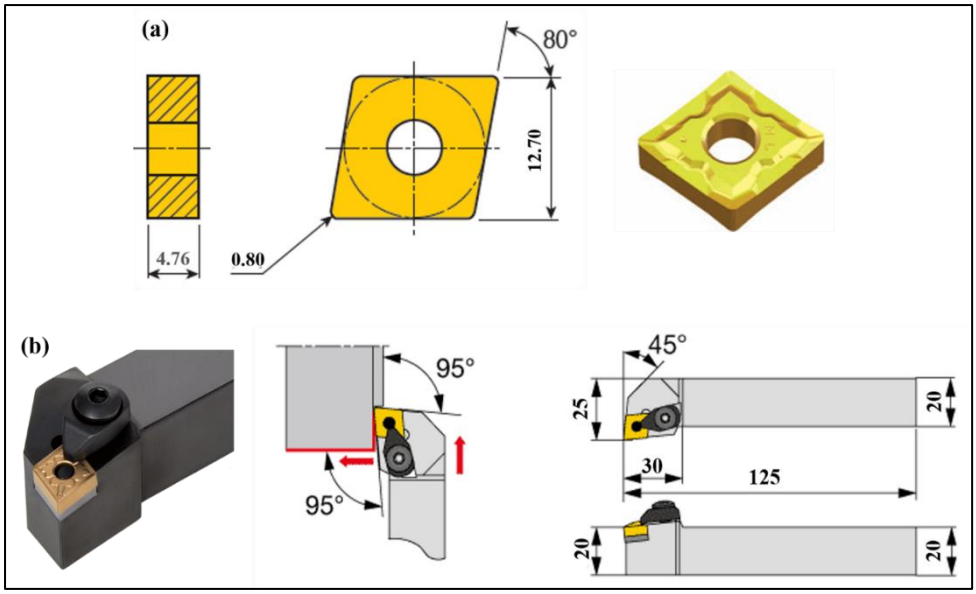

Figure 2.12 Geometry of (a) cutting tool insert (b) Tool holder

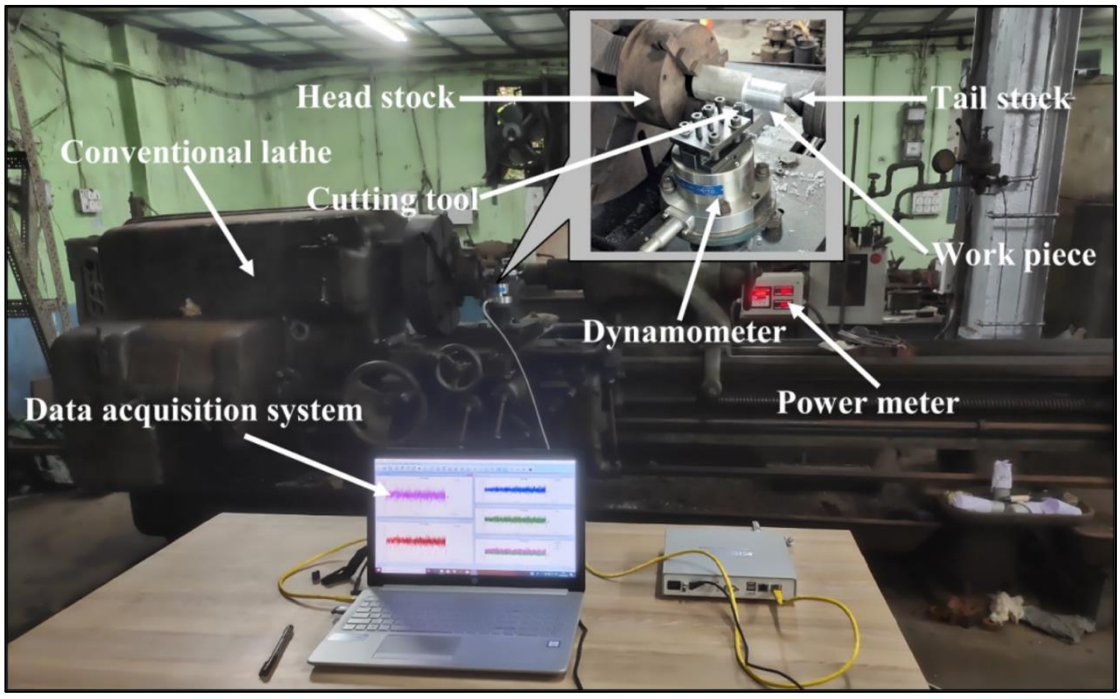

Figure 2.13 Photograph of experimental setup (inset: shows zoomed image of tool workpiece interface indicating dynamometer)

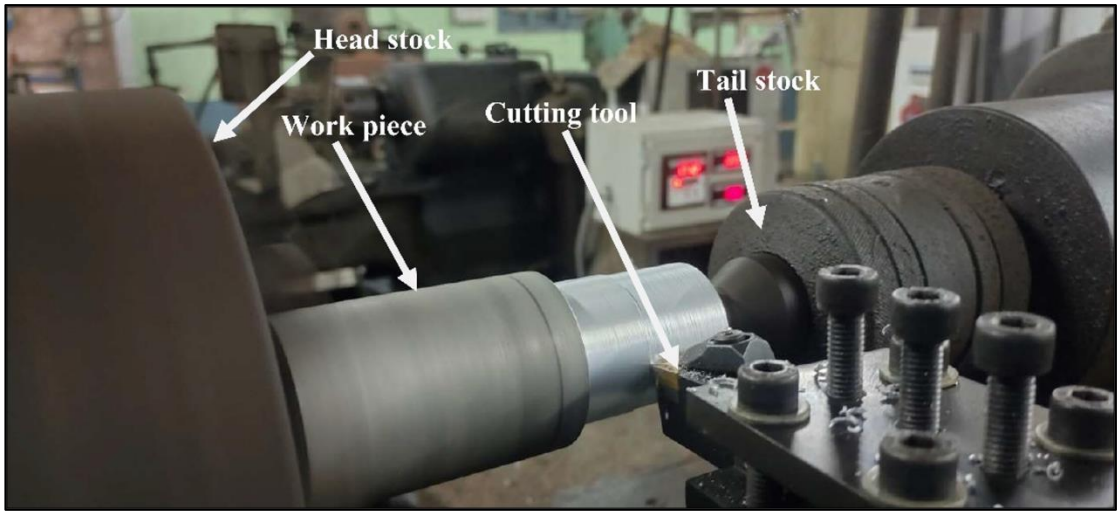

Figure 2.14 Close up view of tool workpiece interface

2.6.2. Parameters selection

Any experimental investigation should follow a well thought plan to reduce the time and material loss which reduces the cost of analysis. The basic step in experimental planning is to identify the parameters of the experiments. All system of experiments consists of two major set of variables one is independent other wise said as input or process parameters and the other ones are dependent or responses generally referred as output. The input parameters are user controlled while the outputs are process or system controlled. The inputs clearly influence the responses. Thus, selection of process parameters and responses are critical in any experimental study. In this machinability analysis the process inputs are selected as weight percentage of cupola slag (wt.%), feed rate (mm/rev) and spindle speed (rpm) based on literature and pilot experimentations. The influence of slag inclusion can be determined by the first process input while the other two are necessary to introspect the dependency on machining. The other well-known machining parameter depth of cut (mm) has been kept constant intentionally throughout the experimentation due to the fact that the effect of depth of cut on machinability indices is well established in present academia [129, 130]. The ranges of input parameters have been selected through literature study and rigours pilot experimentation. The range of process parameters has been tabulated in Table 2.6.

Table 2.6 Process inputs of machining with ranges

Condition	Description
Feed rate (mm/rev)	0.083, 0.109 and 0.125
Spindle speed (rpm)	495, 620 and 800
Depth of cut (mm)	1
Cupola slag content (wt.%)	0, 3, 5, 7
Cutting condition	Dry

The machinability has been accessed in terms of various indices these indices has been taken as response in this experimental investigation. The quality of the finished product and economy of machining are highly dependent on indices like surface roughness (μm), chip thickness (mm) and material removal rate (g/min) while cutting force (N) and power consumption (kW) are other indices of interest, as they are responsible for the energy aspects of machinability. In addition, tool wear (μm) is another important response as it influences tool life and economy of machining. Thus, in this work six machinability indices such as cutting force, power consumption, material removal rate (MRR), surface roughness of machined surface, chip thickness and tool wear has been selected as responses.

2.6.3. Design of experiments

The experimental investigation of machinability of novel slag reinforced composites requires a detailed experimental design. The proper design of experiments reduces the material and time loss of experimentation resulting in cost reduction. The experimental setup and selection of process parameters has been presented in previous paragraphs. This work adopts a full factorial experimental design with three input factors as discussed in section 2.6.2. The full factorial design is very effective as it allows introspection of multi factor influence along with their interactions. This provides more comprehensive information about the system of experiments. A full factorial design estimates all main effect plots and is said to be orthogonal as the influence of every factor can be isolated and quantified independently. Although, it requires more numbers of experiments, this gives the fullest insight about the experimental system. The full factorial design matrix used in this work has been presented in Table 2.7. The bounds of process input have been taken from Table 2.6. A total of 36 experiments has been conducted according to experimental design. Each run of experiments has been conducted using new tool inserts to depict tool wear post operation.

Table 2.7 Design of experiments for machining

Exp. No.	Spindle Speed	Feed Rate	Weight percentage	Exp. No.	Spindle Speed	Feed Rate	Weight percentage
1	495	0.083	0	19	620	0.109	5
2	495	0.083	3	20	620	0.109	7
3	495	0.083	5	21	620	0.125	0
4	495	0.083	7	22	620	0.125	3
5	495	0.109	0	23	620	0.125	5
6	495	0.109	3	24	620	0.125	7
7	495	0.109	5	25	800	0.083	0
8	495	0.109	7	26	800	0.083	3
9	495	0.125	0	27	800	0.083	5
10	495	0.125	3	28	800	0.083	7
11	495	0.125	5	29	800	0.109	0
12	495	0.125	7	30	800	0.109	3
13	620	0.083	0	31	800	0.109	5
14	620	0.083	3	32	800	0.109	7
15	620	0.083	5	33	800	0.125	0
16	620	0.083	7	34	800	0.125	3
17	620	0.109	0	35	800	0.125	5
18	620	0.109	3	36	800	0.125	7

2.6.4. Responses measurements

The machinability analysis has been conducted by measuring six machinability indices as discussed earlier. Among all the responses only cutting force has been measured in-situ while machining. The cutting force has been measured using a piezoelectric dynamometer (Make: Kistler, Model: 9272) equipped with computer-based data acquisition system. The resultant of 3 axis force (F_x, F_y and F_z) has been reported as cutting force. The power consumption has been measured using in-built power meter. The cutting force and power consumptions have been measured in real time while machining and the arrearage value has been reported. The tool wear has been measured by using optical imaging of cutting tool inserts before and after turning. A surface roughness tester (Make: Taylor Hobson) was used to measure the machined surface integrity. It was measured after each machining pass with a sample length of 4 mm. The roughness was measured at five different positions and the mean was reported. The experimental MRR was calculated by weight loss method, samples initial and final weights were taken using high precision weighing scale (Make: Mettler Toledo - BBA236-4A3N) with accuracy up to 0.001 g after each machining pass. The chips were

collected after each pass of turning. Chip thickness was measured using a pointed micrometre. The chip thickness was measured at various points in a chip and the average value had been reported. Moreover, a rigorous introspection of chips formed in various cutting parameters was performed using chip analysis.

2.6.5. Methodology of Analysis

The analysis of the experimental data from the machinability studies has been performed using Minitab – 18 software. The main effect plots of each response have been obtained to introspect the influence of process parameters on the responses. The infographic presentation of responses with respect to individual process inputs yield robust observations on machinability properties of novel composites. The detailed chip analysis has been performed to introspect the underlying mechanism of chip formation. A comparative analysis of machinability has been presented with the help of radar diagram, which has been constructed by normalizing the values of machinability indices from 0 to 100, as the maximum value for each index has been assigned as 100 and subsequently the other values have been converted to percentage of the maximum value. This eases the comparisons of machinability visually.

2.7.Heat treatment of cupola slag reinforced composites

The base LM11 alloy are highly responsive to solution heat treatment. This significantly improves the properties and internal orientations of the alloy. The copper present in LM11 alloy effectively dissolved back into aluminium matrix during the solution treatment. This reintroduction of copper into the microstructure with uniform dispersion throughout the matrix can form strengthening precipitates upon subsequent natural aging. This improves the overall properties and performance of the LM11 alloy. Given the importance of this heat treatment-induced strengthening mechanism in the base LM11 alloy, it is essential to investigate the impact of heat treatment on novel cupola slag-reinforced LM11 composites. The presence of the cupola slag reinforcement may influence the alloy's response to heat treatment, potentially altering the microstructural changes along with the resulting mechanical and machinability properties. In this section detailed heat treatment process adopted in this work has been presented.

2.7.1. Selection of schedule

The heat treatment schedule followed in this work has been based on the literature review and trial and error experimentations. The literatures indicate the parameters of heat treatment as heat treatment temperature, holding time, aging temperature and aging time. These parameters have been selected as per the literature as, heat treatment temperature 500 ºC to 530 ºC, holding time as 2 to 6 hrs, aging temperature as 80 ºC to 120 ºC and aging time as 4 to 8 hrs [131, 132]. The trial-and-error experiments has been designed using 4 factor 3 level Taguchi L_9 orthogonal array with hardness as decision variable. The 7 wt.% slag reinforced composites have been treated in these pilot experiments, as this has the maximum amount of slag included in the metal matrix. These pilot experimentation reveals the optimum parameter for solution treatment as heating at 530 ºC for 6 hours followed by water quenching at 70 ºC and aging at 100 ºC for 4 hours. This decision has been based on the maximum enhancement of hardness when compared with as cast composites.

2.7.2. Process of heat treatment

This solution treatment process consists of heating the composites to a specific temperature, holding it at that point for a predetermined duration, and then cooling at room temperature. This followed by an aging of composites to a certain aging temperature for predetermined amount of time. The cast composites have been heat-treated according to T6 condition as per selected parameters. The T6 condition is a common heat treatment for aluminium alloys that involves three steps: solution heat treatment, quenching, and artificial aging. The alloy is heated (490–540 °C) to dissolve soluble phases, rapidly quenched to form a supersaturated solid solution, and then aged (100–190 °C) to precipitate fine, coherent phases that strengthen the matrix. This treatment gives higher hardness and strength and is widely used in aerospace, automotive, and industrial parts. In AMCs, T6 also improves hardness and strength, but the presence of reinforcement particles affects how precipitates form, so the treatment schedule is adjusted for each composite. The samples are heat-treated in a muffle furnace and aged in an induction heating chamber. The schedule of heat treatment followed for all the composites is treating at 530 ºC for 6 hours followed by water quenching at 70 ºC and aging at 100 ºC for 4 hours and natural aging which further artificially aged at 100 ºC for 4 hours. The heat-treated samples have been cut and prepared metallographically for microstructural characterizations. Moreover, the heat-

treated composites have been characterized for physical properties, mechanical and machinability analysis similar to the as cast composites. Detailed comparisons of all properties and machinability studies of heat-treated and as cast composites has been discussed in this work.

2.8.Summary

This experimental study on novel cupola slag reinforced aluminium metal matrix composites has followed a well-structured methodology presented as flowchart in Figure 2.15. The work has been conducted in four major steps, first cupola slag has been procured, processed and general characterizations has been done. This followed by inspection of effect of particle size and further studies on weight percentage variation and finally study on heat-treated composites, as depicted in Figure 2.15. The experimentation, raw material analysis and reinforcement procurement, development along with characterization has been already discussed in Section 2.1.

The influence of particle size has been analysed by fabricating cast composites with constant 5 wt.% cupola slag inclusion and varying average reinforcement particle size as 40 µm and 100 µm along with base metal. The cast composites have been introspected on the basis of microstructural alterations, grain refinements, physical and mechanical property enhancement and comparative study with base metal. The decision taken from this stage of experimentation has been carried to the next stage along with-it detailed understanding of particle size influence in composite has been presented.

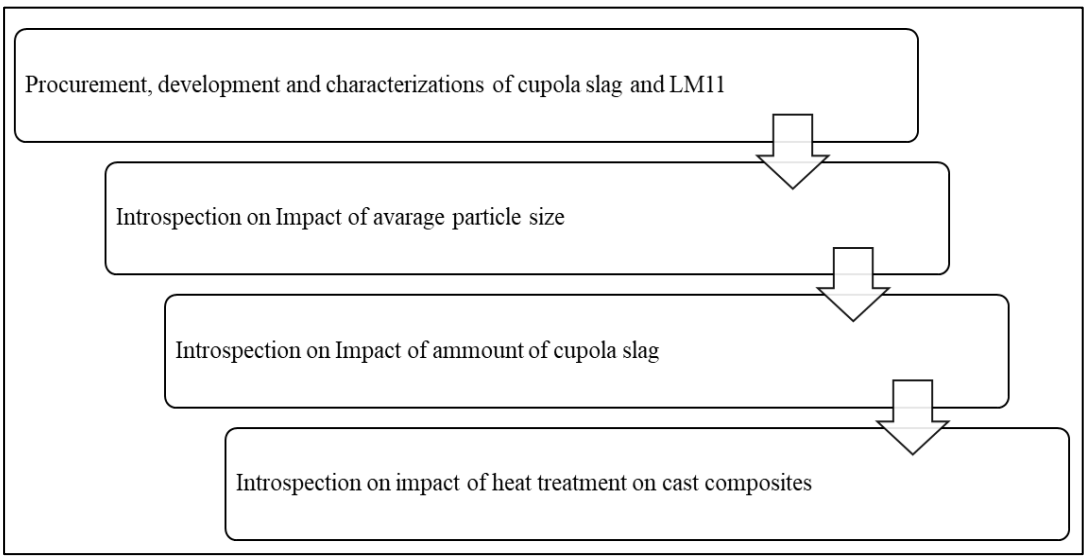

Figure 2.15 Flowchart of methodology adopted

The selected particle size of the cast composites has been taken constant for further stages of experimentation. The impact of slag content has been studied by fabrication of cast composites with varying wt.% of cupola slag as 0, 3, 5 and 7 wt.%. The slag content is varied only up to 7 wt.% because in the pilot experimentation it has been observed that beyond 7 wt.% slag inclusion highly defective casting with pores and agglomerations are formed which are visible even by naked eye. This reduction of quality is the result of reduced wettability beyond 7 wt.% slag inclusion. These cast composites have been undergone rigorous microstructural, physical, mechanical and machinability characterizations as discussed in previous paragraphs of this chapter. This study concluded with detailed discussion and comparison on enhancement of material properties by inclusion of waste cupola slag.

The last stage in this experimental study is the heat treatment analysis. The cast composites with varying weight percentage have been undergone heat treatment as per the procedure discussed in Section 2.7. The solution treated composites has been analysed in terms of mechanical, physical and microstructural investigations. Moreover, analysis on machinability behaviour and comparisons with LM11 as well as as-cast composites has been performed. The detailed analysis on property enhancement and justification of cupola slag as reinforcement particles has been introspected.

Chapter 3

Study on Particle Size Variation of Reinforced Cupola Slag Particles

New era of innovation requires noble materials with tailored properties. AMCs are one of such new age materials with light weight, high performance along with desired application-based properties. However, mass-scale production of AMCs has not been observed since the cost of AMCs is higher than conventional monolithic alloys. This leads to compromise property improvement in most of the application areas. Only specific applications have been accepted AMCs as an alternative due to the higher cost [137].

The cost may be reduced by lowering the cost of fabrication and the cost of reinforcement material. Stir casting is an economic alternative for the fabrication process. It is simple in operation and greater control over the process can be established [138]. The cost of reinforcement particles can be reduced by using non-conventional reinforcement cupola slag. Cupola slag is an industrial waste that has no material cost. Only transportation and cost of reinforcement particle development will occur to use it as reinforcement. Mechanical property improvement may be expected in cupola slag reinforced AMCs. The added advantage would be in conversion of industrial waste to resource for the development of engineering material. The attempts have been made to fabricate and introspect the cupola slag reinforced composites. The effect of average particle size of reinforcement has been investigated. The average reinforcement particle size is important as the properties and strengthening mechanisms of the composites

highly dependent on the particle size. The microstructural, physical and mechanical properties of cupola slag reinforced composites have been evaluated and the results have been reported in this chapter.

In this experimental investigation on effect of average particle size of reinforcements, as received stony cupola slag has been used to develop two types of reinforcement material for the fabrication AMCs those are cupola slag of 40 μm and 100 μm particle size. Now, three types of AMCs have been fabricated using stir casting route, LM11 casting without any reinforcement, LM11 AMC with 5 wt.% cupola slag of 40 μm particles size as reinforcement and LM11 AMC with 5 wt.% cupola slag of 100 μm particles size as reinforcement. The selection of 5 wt.% reinforcement was based on prior studies where lower percentages of waste-based reinforcements ensured uniform dispersion and improved properties. Literature also indicates that particles in the 40–100 μm range provide better wettability and bonding. Pilot trials confirmed that 5 wt.% with 40 μm and 100 μm sizes offered optimal dispersion and interfacial bonding. The quality of developed composites (LM11/5wt.% 40 μm CS composites, LM11/5wt.% 100 μm CS composites) has been characterized for density, porosity, hardness, grain refinement along with optical and SEM – EDS microstructural analysis. Detailed experimental procedures and setups have been discussed in Chapter 2. The feasibility of the process to develop low-cost cast composites with improved properties has been assessed. The confirmation of the successful development of AMCs has been observed with the help of EDS and elemental mapping. The influence of the average particle size on the properties of cast composites has been discussed. The insights on underlying mechanisms of property enhancement have been presented. Moreover, the reinforcement particle size showing better properties has been chosen for further investigations.

3.1.Effect on microstructure

Optical microstructures of base LM11 along with two variants of cast composites have been shown in Figure 3.1 (a – c). The microstructure indicates a uniform dispersion of cupola slag throughout the matrix as well as the grain boundaries as illustrated in Figure 3.1 (b) and Figure 3.1 (c). Clean interfacial bonding has been found between cupola slag particles and the LM11 matrix. There is very low amount of agglomeration has been present as a small amount of Mg is used while fabrication to improve wettability [139]. The reinforcement-matrix interfaces have been identified as clean and

free from any intermediate phases which lead to higher interfacial bond strength [140]. A more detailed analysis of the microstructure, interfaces and cupola slag inclusion has been discussed using scanning electron microscopy results.

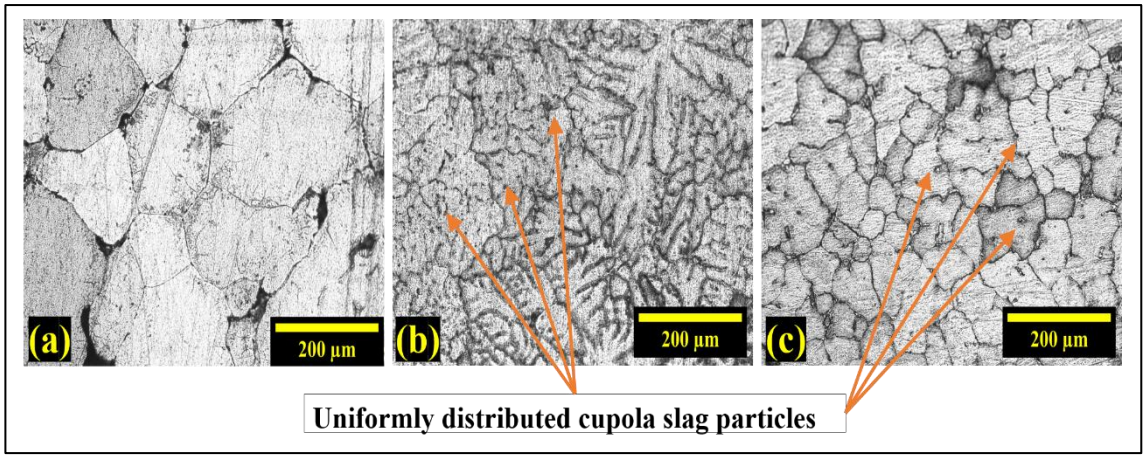

Figure 3.1 Optical micrographs of (a) LM11, (b) LM11/5wt.% 40 µm CS and (c) LM11/5wt.% 100 µm CS composites

The optical microstructures shown in Figure 3.1 indicate refinements of grains as cupola slag is dispersed in the metal matrix. The grain size has been measured by the masking technique. The process is described with the help of Figure 3.2 (a – f). Figure 3.2 (a) is the microscopic image of base LM11 alloy which is masked to find the grain boundaries prominently in Figure 3.2 (b). Similarly, Figure 3.2 (c) represents LM11/5wt.% 40 µm CS composite's microstructure and its masked grain boundaries have been shown in Figure 3.2 (d). LM11/5wt.% 100 µm CS composite's microstructure and its masked grain boundaries have been depicted in Figure 3.2 (e) and Figure 3.2 (f) respectively. The grain size has been extracted from the masked images in Figure 3.2 using the line interception method in accordance with ASTM E112 standard. After masking, the grain boundaries become clearly distinguishable, as shown in Figure 3.2 (b), (d), and (f). A set of uniformly spaced straight lines were overlaid on these masked images, and the number of grain boundary intersections per unit length was counted. The average grain size was then calculated from the reciprocal of the lineal intercept length. This procedure was repeated over multiple fields of view to minimize statistical error. The histograms for particle size for base LM11, LM11/5wt.% 40 µm CS and LM11/5wt.% 100 µm CS composites have been presented in Figure 3.3 (a), Figure 3.3 (b) and Figure 3.3 (c) respectively. The average particle sizes have been reported in Table 3.1. It is clearly observed from Figure 3.2 and Figure 3.3 that grains have been refined due to cupola slag inclusion. Same kind of grain refinements has been

investigated in the previous works [141,142]. Table 3.1 suggests that LM11/5wt.% 40 µm CS composites have lower grain size than LM11/5wt.% 100 µm CS composites. Smaller particle size creates dense dispersion of reinforcement in the case of 40 µm which upon solidification creates smaller grains [143]. This smaller grain size can also be a result of incomplete grain growth of the matrix while solidification due to dense dispersion of the second phase [144]. The overall percentage reduction in grain size, when compared with base LM11, was observed to be 82.84 % for LM11/5wt.% 40 µm CS composites and 71.08 % for LM11/5wt.% 100 µm CS composites which indicates the improvement of mechanical properties of the developed cast composites [145].

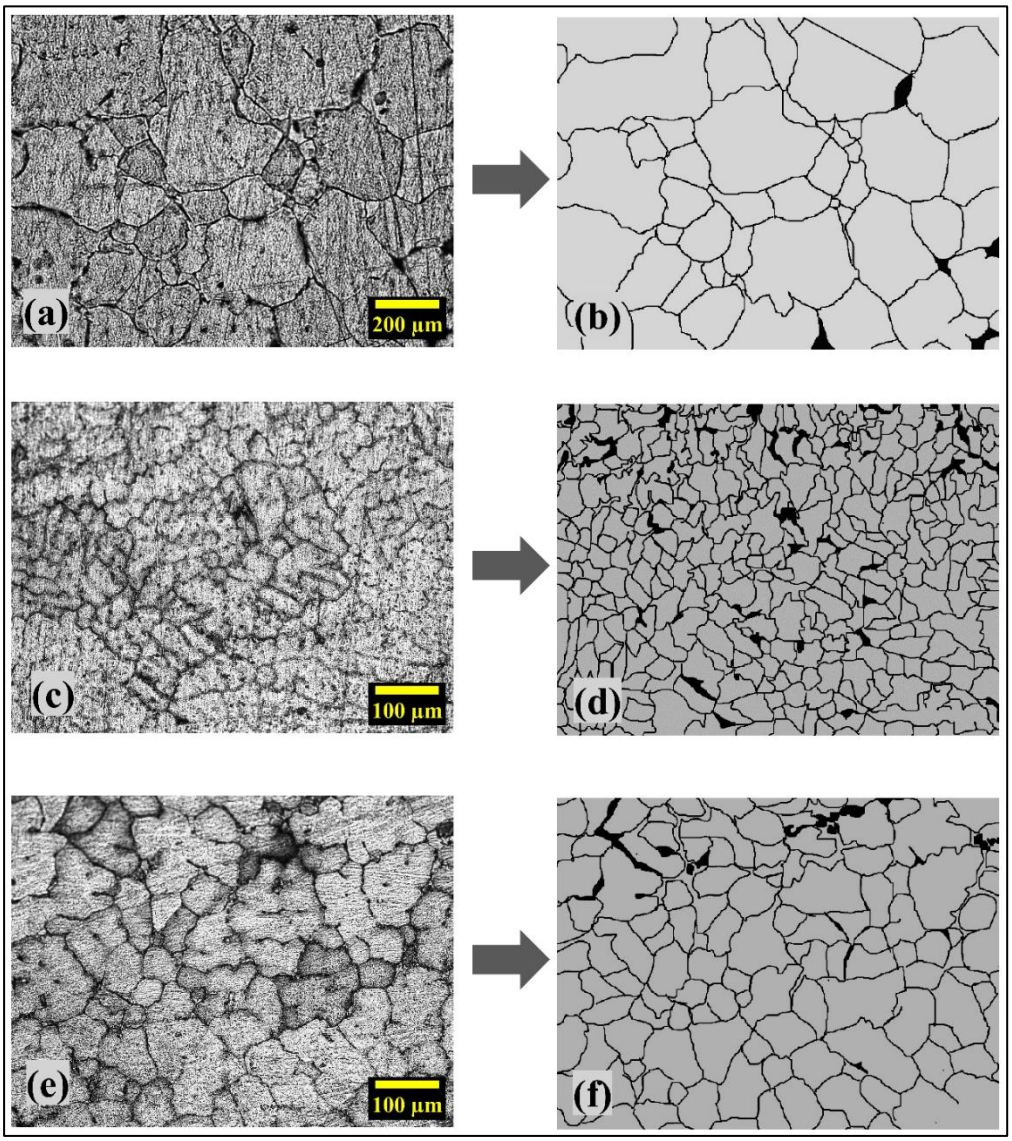

Figure 3.2 Optical microscopic images of (a) LM11, (c) LM11/5wt.% 40 µm CS, (e) LM11/5wt.% 100 µm CS composites and masked grain boundaries for grain size measurement for (b) LM11, (d) LM11/5wt.% 40 µm CS, (f) LM11/5wt.% 100 µm CS composites

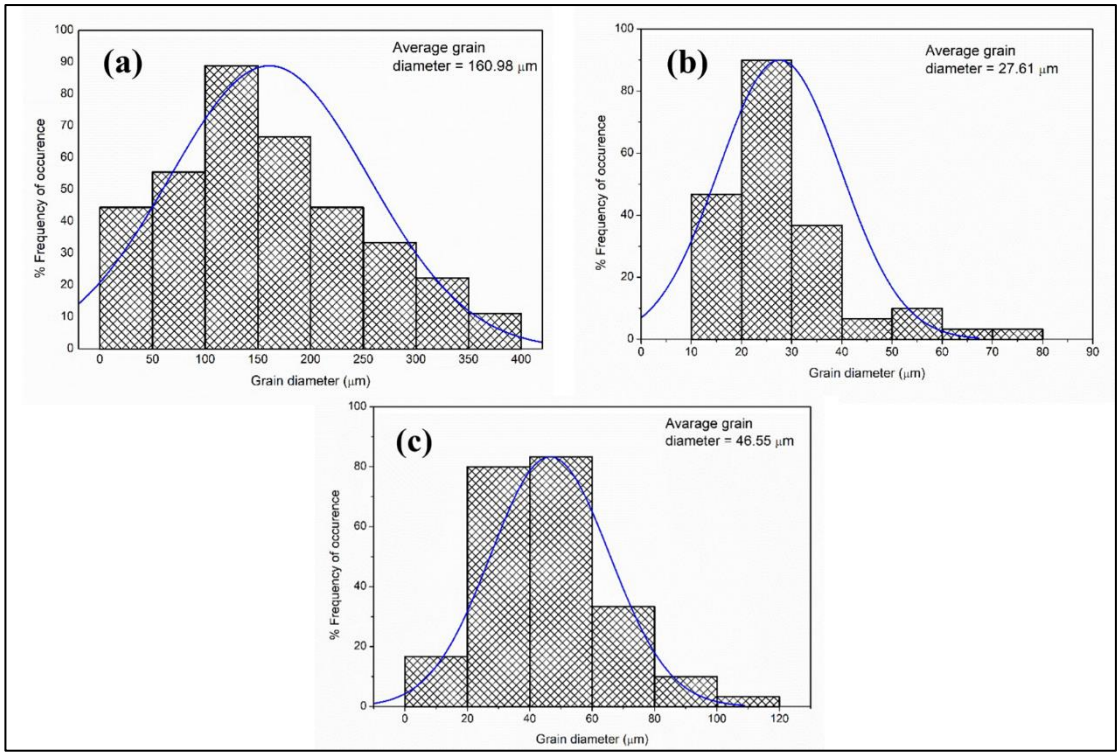

Figure 3.3 Histograms of particle size of (a) LM11, (b) LM11/5wt.% 40 µm CS, (c) LM11/5wt.% 100 µm CS composites

Table 3.1 Average grain size results

Composites	Average grain size (µm)
LM 11	160.98
LM 11/5wt.% 40 µm CS	27.61
LM 11/5wt.% 100 µm CS	46.55

SEM micrographs have been shown in Figure 3.4 (a – c). Figure 3.4 (a) depicts no presence of the second phase in base LM11 alloy but nearly equiaxed grains are visible. Figure 3.4 (b) represents LM11/5wt.% 40 µm CS composites with visible reinforcement and interface. Similarly, in Figure 3.4 (c) LM11/5wt.% 100 µm CS composites have been shown with visible slag sites and interface. It is clear from Figure 3.4 (b) and Figure 3.4 (c) that successful slag inclusion along with good interfacial bonding has occurred in the process of development of these low-cost cast composites. It is also visible from SEM micrographs that cupola slag particles dispersed not only at the grain boundaries but also inside the grain which would show property improvement of the base materials [146].

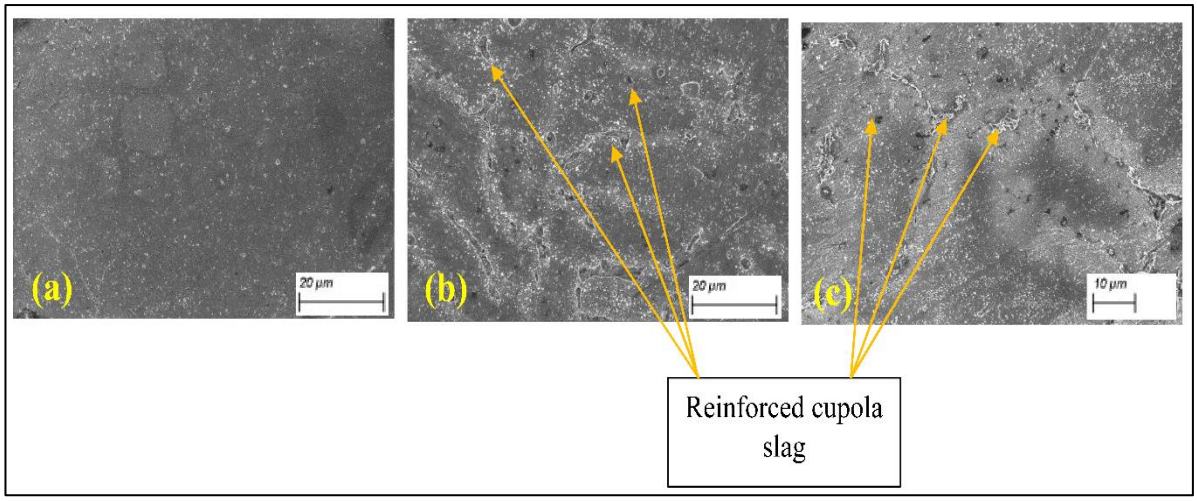

Figure 3.4 SEM micrograph of (a) LM11, (b) LM11/5wt.% 40 µm CS and (c) LM11/5wt.% 100 µm CS composites

The confirmation about cupola slag inclusion was further analysed using EDS. The results of EDS have been shown in Figure 3.5 (a – c). Figure 3.5 (a) shows the spot of EDS along with the EDS curve for the base LM11 alloy. The results show the presence of Al and Cu elements which are the major constituents of the LM11 alloy. No oxygen peak has been observed in the EDS curve of the base which suggests that no oxides have been formed during casting. Figure 3.5 (b) indicates the EDS analysis of LM11/5wt.% 40 µm CS composites. The presence of elements such as O and Si ensures cupola slag addition as these element maps to SiO_2 which is the major constituent of cupola slag. The presence of Mg in the EDS is due to the addition of Mg to improve wettability while casting. Similar results have been seen for LM11/5wt.% 100 µm CS composites in Figure 3.5 (c). The other elements of cupola slag have been not traced using EDS due to the low weight percentage and smaller size of cupola slag particles [147]. The EDS analysis confirms the inclusion of slag in the metal matrix of developed composites.

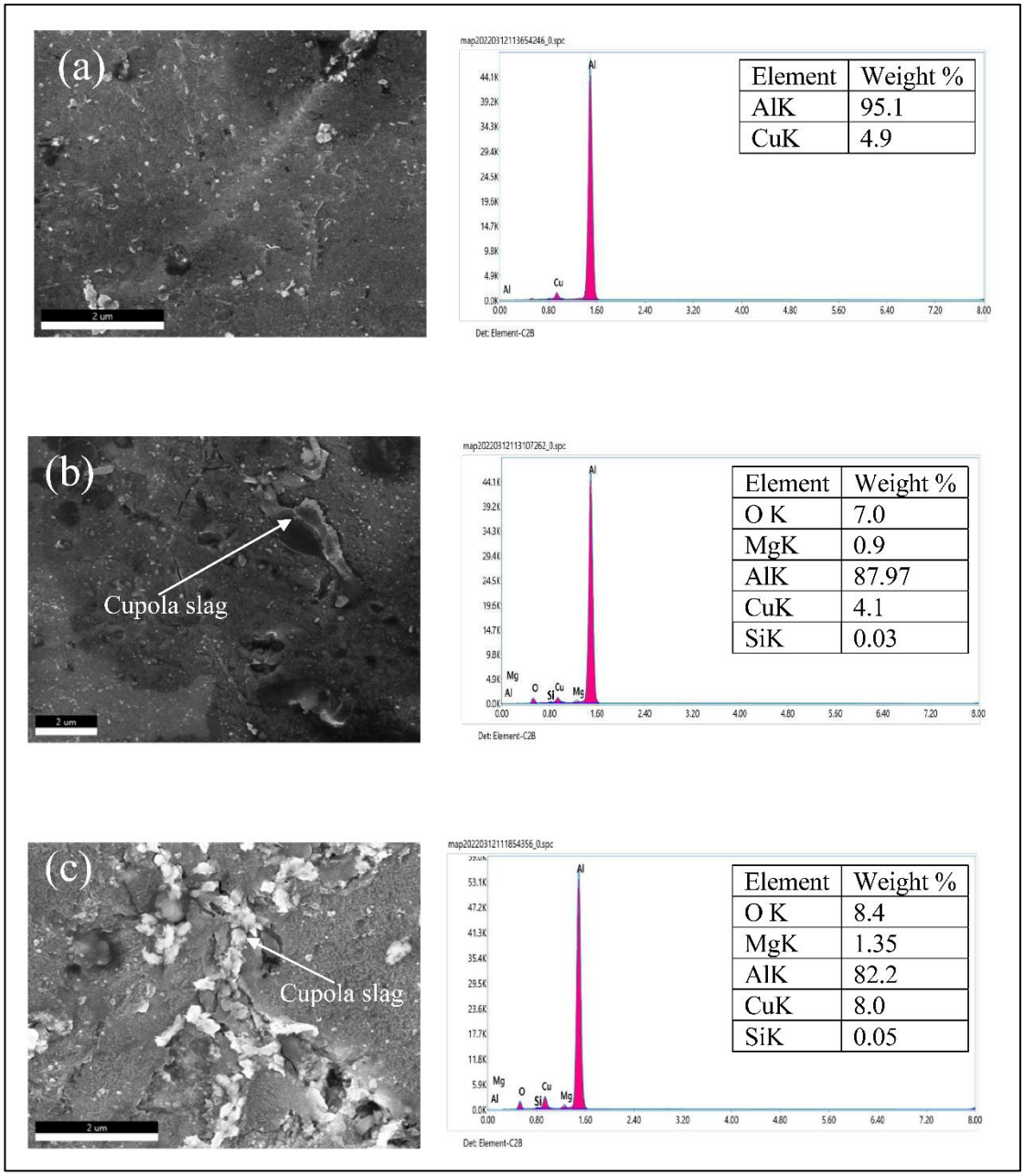

Figure 3.5 EDS analysis results for (a) LM11, (b) LM11/5wt.% 40 µm CS and (c) LM11/5wt.% 100 µm CS composites

Positional analysis by elemental mapping has provided robust proof of slag inclusion. The elemental mapping for each element has been shown in Figure 3.6 (a, b). The highlighted sections in Figure 3.6 show the corresponding elements. Figure 3.6 (a) shows elemental mapping for LM11/5wt.% 40 µm CS composites. It is clear from the figure that the position identified as cupola slag has rich O and Si which may validate the claim of cupola slag inclusion in developed metal matrix composites. Consequently, Figure 3.6 (b) depicts that O and Si-rich regions are part of identified cupola slag particle. Thus, detailed microstructural analysis supports the claim of the successful

casting of low-cost AMCs and the feasibility of the method has been proven. Kok [148] has previously reported similar results in microstructural analysis.

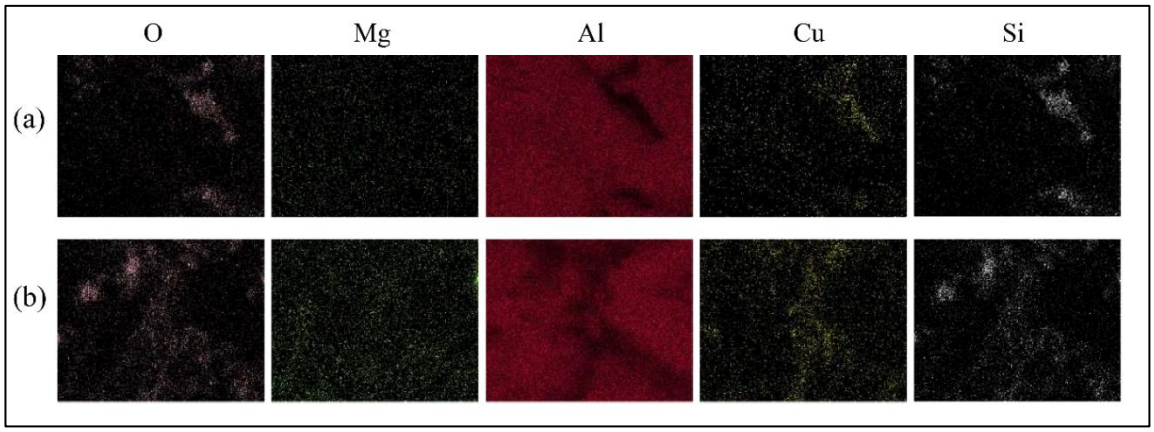

Figure 3.6 Elemental mapping of EDS spot on (a) LM11/5wt.% 40 µm CS and (b) LM11/5wt.% 100 µm CS composites

3.2.Physical properties analysis

Density and porosity of the base alloy LM11 along with two variants of cast composites namely, LM11/5wt.% 40 µm CS and LM11/5wt.% 100 µm composites have been reported in Table 3.2. It is clear from Table 3.2 that density has been decreased in cast composites when compared with base alloy. It is due to the fact that cupola slag particles have a lower density when compared with base LM11. Sridhar Raja et al. [149] has observed similar decrease in density by incorporating steel slag in Al356 alloy. These developed cast composites of aluminium alloy with low density could be a potential member for rotary parts in automobiles and other applications in transportation [150].

Table 3.2 Density and porosity percentage results

Composites	Density (g/cm^3)	Porosity Percentage (%)
LM11	2.489 ± 0.006	5.74 ± 0.29
LM11/5wt.% 40 µm CS	2.415 ± 0.006	3.75 ± 0.19
LM11/5wt.% 100 µm CS	2.381 ± 0.006	12.34 ± 0.61

The variation of density and porosity with respect to the increasing particle size of reinforcement has been plotted in Figure 3.7. The density has been observed to be decreased in the case of both variants of cast composites. The density has been observed to be lower in the case of LM11/5wt.% 100 µm CS composites as shown in Figure 3.7. Inclusion of larger cupola slag particle of 100 µm results in larger grains as compared with composites with 40 µm CS addition as described in microscopic analysis [151]. The porosity on the other hand decreased initially when compared between base LM11

and LM11/5wt.% 40 µm CS composites. This has been identified as another supporting fact for the claim of grain refinement which may result in better mechanical properties [152]. Porosity percentage has been observed to be increased when 100 µm CS particles are reinforced which is a result of more voids due to the larger grain size of the cast composites [153].

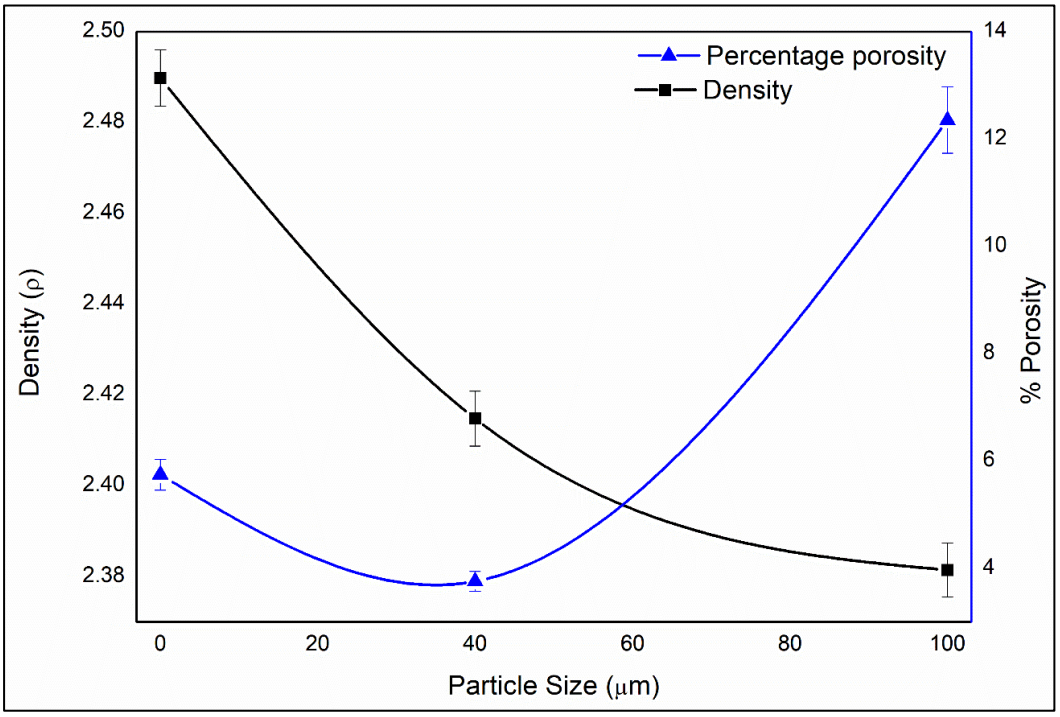

Figure 3.7 Variation of density and porosity with respect to particle size

3.3.Microhardness analysis

Improvement of mechanical properties in the developed low-cost composites has been indicated by the microstructural and physical property analysis. The effect on microhardness has been analysed in this work and reported in Table 3.3. Figure 3.8 pictorially represents the microhardness analysis results. Improvement of microhardness of cast composites, when compared with base LM11, has been observed. This improvement in hardness is the result of hard ceramic inclusion in the form of cupola slag. Hamid et al. [154] has concluded a similar increment in hardness of aluminium alloy by hard ceramic inclusion. The load applied while hardness has been distributed over the hard reinforcement which leads to greater hardness values. In the works of Sridhar Raja et al. [155] improvements of hardness due to steel slag inclusion in Al 356 alloy have been investigated and observed to be in line with the current experimental investigation. It is evident from Figure 3.8 that a maximum hardness of 82.8 Hv has been observed in LM11/5wt.% 100 µm CS cast composites. Interestingly

grain size of LM11/5wt.% 100 µm CS composites is higher than LM11/5wt.% 40 µm CS. This larger value of hardness by using larger particle size as reinforcement is due to the dense distribution of smaller 40 µm cupola slag leads to limited grain growth which acts as potential crack sites. These potential crack sites may take the indentation load and decreases the hardness value although 40 µm CS reinforced composites have smaller grains [156]. The higher porosity in the 100 µm composite does not reduce the microhardness because the larger slag particles act as load-bearing agents during indentation. Since microhardness is a localized test of limited depth, values may also vary depending on whether the indentation falls on a grain or reinforcement-rich region. Therefore, bulk hardness tests such as Brinell or Rockwell are recommended for a more representative assessment of the overall hardness of the composites. The analysis has indicated microhardness improvement in cast composites which make them a potential member of application in various automobile, aerospace and defence industries.

Table 3.3 Microhardness results

Composites	Microhardness (Hv)
LM 11	73.1 ± 2
LM11/5 wt.% 40 µm CS	80.8 ± 1.2
LM11/5 wt.% 100 µm CS	82.8 ± 1.7

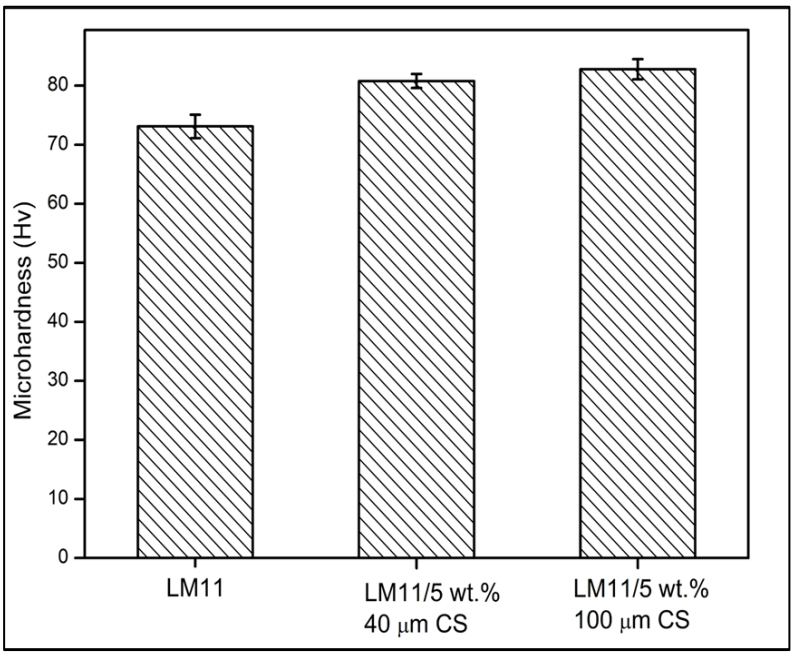

Figure 3.8 Microhardness analysis results

3.4.Summary

The study on reinforcement particle size variation indicates that it is feasible to use cupola slag as a reinforcement in AMCs which yield enhancement of properties. The major findings indicates that,

- Successful fabrication of cupola slag composites using the liquid metallurgy stir casting process has been identified.
- Microstructural analysis shows uniform dispersion of cupola slag in the base LM11 matrix.
- Grain refinement indicated, yielding improved mechanical properties of the LM11 alloy.
- SEM analysis indicates good interfacial bonding with a clean interface.
- EDS and elemental mapping confirm cupola slag inclusion in both cast composite variants.
- The density of base LM11 decreases by cupola slag inclusions.
- Density further decreases with increasing particle size, making the composites lighter as hardness is governed more by particle strengthening than bulk density, with 100 µm particles acting as load-bearing sites despite lower density, while 40 µm particles refine grains but introduce crack sites.
- Composites with smaller cupola slag particles (40 µm) exhibit higher density compared to those reinforced with larger particles (100 µm).
- The microhardness of LM11 increases with incorporation of cupola slag particles as reinforcements.
- Microhardness trends upward with increasing particle size, reaching a maximum of 82.8 Hv in composites with 100 µm cupola slag reinforcement.
- Composites with 100 µm particle size show better particle dispersion, grain refinement, microhardness, and clean matrix–reinforcement interface.
- The average reinforcement particle size of 100 µm is selected for further investigations.

Chapter 4

Study on Weight Percentage Variation of Reinforced Cupola Slag Particles

Rapid evolution in engineering and manufacturing demands light weight material with enhanced mechanical properties. Aluminium metal matrix composites with ceramic reinforcement particulates serve this demand due to their reduced density, improved strength and hardness along with higher resistance to wear and corrosion. However, the material cost hinders the full potential of utilization. To overcome these challenges, in this work cupola slag, has been incorporated as reinforcement of aluminium composites using low-cost stir casting method. The enhancement of material properties by cupola slag inclusion on base alloy has been investigated in detail. The impact of amount of slag inclusion has been introspected. Moreover, discussion about the underlying mechanisms responsible for the improvement in material properties has been presented with detailed microstructure and fractographic analysis. This chapter is dedicated to reporting and discussion of microstructural, physical and mechanical property enhancement, providing thorough insights about the impacts of cupola slag content in the composites, mechanisms responsible for improvement of properties. Additionally, the effectiveness of incorporating an industrial waste to develop an economic novel AMCs has been judged.

The investigation of reinforcement weight percentage variation in the properties of LM11 cast composites has been analysed by fabricating the composites with inclusion of cupola slag particle in varying weight percentage as 0, 3, 5 and 7wt.%. The average particle size of cupola slag particle has been kept constant as 100 μm as discussed in Chapter 3. The fabrication has been followed economic stir casting process. The cast

composites have undergone rigours microstructural, physical and mechanical characterizations following the detailed methodology presented in Chapter 2. The grain refinements, particle dispersion, density, porosity, hardness, tensile properties along fractography have been studied in detailed. The comparative analysis of increase in cupola slag content along with best weight percentage selection has been discussed.

4.1.Effect on microstructure

The optical microscopic image of base LM11 matrix, which is free from slag particles and with larger grains as presented in Figure 4.1 (a). The inclusion of slag is clearly visible in the case of cast composites with 3 wt.%, 5 wt.% and 7 wt.% of cupola slag reinforced composites in Figure 4.1 (b – d). The yellow arrows in Figure 4.1 are the slag particles and the red circles show the porosity. The grain size has been reduced with increasing slag percentage as depicted in grain distribution curve shown in Figure 4.2 (a - d).

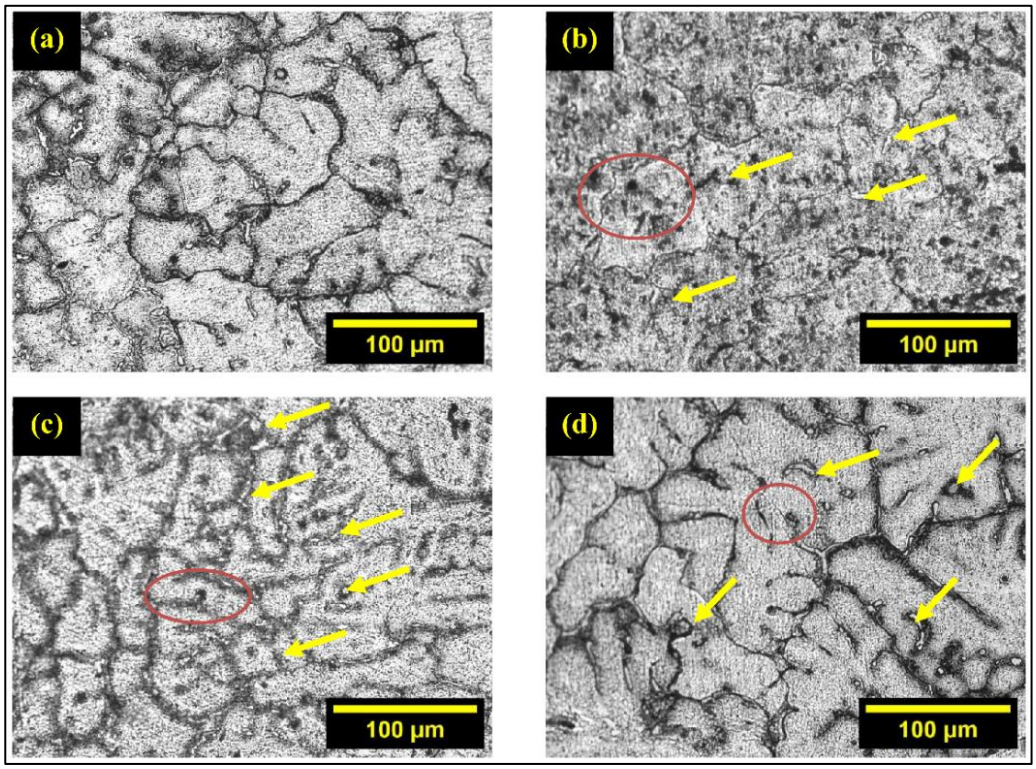

Figure 4.1 Optical micrographs of (a) LM11, (b) LM11/3wt.%CS (c) LM11/5wt.%CS and (d) LM11/7wt.%CS where yellow arrows show slag particles and the red circles show porosity

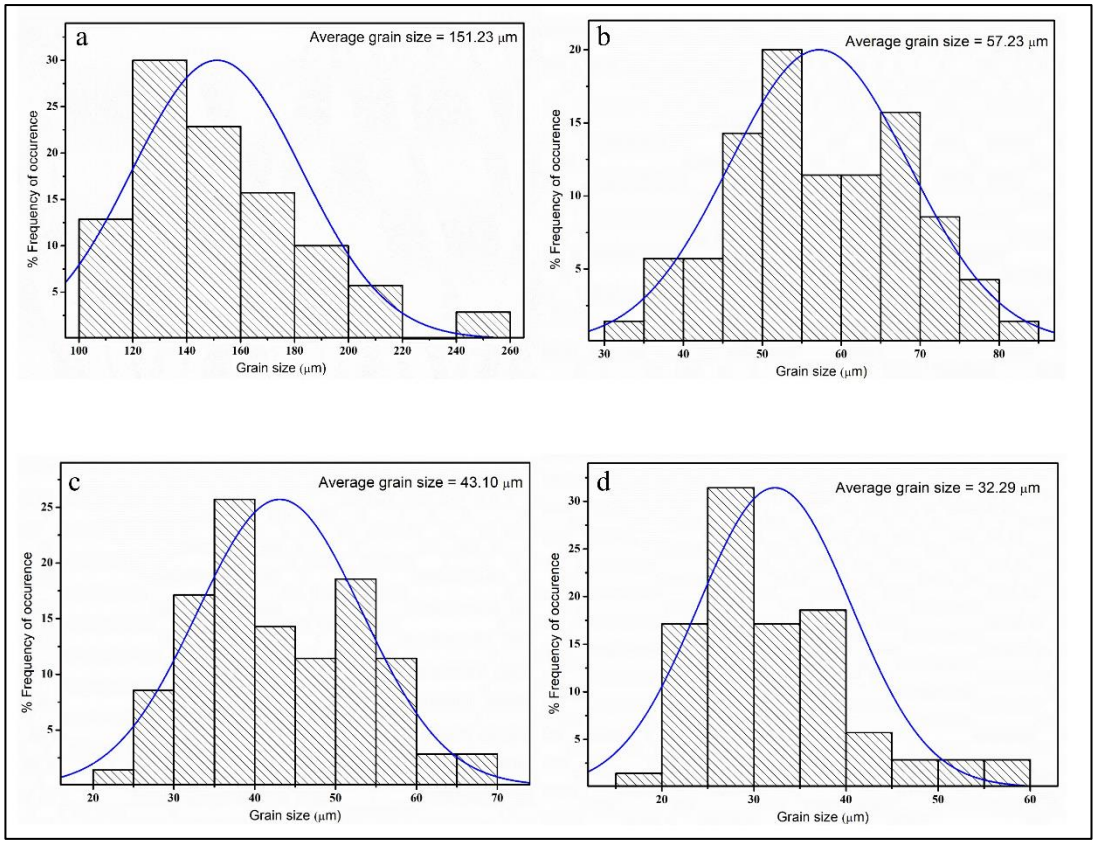

Figure 4.2 Grain size distribution of (a) Base LM11 alloy (b) 3 wt.% CS/LM11 composites, (c) 5 wt.% CS/LM11 composites and (d) 7 wt.% CS/LM11 composites

More detailed view of microstructure along with matrix reinforcement interfaces has been observed using scanning electron microscopy imaging as depicted by Figure 4.3 (a – d). Figure 4.3 (a) shows the SEM image of base LM11 where Cu precipitation is visible in the grain boundaries. The included slag in the matrix has been indicated by yellow arrow in Figure 4.3. The black dots as visible clearly in Figure 4.3 (b) represent the porosity which generated as a result of gas entrapment while casting. However, the porosity found to be minimized with increasing weight percentage of cupola slag. It is also observed from scanning electron microscopy imaging that the matrix reinforcement interface improves with increasing cupola slag content as the interface becomes cleaner.

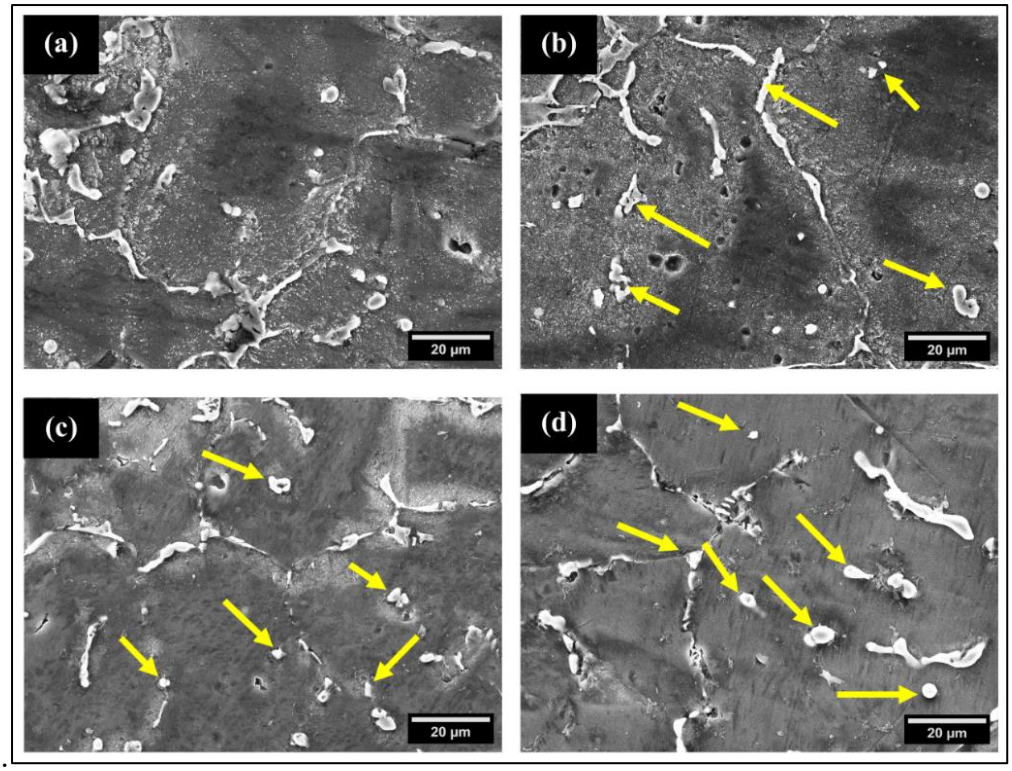

Figure 4.3 Scanning electron microscopy micrographs of (a) LM11, (b) LM11/3wt.%CS (c) LM11/5wt.%CS and (d) LM11/7wt.%CS where yellow arrows show slag particles.

The evidence of slag inclusion has also been observed in energy dispersive spectroscopy results along with elemental mapping presented in Figure 4.4 (a – d). The major constituent of LM11 has been observed from Figure 4.4 (a) as aluminium and copper along with 5.3 wt.% Cu in elemental mapping. Figure 4.4 (b – d) made it evident that cupola slag particles which contain various metallic and non-metallic oxides such as silicon dioxide (SiO_2), calcium oxide (CaO), ferrous oxide (Fe_2O_3) etc. has been successfully incorporated in the metal matrix of LM11 as the trace of oxygen (O), calcium (Ca), silicon (Si) and iron (Fe) can be observed in energy dispersive spectroscopy of cast composites whereas, base material are free from these particles. The microstructural results observed to be in agreement with the previous literatures with fly ash reinforcement and rice husk ash reinforcement [37,157].

Properties of cast composites is highly dependent on the microstructure of the material [158]. The microstructure studies using optical microscopy show the refinement of grains with increasing amounts of cupola slag in the matrix. It should be noted that the optical micrographs of base LM11 alloy as presented in Figure 4.1 (a)

have no cupola slag particles and has larger grains as compared with other cast composites. Cupola slag has been introduced in the matrix and the slag particles act as the site of nucleation and generate new grains while solidification. The numbers of refined grains have been increased with increasing slag content. This is attributed to the fact that with increasing cupola slag, the amount of grain nucleation sites increases along with-it resistance to growing grains, generating finer grains. The porosity, on the other hand, has been observed to be reduced with increasing slag content. This can be explained by the phenomenon of void packing with increased amount of slag. Void packing refers to the arrangement of empty spaces within the material. Its importance lies in controlling mechanical properties by minimizing void concentration and size, ensuring enhanced strength and stiffness. Efficient void packing contributes to a higher material density, crucial for lightweight applications. When amount of slag is very less, maximum of particles act as grain nucleation site and irregular grains have been formed with inherent porosities. On the other hand, when amount of slag has been increased, the slag particles have been dispersed uniformly in the grain boundary and inside the grains which pack the porosity generated while solidification [159].

The SEM micrographs shown in Figure 4.3 indicates a clean matrix reinforcement interface with nominal agglomeration of slag particles in the matrix. The inclusion of slag has been evidenced by energy dispersive spectrometer analysis. The amount of Si, Fe and Ca has increased with increasing slag percentage has been observed in Figure 4.4, which indicates successful inclusion of cupola slag particle in cast composites. The scanning electron microscopy along with elemental mapping indicates the presence of cupola slag in the grain boundary along with inside the grains which evidenced the two reasons of grain refinement such as by acting as nucleation sites and by prohibiting the grain growth to form new grains [37,146].

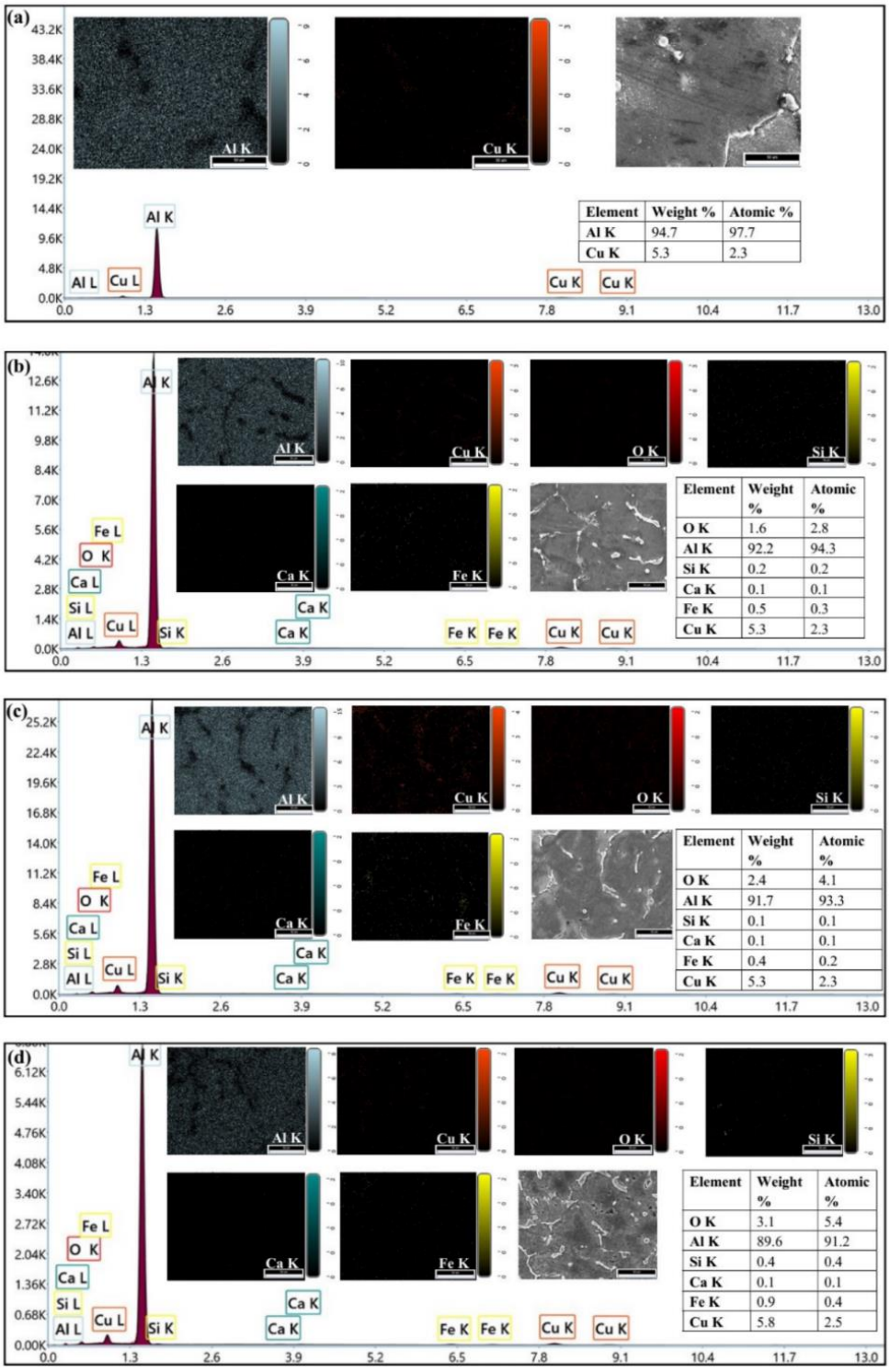

Figure 4.4 Energy dispersive spectroscopy analysis along with elemental mapping for (a) LM11, (b) LM11/3wt.%CS (c) LM11/5wt.%CS and (d) LM11/7wt.%CS

4.2.Improvements of density and porosity

The bar chart comparing theoretical density, experimental density and porosity percentage of base LM11 along with cast composites has been presented in Figure 4.5.

Inclusion of cupola slag reduced the density and percentage porosity and minimum density with much lower porosity have been observed for the case of LM11/7wt.%CS composites as depicted from Figure 4.5. It is noteworthy that the theoretical density remained more or less similar for all the cast samples. Previous works with waste reinforced AMCs reported similar decrease of density and porosity [160,161].

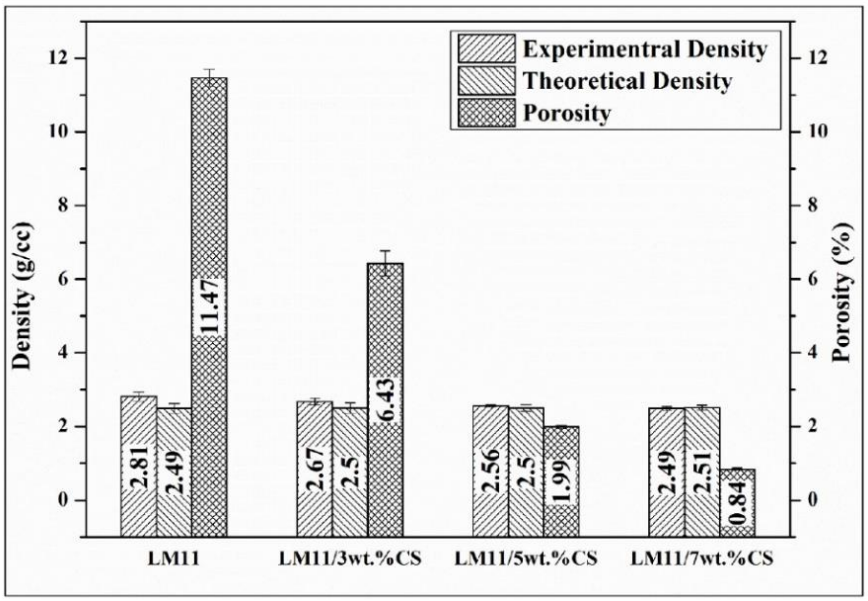

Figure 4.5 Bar diagram of density and porosity for all the cast samples

The experimental density has been observed to be reduced with increasing cupola slag percentage according to Figure 4.5. Density of cupola slag is lower than the density of base metal, thus while mixing by fabrication of composites the density of cast composites has been reduced. The porosity percentage has also been observed to be reduced with increasing cupola slag content, which is in accordance with the optical micrograph presented in Figure 4.1. The reduction in porosity may be due to increased cupola slag content, which fills the gaps between grains. The comparative analysis of reduction of density and porosity show that composites with slag contents have lower density and porosity percentage which results in higher strength to weight ratio and higher hardness. Moreover, 7 wt.% of cupola slag inclusion has the highest reduction of density and porosity percentage as 11.39% and 92.67% respectively. This suggests that with low density cast composites with 7 wt.% cupola slag inclusion has better strength at low weight and lower porosity yields higher hardness. Incorporating low density hard ceramic like particulate reinforcement results in reduction of density and porosity [162,163].

4.3.Hardness enhancement

The results of microhardness test by varying weight percentage of cupola slag has been presented in Figure 4.6. The increasing cupola slag reinforcement weight percentage increased the microhardness. It shows that base material has the lowest hardness of 72 Hv whereas it increases with increasing cupola slag percentage. The 7 wt.% cupola slag reinforced composites observed to have the maximum hardness of 93.43 Hv. Inclusion of secondary phase resulting improved hardness has also been observed in other waste reinforced composites [157,164].

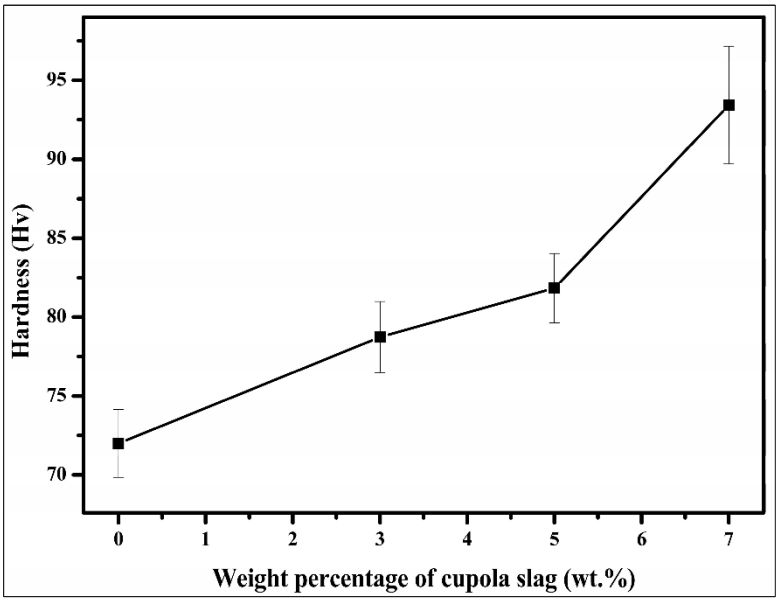

Figure 4.6 Variation of microhardness with respect to slag content

It has been observed from Figure 4.6 that with increasing cupola slag percentage, micro-hardness value in terms of Vickers hardness number increases. The percentage enhancements for 3, 5 and 7 wt.% cupola slag reinforced composite when compared with base LM11 alloy are 9.35%, 13.65% and 29.76%, respectively. The observation indicates continuous improvement of hardness with increasing cupola slag content in aluminium composites. There are two major reasons for this improved hardness, firstly, with increased slag percentage, the grain size has been reduced, as discussed in section 4.2. Hence, according to Hall patch equation, the hardness is increased with decreasing grain size [165]. Secondly, the closely placed grain boundaries and slag contents resist the movement of dislocation inside the matrix after indentation which resulted in increased resistance to indentation. Moreover, cupola slag is a mixture of various hard abrasive ceramics like silicon, alumina etc. and appears to be hard and stony which increases the hardness of the cast composites by bearing the load of indentation. It is

clearly observed that 7 wt.% cupola slag reinforced composites have the highest hardness of 93.43 Hv which is 1.29 times higher in comparison with respect to base LM11 alloy. This enhancement of hardness makes this novel material applicable in applications which require higher hardness to withstand a larger amount of wear and tear such as clutch plate, bearing ring in automobile and aerospace industries. The improvements in hardness of base materials by incorporating particulate reinforcements have been in line with the previous works of various academicians [30,166].

4.4.Tensile property enhancement

The load versus elongation curve obtained by tensile test of base alloy along with composites shown in Figure 4.7 which depicts the loading behaviour along with the breaking loads for different cast composites. The stress-strain diagram presented in Figure 4.8 (a – d) indicates the tensile behaviour of cast composites along with the samples after tensile with ultimate tensile stress and yield stress marked. The tensile test results such as breaking load, ultimate tensile stress, yield stress, % elongation, specific strength and braking strain have been reported in Table 4.1. It is evident from the tensile test results that with increasing slag percentage the tensile behaviour of cast composites improves.

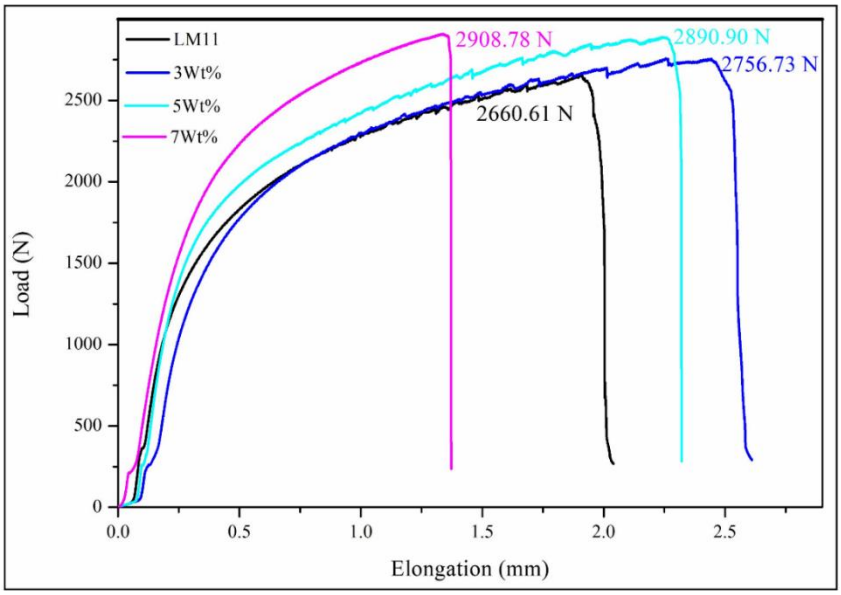

Figure 4.7 Load versus elongation curve of cast composites

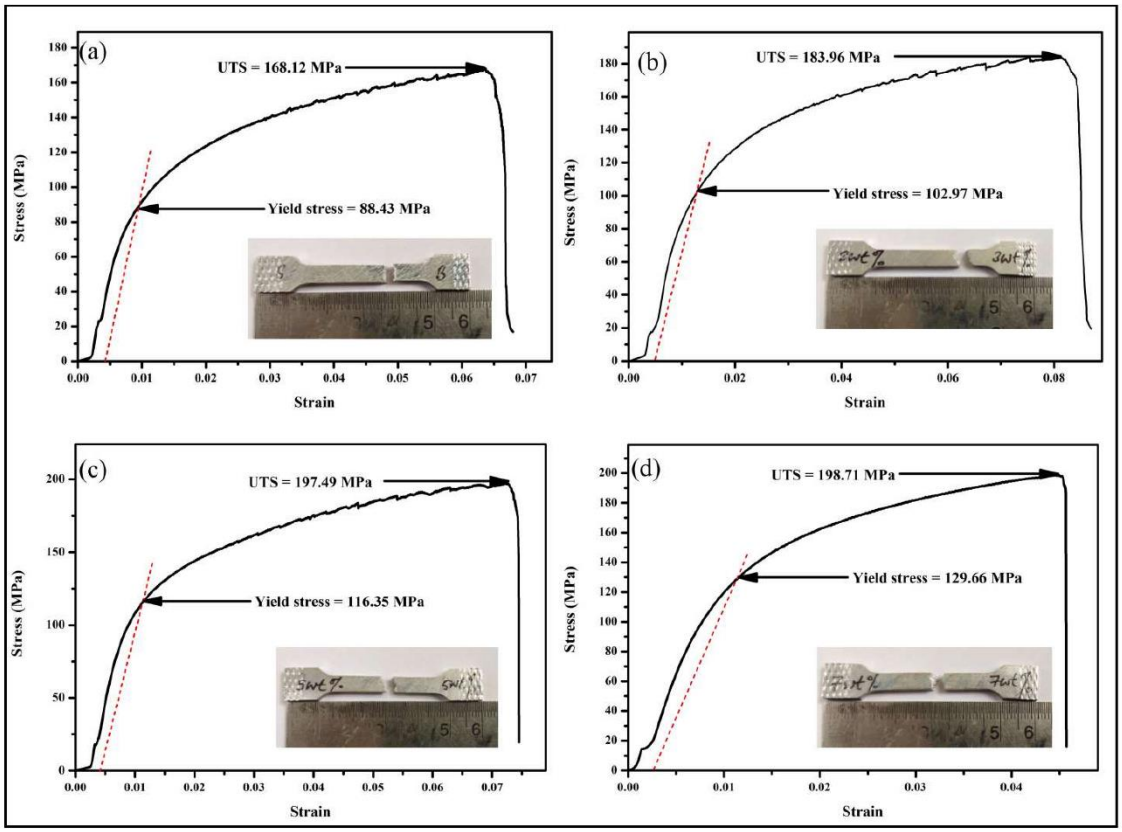

Figure 4.8 Stress-strain plots of (a) LM11, (b) LM11/3wt.%CS (c) LM11/5wt.%CS and (d) LM11/7wt.%CS

Table 4.1 Tensile test results

Weight %	Breaking Load (N)	Ultimate Tensile Stress (MPa)	Yield Stress (MPa)	Specific Strength (kN-m/kg)	Breaking Strain	% Elongation
0	2660.61	168.12	88.43	59.77	0.063	6.338
3	2756.73	183.96	102.97	68.81	0.081	8.141
5	2890.90	197.49	116.35	77.14	0.072	7.202
7	2908.78	198.71	129.66	79.63	0.045	4.465

The tensile test results show that with increasing slag percentage the tensile behaviour of cast composites improves. The percentage change in tensile properties shows improvement of all the properties by incorporating cupola slag particle as reinforcement except the percentage elongation for 7 wt.% slag incorporated composites as reported in Table 4.2. It has been observed to be reduced by 29.55% (denoted by negative sign) due to increased brittleness of composites with higher amount of cupola slag. The breaking load is the maximum tensile load that can a material withstand. The LM11/7wt.%CS composites observed withstand 9.33% more load when compared with base LM11. All other cast composites possess higher breaking load when compared with base alloy. The enhanced breaking load is attributed

to distribution of load to the hard ceramic reinforcement from the matrix. Moreover, hindrance in movement of dislocation due to refined grains results in higher load capacity [167]. This increased breaking load made the cast composites usable in higher strength applications. The breaking load improves with increasing weight percentage of cupola slag.

Table 4.2 Percentage change in tensile properties with respect to base alloy

Composite	Percentage change in				
	Breaking Load	Ultimate Tensile Stress	Yield Stress	Specific Strength	% Elongation
LM11/3wt.%CS	3.61	9.42	16.44	15.12	22.15
LM11/5wt.%CS	8.66	17.47	31.57	29.06	13.63
LM11/7wt.%CS	9.33	18.20	46.62	33.23	-29.55

Table 4.2 depicts that the ultimate tensile stress increases by 9.42, 17.47 and 18.20% by compositing with 3, 5 and 7 wt.% cupola slag reinforcements respectively. Yield stress has been found to be improved with incorporation of slag particle into LM11 matrix. The percentage increases as 16.44, 31.57 and 46.62% increase by introducing cupola slag of 3, 5 and 7 wt.% respectively. The increase in ultimate tensile stress and yield stress is attributed to various factors such as, the incorporation of slag particle enhances the refinement of grains which results in higher strength. The strengthening of material due to smaller grains has been achieved through Hall-Petch strengthening [168]. Moreover, presence of discontinuous phases of hard cupola slag particles in the matrix hinders the movement of dislocation while tensile loading which results in prevention of crack propagation hence, higher strength has been reached. The strength has been increasing with increasing slag percentage as with increasing slag amount of more refined grains with a greater number of nucleation sites has been formed which can be evidenced by Figure 4.1. The percentage in elongation increases by addition of 3 wt.% cupola slag when compared with base LM11 alloy. The elongation then reduced with increased slag amount. The variations in percentage elongation as reported in Table 4.2 from base LM11 alloy are 22.15% and 13.63% increase for 3 wt.% and 5 wt.% slag reinforced composites while 29.33% reduction in case of 7 wt.% cupola slag addition. The increase in elongation percentage due to incorporation of 3 wt.% and 5 wt.% cupola slag as reinforcement to monolithic LM11 matrix is the result of three major phenomenon those are, refined grains of composite, increased strain hardening rate and crack inhabiting nature of cupola slag particles [169]. The cupola slag particles provide

new nucleation sites which refines the grain resulting in higher capacity to withstand deformation. Along with it the reinforced cupola slag particles restrict the movement of dislocation and creates a stress field around itself which pile up other dislocations resulting in higher elongation percentage. The cracks generated while tensile loading also get trapped by the hard cupola slag particles which enhances the elongation percentage. It has been also notable that with increasing wt.% of cupola slag the elongation has been reduced, this may be attributed to the fact that with increasing cupola slag particles number of stress concentration sites increases which results in premature failure of the material. Moreover, higher amount of hard ceramic reinforcement like cupola slag increases the stiffness of composites which make it more brittle [170].

The percentage increase in specific strength when compared with base LM11 has been observed to be 15.12%, 29.06% and 33.23% for 3 wt.%, 5 wt.% and 7 wt.% cupola slag reinforced composite, respectively. The comparative bar diagram for specific strength indicating progressive increment has been presented in Figure 4.9. The enhancement of specific strength is the result of lower density and higher strength of cupola slag reinforced composites as discussed earlier. The increasing amount of cupola slag increases the strength due to grain refinement, strain hardening and crack inhibition and low density of cupola slag reduces the density, hence the specific strength increases and highest specific strength has been observed for LM11/7wt.%CS composites. The higher specific strength of composites made it suitable for light weight high strength application in aerospace and transportation industries.

Cupola slag reinforced AMCs show enhanced tensile properties with improved efficiency and ductility than conventional ceramic reinforcements. This work inferred that incorporation of 7wt.% CS outperformed the conventional reinforcements by 18.2% with a reinforcement efficiency of 4.4 MPa per wt.%. SiC composites achieve an UTS of 365 – 430 MPa but require 15 – 25 wt.% reinforcement, while WC and B_4C systems shows lower tensile strengths [29,147,171]. The increase in yield strength also shows a typical 15 – 24% higher than conventional TiC system [169]. The ductility and specific strength also improved highlighting cupola slags potential for lightweight, high performing sustainable composite applications.

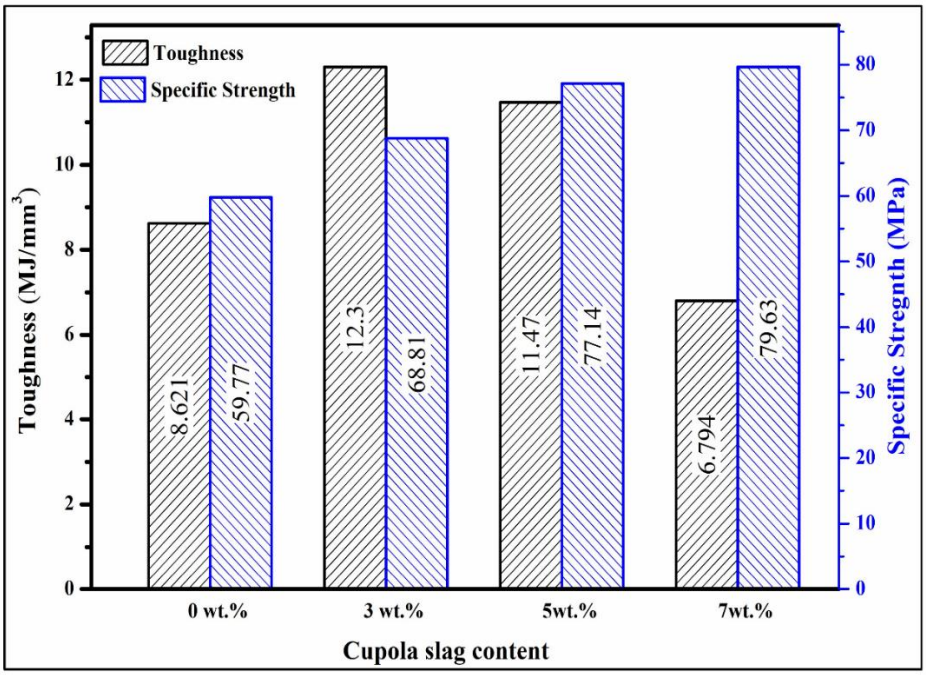

Figure 4.9 Comparison of specific strength and toughness

Another important property that can be inferred from tensile test, more precisely from stress strain curve is toughness of the material. The toughness can be calculated using area under the curve until fracture of stress strain curve using Origin 8 software. Incorporation of cupola slag enhances the toughness of base material by 42.67% for LM11/3wt.%CS composites which reduced by further addition of cupola slag into the matrix as reported in Table 4.3. The comparative bar diagram for toughness indicates increase of toughness which reduced by addition of higher weight percent of cupola slag as depicted in Figure 4.9. The increase in toughness by 3 wt.% cupola slag addition is the result of refined grain and hindered dislocation movement which reduced as with increasing cupola slag percentage the brittleness of the material increases due to more stress concentration sites. The toughness also increases by cupola slag particles which are mainly hard ceramic by crack deflection and crack bridging [172]. Slag particulates can bridge a crack and prohibit its propagation due to higher strength as compared to the matrix and enhances the toughness. Along with it, the hard cupola slag particles resist the crack tip deflecting its straight-line propagation and requires more energy for failure. The toughness begins to decline as weight percentage of cupola slag rises as the slag particle starts to interfere with each other which make it difficult to deform plastically and absorb energy. Moreover, reinforcements serve as stress concentrators which spread the cracks to facilitate brittle fracture like ceramics.

Table 4.3 Toughness values along with percentage change

Composites	Toughness (MJ/m^3)	Percentage Change (%)
LM11	8.621	-
LM11/3wt.%CS	12.300	42.67
LM11/5wt.%CS	11.470	33.05
LM11/7wt.%CS	6.794	-21.19

The tensile test samples after fracture have been prepared metallographically and fractographic analysis has been performed for detailed introspection of fracture mechanisms. Figure 4.10 (a – d) presented fractographic images in lower magnification. The mountain and valley feature with higher depth of dimples which indicate ductile failure of LM11 alloy in Figure 4.10 (a). However, presences of aluminium copper intermetallic in the alloy lead to formation of some tear ridges which indicate the failure to be brittle. Hence, it can be stated that the failure mechanism follows majorly ductile mode with nominal brittle fracture. Mixed mode of fracture with dimples, cleavages and tear ridges has been observed for cast composites as depicted from Figure 4.10 (b – d). Moreover, with increasing weight percentage of cupola slag from 3 wt.% to 7 wt.% of amount brittle fracture increases as per Figure 4.10 (b – d). Figure 4.10 also show that the depth and number of dimples decrease with increasing cupola slag. The tear ridges along with flat facet have been observed to be increased with increasing slag content. This fractographic analysis evidenced the ultimate tensile stress and elongation trends identified from tensile test.

Introspection of micro void coalescence along hindrance in crack propagation has been clearly visible from higher magnification fractography presented in Figure 4.11 (a – d). Micro void coalescence along with intra-granular and trans-granular crack propagation without any hindrance as shown in Figure 4.11 (a) indicates lower strength of base alloy when compared with slag reinforced composites. The propagating cracks has been resisted by reinforcement particles, clearly visible in Figure 4.11 (b – d), these raised the stress required for plastic deformation. Figure 4.11 (b – d) also indicates the amount of flat facet and tear ridges increases with increasing slag percentage. This confirms reduction of elongation and toughness with increasing slag content. The fractography for LM11/7wt.%CS composites shown in Figure 4.11 (d) depicts higher amount of crack resistance and cleavages which indicates increase in strength by resistance to dislocation movement but the induced brittleness decreases the elongation and toughness [173,174].

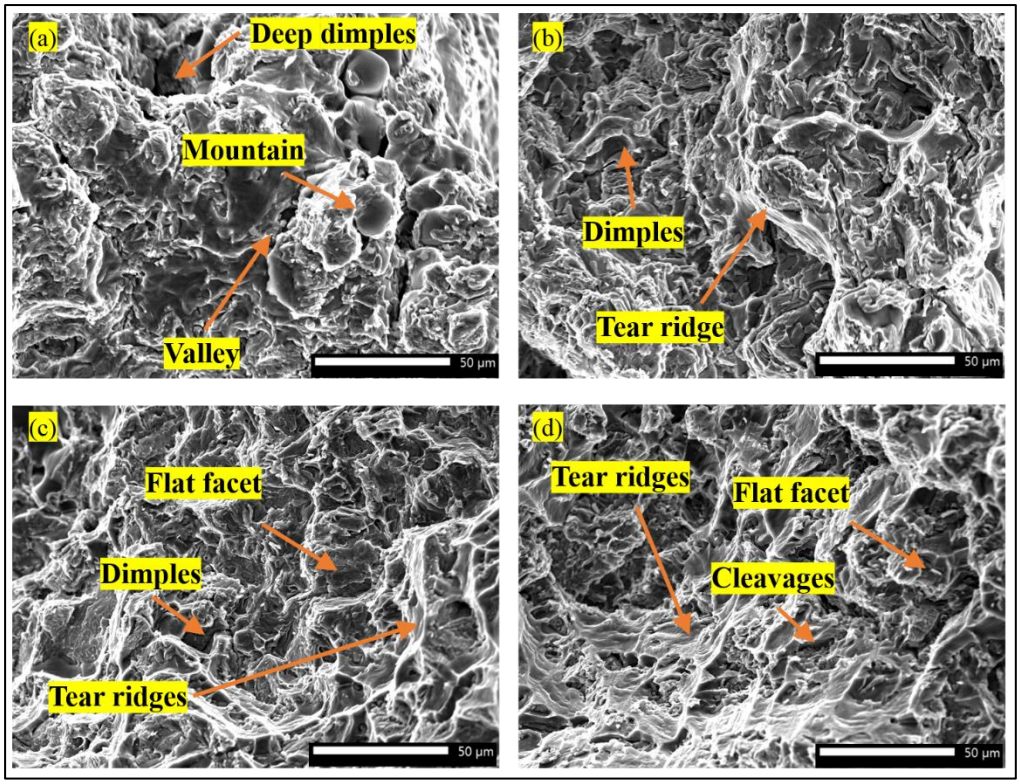

Figure 4.10 SEM fractography for (a) LM11, (b) LM11/3wt.%CS (c) LM11/5wt.%CS and (d) LM11/7wt.%CS

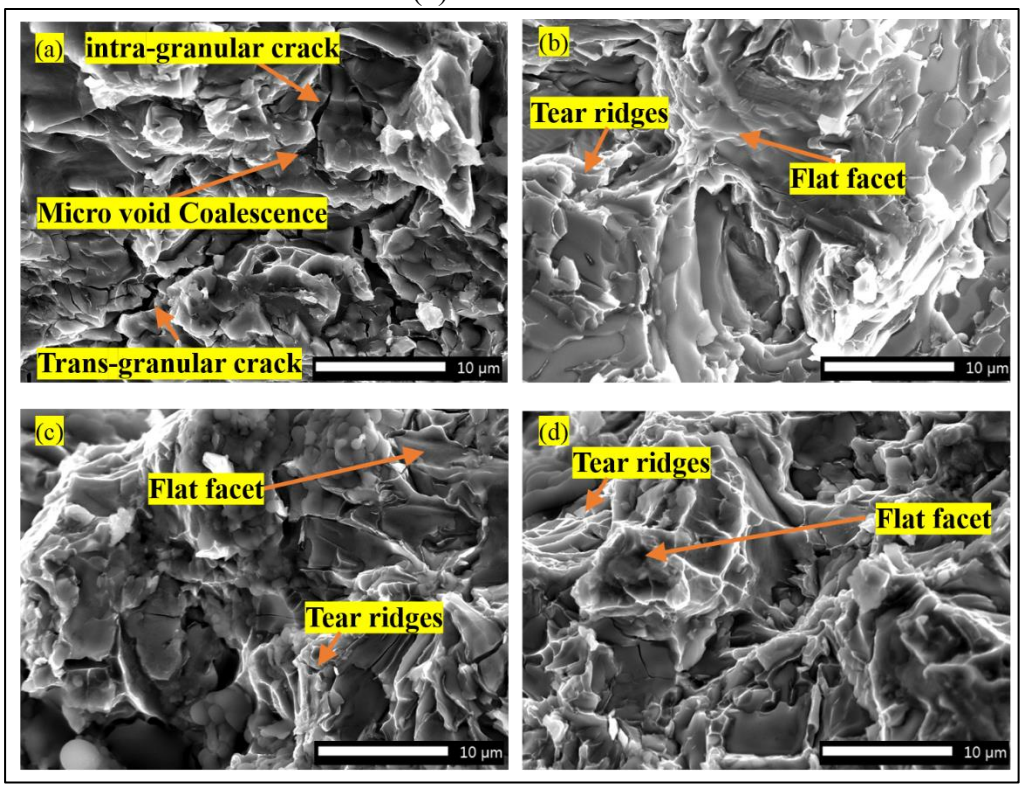

Figure 4.11 Higher magnification (2000×) SEM fractography for (a) LM11, (b) LM11/3wt.%CS (c) LM11/5wt.%CS and (d) LM11/7wt.%CS

4.5.Summary

This work investigates the influence of weight percentage of industrial waste cupola slag particle reinforcement on enhancement of properties of Base LM11 matrix composites, the introspection indicates that,

- The fabricated specimens are defect free and sound up to 7 wt.% slag inclusion, beyond which deterioration occurs due to reduced wettability.
- Microstructural analysis reveals grain refinement and new nucleation sites with cupola slag incorporation in the LM11 matrix, indicating improved material properties.
- Density and porosity of the composites are reduced, while hardness increases with higher slag content, making the material lightweight, stiffer, and harder.
- The material's enhanced properties make it suitable for applications requiring higher wear resistance.
    - Tensile properties, including breaking load, ultimate tensile stress, and yield stress, improve with increasing slag content. The highest tensile property values are observed in composites with 7 wt.% cupola slag reinforcement: Breaking load increased by 9.33%; Ultimate tensile stress increased by 18.20%. Yield stress increased by 46.62% compared to the base alloy.
- Fractography analysis indicates a mixed mode of failure, with increased brittleness at higher slag content.
- Fractography also evidences enhanced tensile properties due to crack propagation hindrance and dislocation movement prohibition.
- Improved specific strength results in a higher strength-to-weight ratio, making these composites suitable for lightweight applications.

Chapter 5

Machinability Analysis of Novel Cupola Slag Reinforced Composites

Composites fabricated using a low cost easy to operate stir casting method generates a near net shape design. However, machining is an essential process to achieve a high quality precise final product with the desired dimension and surface finish. AMCs contain hard and abrasive reinforcements, which hinder the machining process reducing tool life and machining efficiency. Thus, an investigation of the machinability of AMCs can help optimize the process of machining to improve the integrity of machined parts. Machining operations that involve turning are highly significant due to their ability to generate a diverse range of desired surfaces. Hence, the machinability of a novel material should be studied in terms of turning. The machinability can be assessed as per the machining indices which include surface roughness, MRR, chip analysis, tool wear, power consumption and cutting force. The process inputs of the machinability analysis can be cutting process inputs such as depth of cut, feed and speed along with cutting tool and workpiece materials, use of cutting fluid. A thorough investigation into machinability must involve a detailed analysis of how process parameters affect the outcomes. Investigating the impact of inputs on responses commonly requires the use of a statistical design of experiments, such as a full factorial design.

The machinability has been accessed in terms of various machinability indices. The cutting force, power consumption, tool wear, surface roughness, MRR, chip thickness

has been measured in dry turning. The turning experimentation has been designed using process inputs as weight percentage of cupola slag, feed and spindle speed. The details of experimentation in turning have been presented in Section 2.6 of Chapter 2. The term better machinability is used for turning that yield low cutting force, power requirement, tool wear and surface roughness with higher MRR, chip thickness. In this work first the machinability indices have been measured some in-situ while others after the turning. The chips have been collected after every run and a detailed chip analysis has been presented. The effect of weight percentage of cupola slag on machinability has been compared and discussed. A note should be taken that the outputs have been measured several times while experimentation and the average has been tabulated.

5.1.Machinability results

The experimental investigation of machinability of novel slag reinforced composites requires a detailed experimental design. This work adopts a full factorial experimental design with three input factors as discussed in section 2.6.2. The full factorial design is very effective as it allows introspection of multi factor influence along with their interactions. A full factorial design estimates all main effect plots and is said to be orthogonal as the influence of every factor can be isolated and quantified independently. Although, it requires more numbers of experiments, this gives the fullest insight about the experimental system. The full factorial design matrix used in this work has been presented in Table 2.7. The process input ranges have been taken from Table 2.6. A total of 36 experiments has been conducted according to experimental design. Each run of experiments has been conducted using new tool inserts to depict tool wear post operation. The variations in machinability results could not establish conclusive trends, may be due to limited levels and narrow process input range. Along with it. the robust turning operation in conventional lathe and measuring systems has some limitations which leads to these results. However, the purpose of this work is to gain better understanding of comparative behaviour of slag composites with varying wt.% which could be well established by the machinability results.

Experimental output as per the Table 2.7 design matrix has been presented in Table 5.1. It is evident from Table 5.1 that the experiments with base alloy have the lowest machinability. The machining has been observed to be easy with a larger amount of CS content in LM11/CS composites. The results table also indicates that by CS addition the cutting force, power consumption and tool wear has been reduced. Maximum reduction

has been observed in case of LM11/7wt.%CS composites. Detailed discussions on responses and their dependency upon process input have been discussed in subsequent paragraphs.

Table 5.1 Machinability results

Exp. No.	Cutting Force (N)	Power Consumed (kW)	Tool Wear (µm)	Surface roughness (µm)	MRR (g/min)	Chip thickness (mm)
1	14.347	13.9	415.825	3.713	7.50	0.110
2	24.048	14.1	52.091	6.833	7.50	0.137
3	29.482	14.3	304.668	4.727	11.25	0.127
4	9.619	14.6	29.580	1.353	11.25	0.127
5	28.135	14.2	327.351	4.510	9.23	0.220
6	31.566	14.3	236.824	4.633	9.23	0.223
7	29.891	14.5	447.793	5.750	13.85	0.230
8	9.629	13.9	339.714	3.033	9.23	0.227
9	31.219	13.8	89.542	6.537	15.00	0.280
10	33.117	15.5	131.103	7.953	10.00	0.293
11	34.410	15.3	436.374	5.400	10.00	0.277
12	16.564	15.1	42.053	2.923	15.00	0.270
13	27.071	15.2	47.828	3.670	9.23	0.160
14	29.972	16.2	52.711	5.640	13.85	0.157
15	29.761	15.9	53.137	4.880	9.23	0.150
16	12.823	15.6	70.854	1.397	4.62	0.140
17	62.320	15.7	102.826	3.807	10.91	0.227
18	43.771	15.2	82.481	5.990	11.54	0.230
19	42.156	15.8	544.478	4.023	11.54	0.230
20	14.202	14.9	294.707	1.423	11.54	0.200
21	63.464	14.6	529.460	7.363	13.33	0.290
22	52.971	16.5	128.986	8.660	13.33	0.287
23	63.730	16.7	61.013	5.437	13.33	0.283
24	25.778	16.6	399.099	1.783	13.33	0.237
25	29.612	15.9	303.581	7.557	17.31	0.190
26	35.625	17.2	64.167	6.643	12.00	0.173
27	28.959	16.1	286.848	6.613	12.00	0.173
28	18.147	16.8	293.546	1.004	12.00	0.120
29	41.785	15.3	99.992	4.593	15.00	0.607
30	51.926	16.4	46.389	6.820	15.00	0.543
31	73.883	16.3	98.888	6.750	15.00	0.523
32	16.379	17.2	312.162	1.220	22.50	0.257
33	66.037	16.2	53.811	6.183	17.14	0.563
34	62.760	16.5	64.414	6.503	8.57	0.453
35	73.729	16.8	60.800	6.620	17.14	0.497
36	20.871	15.2	281.352	1.917	8.57	0.310

5.1.1. Analysis on cutting force

Cutting force is significant parameters for energy aspects of machinability. The cutting force should be as small as possible for better machinability. The cutting force main effect plots have been used to introspect the effects of process inputs on force requirements. The main effect plots for cutting force have been presented in Figure 5.1 indicating cutting force increases with increasing spindle speed and feed rate. This happens because with increasing cutting speed and feed rate, the contact length in workpiece-tool interface increases inducing more friction and thus, more force would be required to overcome it [175]. The cutting force reduces at higher speed because of localized thermal softening due to heat generated by friction. The cutting force was found to be reduced in the base alloy but increased with the inclusion of 5wt.% CS, which then decreased significantly with the inclusion of 7wt.% CS. This reduction of cutting force is due to more amount of slag inclusion. Higher amount of abrasive CS particles with sharp edges and small protrusions while turning these CS particles deboned from the matrix and accumulate in tool-workpiece interface resulting micro cutting of the samples. This micro cutting reduces the force requirements and eases the machining process [176]. Figure 5.2 shows bar diagram of cutting force versus spindle speed for different weight percentage and feed. Figure 5.2 depicts that the cutting force has been increased in higher spindle speed for all the feed and weight percentage.

It is noteworthy that the base alloy, 3wt.% and 5wt.% CS reinforced composites turning requires more or less similar cutting force while major drop in cutting force has been observed in turning of 7 wt.% CS reinforced composites for all feed and spindle speed. This is because with increasing CS percentage abrasive SiO_2 content in the matrix increases which breaks while turning and assists the cutting process. Similarly, Figure 5.3 presents the bar diagrams of cutting force versus feed rate for various spindle speed and CS percentage. Figure 5.3 depicts increase of cutting force with increasing feed for all weight percentage and spindle speed similar to the main effect plots. The increased feed rate increases the contact length between cutting tool and workpiece which in turn increases the cutting force. Figure 5.3 also shows major drop of cutting force while machining of LM11/7wt.% CS composites. These results indicate improvement of machinability in terms of cutting force by 7wt.% CS reinforcement when compared with base LM11 alloy.

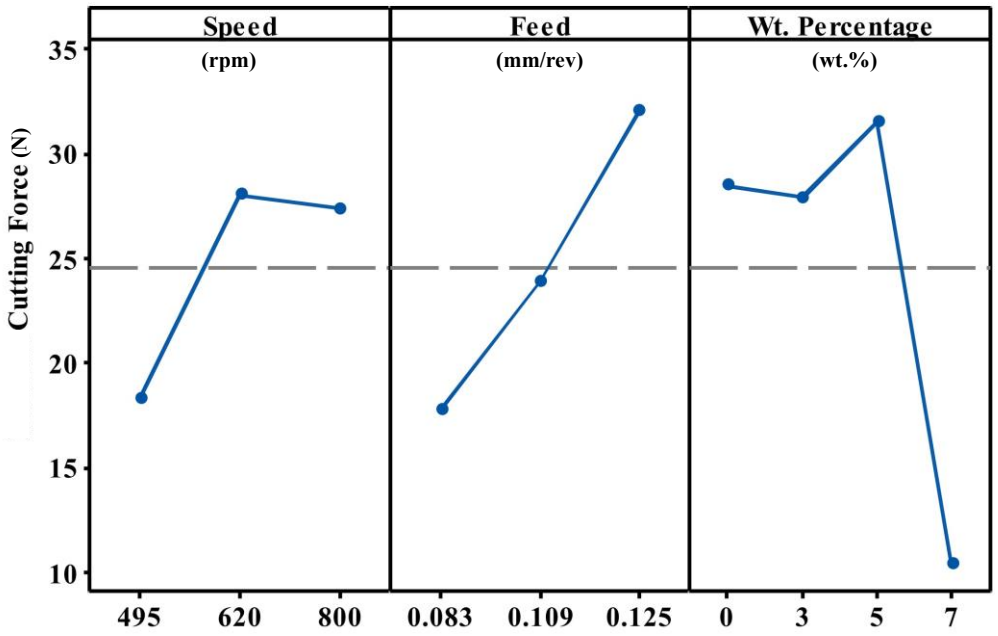

Figure 5.1 Main effect plots for cutting force

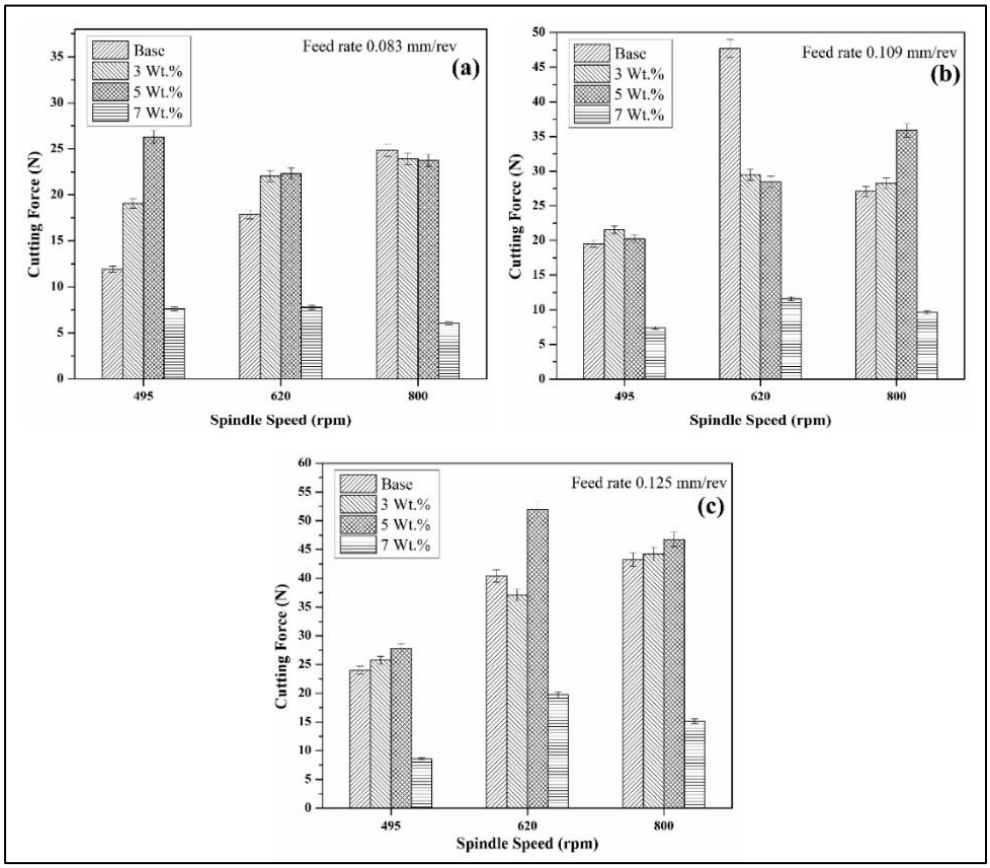

Figure 5.2 Cutting force versus spindle speed plots for feed rate (a) 0.083 mm/rev, (b) 0.109 mm/rev, (c) 0.125 mm/rev

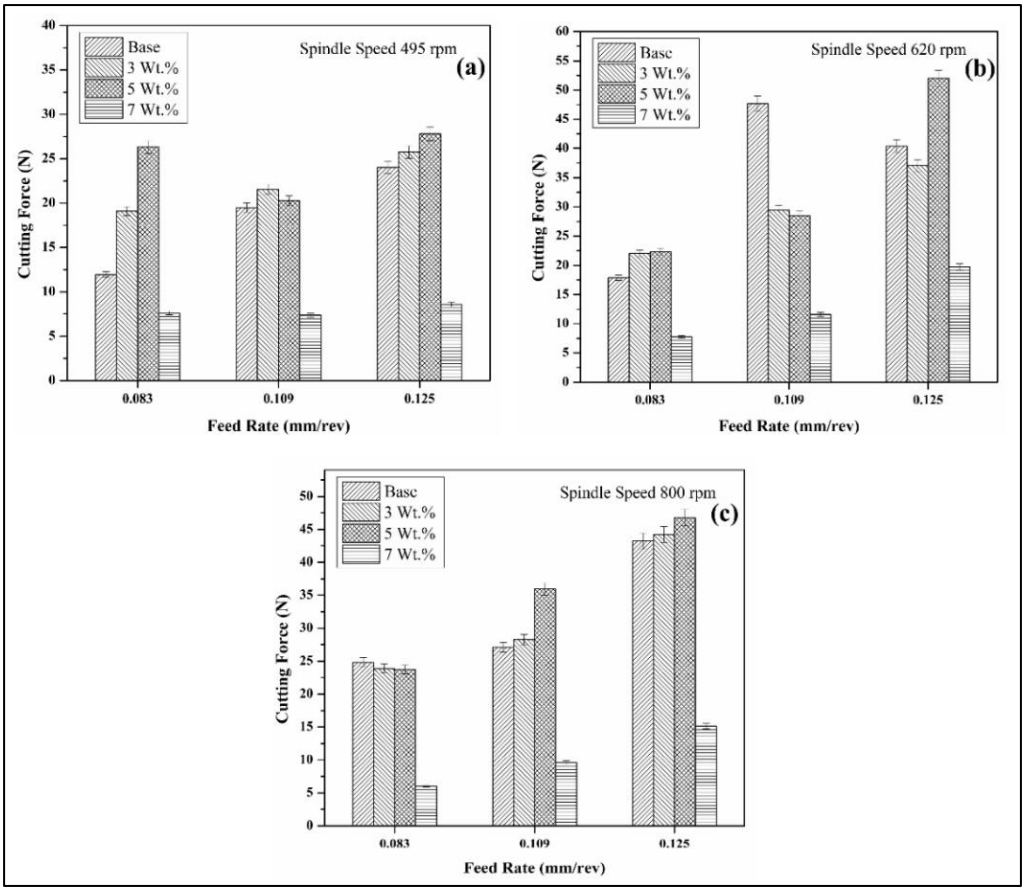

Figure 5.3 Cutting force versus feed rate plots for spindle speed(a) 495 rpm, (b) 620 rpm, (c) 800 rpm

5.1.2. Analysis on power consumption

Improved machinability has been identified as the machining which consumes lower power. The main effect plots for machining of base LM11 alloy along with CS reinforced cast composites with varying weight percentage have been presented in Figure 5.4. Consumed power has been observed to be increased with increasing feed and speed as observed in Figure 5.4 as force requirement for machining increases at higher feed and spindle speed which requires more power [177]. The power consumed was found to be lowest in base alloy which increases with 3 wt.% CS inclusion and then reduces with increasing weight percentage of CS. The presence of abrasives in CS composites hinders the machining process and thus requires more power. The power requirement reduces with increasing slag percentage due to the self-lubricating nature of abrasive CS particles which assisted the machining process [178]. The range of power consumed when machining of 7wt.% CS composites is within the range of 0.5 kW when compared with base alloy turning. Figure 5.5 shows the spindle speed versus power consumption plots for different feed and weight percentage of CS. It is observed from the bar graphs presented in Figure 5.5 that the variation of power consumption is very

nominal due to the robustness of conventional engine lathe used in the experimentation. Yet, the power requirement found to be increase with increasing spindle speed for all feed rate and weight percentage. Feed rate versus power consumption graphs have been shown in Figure 5.6 which indicates that with increasing feed rate the power requirement increased. The effect of weight percentage on power consumption has been clearly presented in Figure 5.5 and Figure 5.6 indicates that CS inclusions of 7 wt.% in metal matrix require same or lower power than the base alloy which indicates improvement in machinability.

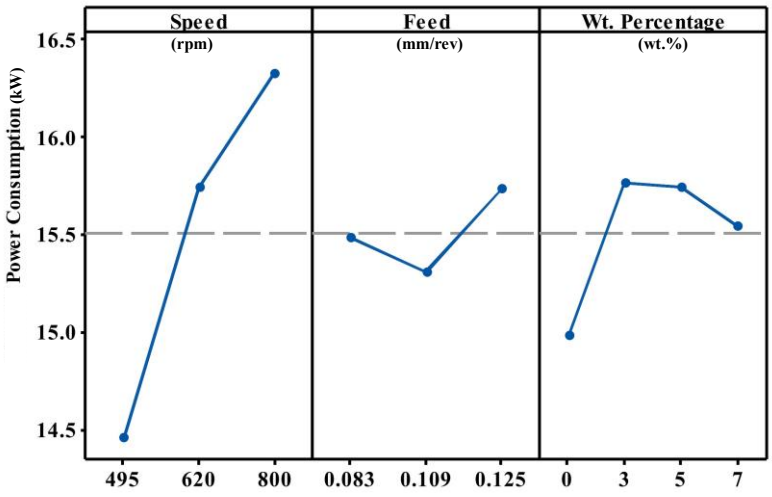

Figure 5.4 Main effect plots for power consumption

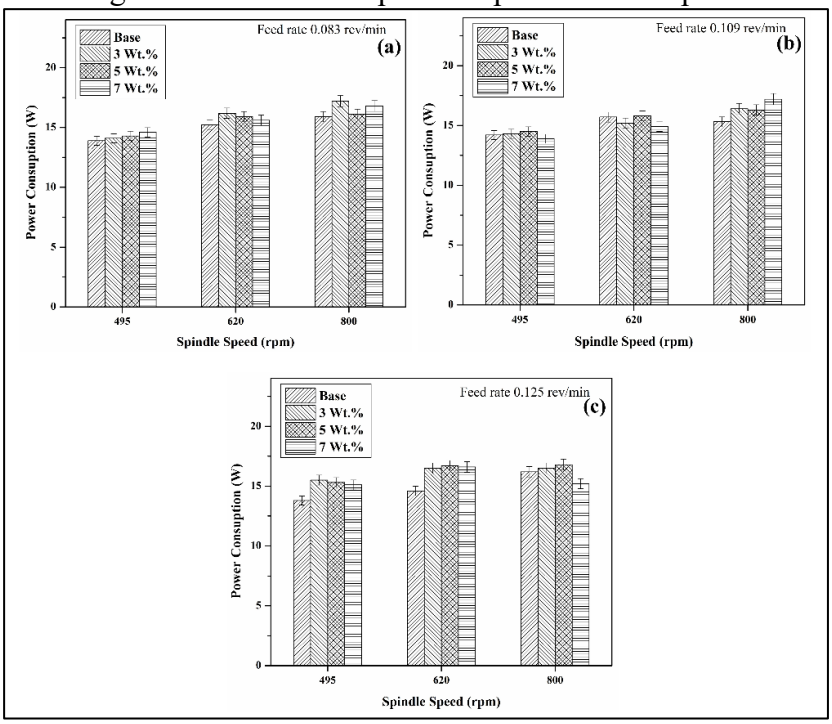

Figure 5.5 Power consumption versus spindle speed plots for feed rate (a) 0.083 mm/rev, (b) 0.109 mm/rev, (c) 0.125 mm/rev

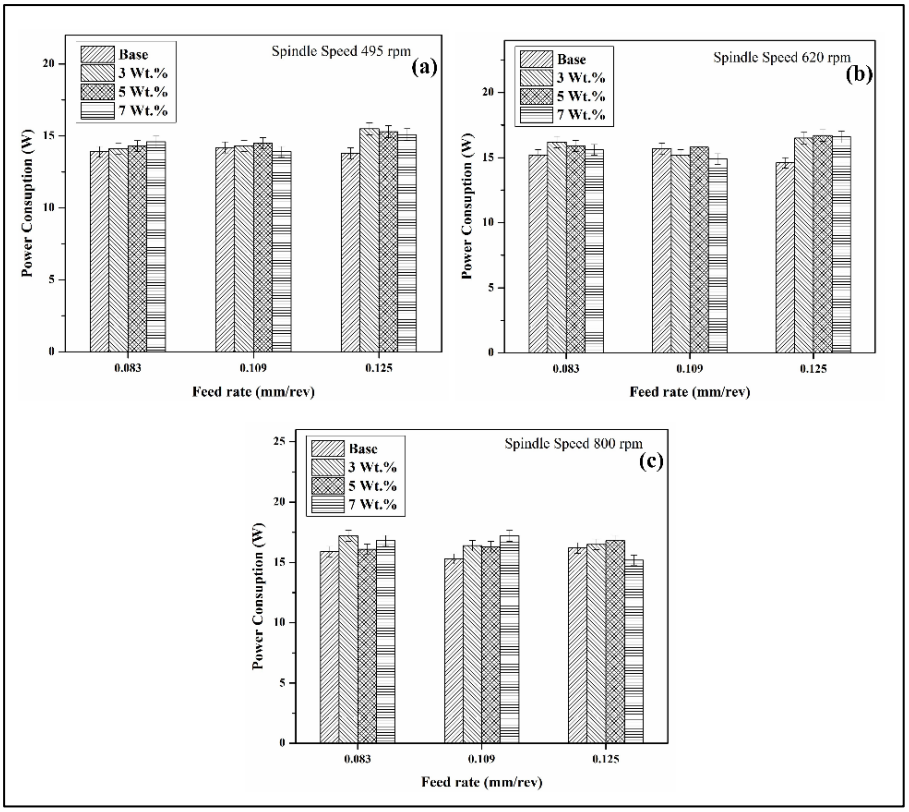

Figure 5.6 Power consumption versus feed rate plots for spindle speed (a) 495 rpm, (b) 620 rpm, (c) 800 rpm

5.1.3. Analysis on tool wear

Tool wear is an important characteristic of machinability as it directly affects the tool life. In this experimental work TiN coated carbide tool has been used. This tool has shown very nominal wear in the observation. Built up edge (BUE) is most prominent wear mechanism that generates wear in the cutting tool in this turning of LM11/CS AMCs. This formation of BUE is attributed to the fact that while machining of LM11/CS AMCs the CS particles hinder the cutting process due to hard abrasive nature of CS particles. This would increase the friction in tool tip and workpiece interface leading to increase in tip temperature. Along with it the abrasive particles get deboned due to turning, these free CS particles got stuck on the cutting edge by localized welding by fictional heating at tool tip. This creates BUE at the cutting edge of the tool [179]. The other tool wear such as flank and crater wear has not been observed due to higher hardness of the cutting tool [180]. Thus, in this experimental work tool wear has been measured as the width of BUE formed. The morphology of flank face and rake face views of cutting tool before and after cutting has been shown in Figure 5.7 (a – f). Figure 5.7 (a – b) depicts that before cutting the flank face and rake face had no wear with clean tool tip and nose radius. Nominal tool wear of 29.580 μm has been measured in case of process input such as spindle speed 495 rpm, feed rate 0.083 mm/ rev and 7

wt.% CS inclusion and has been presented in Figure 5.7 (c – d). Figure 5.7 (e – f) shows morphology of tool for maximum observed tool wear of 544.478 µm for process inputs 620 rpm spindle speed, 0.109 mm/ rev feed and LM11/5wt.%CS composites turning with prominent BUE. The detailed analysis of input influence on tool wear has been presented in terms of main effect plot in Figure 5.8. The tool wear has been observed to be reduced with increasing cutting speed as shown in Figure 5.8, because with increasing speed the time of contact between tool tip and workpiece reduced which leads to reduced temperature rise due to friction thus reducing the tool wear [181]. The impact of feed and weight percentage of CS on tool wear has been found inconsistent as it increases and decreases with increasing feed and wt.% of CS. However, it should be noted from Figure 5.8 that the lowest tool wear has been observed for a feed of 0.083 mm/rev and for LM11/3 wt.%CS composites. The tool wear versus spindle speed plots in terms of bar graph has been shown in Figure 5.9 for all the feed rates and weight percentage of CS. It is evident from Figure 5.9 that with increasing speed tool wear reduces and addition of CS in base material reduces the tool wear in most of the spindle speed and feed inputs. LM11/3wt.%CS composites have been observed to produce nominal tool wear in most of the spindle speed, feed settings. Influence of feed has been observed in detail by the bar graphs of tool wear versus feed rate as shown in Figure 5.10. It is clear from Figure 5.10 that with increasing feed rate the tool wear has been increased for all speed and weight percentage. This attributed to increasing feed rate that increases the contact length between tool and workpiece resulting more friction thus tool wear has increased [182].

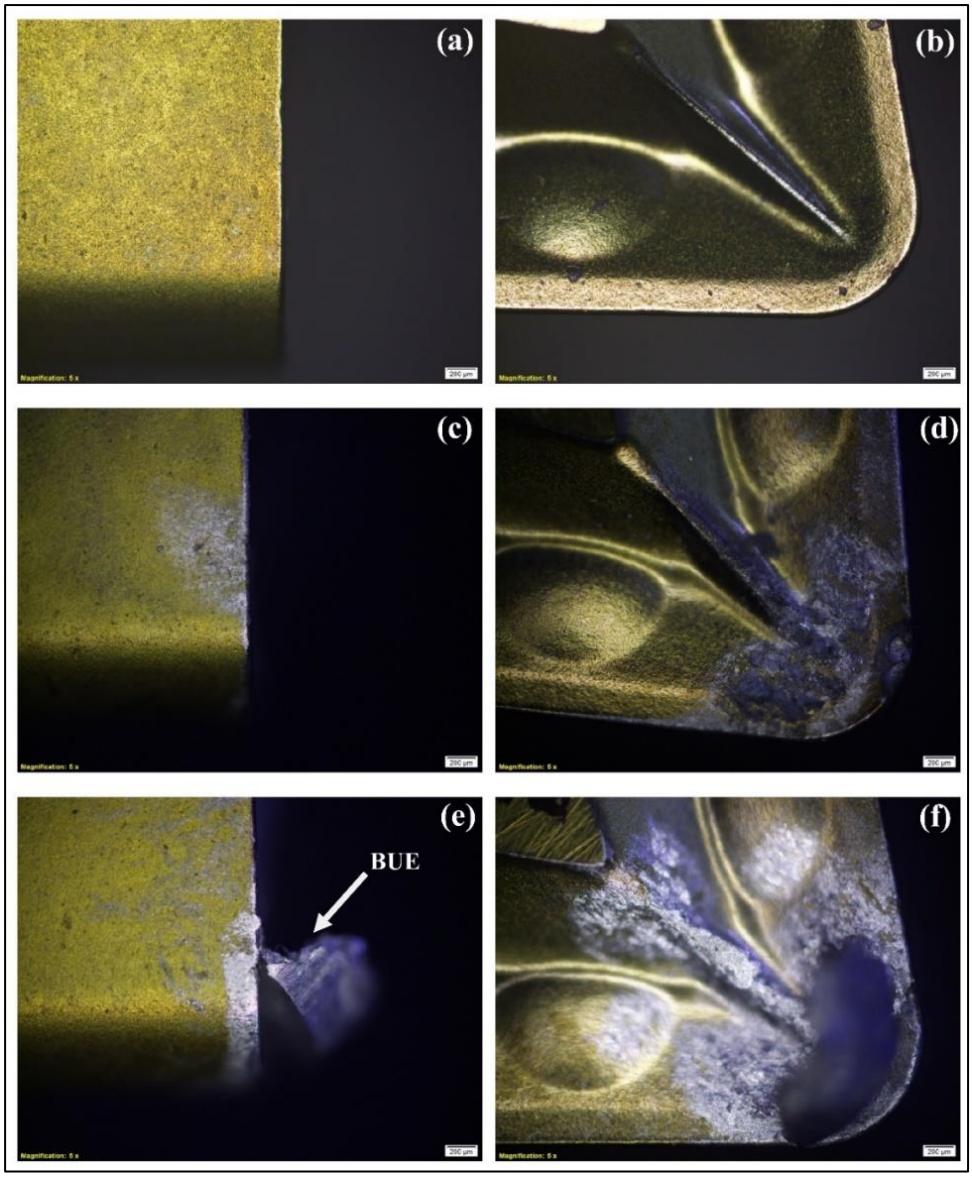

Figure 5.7 Tool wear morphology for cutting tool (a) flank face before cutting, (b) rake face before cutting, (c) minimum tool wear flank face, (d) minimum tool wear rake face, (e) maximum tool wear flank face, (f) maximum tool wear rake face

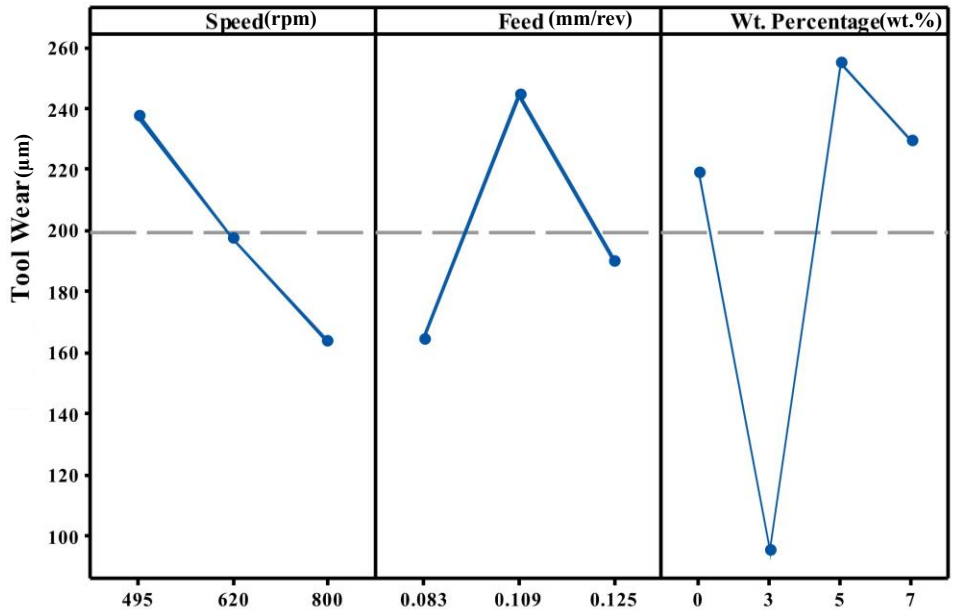

Figure 5.8 Main effect plots for tool wear

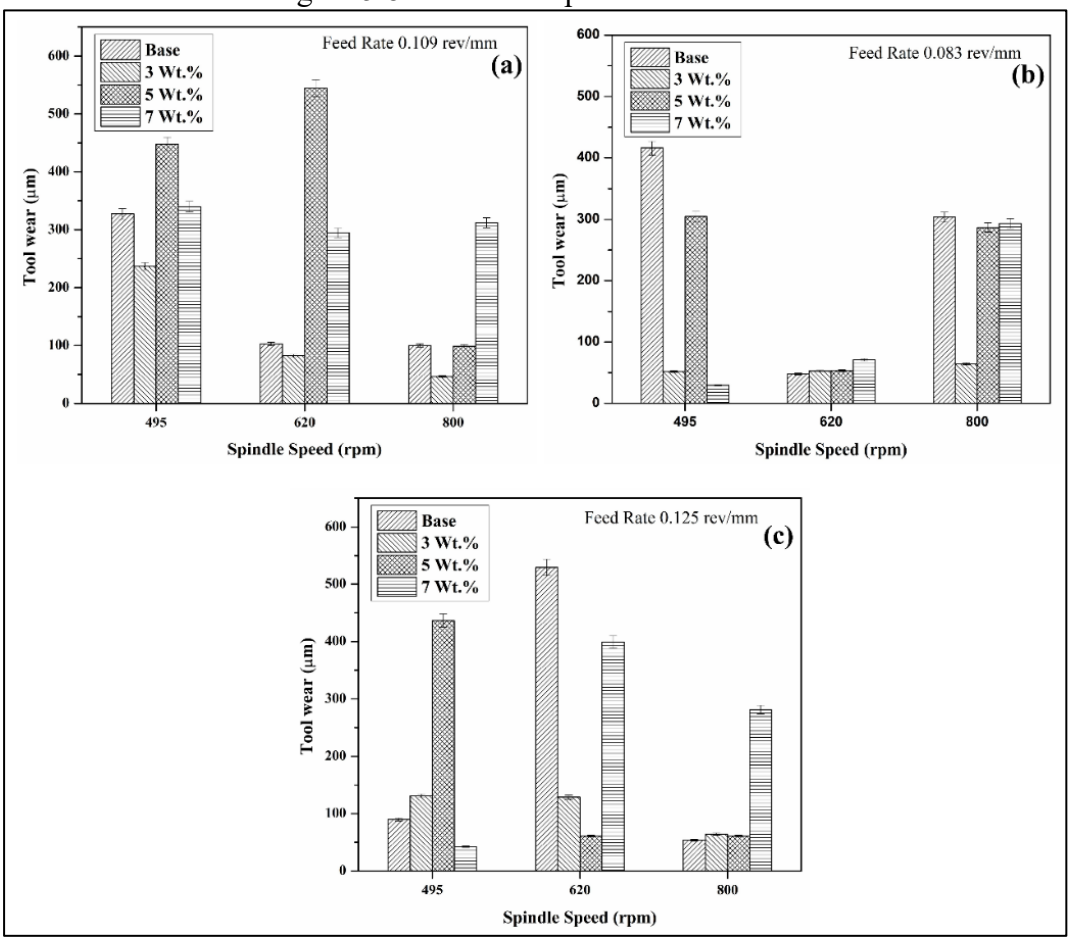

Figure 5.9 Tool wear versus spindle speed plots for feed rate (a) 0.083 mm/rev, (b) 0.109 mm/rev, (c) 0.125 mm/rev

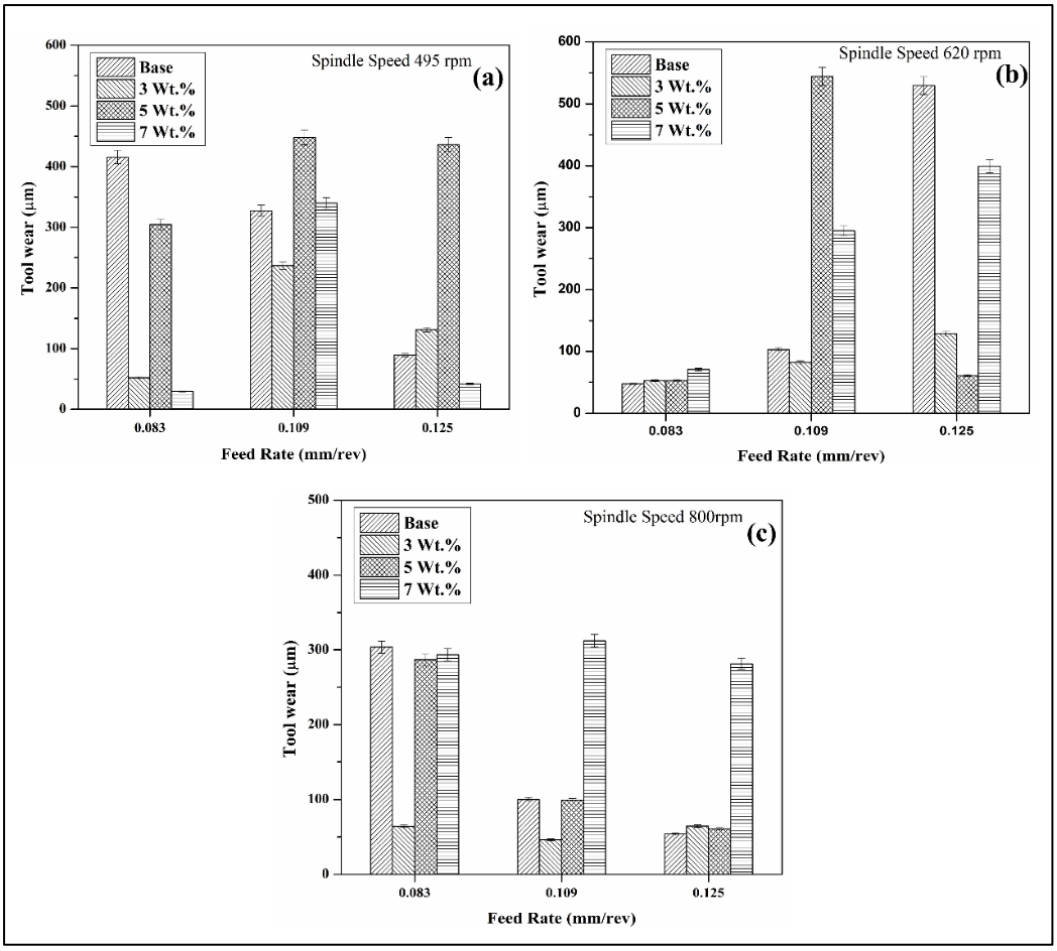

Figure 5.10 Tool wear versus feed rate plots for spindle speed (a) 495 rpm, (b) 620 rpm, (c) 800 rpm

5.1.4. Analysis on surface roughness

Better machinability can be defined by the integrity of the surface generated through the machining. The surface roughness should be nominal which indicates better quality of machined surface. The surface roughness main effect plots have been presented in Figure 5.11. It indicates that surface quality deteriorates at higher feed and spindle speed. This is caused by the fact that at higher feed and spindle speed the force acting while cutting would be increased which leads to higher chatter and vibrations and deteriorates the surface integrity [183]. According to the main effect plots, slag inclusion improves the surface quality. This is because the CS particles have a special shape with sharp edges and small protrusions that act like tiny cutting tools and make the machined surface smoother. Moreover, metallic oxides and sulphide contents of CS act as self-lubricating material while turning which reduces the tool-workpiece interface friction hence the quality of the surface improved. Similar improvement of surface roughness by the addition of reinforcement has been reported by several academicians [56,73,183]. Figure 5.12 (a – c) presents the feed rate versus surface roughness plots. It

is evident from Figure 5.12 (a – c) that surface quality reduces with increasing feed rate and improves with increasing CS percentage for all spindle speeds. The cutting speed versus surface roughness plots for different feed rate and weight percentage has been shown in Figure 5.12 (d – f). It has been clearly seen from Figure 5.12 (d – f) that with increasing spindle speed the surface integrity reduces for all feed rates and weight percentages. It is interesting to notice that surface finish improves with increasing CS percentage in the matrix and LM11/7wt.%CS composite has the lowest surface roughness. This may be attributed to the mechanical effect of sharp-edged CS particles acting as micro-cutting tools and the self-lubricating effect of metallic oxides and sulphides. These reduce friction and vibrations at the tool–workpiece interface during machining leading to better surface finish. The surface roughness analysis indicates improved machinability for CS reinforced composites compared to the base LM11 alloy.

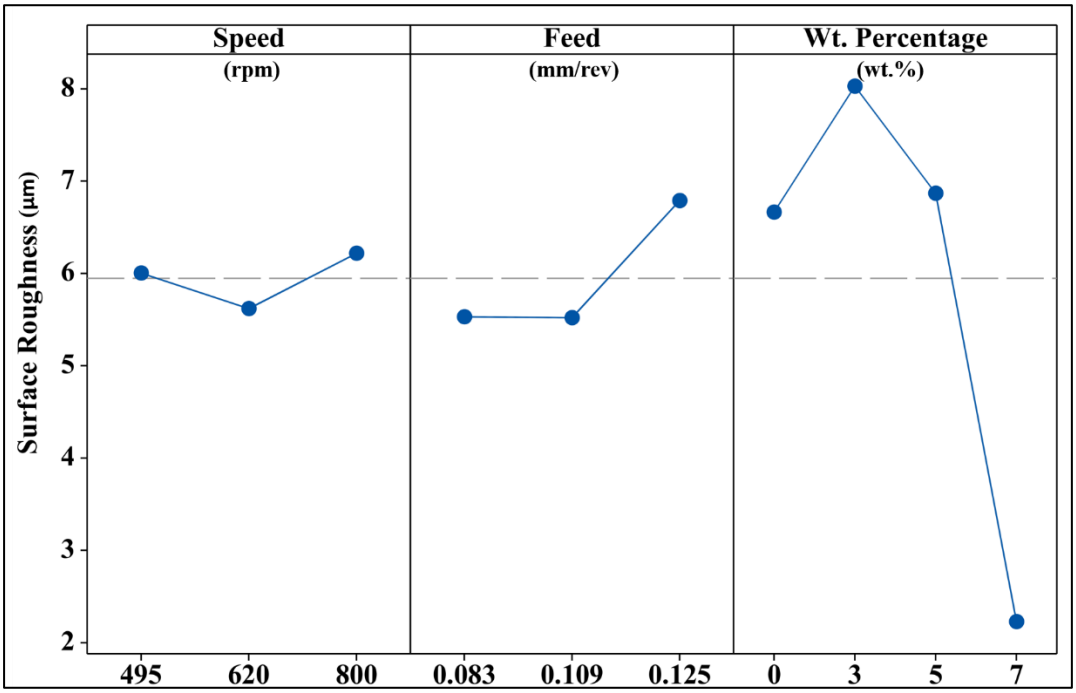

Figure 5.11 Surface roughness main effect plots

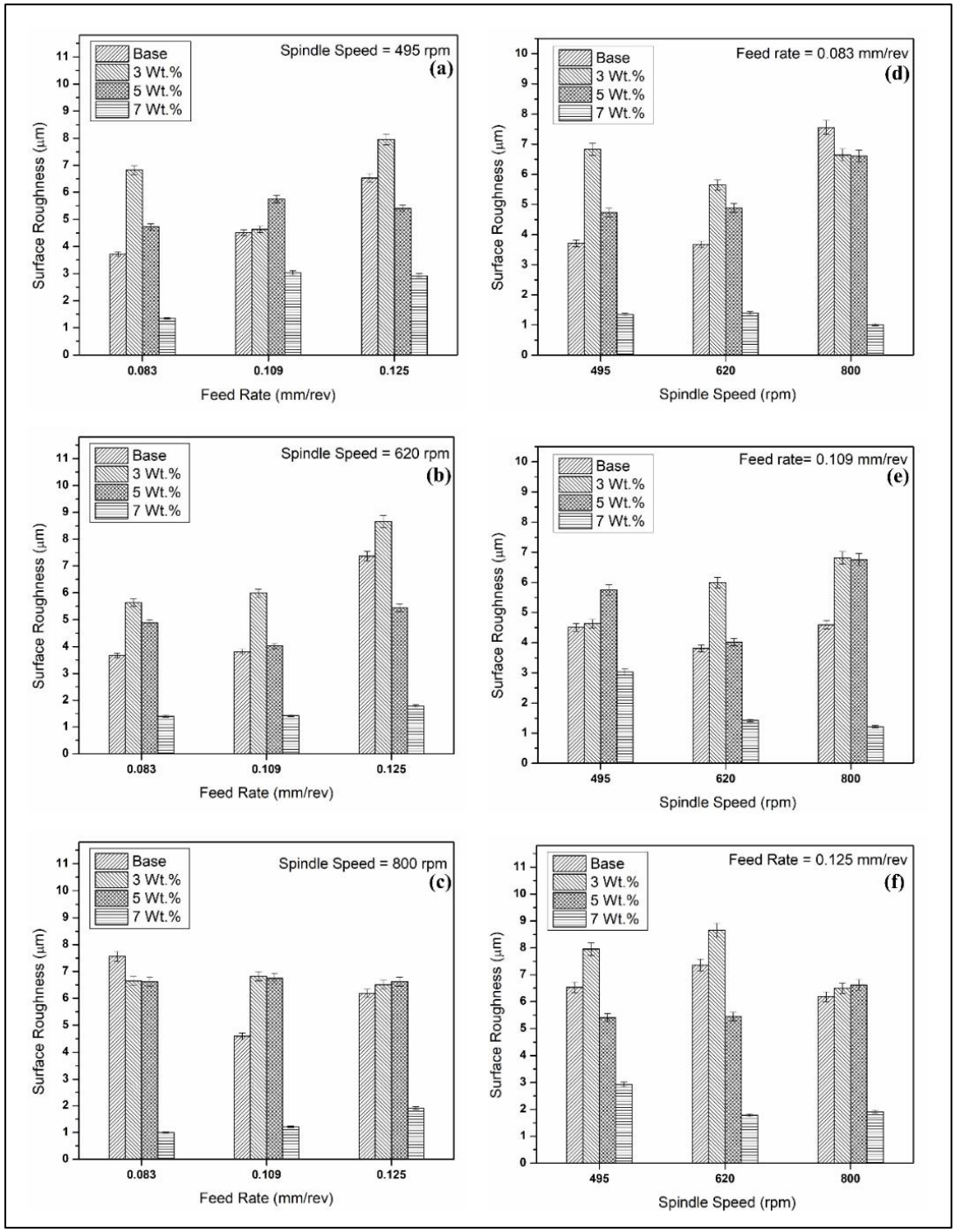

Figure 5.12 (a – c) Feed Rate vs. Surface roughness plots for constant speed and weight percentage, (d – f) Spindle Speed vs. Surface Roughness plots for constant feed and weight percentage

5.1.5. Analysis on material removal rate

The MRR holds an important place for the analysis of machinability in the conventional machining process. Machinability is highly dependent on MRR as it is one of the greatest factors that are directly related to economy of machining. The MRR should be as high as possible for higher machinability since higher MRR results in desired surface generation in a shorter time. The main effect plots for MRR have been

presented in Figure 5.13. It has been depicted from Figure 5.13 that MRR increases with increasing spindle speed since, with increasing speed, stress developed in the tool-work piece interface is more which eases the machining and thus, more material has been removed. Feed rate increase results in an increase of MRR as with increasing feed rate the tool and workpiece contact length increases per revolution which results in increased chip thickness and hence MRR has been increased. In the works of Suresh et al. [64] similar influence of inputs on MRR have been reported. The influence of weight percentage on MRR observed to be inconstant. The dependency of MRR on feed rate has been presented as feed rate versus MRR plot in Figure 5.14 (a – c) for all spindle speeds and weight percentages. Figure 5.14 (a – c) indicates an increase in MRR with the increasing feed rate which is the same as observed from the main effect plots. The spindle speed versus MRR graphs for different feed rates and weight percentages has been illustrated in Figure 5.14 (d – f). Figure 5.14 (d – f) depicts similar results of increasing MRR with increasing spindle speed for all feed rate and weight percentage. It is evident from Figure 5.14 that the MRR, in case CS addition in all the weight percent is the same or more than that of base LM11 alloy. This indicates that, although the trend of MRR versus weight percentage is inconstant but an overall improvement in MRR has been observed. Hence, it can be inferred that CS addition modifies the MRR and results in better machinability than base LM11 alloy.

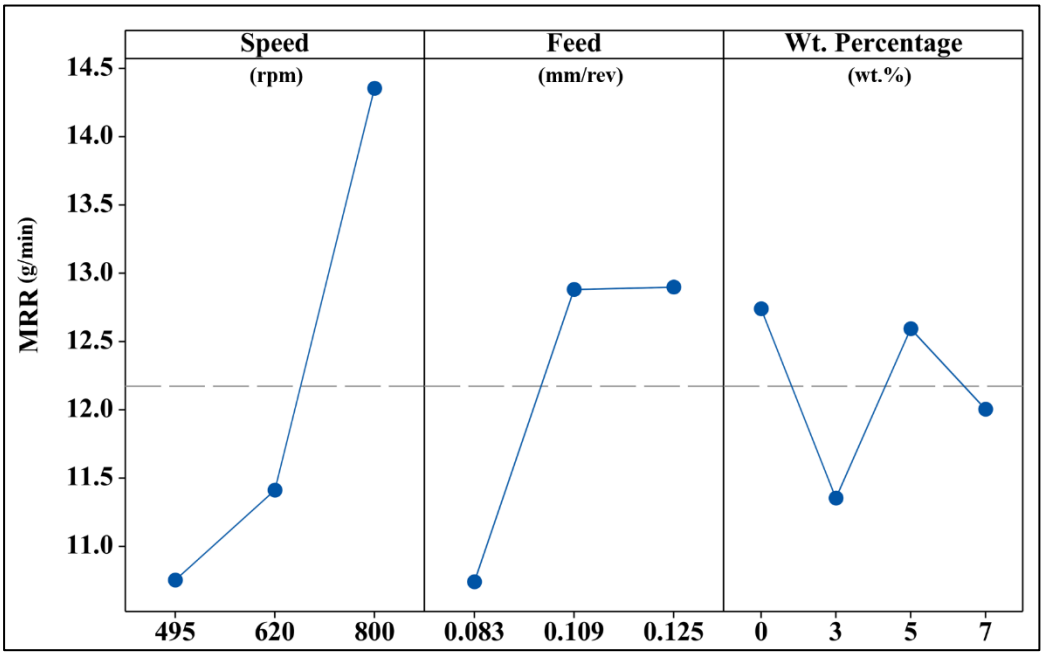

Figure 5.13 Main effect plots for MRR

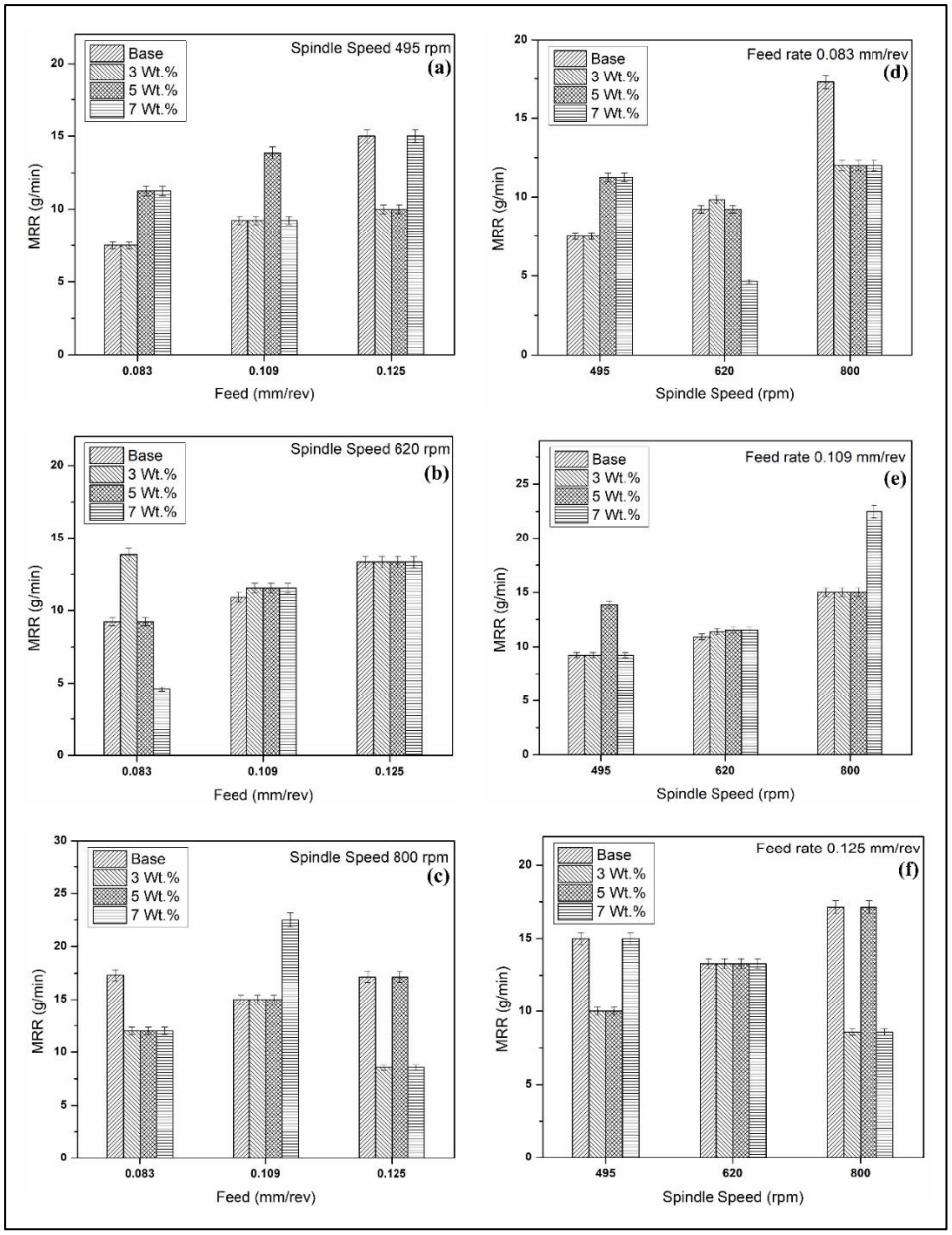

Figure 5.14 (a – c) Feed Rate vs. MRR plots for speed and weight percentage, (d – f) Spindle Speed vs. MRR plots for feed and weight percentages

5.1.6. Analysis on chip thickness

The machinability indices have an indirect dependency on chip thickness. Hence, it is necessary to analyse the thickness of cut chips. The main effect plot generated from the experimentation has been presented in Figure 5.15. Figure 5.15 shows that speed increase results in increased chip thickness. Since increase in spindle speed increases chip – tool interface strain which initiates larger shear cracks leading to higher chip thickness. This increased chip thickness at a higher speed also results in higher MRR. Feed rate increase yields increase in chip thickness as the contact length between tool and work piece increases with increased feed which results in a larger contact area increasing the chip thickness [184]. The impact of weight percentage on chip thickness

shows an opposite trend that is the chip thickness reduces with increasing CS content this is due to the fact that the presence of abrasive particles like SiO_2, Al_2O_3 in CS the composite workpiece has discontinuity which leads to reduced chip thickness. This reduction in chip thickness by reinforcement addition observed to be similar with the investigations by Kannan et al. [69]. This reduced chip thickness compromises the MRR but as the material is removed in small steps the surface roughness found to be improved in composites with higher concentrations of CS. Figure 5.16 (a – c) shows feed rate versus chip thickness plots for all the spindle speeds and weight percentages. The influence of feed on chip thickness as per Figure 5.16 (a – c) has been indicated to be similar to the main effect plot for all the spindle speeds and weight percentages. Spindle speed versus chip thickness plots for all feed rates and weight percentages have been presented in Figure 5.16 (d – f). Figure 5.16 (d – f) depicts that chip thickness increases with spindle speed for all feed rate and weight percentage. The lowest chip thickness has been observed for LM11/7wt.%CS composites for all feed rates and spindle speeds. This reduces the MRR but the surface integrity improved many times. Further depiction from Figure 5.16 shows chip thickness reduces with increasing weight percentage and surface roughness has improved in the expense of a reduction in MRR.

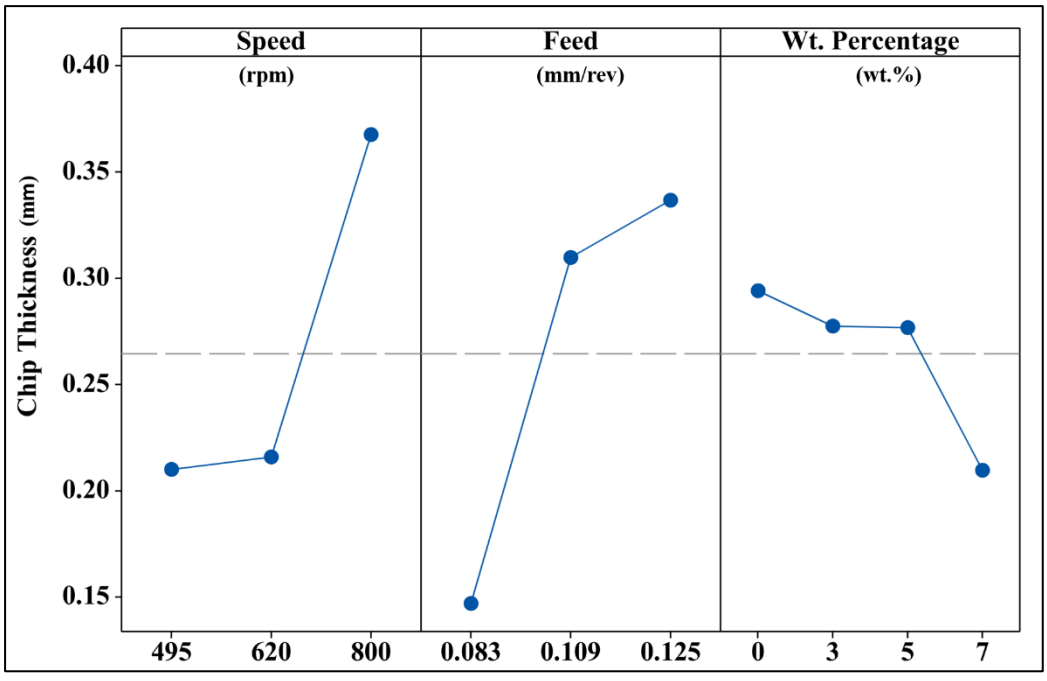

Figure 5.15 Main effect plots for chip thickness

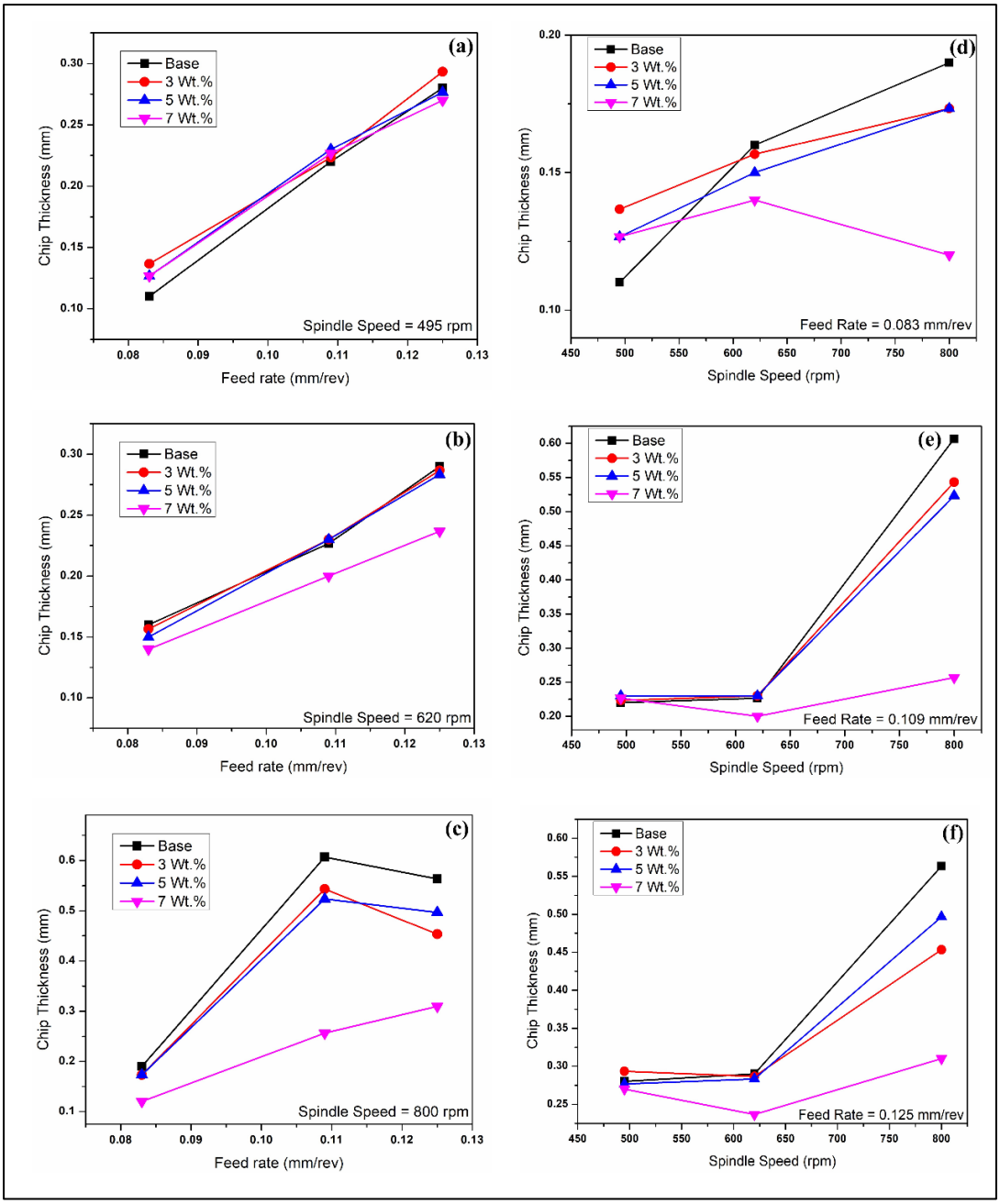

Figure 5.16 (a – c) Feed Rate vs. Chip thickness plots for speed and weight percentage, (d – f) Spindle Speed vs. Chip thickness plots for feed and weight percentages

5.1.7. Chip analysis

The machinability can also be assessed by analysing the chip formation due to various process parameters and the composition of materials. In dry turning chips can be segmented, C-type, spring type or helical and continuous in nature [49]. The formation of chips while turning of composites mainly depends on feed rate and spindle speed. The typical photographs of chips formed during machining have been shown in Figure 5.17 (a – l) to Figure 5.19 (a – l). The photographs depict that at lower spindle speed, the chips are segmented and of C-type as observed from Figure 5.17 (a – d),

Figure 5.18 (a – c) and Figure 5.19 (a – c). Since, at lower speed the composites show brittle fracture as there is no major effect of strain rate due to machining [185]. Increasing feed rate at low-speed results in change in chip formation such as segmented C-type chips converted to connected C type and ¼ circle C-type chips as with increasing feed the tool-workpiece contact length increase leads to higher MRR yielding heavier chips with different form [186]. The effect of weight percentage at low speed observed to be nominal until LM11/5wt.%CS composites. However, a major change in chip formation reported in case of LM11/7wt.%CS composites at medium and higher feed rate as investigated from Figure 5.18 (d) and Figure 5.19 (d). Shape of chips has been changed from C-type to spring type in LM11/7wt.%CS composites as the higher percentage of CS acts as a solid lubricant and enhances the reinforcement particle displacement thus, chips tend to be continuous and spiral.

At medium spindle speed the segmented chips tend to continuous spiral chips as a results connected C-type chips are formed as per Figure 5.17 (e –g), Figure 5.18 (e – g) and Figure 5.19 (e – g). The feed rate increase increases the chip thickness and formed heavier chips with ½ circle C-type chips and connected C-type as the cutting temperature increased due to larger contact length due to larger feed rate. It is also observed from Figure 5.17 (h), Figure 5.18 (h) and Figure 5.19 (h) that the curls become more frequent for LM11/7wt.%CS composite at medium speed and increasing feed rate which indicates that CS particle assisted the machining. This indicates ease of machining by CS inclusion. Particularly for LM11/7wt.%CS, the chip thickness is observed to be lower, which can be attributed to the lubricating effect of the higher slag content that reduces cutting forces and promotes easier shearing of material. However, the same slag particles assist in localized plastic flow, leading to the formation of curly or helical chips despite their reduced thickness [182].

The influence weight percentage of CS and feed rate on chip formation at high spindle speed has been shown in Figure 5.17 (h – l), Figure 5.18 (h – l) and Figure 5.19 (h – l). The photographs show conversion from large radii C-type to large radii helix type as the feed increases. Since, at higher speed the brittleness of composites has been converted to ductile due to a rise in temperature and strain rate which results in helical chips [187]. In high speed also for 7 wt.% slag included composites show spring like chips due to the self-lubrication nature of metal oxides present in the CS reinforcement particles. The 7 wt.% CS, chips appear thinner but tend to curl or form helical shapes,

as the reduced cutting resistance lowers chip thickness while the enhanced ductility from lubrication and particle displacement facilitates continuous curling.

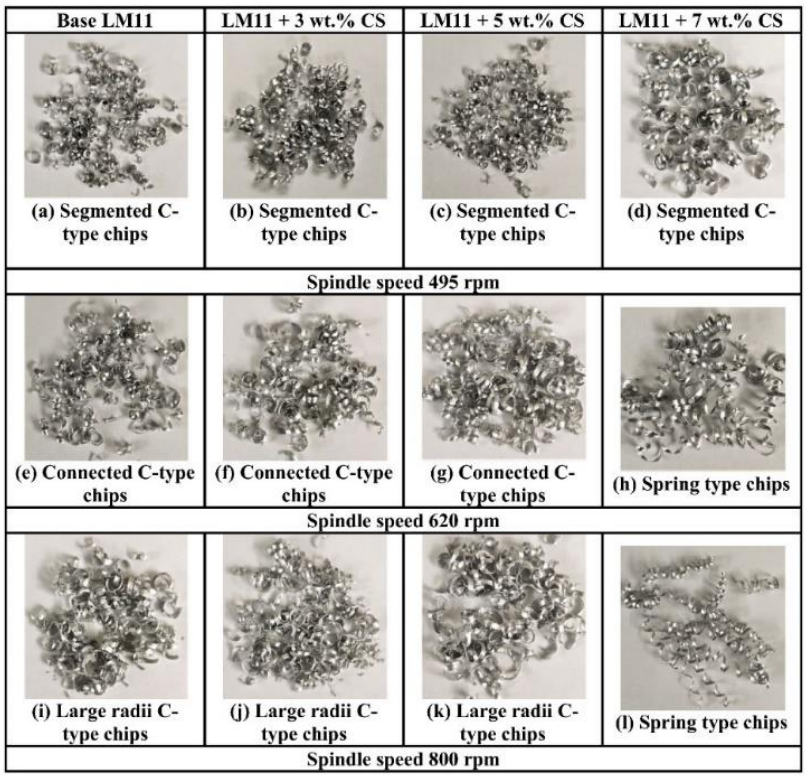

Figure 5.17 (a – l) Photographs of chips formed at different spindle speed for feed rate 0.083 mm/rev

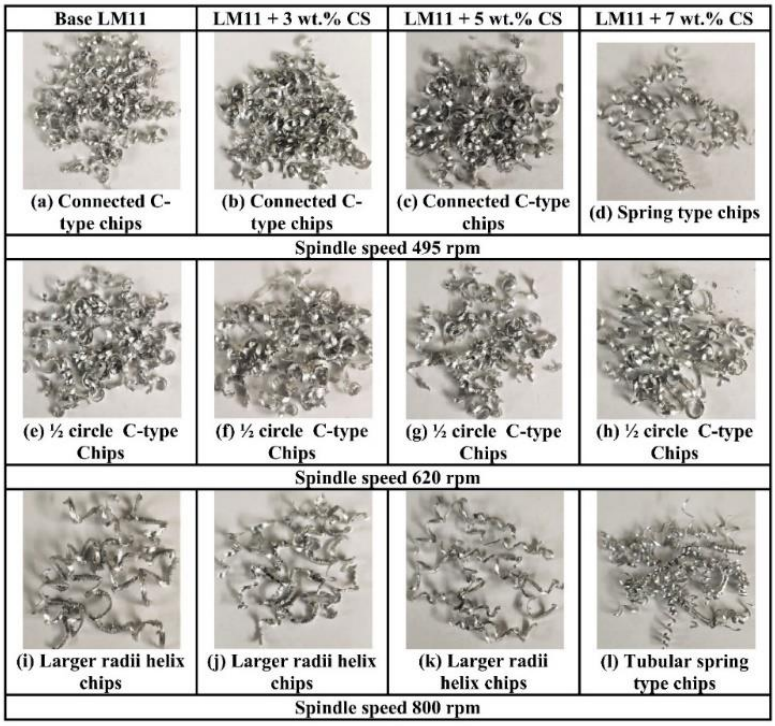

Figure 5.18 (a – l) Photographs of chips formed at different spindle speed for feed rate 0.109 mm/rev

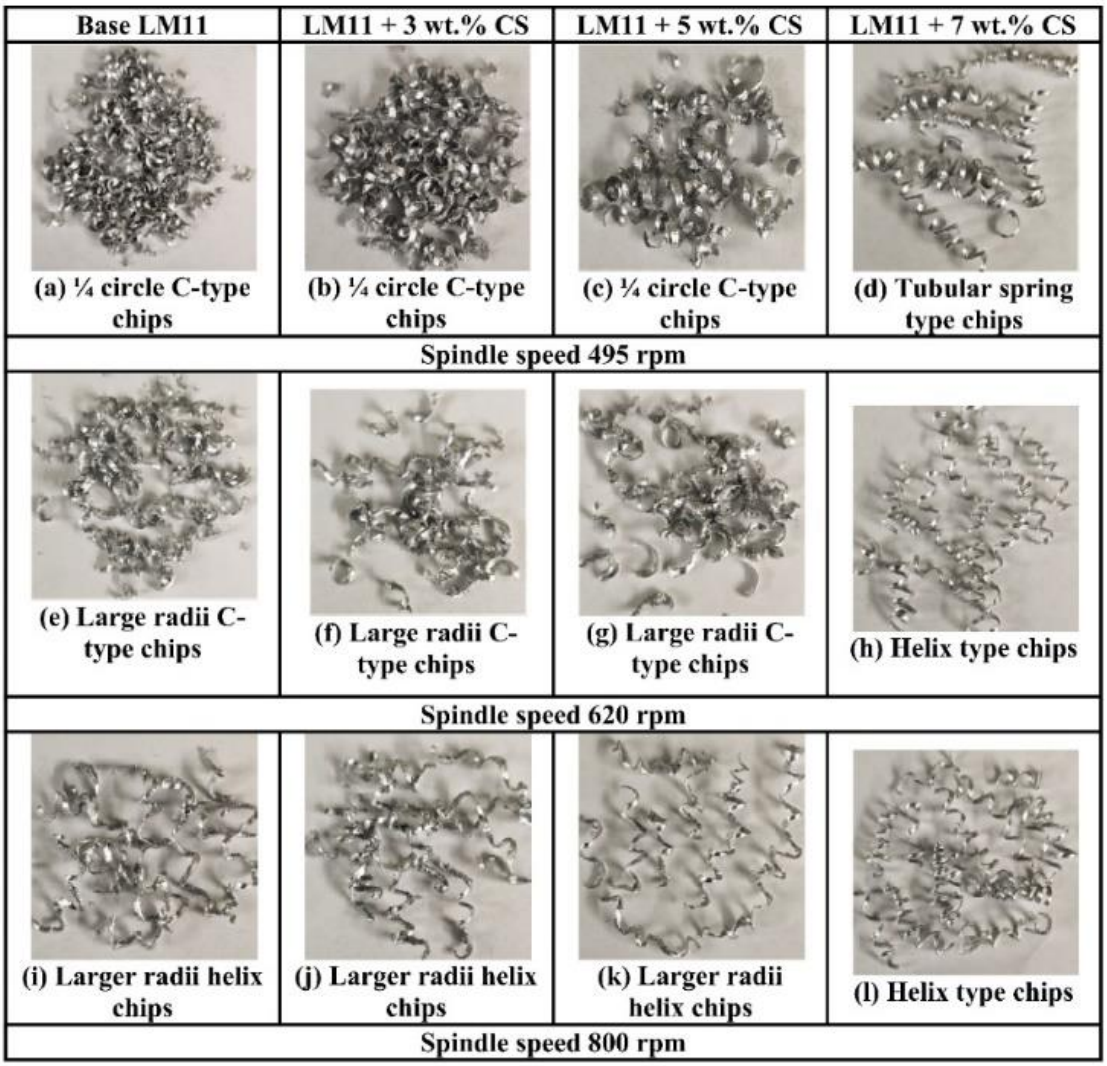

Figure 5.19 (a – l) Photographs of chips formed at different spindle speed for feed rate 0.125 mm/rev

5.2. Comparisons of machinability indices

The effect of slag content on machinability has been studied in depth. Table 5.2 shows different values of average machining indices respective to all the cast composites. The data suggests that good machinability with low cutting force, power consumption, chip thickness, tool wear and surface roughness along with higher material removal rate has been achieved in composite turning when compared with base LM11 alloy. The percentage change in machinability indices has been reported in Table 5.3. The increment in the investigated machining indices has been taken positive and the decrement of indices from base has been chosen negative.

Table 5.2 Average machinability indices respective to all cast composites

Samples	Force (N)	Surface Roughness (µm)	Power Consumption (kW)	MRR (g/min)	Tool Wear (µm)	Chip Thickness (µm)
LM 11	40.44	6.66	14.98	12.74	218.91	0.29
LM11/3wt.%CS	40.64	8.03	15.77	11.22	95.46	0.28
LM11/5Wt.% CS	45.11	6.87	15.74	12.59	254.89	0.28
LM11/7wt.% CS	16.00	2.23	15.54	12.00	229.23	0.21

Table 5.3 Percentage change in machinability indices with respect to base composite

Samples	Percentage change in					
	Force (%)	Surface Roughness (%)	Power Consumption (%)	MRR (%)	Tool Wear (%)	Chip Thickness (%)
LM11/3wt.%CS	0.49	20.57	5.27	-11.93	-56.39	-3.45
LM11/5Wt.% CS	11.55	3.15	5.07	-1.18	16.44	-3.45
LM11/7wt.% CS	-60.44	-66.52	3.74	-5.81	4.71	-27.59

Effective comparison and estimation of machinability has been presented as radar diagram as shown in Figure 5.20. The cutting force has been increased with adding cupola slag particles up to 5 wt.% which then reduced many times for 7 wt.% cupola slag reinforced composites as observed from Table 5.3 and Figure 5.20. The presence of hard ceramic like cupola slag reinforcements in 3 and 5 wt.% cupola slag reinforced composites gets rubbed with the cutting edge while turning increasing the friction in the tool workpiece interface and the force required to initiate cutting by shearing should overcome this friction. Moreover, abrasive cupola slag particles increase the temperature workpiece which harden the cutting interface locally and increases the cutting force requirement [188]. Now for composites reinforced with 7 wt.% cupola slag, higher amount of slag creates a nearly homogeneous distribution in the matrix with finer grains. This composite when turned the crack initiated by the cutting edge propagates through the grain boundaries and force requirement becomes nominal [189]. Apart from this, the slag particles which come out from the composites while turning rubs against the workpiece in chip tool interface which generates additional micro cutting of workpiece due to abrasive action and reduces the cutting force. The maximum reduction on cutting force of 60.44% has been observed in LM11/7wt.%CS.

The surface integrity analysis of the machined surface inferred that inclusion of slag particle first deteriorates the machined surface but finally at 7 wt.% cupola slag inclusion results in improvements of 66.52% as compared to the base as visualized in Table 5.3 and Figure 5.20. This can be attributed to higher cutting force in case of turning of 3 and 5 wt.% cupola slag reinforced particles. In case of LM11/7wt.%CS

composites low cutting force along with abrasive rubbing action of loose slag particle improves the surface roughness. It should be noted that the worst machined surface with maximum surface integrity deterioration of 20.5% has been observed in case of LM11/3wt.%CS composites because of formation of built-up edge in the tool tip while cutting. The abruptly present cupola slag particle in 3wt.% cupola slag incorporated particle while cutting initiate very high amount of friction and heat when tool tip came in contact with slag particles. This friction and heat create a localized welding of cut chips to the tip of the tool making the tip blunt and hence deteriorate the surface integrity.

The power consumption while machining does not vary much as for the rigid and robustness of the conventional lathe used in this investigation. Although, A trend of reducing power required has been observed as wt.% of slag particle increased. This has been in line with the results of cutting force. The lowest increase in power consumption has been observed as 3.74% from the base metal in case of LM11 composites with 7 wt.% of slag. The increase in power consumption can be reasoned by the vibration of rotating spindle holding the workpiece while each encounter of hard abrasive cupola slag particle in the matrix [190]. In case of LM11/7wt.%CS composites the cutting eases with every encounter thus required power is less than that of other cast composites.

The MRR has been observed to be similar in all the cast composites except LM11/3wt.%CS composites may be because of bluntness of tool generated by built up edge. A reduction of 11.93% of material removal rate when compared with base LM11 has been obtained in case of LM11/3wt.%CS composites while 5 and 7 wt.% composites reduce the material removal rate by 1.18% and 5.81% respectively. The tool wear has been observed to be reduced in case of LM11/3wt.%CS composites by 56.39% which increases in case of 5 and 7 wt.% slag inclusion with respect to LM11.

The decrease of tool wear is due to the deposition of abrasive particle into the tool tip due to localized welding by the heat generated due to friction, this deposition works as a coating over the tool workpiece interface hence protects the tool from wear out. The Chip thickness has been reduced for all the composites while maximum reduction of 27.59% has been observed in LM11/7wt.%CS composites. This lower chip thickness indicates better surface finish with low tool wear which are in accordance with the experimental investigation.

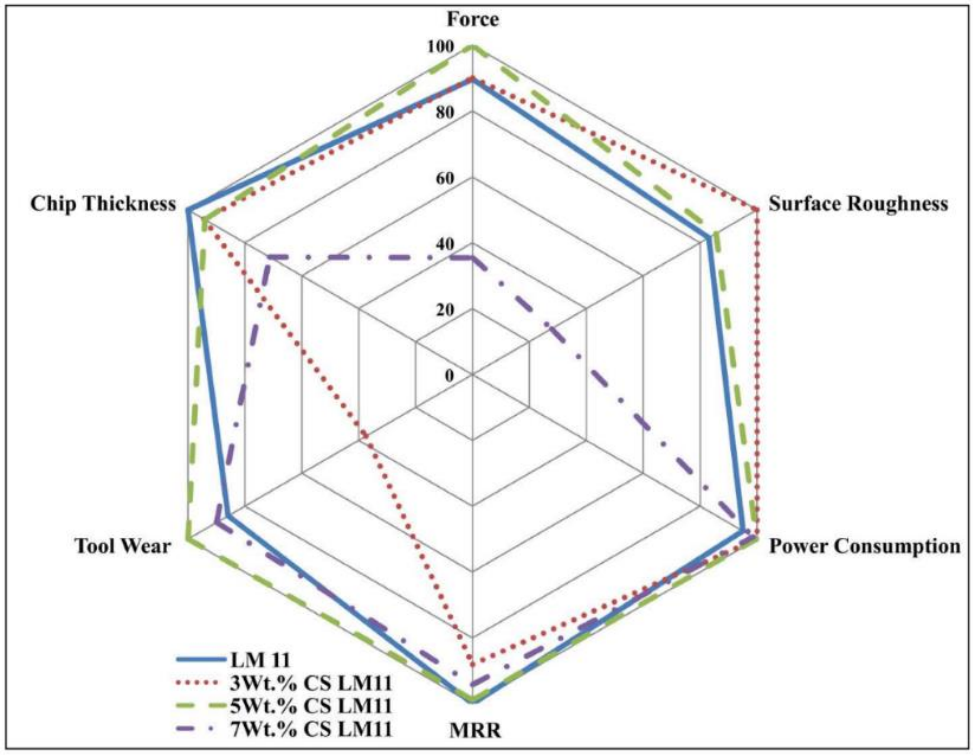

Figure 5.20 Radar chart for comparison of machinability for as cast composites

The aim is to judge the machinability of novel slag reinforced composites has been successfully justified using radar diagram shown in Figure 5.20. The better machinability means ease of machining which in terms of machining indices can be written as low cutting force, surface roughness, power consumption, tool wear and chip thickness along with high material removal rate Now, it is clearly visible from Figure 5.20 that cutting force and surface roughness is minimum for 7 wt.% slag included composites while other two slag reinforced composites show similar results as base alloy. Power consumption shows similar range as base material for all the cast composites. The material removal rate has been observed to be in range of 12% deviation when compared with base alloy for all the cast composites. The MRR slightly decline for LM11/3 wt.% CS composites may be due to tool bluntness resulting from built-up edge formation. Conversely, LM11/5 wt.% and LM11/7 wt.% CS composites exhibit only marginal reductions in the range of 1–6%, indicating that the overall MRR remains nearly constant, with no marked improvement or deterioration. The tool wear and chip thickness reduced for all the cupola slag included composites. The LM11/3wt.%CS composites yield lowest tool wear and LM11/7wt.%CS composites generate least chip thickness. Hence, overall machinability of cast cupola slag

reinforced composites said to be enhanced from the base LM11 alloy and 7 wt.% cupola slag inclusion in the matrix gives best machinability in terms of cutting force, surface roughness and chip thickness and 3 wt.% slag included composites yield best machinability character in terms of tool wear. The distinct behaviour at 7 wt.% arises because increasing slag fraction changes particle distribution and the dominant cutting mechanism: while 3–5 wt.% samples have isolated hard particles that raise local friction, promote built-up edge formation and local work-hardening (increasing cutting force and roughness), the 7 wt.% material shows a more homogeneous/fine dispersion and stronger particle–particle interactions that favour crack propagation along grain boundaries and micro-abrasive chip formation. These changes reduce the average cutting resistance and improve surface finish.

5.3. Summary

The machinability study of novel cupola slag reinforced composites with varying cupola slag weight percentage has depicted the following observations:

- The cupola slag inclusion reduces cutting force requirement likely due to hard and abrasive nature of slag particles. Nominal cutting force has been required for turning of LM11/7wt.%CS composites and the cutting force increases with increasing spindle speed and feed rate.
- Power consumption during machining increased with increasing speed and feed rate. The lowest power was consumed for machining of base LM11 alloy, however, it increased for LM11/3wt.%CS composite and then decreased with increasing weight percentage.
- Tool wear has been decreased with increasing spindle speed. LM11/7wt.%CS composite shows nominal tool wear while turning.
- The surface finish is deteriorated with increased spindle speed and feed rate while it is improved with increased weight percentage of CS. Composites with 7 wt.% CS when machined in low speed and feed have shown a nominal surface roughness of 1.36 μm.
- The MRR is increased with increasing feed and spindle speed. Maximum MRR of 22.50 g/min is reported in LM11/7wt.%CS composites when machined with speed 800 rpm and feed 0.109 mm/rev.

- The chip thickness is increased with increasing feed and spindle speed but reduces with increasing weight percentage of CS. The lowest chip thickness has been observed in composites incorporated with the highest amount of CS.
- Chip analysis indicates that slag inclusion changes the chip morphology from segmented type to continuous spring type chips with increasing weight percentage while increasing speed resulted in an increase in the radii of chip curls and increasing feed resulted in increasing chip curls.
- The results suggest that incorporation of cupola slag enhances the machinability of cast composites. The comparison of machinability depicts that with increasing slag weight percentages in cast composites, machinability has improved by considering lower cutting force, similar power consumption, and lower tool wear, lower surface roughness, along with higher MRR and chip thickness. The best machinability can be seen in LM11/7wt.%CS composites, as the turning of this cast composite generates a surface with a better surface finish, reduced chip thickness and similar MRR when compared with the base LM11 alloy. The increase in CS content may lead to better machinability. However, due to reduced wettability of reinforcement CS particle the fabrication of composites via stir casting route is not feasible.

Chapter 6

Effect of Heat Treatment on Novel Cupola Slag Reinforced Composites

The LM11 alloy are well known to be highly responsive to the heat treatment. The heat treatment of LM11 alloy primarily aims to dissolve alloying elements, particularly copper, into the aluminium matrix during the solution treatment stage, followed by the controlled precipitation of strengthening phases during aging. This sequence results in the formation of finely dispersed precipitates that significantly improve hardness, tensile strength, and wear resistance. The heat treatment for LM11–cupola slag composites, additionally contributes to microstructural refinement and promotes more effective load transfer between the matrix and the reinforcement. Consequently, both the mechanical performance and machinability of the composites are expected to be enhanced. In this chapter the experimental investigation results of solution heat treatment of cast composites have been presented along with comparisons with as cast composites.

The as cast composites have been solution treated in T6 condition which refers to solution heat treatment, quenching, and artificial aging of aluminium alloys to increase hardness and strength. The schedule of heat treatment has been selected by performing rigorous literature review and pilot experiments as described in Chapter 2. The final schedule has been selected based on hardness value of pilot experiments. A common schedule of heat treatment followed for all the composites is heating at 530 ºC for 6 hours followed by water quenching at 70 ºC which further artificially aged at 100 ºC for

4 hours. The heat-treated samples have been cut and prepared for microstructural characterizations. The heat-treated composites have been characterized in same manner as for as-cast composites presented in Chapter 2. The heat-treated composites have been undergone machinability analysis in turning at a conventional lathe without using any cutting fluid (Dry turning). The details of machinability experimentation parameters have been presented in Chapter 2. The machinability experimentation utilizes full factorial experimental design for robust understanding the process parameters influence on output. The cutting parameters such as feed rate, spindle speed and slag weight percentage has been selected as input whereas machinability indices like, surface roughness, cutting force, MRR, power consumption, tool wear, chip thickness are responses. A constant depth of cut has been kept influence of it on turning is well established in literature. Total 36 numbers of experiments have been performed for all combinations of levels and factors of inputs. This work followed the same scheme of machinability experiments that has been followed for machinability studies of as cast composites as presented in Chapter 2. Detailed chip analysis and chip thickness measurement has been done using the collected chips. The observations have been analysed in a rigorous manner to introspect process input effects and underlying mechanisms. The comparative study of machinability has been performed as the last step of this work. The comparison has been done among the heat-treated composites and along with the as cast composites. The comparison of machinability performance has been done by normalising the experimental data and processing it subsequently.

6.1.Effect on microstructure

The heat-treated composites micrographs along with grain distribution has been presented in Figure 6.1 (a – h). It is observed from the optical micrographs that homogeneous distribution of slag particles had been occurred along with minimal agglomerations. The white arrows in Figure 6.1 (c, e and f) shows incorporated cupola slag particles. The interface between slag and matrix has been observed to be clean and free from intermetallic compounds indicating good bonding between matrix and reinforcements [191]. The slag inclusion majorly effects in refinement of grains as observed from Figure 6.1 (b, d, f, h). Base LM11 has mean size of 138.89 μm which reduces to 48.46 μm, 38.83 μm and 27.70 μm respectively for LM11/3wt.%CS, LM11/5wt.%CS and LM11/7wt.%CS. This refinement has been resulted from the initiation of solidification surrounding reinforced slag particles [192]. Moreover,

homogenization of grains has been resulted from solution treatment [193]. The effect of this refinement in microstructure would result in enhancement of machinability and mechanical properties. The grain size is gradually reducing with increasing reinforcing cupola slag content as per Figure 6.1. This is due to the fact that with increasing slag content number of nucleation sites increases while solidification. The grain size of as cast composites has been reported in Chapter 4, was much higher than that of heat-treated composites due to homogenization and result in enhanced properties. A detailed comparison chart has been presented in Figure 6.2 depicting the reduction of grain size with increasing slag content, moreover heat treatment reduces grain size even more.

Figure 6.3 (a – d) presents SEM images for heat-treated composites. Base LM11 depicts larger grains with porosities as observed form Figure 6.3 (a). The cupola slag inclusion in grain boundaries and inside the grains has been observed in Figure 6.3 (b – d), the reinforcement – matrix interfaces are free from intermetallic formation and clean yielding better mechanical and machinability properties [194]. The grains are observed to be reduced with increasing slag content and there are minimal agglomerations of reinforcement particle ode to the successful stirring. Composites with 7 wt.% cupola slag have clean interface showing better bonding between matrix and reinforcement as per Figure 6.3 (d). The inclusion of slag particle has been further evidenced by elemental analysis using EDS plots shown in Figure 6.4 (a – c). The slag particle content oxides of iron (Fe), calcium (Ca), aluminium (Al), silicon (Si) etc. Hence, presence of oxygen (O), Si, Al, Ca, Cu and Fe in low electron level as presented in Figure 6.4, indicate presence of cupola slag in the composites. The quantitative analysis indicates the composition of the mapped area shown. The total amount of foreign element to Al and Cu has been increases with increasing slag content. These, indicates successful inclusion reinforcement in matrix. Similar studies on reinforcement inclusion have been reported by pervious authors [195–197].

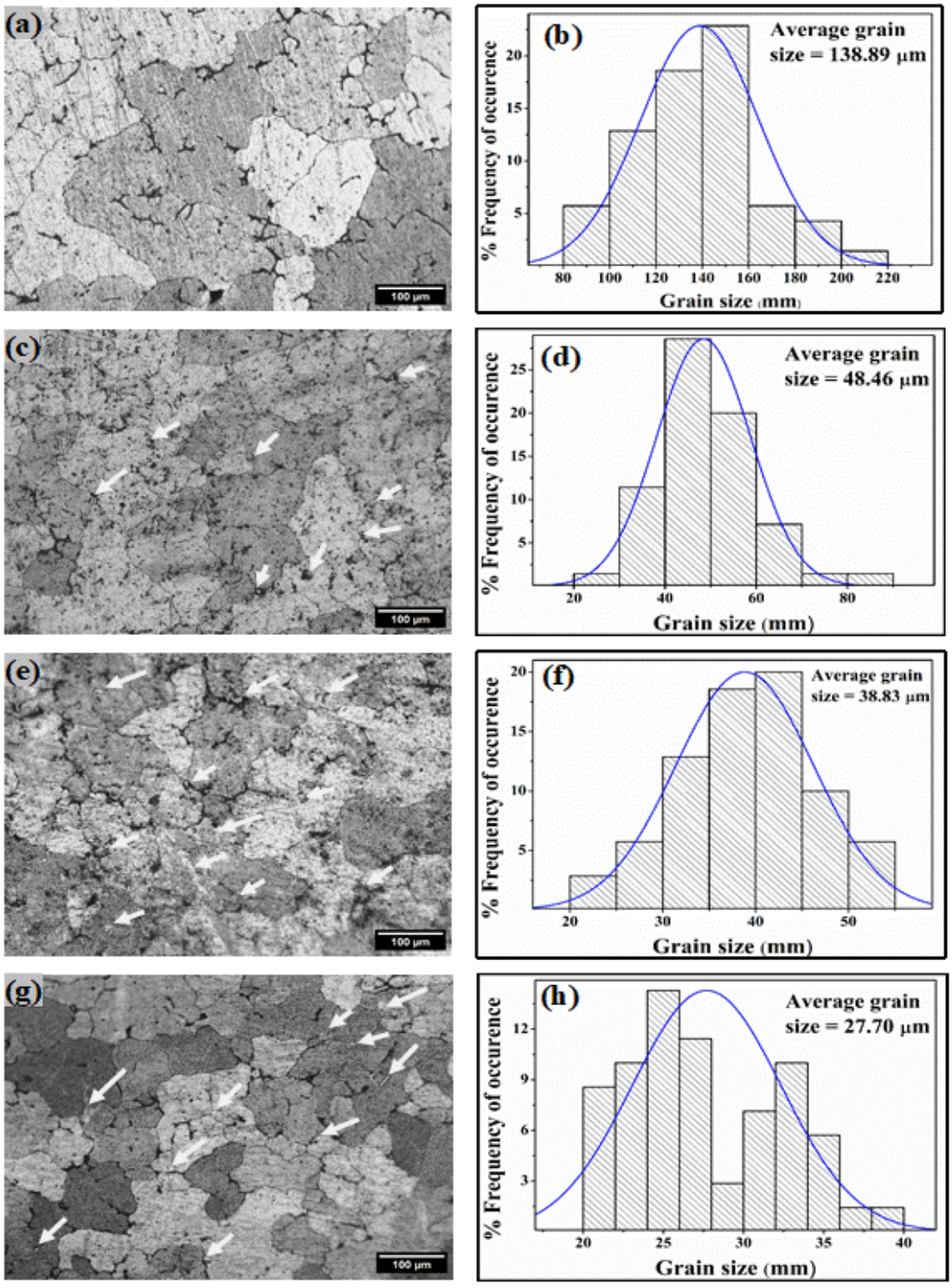

Figure 6.1 Optical micrographs and particle size distribution curve for heat-treated LM11 (a, b), LM11/3wt.%CS (c, d), LM11/5wt.%CS (e, f) and LM11/7wt.%CS (g, h)

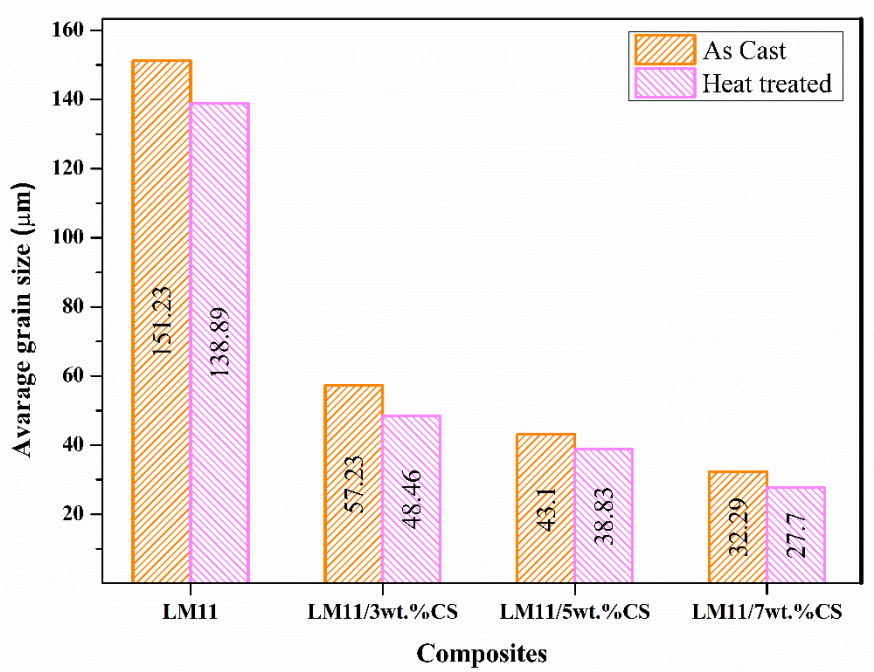

Figure 6.2 Comparison chart for grain size refinement

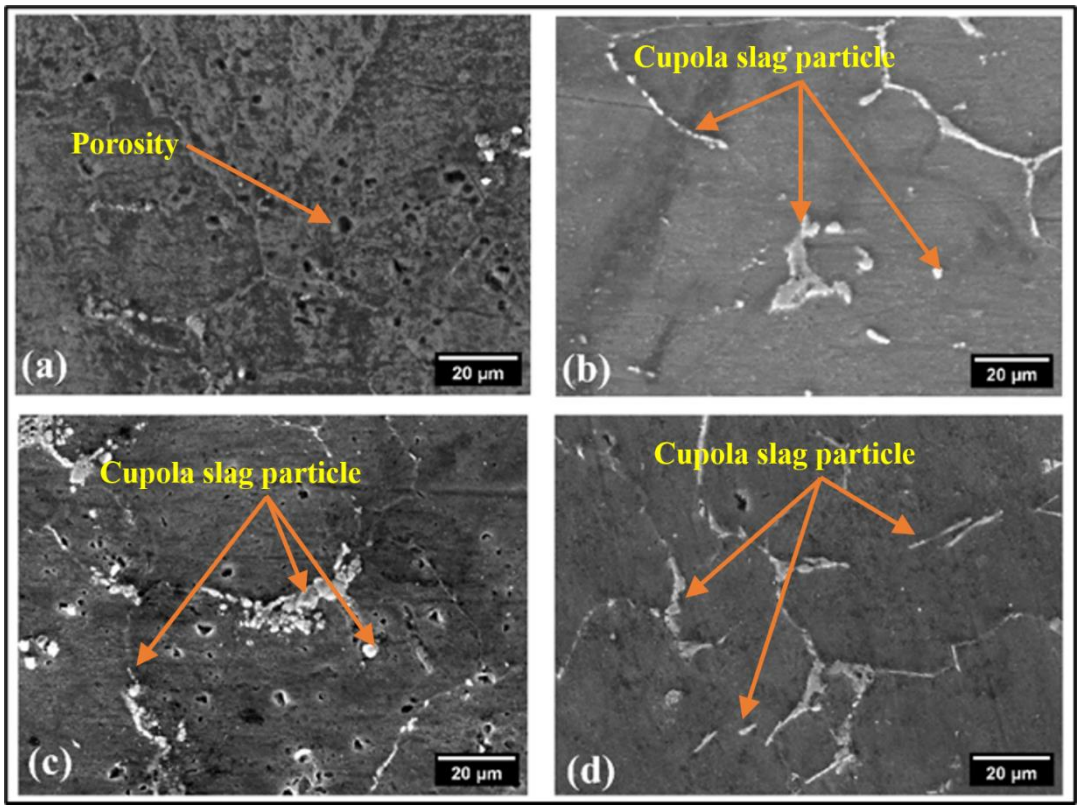

Figure 6.3 SEM images of heat-treated (a) LM11, (b) LM11/3wt.%CS, (c) LM11/5wt.%CS and (d) LM11/7wt.%CS

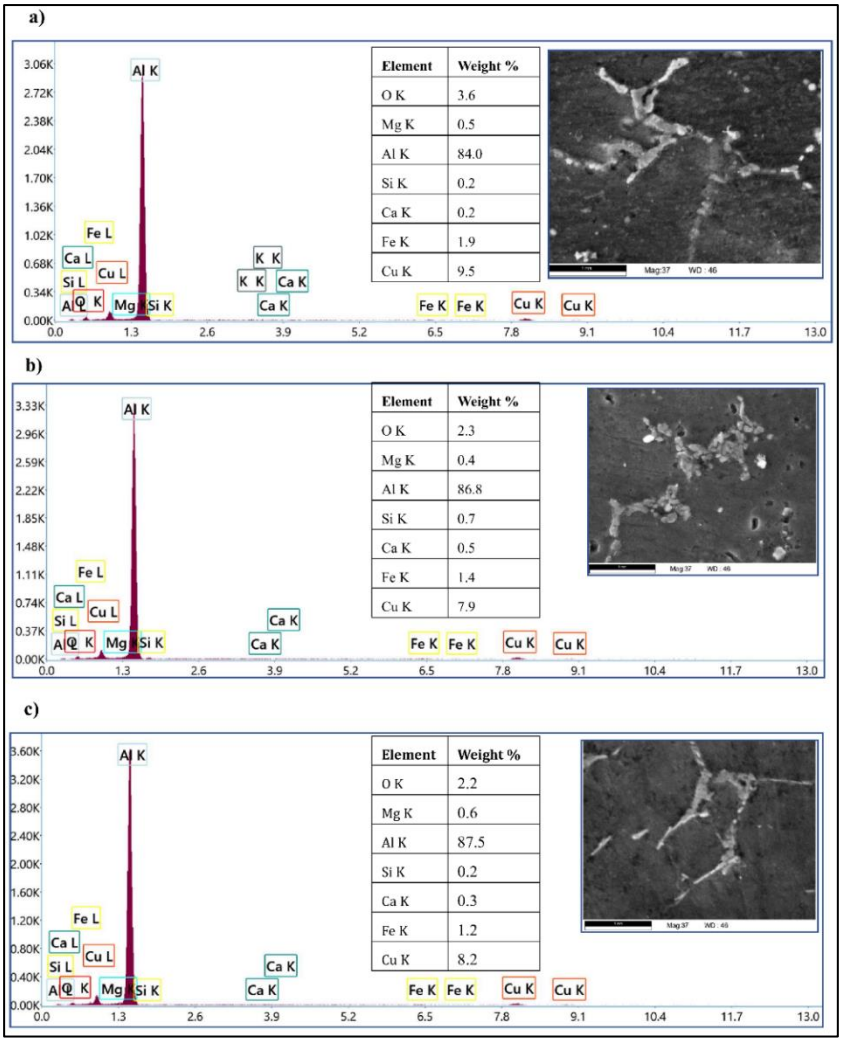

Figure 6.4 EDS plots for heat-treated (a) LM11/3wt.%CS, (b) LM11/5wt.%CS and (c) LM11/7wt.%CS

6.2.Effect on density and hardness

The heat-treated composites density along with as cast composites has been presented in Figure 6.5. It is depicted from Figure 6.5 that higher cupola slag content reduces the density as cupola slag possesses comparatively lower density. The variation in density for as cast composites has been observed to be more as slag percentage increase whereas it is consistent in case heat-treated composites due to homogenisation of Cu into aluminium solid solution. The percentage decrease in density has been observed as 5.82, 2.83 and 0.382% for base, 3% and 7% slag included composites whereas, 0.898% increase in density observed for 5wt.% slag reinforced composites.

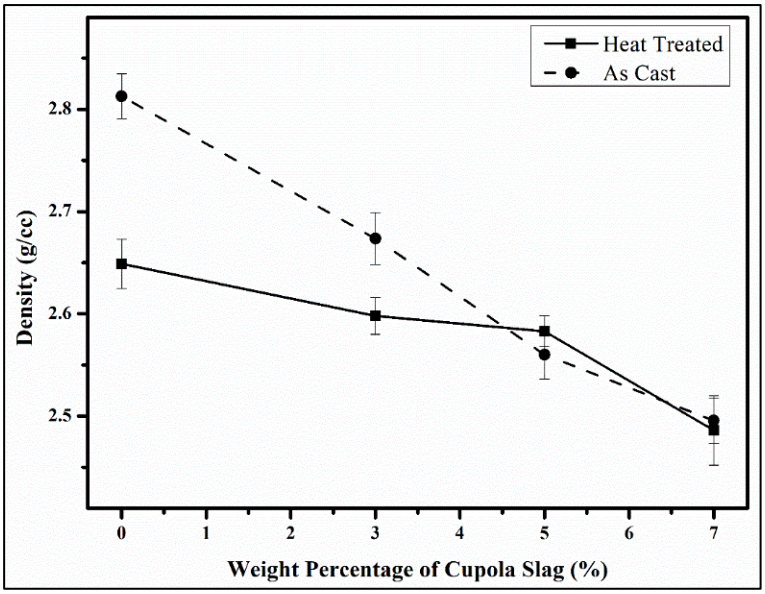

Figure 6.5 Graphical representation of density results of heat-treated samples

The microhardness plots for heat-treated and as cast composites has been presented in Figure 6.6. It has been noted that microhardness increases as the slag percentage rises, owing to the refinement of grains associated with the higher slag content. This is governed by three major mechanisms such as load transfer, dislocation strengthening and grain refinement. Load transfer strengthening in composite occurs when reinforcing particles resist deformation, leading to dislocation at the particle-matrix interface. This creates a stress field hindering dislocation movement, enhancing composite strength. Interfacial strength is vital for efficient load transfer. Dislocation strengthening further boosts hardness by impeding dislocation movement through the introduction of numerous dislocations at the interface [198]. The inclusion of slag reinforcement can lead to grain refinement, which increases the hardness and strength of the composite according to the Hall-Petch relationship [199]. Sharma et al. [200] has reported that the brass slag reinforcement results in remarkable improvement in hardness for Al-Si alloy (LM30) composites. Improved hardness of solution treated composites has been observed when compared with as cast composites. An improvement of 28.71%, 25.33%, 23.84% and 13.10% from as cast composites has been obtained respectively for base, 3wt.%, 5wt.% and 7wt.% slag included composites. The improvement of hardness is due to formation of Al_2Cu, which stops movement of dislocation to increase material strength [201]. Sun et al. reported similar enhancements of hardness and density in heat-treated SiC/Al-Cu composites [202].

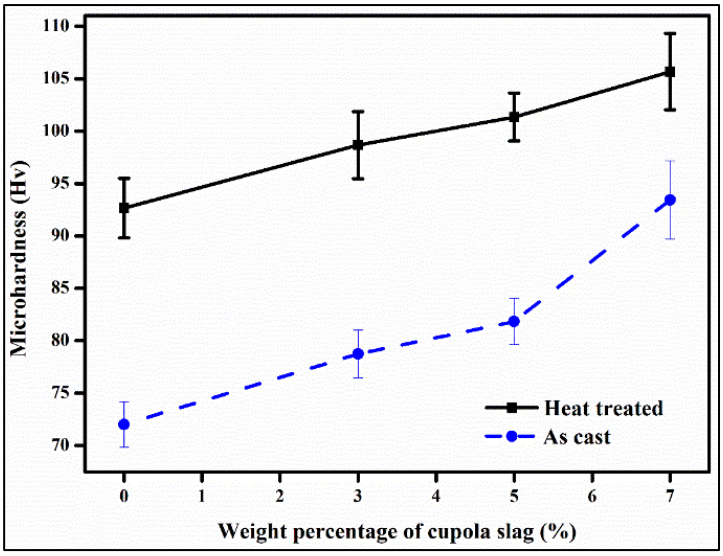

Figure 6.6 Graphical representation of microhardness

6.3.Effect on tensile properties

The stress stain curve for heat-treated composites is presented in Figure 6.7, which shows that higher slag content yields increased ultimate tensile stress. Moreover, the stress strain curve area denoting the modulus of toughness increases with increasing slag percentage. The yield strength is also observed to be increased with increasing slag content as per Figure 6.7. This enhancement of tensile properties is the result of increased strength due to good interfacial bonding, refinement of grains and strengthening due to inclusion of reinforcements [203,204]. Moreover, as the microstructure shows in Figure 6.1 that the reinforcement particles are reduced in size, which can distribute the stress within the matrix yielding higher tensile strength.

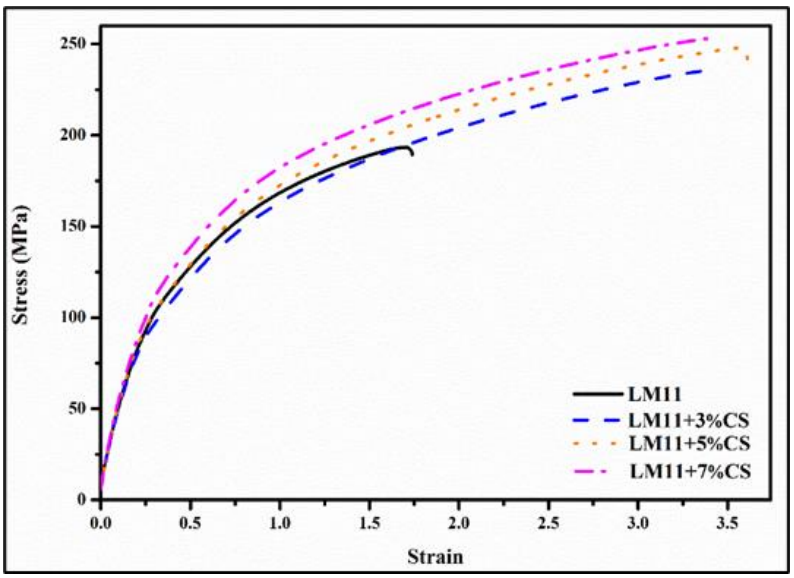

Figure 6.7 Stress strain curve for all heat-treated composites

The ultimate tensile strength (UTS), yield stress along with the comparisons with the as cast tensile values has been presented in Figure 6.8. The UTS increasing with increasing cupola slag percentage and heat-treated composites show better UTS. The uniform distribution of grains achieved in solution heat treatment has resulted in this betterment [205]. The UTS indicate the overall strength of material and heat-treated composites with 7 wt.% slag inclusion with UTS value 243.26 MPa observed to be approximately 25% higher when compared to solution treated base LM11 (193.38 MPa) and more than 70% enhancement comparing with as cast base alloy (141.45 MPa). The yield stress also increases with increasing slag content but heat-treated composites show more uniform increase. This increase is the result of strengthening effect of the cupola slag particles within the composite material [206]. The implications of this increase in yield stress include enhanced mechanical properties, such as improved strength and durability. The UTS has been enhanced due to heat treatment as 37.03%, 26.81%, 32.26% and 22.88% respectively for base, 3, 5 and 7 wt.% slag incorporated composites.

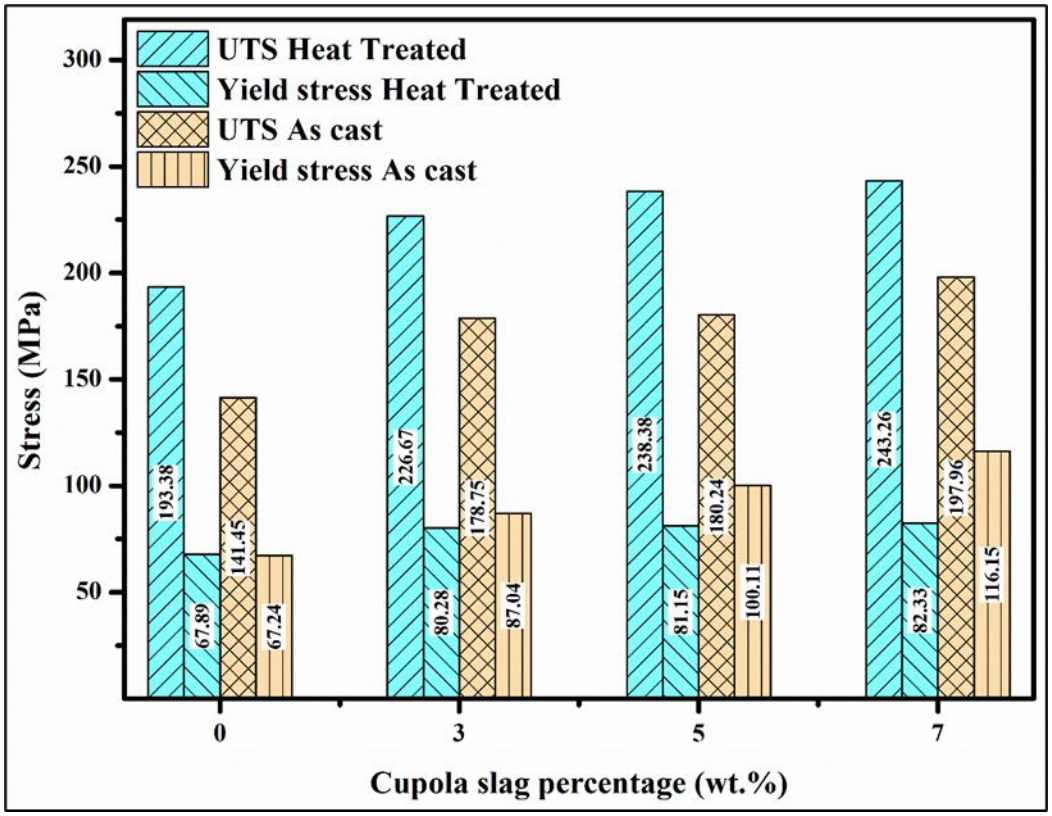

Figure 6.8 Comparison of UTS and yield stress

The ultimate load indicates maximum load bearing capacity of any material which is another important mechanical property for structural applications. Along with-it

specific strength gives the strength to weight ratio which is most important property for light weight composites. The ultimate load and specific strength results has been plotted in Figure 6.9, which shows that the ultimate load increases with slag inclusion although with increasing slag weight percentage it becomes consistent. However, the ultimate load of heat-treated composites significantly surpasses that of as-cast composites, which can be the outcome of the homogenization resulting from solution heat treatment [207]. The increase in ultimate load is due to overall strengthening. This indicates enhanced mechanical property result from waste material inclusion. The specific strength increases with increasing slag percentage for both heat-treated and as cast specimens, although, heat-treated composites show better specific strength. This improvement arises from the dissolution of alloying elements during solution treatment and subsequent precipitation hardening, which refine the microstructure and enhance the load transfer between the aluminium matrix and slag reinforcement. The highest specific strength has been observed for solution treated 7 wt.% slag reinforced specimens. The enhanced specific strength indicates higher strength to weight ratio of waste incorporated aluminium matrix composites. Similar enhancement in tensile properties has been reported in the works of Kumar [208], Saini et al. [161].

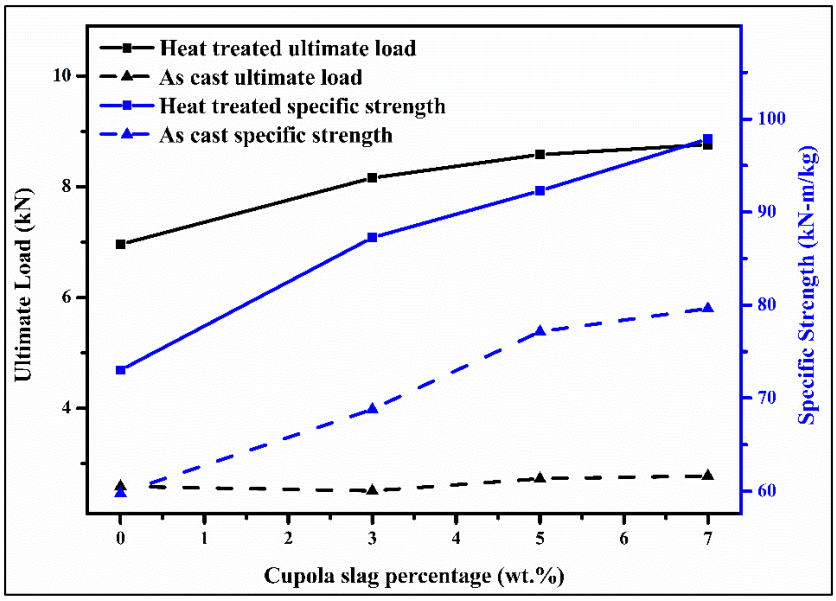

Figure 6.9 Ultimate load and specific strength vs slag content plot

The toughness has been calculated using area under the curve of stress-strain diagram. The results of toughness have been demonstrated in Figure 6.10 showing enhanced toughness for 7 wt.% slag reinforced composites. The heat-treated composites

observed to have better toughness as expected from the tensile property results. This increased toughness would allow the novel slag reinforced composites to be used in applications required sudden contact and release such as clutch plates of automobile [209,210].

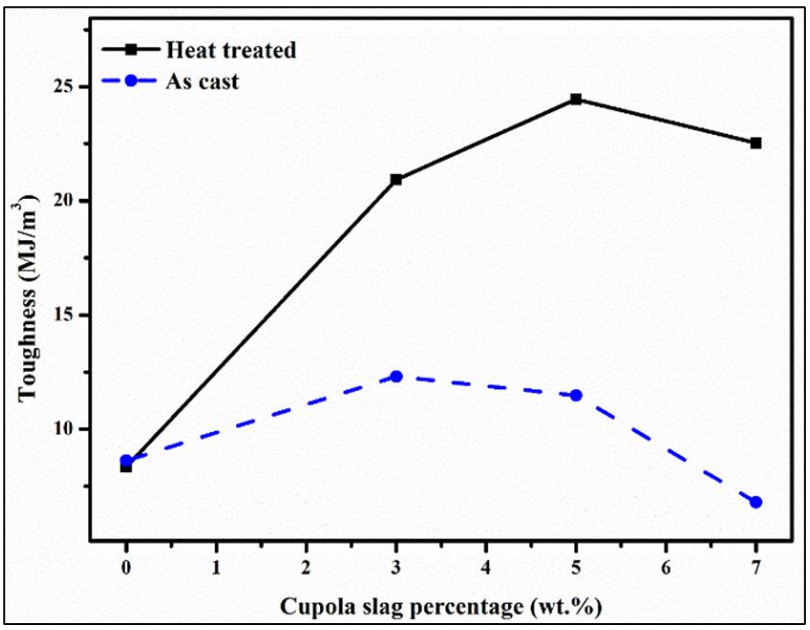

Figure 6.10 Toughness plot

The fractured surface of the tensile test specimens has been analysed using SEM to introspection into fractography which may reveal the fracture mechanisms. The low magnification fractography images has been presented in Figure 6.11 (a – d). Figure 6.11 (a) depicts fracture surface for base LM11 alloy showing a cleavage and dimples indicating ductile fracture. The cupola slag inclusion has induced brittleness into the composites as evidenced by flat facets with nominal grooves and tear ridges as depicted in Figure 6.11 (b – d). The higher magnification fractography has been presented in Figure 6.12 (a – d). The mountains and valley structure has been visible in case of base LM11 alloy where as other composites show flat faces with depth of valleys and ridges of tearing indicating a mixed mode of fracture. The strengthening by hindrance in crack propagation has been visible in Figure 6.12 (b) and (d). The fractography indicates similar results when compared with as cast composites however the amount of tear ridges increased in heat-treated composites which indicates greater strength in case of heat-treated composites.

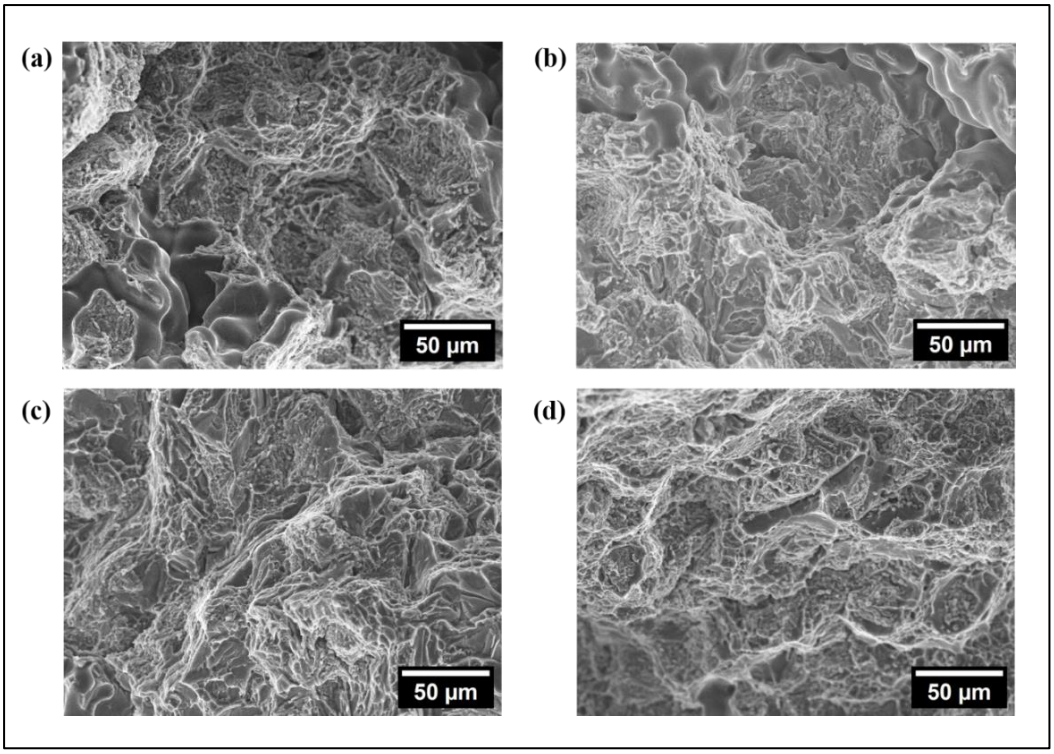

Figure 6.11 Scanning electron microscopy fractography for heat-treated (a) LM11, (b) LM11/3wt.%CS (c) LM11/5wt.%CS and (d) LM11/7wt.%CS

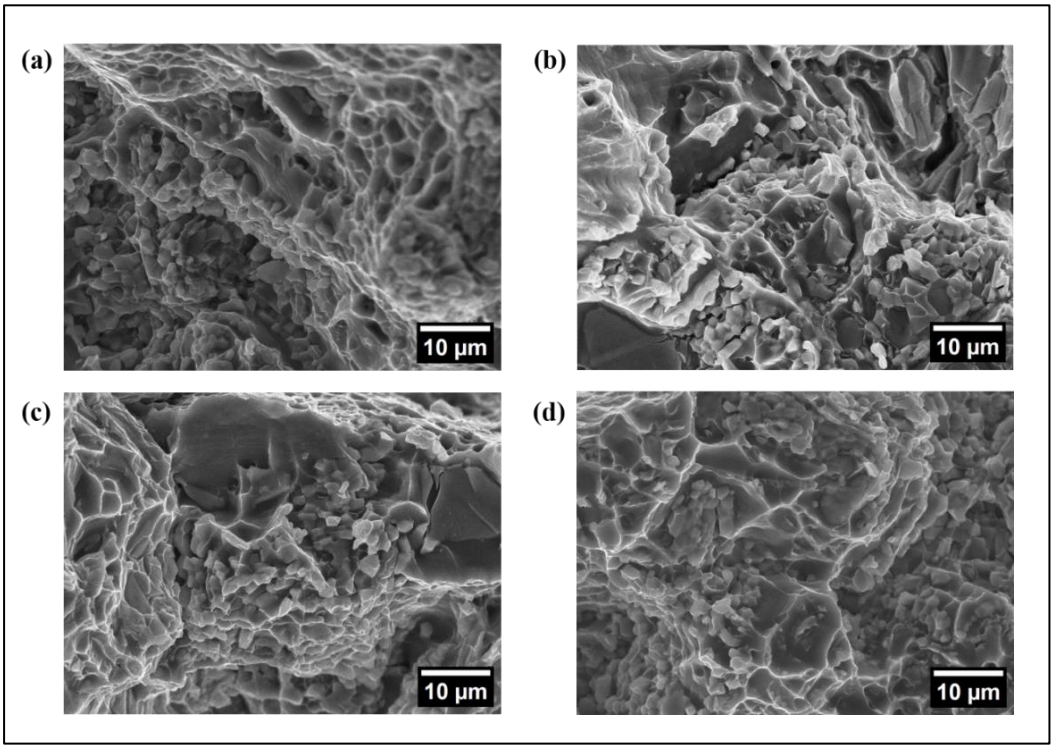

Figure 6.12 Higher magnification (2000×) scanning electron microscopy fractography for heat-treated (a) LM11, (b) LM11/3wt.%CS (c) LM11/5wt.%CS and (d) LM11/7wt.%CS

6.4.Effect on machinability

The results have been documented in this section with adequate explanation of underlying mechanisms and trends. The efficiency and quality of novel composites depend on the machinability behaviour.

6.4.1. Cutting force

The machinability of a material is highly influenced by the force requirement for machining. Thus, cutting force is measured. The cutting force is obtained in 3 directions (F_x, F_y and F_z) and the resultant force has been treated cutting force (F). The force required for cutting for all the variations of process inputs has been presented in Figure 6.13. In the inset of Figure 6.13 the cutting force factorial plot has been presented. It is evident from Figure 6.13 that with higher feed and spindle speed the force increases. This increasing trend is visible as higher speed and feed yields increased uncut chip thickness which increases the shear zone which requires more force to shear leading to increased force requirements [202,211]. Initially the cutting force reduces slightly with addition of cupola slag particle but it increases sharply with addition of 7 wt.% of cupola slag. The decrease of cutting force with slag inclusion is the result of self-lubrication and refined grains that allows the cracks to propagate easily facilitating ease of cutting [173]. However, the sudden increase with 7 wt.% slag is due to agglomeration and excessive porosity which hinders the cutting by hardening of the workpiece [212]. It is noteworthy, that in heat treated condition cutting force requirement increases as compared to the cutting force requirement at as cast condition shown in Figure 5.1. This is attributed to the fact that in the as-cast state, cupola slag particles are weakly bonded to the LM11 matrix, leading to easier particle pull-out that actively participate in micro cutting and fracture during machining, which lowers resistance to cutting. However, the matrix undergoes strengthening due to phase redistribution and spheroidization of silicon after solution treatment. Particle–matrix interfaces become stronger and more effective in load transfer, reducing pull-out and forcing the cutting tool to shear through intact, harder regions increasing the required cutting force. Kannan et al. [69] and Saini et al. [73] have reported similar trends of force requirement in turning of AMCs without cutting fluid.

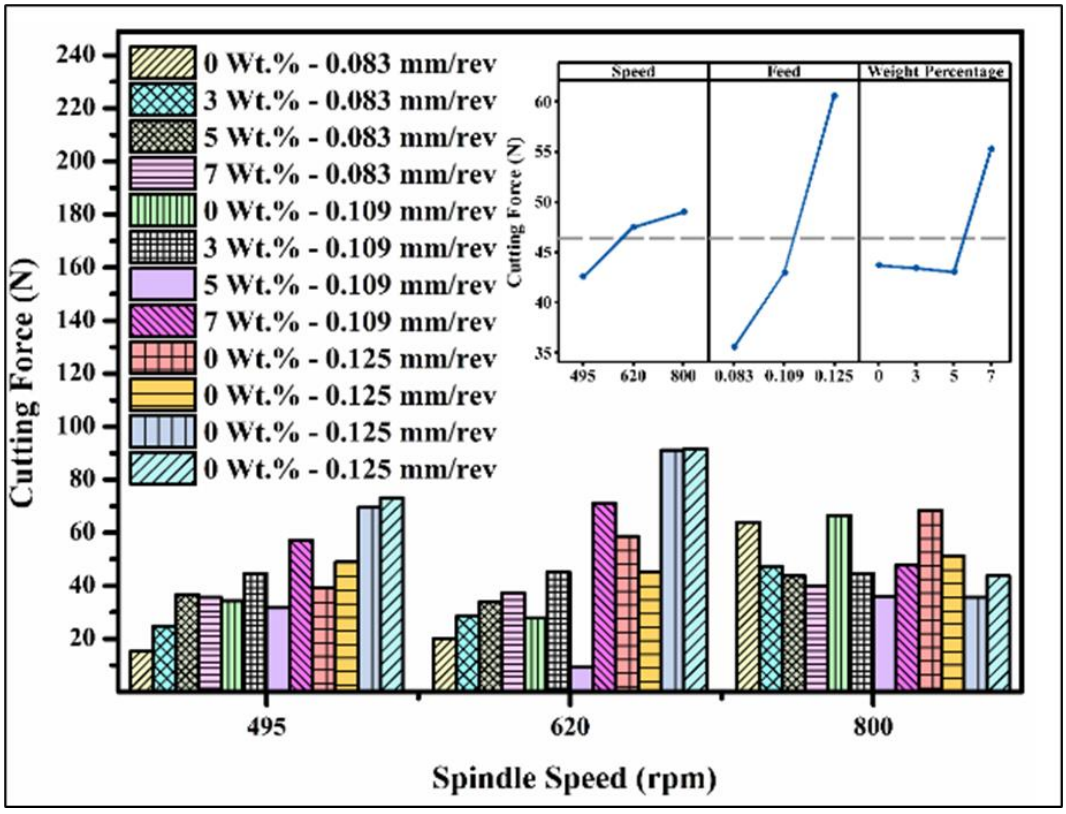

Figure 6.13 Impact of process inputs on cutting force for dry turning of heat-treated composites (inset: factorial plots for cutting force)

6.4.2. Surface roughness

The quality of the machining is accessed by the smoothness of the generated surface. Hence, surface roughness becomes an important index of machinability analysis. The roughness is measured at different position along the surface for each experimental run and the average roughness in terms of R_{rms} has been reported. The R_{rms} has been calculated from the peek and valley observed in measured surface profiles. The surface profile for the extremities such as highest (R_{rms} = 10.222 µm at speed = 495 rpm, feed = 0.0125 mm/rev on heat treated base LM11 alloy) and lowest (R_{rms} = 2.567 µm at speed = 495 rpm, feed = 0.083 on heat treated 7wt.% slag incorporated LM11 composites) value of surface roughness values has been shown in Figure 6.14. Figure 6.14 depicts that profile of machined surface has been changes greatly with changing parameters.

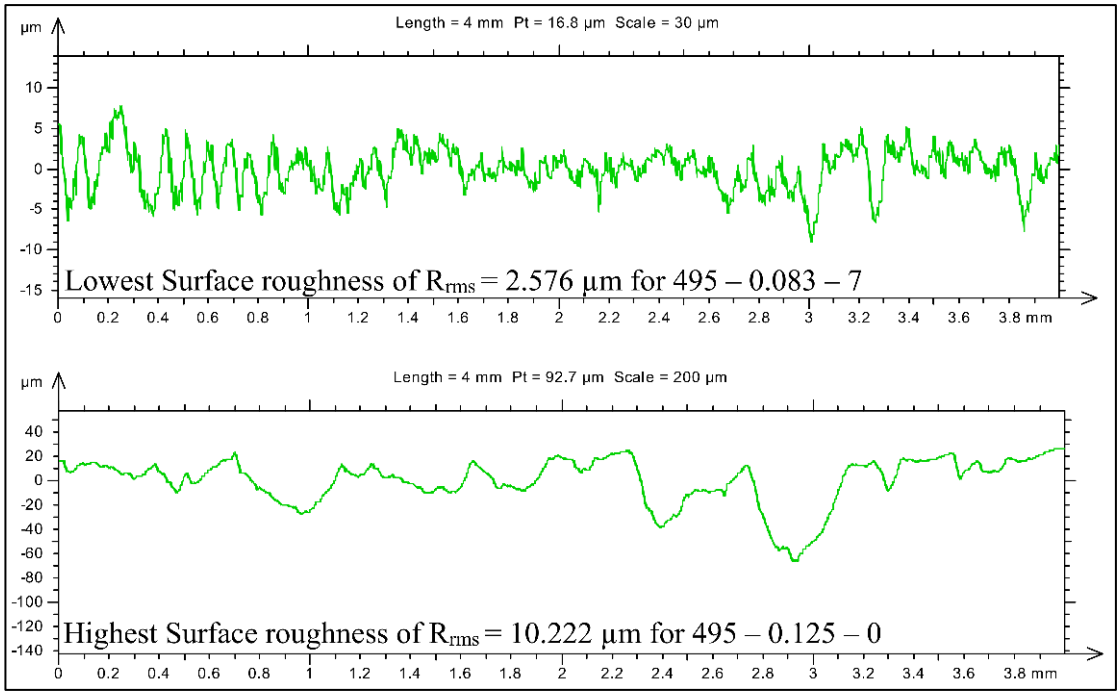

Figure 6.14 Surface profiles of best and worst machined surface of heat-treated composites

The dependency of the surface roughness on inputs has been represented graphically on spindle speed versus surface roughness plot presented in Figure 6.15. The best surface has been obtained for 7 wt.% slag included composite in low feed and low speed. The inset of Figure 6.15 represents the factorial plot for surface roughness. Figure 6.15 depicts that higher speed and feed rate results in deteriorated surface integrity. As that with higher values of spindle speed and feed, area of tool-work piece contact increases which in result increases the rubbing action leading to higher surface roughness [213]. Moreover, increasing feed rate and spindle speed results in increase of frictional heat in tool workpiece interface which may blunt the tool tip by softening that changes the nose radius resulting deteriorated surface integrity [214]. The factorial plot shows that with addition of secondary CS particulate the surface roughness improves and 7 wt.% slag reinforced composites yield lowest roughness. The improvement of machined surface integrity by cupola slag reinforcement can be explained by assisted micro cutting and self-lubrication of the reinforcements. The hard abrasive ceramic cupola slag particles have small protrusions with sharp cutting edges, thus when breaks from the matrix and rub between tool workpiece surface acts as micro cutting tool and smoothen the machined surface. The self-lubricating properties of oxides and sulphides of cupola slag lowers the tool interface friction which improves the surface integrity.

Research by Pugazhenthi et al. [56], Saini et al. [73] on machining behaviour of Al-TiB_2 and Al-granite marble dust composites, respectively concluded similar observations.

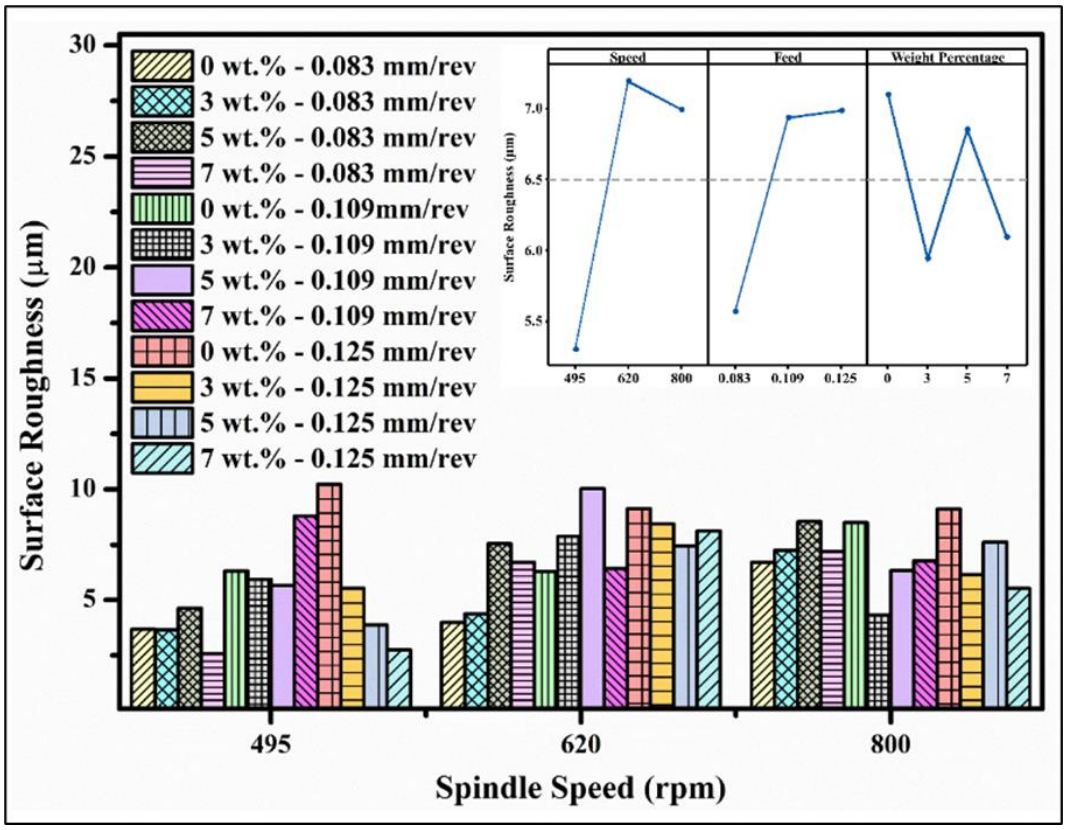

Figure 6.15 Impact of inputs on surface integrity for dry turning of heat-treated composites (inset: factorial plots for surface integrity)

6.4.3. Material removal rate

MRR in conventional machining directly relates to the machining cost as with higher MRR the cost would reduce due to lower running time. Hence, MRR is one of the necessary indices in machinability study. The MRR for all the experimental runs has been presented in Figure 6.16. The highest MRR has been observed in 3 wt.% slag reinforced composites machined with high speed and high feed as shown in Figure 6.16. The factorial plot for MRR has been presented in the inset of Figure 6.16. The increase in feed and speed yields higher MRR as per Figure 6.16. Inclusion of cupola slag first increases the MRR then it's become stagnant with increasing cupola slag content. The rise in MRR with higher spindle speeds is because increased speed amplifies the stress at the chip-tool interface, facilitating crack propagation and thereby boosting MRR [64]. The increased feed rate increases the MRR by increasing the chip tool contact length which yields higher chip thickness [55]. The addition of cupola slag enhances the MRR as homogeneously distributed slag particles creates sites of crack initiation simplifying

the chip formation [188]. The results of MRR analysis are in alignment with the experiments of various academicians on machinability of AMCs [215,216].

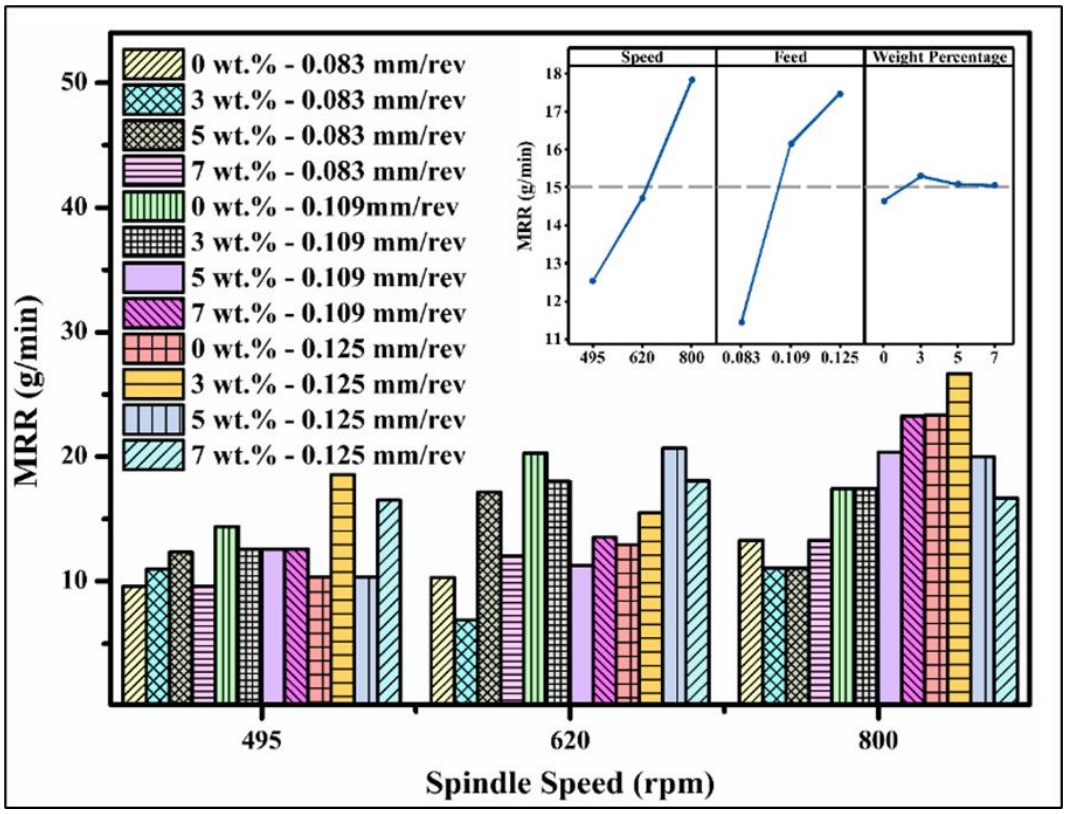

Figure 6.16 Impact of process inputs on MRR for dry turning of heat-treated composites (inset: factorial plots for MRR)

6.4.4. Power consumption

The energy aspect of turning is incomplete without analysis of power consumed while the process. The power consumption gets influenced by work piece material, cutting tool and machine tool. The conventional lathe used here was a robust machine hence very small amount of variation in power consumption has been observed. The variation of power consumed for all the speed, feed and cupola slag content has been shown in Figure 6.17. Although variation has not been visible in bar graphs, the factorial plot presented in the inset shows the influence of inputs on power consumed while turning. Figure 6.17 shows that rising spindle speed and feed first increased the power consumed and then it reduces. This reduction of power consumed indicates lower resistance to chip formation. This trend occurs because, initially, the increasing speed and feed enlarge the contact area, which in turn raises chip-tool friction and the temperature at the tool tip. This increased friction and higher temperature hinders the propagation of cracks in the shear zone resulting increased power consumption. Further

at higher feed and speed the chip tool interface temperature even more leading to localized softening of workpiece leading to lower power requirement for cutting [217]. Figure 6.17 also depicts that cupola slag inclusion decreases the power consumption with increasing slag weight percentage. This results from the lubrication and micro-cutting properties of the cupola slag particles. Moreover, the discontinuous microstructures also assisted the crack propagations reducing the power requirement for chip formation [218]. Bhushan [219] reported the similar trends of power required for turning SiC/Al composites.

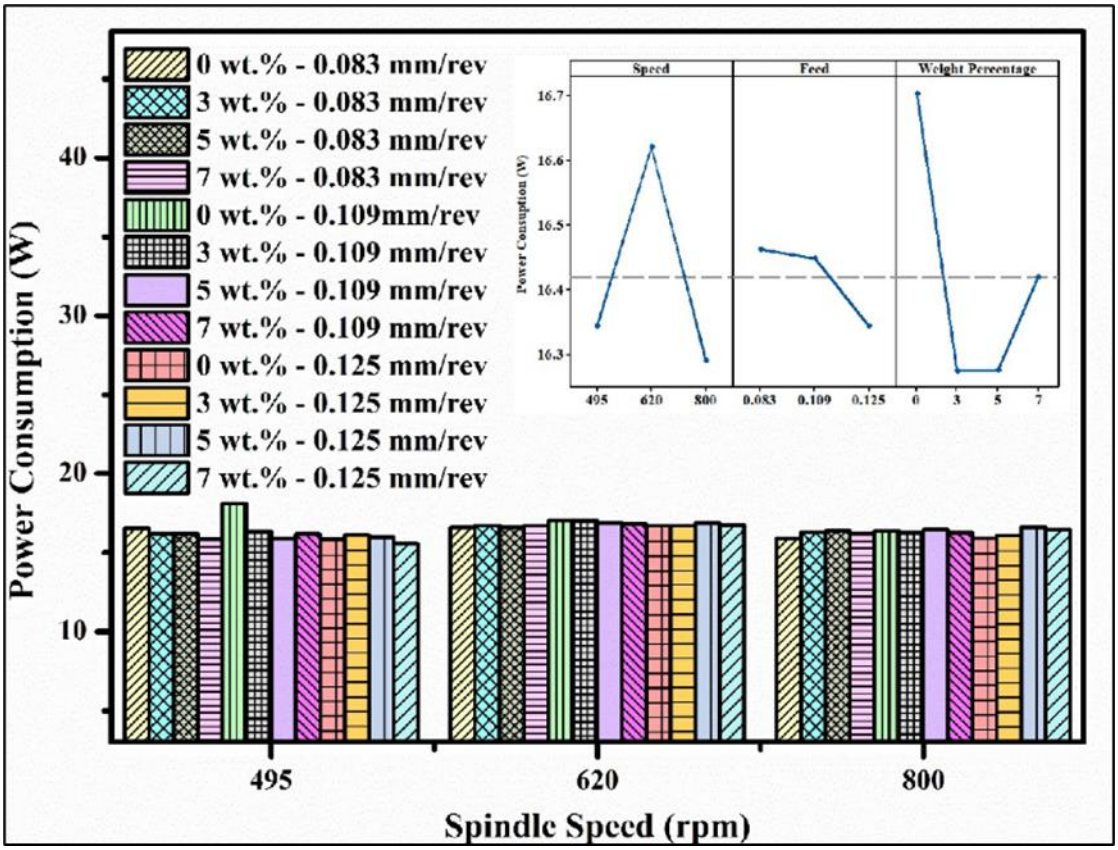

Figure 6.17 Impact of process inputs on power consumption for dry turning of heat-treated composites (inset: factorial plots for power consumption)

6.4.5. Tool wear

The experiments with carbide coated tool produces very nominal tool wear because of hard cutting tool inserts and only a distance of 50 mm has been turned using each cutting tool. The micrographs of tool wear have been presented in Figure 6.18 (a – f). The major wear has been occurred in terms of built-up edge (BUE) formation as there is secondary hard abrasive in composites. These hard abrasives hinder the cutting operation and increases the chip tool interface temperature resulting localized welding of chip material into the tip of tool inserts which creates BUE [179]. The crater and

flank wear were minimal for all the experiments. Hence, in this work only BUE has been considered as tool wear. The experiments indicate minimum tool wear of 12.245 µm for cutting condition 495 rpm spindle speed, 0.083 mm/rev feed rate and for base LM11 alloy. The rake and flank face for the lowest tool wear has been shown in Figure 6.18 (c) and Figure 6.18 (d) respectively. Figure 6.18 (e) shows the flank face of the tool with maximum tool wear where BUE is clearly visible. The rake face for the dame tool insert has been presented in Figure 6.18 (f). LM11/3wt.%CS turned with 800 rpm spindle speed and 0.083 mm/rev feed yields maximum tool wear of 462.338 µm.

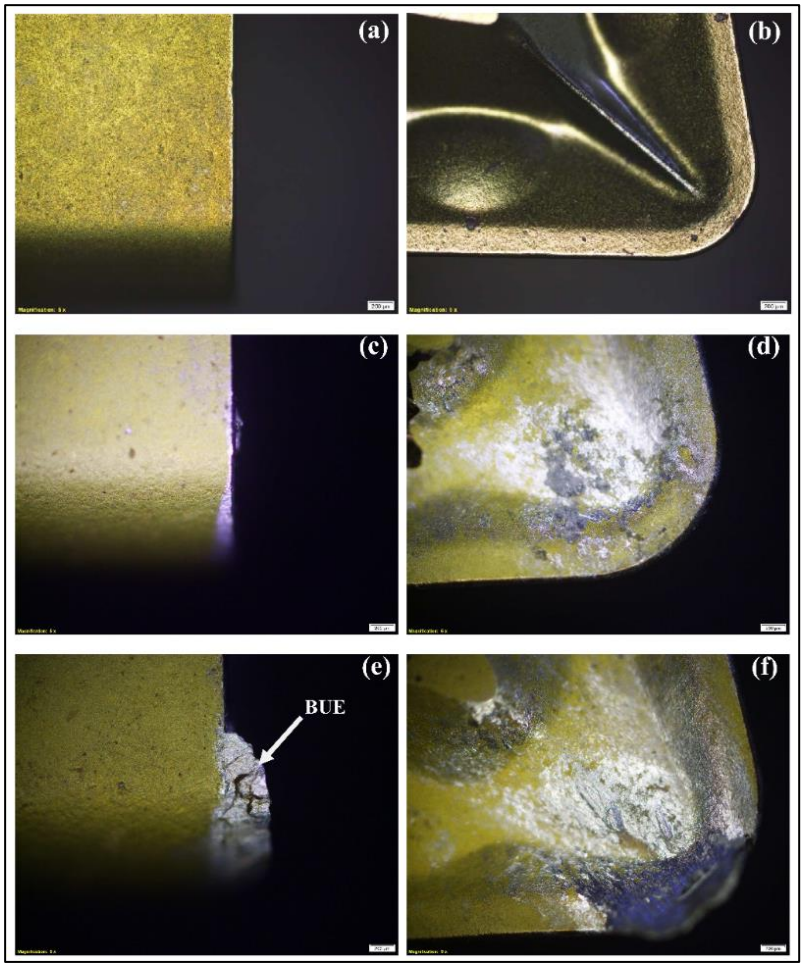

Figure 6.18 Morphology of tool insert for dry turning of heat-treated composites (a) before cutting: flank (b) before cutting: rake (c) nominal tool wear: flank d) nominal tool wear: rake (e) Maximum tool wear: flank (f) Maximum tool wear: rake

The trends of tool wear for all feed rate and cupola slag content have been shown in Figure 6.19, along with that in the inset the factorial plot for tool wear has been shown. Figure 6.19 depict that rising spindle speed and feed rate the wear decreases as at lower feed and spindle speed highest chip tool contact length has been observed. This leads to

higher rubbing action generating more frictional heat resulting in higher wear rate [181,220]. The tool wear increases with addition of secondary slag phase as compared to base LM11 alloy as hard discontinuous phase gets in contact with tool tip and increases the friction yielding higher interface temperature. It is noteworthy that with turning of composites with 7 wt.% slag inclusion shows very nominal wear. This decrease is due to the micro-cutting assistance provided by the hard and sharp abrasive particles. The higher slag content tends to get loose while turning and often get trapped in the chip tool interface. These sharp-edged slag particles rub the workpiece which assist the cutting and reduces the tool temperature and hence, reduces the tool wear [176]. Comparable results regarding tool wear have been reported by Radhika et al. [221] for hybrid AMCs and by Bertolini et al. [222] for Al/SiC composites.

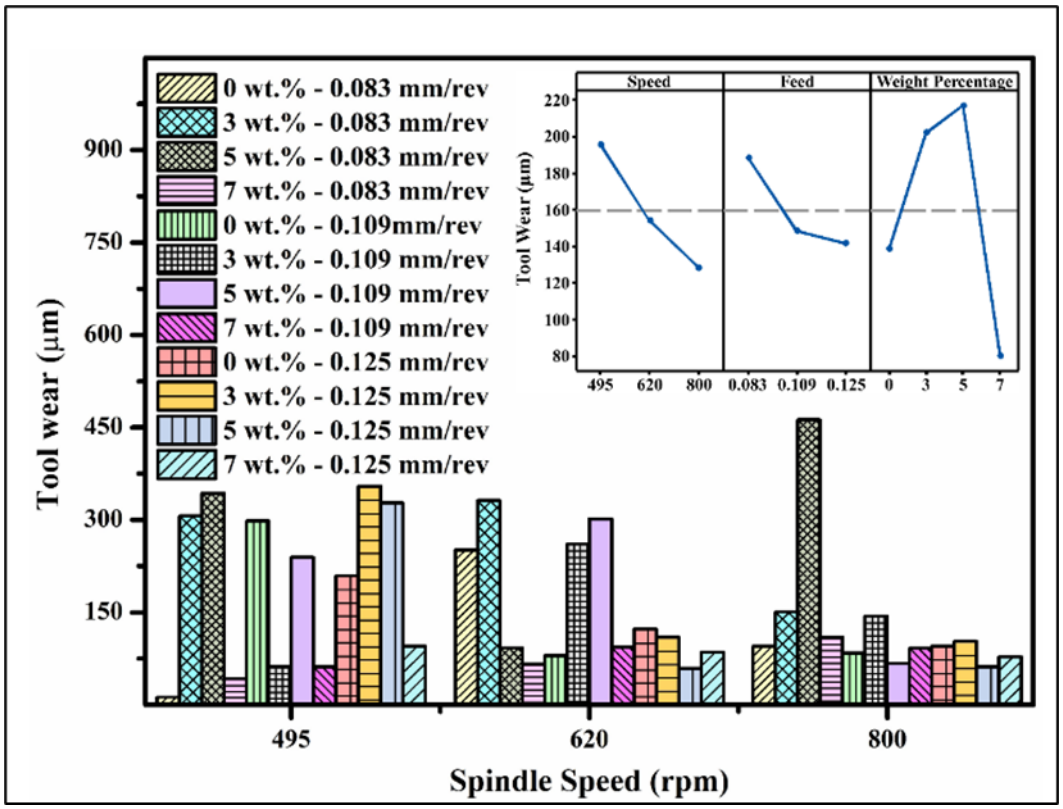

Figure 6.19 Impact of inputs on tool wear for dry turning of heat-treated composites (inset: factorial plots for tool wear)

6.4.6. Chip thickness

Figure 6.20 shows the impact of process inputs on thickness of the cut chips. The factorial plot for the same has been presented as inset of Figure 6.20. At a spindle speed of 495 rpm, feed of 0.083 mm/rev, and 7 wt.% slag-reinforced composites, the nominal chip thickness measures 0.086 mm. However, the maximum chip thickness is recorded

at a speed of 620 rpm, feed of 0.125 mm/rev, and 7 wt.% slag-reinforced composites, resulting in chips with a thickness of 0.764 mm. Figure 6.20 depicts that rising spindle speed and feed chip thickness increases as strain in chip tool interface is higher with higher feed and speed yielding larger cutting shear yielding higher chip thickness [184]. Moreover, it may be result of larger tool and workpiece contact area. This large contact area tends to remove more material increasing the chip thickness [223]. The increasing weight percentage of cupola slag first decreases then increases the chip thickness. The decrease in chip thickness due to presence of discontinuous hard abrasive in composites while in case of turning of LM11/7wt.%CS composites the loose slag particles increases the rubbing area and assist in cutting yielding increased chip thickness. The trends of chip thickness have been in alignment with the works of Kannan et al. [69]. The increased chip thickness results in increased MRR hence improved the machinability.

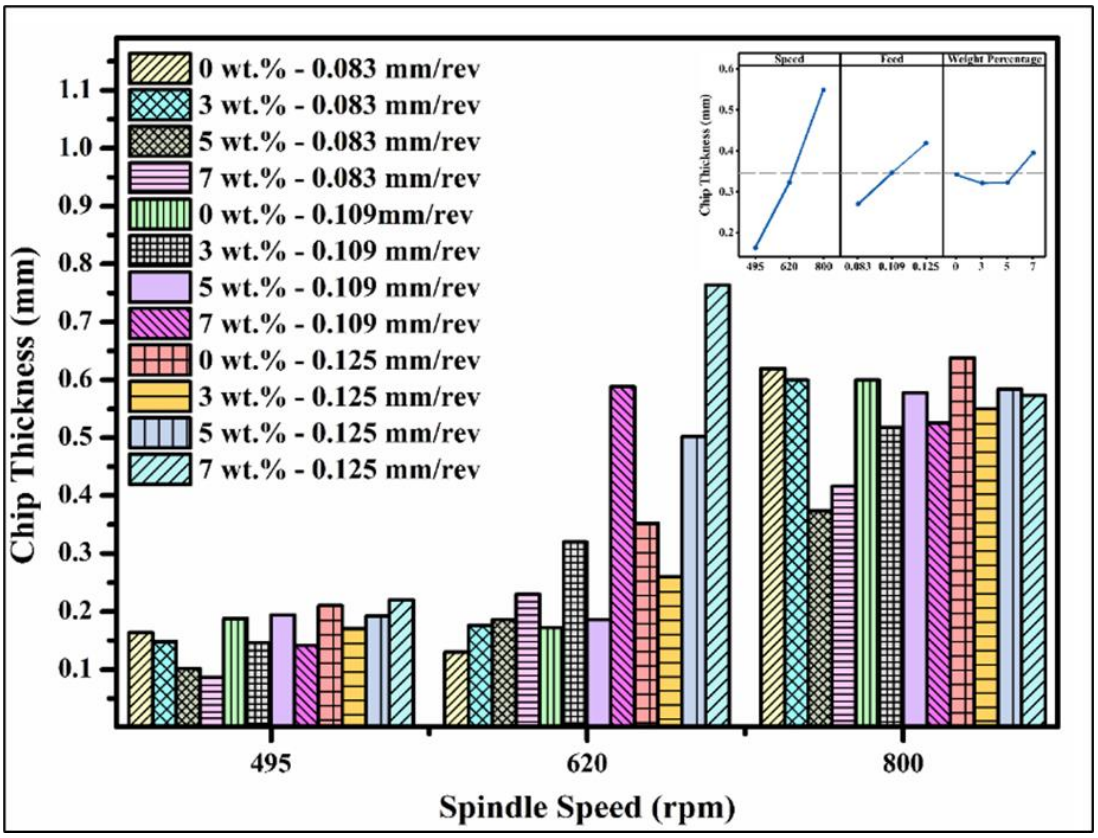

Figure 6.20 Impact of process inputs on chip thickness for dry turning of heat-treated composites (inset: factorial plots for chip thickness)

6.4.7. Chip analysis

Analysis of chips gives an introspection about the physical machining process. The photographs of chips formed for different cutting condition has been illustrated in

Figure 6.21 to Figure 6.23. The chips formed for feed of 0.083 mm/rev has been shown in Figure 6.21 (a – l). It is evident from Figure 6.21 (a, e and i) that turning of base LM11 alloy has produced somewhat continuous tubular spring type chips for all the speed. The increase in weight percentage and speed leads to discontinuous chip formation. This finally leads to formation of segmented C type chip formation for turning of LM11/7wt.%CS composites at 800 rpm spindle speed as shown in Figure 6.21 (l). This chip behaviour trend is noted as both speed and slag content rise, leading to heightened thrust force caused by an increase in hard secondary particles within the matrix, consequently fracturing the chips [49].

Figure 6.22 (a – l) represents the chips formed in turning with medium feed of 0.109 mm/rev. Figure 6.22depicts that the thickness of chips has increased as compared with low feed chips due to larger tool workpiece contact area. The base LM11 turning formed spring type chips while with incorporation of secondary slag particle the spring type chips transformed gradually to segmented C type chips. The increase in speed results in increasing the radii of helix of the spring type and C type chips. The increased speed and weight percentage results in higher strain which results in large radii chips [185]. Heavier chips with BUE have been observed for 0.125 mm/rev feed as per Figure 6.23 (a – l). The increase in slag percentage changes the chips from segmented spring type to large radii C type chips to segmented C type gradually as depicted in Figure 6.23. The speed rise first increases the radii of the chips formed as shown in Figure 6.22 (e – h). Meanwhile, further increase in speed at higher feed rate produces segmented C type chips with higher chip thickness as observed in Figure 6.23 (i – l). The increase in speed feed and slag content make the machining easy due to complex action of higher contact area, micro cutting assistance by loose slag particles, lower chip tool time of contact and easy chip flow [186].

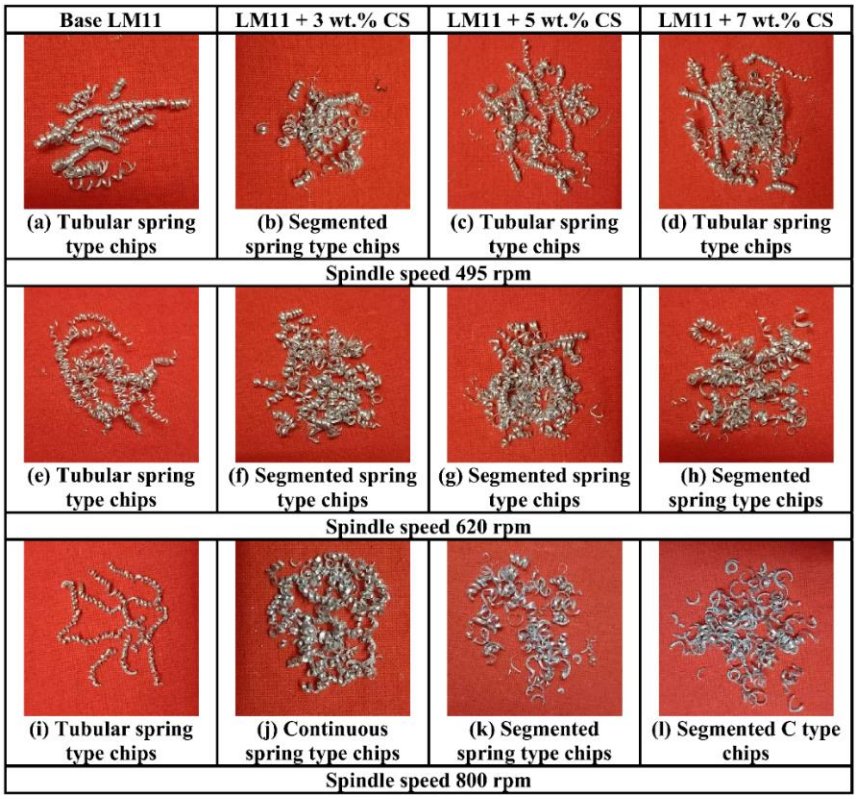

Figure 6.21 (a – l) Photograph of chips formed in turning of heat-treated composites for 0.083 mm/rev feed

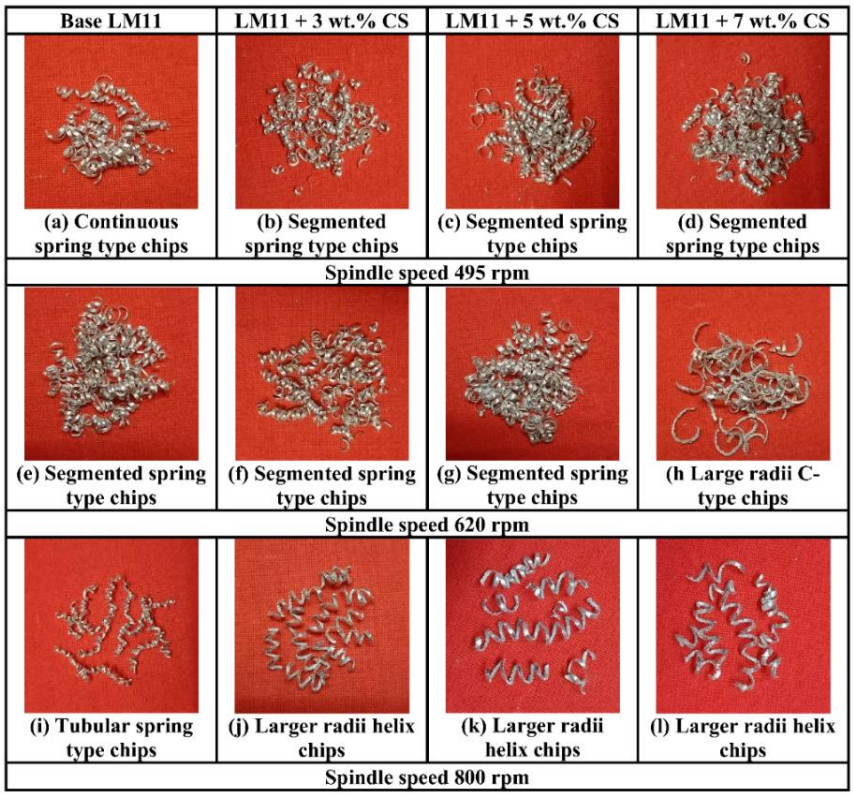

Figure 6.22 (a – l) Photograph of chips formed in turning of heat-treated composites for 0.109 mm/rev feed

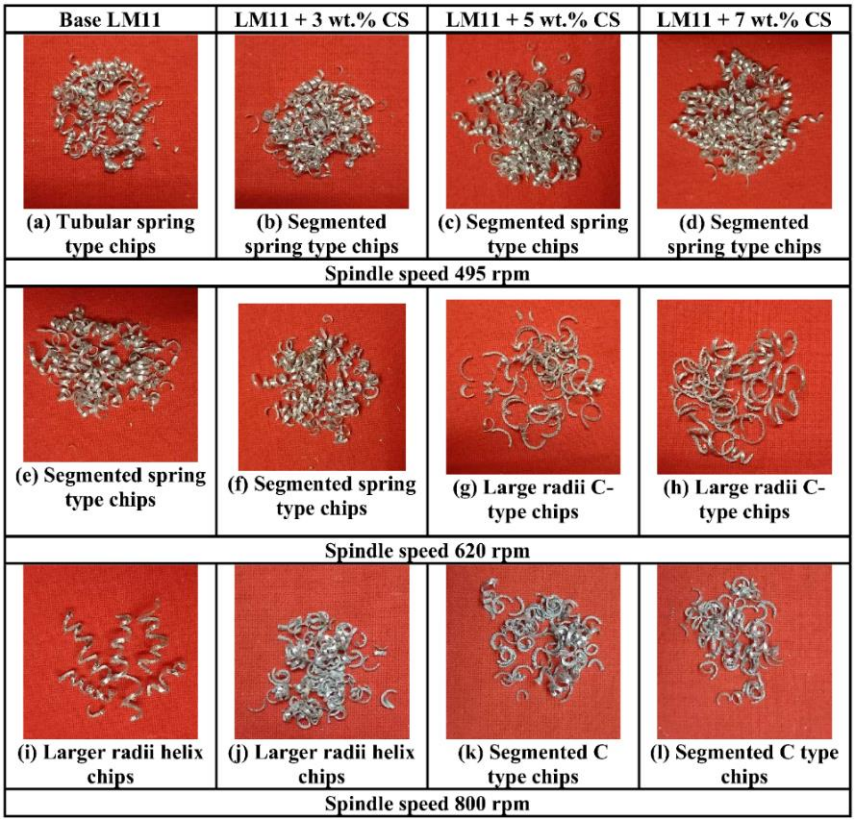

Figure 6.23 (a – l) Photograph of chips formed in turning of heat-treated composites for 0.109 mm/rev feed

6.4.8. Comparative analysis

The responses of machining indices have been normalized to a percentage scale for the sake of comparative analysis. The average machinability indices for as cast composites denoted as LM11, LM11/3wt.%CS, LM11/5wt.%CS and LM11/7wt.%CS have been taken from the previous chapter. The maximum value for each index has been assigned as 100 and subsequently the other values have been converted to percentage of the maximum value. These percentage values have been presented in a radar diagram presented in Figure 6.24. In Figure 6.24, the dashed lines depict machinability data for dry turning of as cast composites, while the solid lines represent the same data for heat-treated composites. It is depicted Figure 6.24 that heat-treated composites show better machinability in terms of similar power consumption, cutting force, lower tool wear, surface roughness, higher MRR and chip thickness when compared with as cast composites. These changes in machinability indices indicate improvement in overall machinability in heat-treated composites. This enhancement in machinability could stem from the segregation of Cu at grain boundaries in the Al-Cu system in its as-cast state, leading to non-uniform distribution. The solution heat treatment homogenizes the alloy and put Cu into the solution yielding better properties with equiaxed

microstructures [224]. The comparative analysis on heat-treated composites as shown in Figure 6.24 depicts that lowest surface roughness and tool wear obtained for LM11/7wt.%CS turning. The same composites yield maximum MRR and chip thickness. Lowest cutting force has been recorded in the machining of LM11/5wt.%CS. The power consumed for turning of heat-treated composites has been observed to be similar for all the composites. Hence, an observation can be drawn from comparative analysis of machining indices that by incorporating cupola slag the machinability has been improved. The hard and abrasive nature of cupola slag facilitated this enhancement, refinement of grains while solidification, homogenisation while solution treatment and assistance in cutting by lose slag particles [189,190].

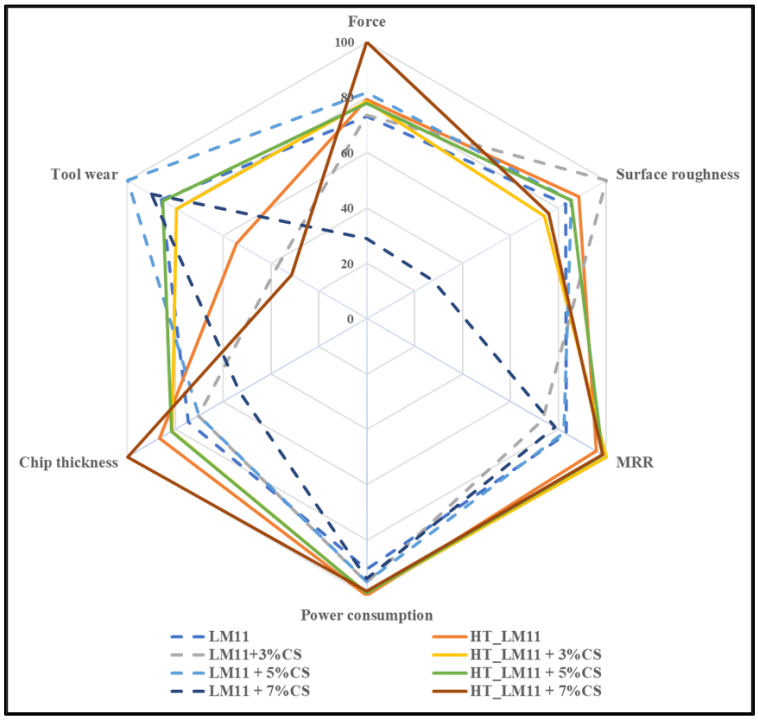

Figure 6.24 Comparison of machinability indices

6.5.Summary

This study presents the fabrication and performance analysis, encompassing physical, mechanical and machinability aspects, of heat-treated newly developed LM11 metal matrix composites reinforced with cupola slag. The key observations drawn from this investigation are outlined below:

- The microstructural analysis shows that successful incorporation of slag particles in matrix. The grain size in the LM11 alloy decreased significantly with the inclusion of cupola slag, from 138.9 µm for the base alloy to 48.5 µm, 38.9 µm, and 27.7 µm with 3%, 5%, and 7% slag reinforcement, respectively. SEM imaging confirmed that

slag particles were well-bonded within the matrix, providing a cleaner interface and minimal porosity.

- The density decreased slightly with higher slag content due to slag's lower density compared to the base LM11. The microhardness increased by 13.1%, 23.8%, 25.3%, and 28.7% for the 0%, 3%, 5%, and 7% slag inclusions, respectively, indicating improved strength due to enhanced load-bearing capacity and grain refinement.
- The tensile properties observed to be improved in terms of ultimate tensile stress, yield stress, ultimate load, specific strength and toughness by incorporation of cupola slag in the base LM11 alloy. Ultimate tensile strength (UTS) showed a marked improvement, with the 7 wt.% slag composites achieving a UTS increase of approximately 25% over the base alloy in heat-treated form and over 70% when compared to the as-cast base. Additionally, specific strength and toughness increased, making the material suitable for high-stress applications, such as in the aerospace and automotive industries.
- The machinability is enhanced in terms of machinability indices lower cutting force, surface roughness, power computation, tool wear and chip thickness with higher MRR, in case of heat-treated composites with slag inclusion. Heat-treated composites with 7 wt.% slag displayed optimal machinability, with reductions in cutting force (approximately 5% less than lower slag composites), surface roughness, and power consumption, while achieving the highest material removal rate (MRR) and chip thickness. The improvement in machinability is attributed to the slag's self-lubricating properties and its assistance in micro-cutting, enhancing both performance and tool life.
- This research demonstrates a sustainable approach by repurposing industrial waste (cupola slag) into value-added composite materials, providing a cost-effective alternative for advanced applications.

This comprehensive analysis indicates that cupola slag-reinforced LM11 composites are promising materials with enhanced mechanical and machinability properties, providing an effective way to utilize industrial waste sustainably. These findings highlight the potential for further applications in lightweight, high-strength engineering fields.

Chapter 7

Concluding Remarks

This comprehensive experimental investigation demonstrated the potential of an industrial waste, cupola slag reuse as reinforcement in AMCs with LM11 alloy as matrix. The rigorous research systematically evaluated mechanical, microstructural and machinability characteristics of newly developed slag reinforced composites. The subsequent sections in this chapter presents the key conclusion and future direction of development in this domain.

7.1. Conclusions

The study introspected the quality of cast composites across various particle size, weight percentage and processing condition while turning along with the effect of solution heat treatment. The key conclusions drawn from the introspection has been presented as follows,

Microstructural analysis and grain refinement

Incorporation of cupola slag was successful and led to grain refinement from approximately 151.23 µm for the base LM11 alloy in as cast condition to 57.25 µm, 43.10 µm, and 32.29 µm for as cast composites with 3 wt.%, 5 wt.%, and 7 wt.% slag reinforcement, respectively. The heat treatment even reduces the grain size reduced to 138.89 µm, 48.46 µm, 38.83 µm and 27.70 µm for heat treated base alloy and composites with 3 wt.%, 5 wt.%, and 7 wt.% slag reinforcement, respectively. Moreover, uniform particle distribution along with clean matrix-reinforcement interface with minimal porosity has been confirmed through SEM-EDS analyses.

Mechanical property enhancement

Cupola slag inclusion as reinforcement to LM11 matrix enhances the mechanical properties of the alloy in terms of microhardness, tensile strength and reduction of density and weight of the composites. The microhardness increased approximately 30% in as cast condition and 47% in heat-treated condition by 7 wt.% cupola slag inclusion reaching a highest value of 105.97 Hv. The heat-treated composites exhibit a massive 70% improvement in ultimate tensile strength, reaching 243.26 MPa for 7 wt.% slag reinforced composites compared to 141.45 MPa for as cast base alloy. The toughness and specific strength also enhanced. The density has been reduced by 11% for 7 wt.% slag addition, contributing to the lightweight material design. These enhancements suggest improved material durability, making the novel cupola slag reinforced composites suitable for high-performance applications.

Machinability

Machining studies revealed improvements in cutting force, tool wear, and surface roughness with increasing slag content due to slag inclusion which enhances further for heat-treated composites. The self-lubricating nature of slag particles contributed to enhanced machinability. Notably, the 7 wt.% slag composite exhibited optimal machinability, with the highest material removal rates (MRR), reduced cutting force and surface roughness. The 7 wt.% heat-treated composite exhibited approximately 5% lower cutting forces compared to lower slag composites, minimum surface roughness of 1.36 μm and the highest material removal rate of 22.5 g/min at 800 rpm and 0.109 mm/rev. In addition, the chips produced were continuous, spring-like with larger curl radii, facilitating ease of machining. Enhanced machinability indicates the potential of high precision machining for novel slag reinforced composites.

Sustainability and Practical Implications

The study demonstrated successful reuse of solid industrial waste providing enhanced material properties while reducing the environmental impact. The development of cupola slag reinforced composites with tailored properties of high-performance lightweight material supports sustainable engineering practices. This work also provides a novel approach to global solid waste management. Such composites can be used in the automotive sector for components like brake rotors, connecting rods, cylinder heads, and suspension parts. They are suitable for brackets, housings, and

structural panels that require both lightweighting and strength in aerospace applications. In machinery and tooling, they are useful for wear-prone parts where improved toughness and machinability are important.

Limitations

The study demonstrated promising results for cupola slag reuse as composite reinforcement but has some limitations. One key concern lies in variability of cupola slag whose chemical composition and particle morphology may differ across foundries, potentially affecting the uniformity and repeatability of fabricated composite properties. Additionally, processing challenges such as lower wettability of slag particles restrict the feasible reinforcement limit to 7 wt.% in stir casting, thereby narrowing the scope for further inclusion. Beyond these, long term durability aspects such as fatigue, thermal stability under cyclic loading, wear and corrosion resistance remain unexplored and must be carefully addressed before these composites can be deployed in critical engineering applications. Moreover, while laboratory-scale fabrication has proven effective, industrial scalability requires additional investigation to validate cost-effectiveness, consistency, and large-scale production feasibility.

7.2. Future scope

The future scope of this experimental work presents several promising avenues for exploration and innovation. Firstly, application based real world properties of the composites can be evaluated through analysing dynamic loading behaviour such as fatigue and impact tests. Secondly, fabrication process parameter can be optimized along with inclusion of additive manufacturing to reach more intricate microstructure with enhanced properties. Thirdly, this work pioneered a way to diversify and expand the sustainable low-cost composite development by establishing the feasibility of waste utilization as reinforcement of composites through sustainability-focused assessments such as life cycle analysis (LCA) and techno-economic evaluations will strengthen the environmental and economic feasibility claims. Such analyses will validate the practicality of utilizing waste-derived reinforcements in real-world scenarios. Additionally, comprehensive investigation into corrosion and wear performance under various condition may facilitate these composites applicability in harsh or marine environments. Moreover, development of hybrid composites with other reinforcement to tailor specific application-oriented properties like thermal or electrical conductivity

can be studied. This work establishes a robust foundation for integration of industrial waste derived economic composites into advanced engineering applications. The industrial collaboration would be explored further for validating large scale feasibility of these waste reinforced composites. The research simultaneously addressed environmental concerns along with growing demand of new age high performance materials.

References

[1] D.B. Miracle, Metal matrix composites - From science to technological significance, Compos. Sci. Technol. 65 (2005) 2526–2540. https://doi.org/10.1016/j.compscitech.2005.05.027.

[2] J. Mukerji, Ceramic matrix composites, Def. Sci. J. 43 (1993) 385–395. https://doi.org/10.14429/dsj.43.4292.

[3] B. Parveez, M.I. Kittur, I.A. Badruddin, S. Kamangar, M. Hussien, M.A. Umarfarooq, Scientific Advancements in Composite Materials for Aircraft Applications: A Review, Polymers (Basel). 14 (2022). https://doi.org/10.3390/polym14225007.

[4] C. Soutis, Fibre reinforced composites in aircraft construction, Prog. Aerosp. Sci. 41 (2005) 143–151. https://doi.org/10.1016/j.paerosci.2005.02.004.

[5] S. Sajan, D. Philip Selvaraj, A review on polymer matrix composite materials and their applications, Mater. Today Proc. 47 (2021) 5493–5498. https://doi.org/10.1016/j.matpr.2021.08.034.

[6] D.K. Rajak, D.D. Pagar, R. Kumar, C.I. Pruncu, Recent progress of reinforcement materials: A comprehensive overview of composite materials, J. Mater. Res. Technol. 8 (2019) 6354–6374. https://doi.org/10.1016/j.jmrt.2019.09.068.

[7] S. Simões, High-Performance Advanced Composites in Multifunctional Material Design: State of the Art, Challenges, and Future Directions, Materials (Basel). 17 (2024). https://doi.org/10.3390/ma17235997.

[8] S.K. Sharma, K.K. Saxena, K.H. Salem, K.A. Mohammed, R. Singh, C. Prakash, Effects of various fabrication techniques on the mechanical characteristics of metal matrix composites: a review, Adv. Mater. Process. Technol. 10 (2024) 277–294. https://doi.org/10.1080/2374068X.2022.2144276.

[9] J.W. Kaczmar, K. Pietrzak, W. Włosiński, The production and application of metal matrix composite materials, J. Mater. Process. Technol. 106 (2000) 58–67. https://doi.org/10.1016/S0924-0136(00)00639-7.

[10] I.A. Ibrahim, F.A. Mohamed, E.J. Lavernia, Particulate reinforced metal matrix composites - a review, J. Mater. Sci. 26 (1991) 1137–1156. https://doi.org/10.1007/BF00544448.

[11] S. Gangwar, V.K. Pathak, A critical review on tribological properties, thermal behavior, and different applications of industrial waste reinforcement for composites, Proc. Inst. Mech. Eng. Part L J. Mater. Des. Appl. 235 (2021) 684–706. https://doi.org/10.1177/1464420720972434.

[12] M.K. Surappa, Aluminium matrix composites: Challenges and opportunities, Sadhana - Acad. Proc. Eng. Sci. 28 (2003) 319–334. https://doi.org/10.1007/BF02717141.

[13] K.U. Kainer, Basics of Metal Matrix Composites, Met. Matrix Compos. Cust. Mater. Automot. Aerosp. Eng. (2006) 1–54. https://doi.org/10.1002/3527608117.ch1.

[14] S. Banerjee, S. Poria, G. Sutradhar, P. Sahoo, Abrasive wear behavior of WC nanoparticle reinforced magnesium metal matrix composites, Surf. Topogr. Metrol. Prop. 8 (2020). https://doi.org/10.1088/2051-672X/ab82a1.

[15] A.K. Yadav, N. Kumar, Mechanical and thermal behaviour of stir cast sillimanite/red mud/LM25 Al-alloy metal matrix composite, Materwiss. Werksttech. 54 (2023) 1648–1658. https://doi.org/10.1002/mawe.202300090.

[16] B.V. Ramnath, C. Elanchezhian, R.M. Annamalai, S. .Aravind, T.S.A. Atreya, V. Vignesh, C. Subramanian, Aluminium metal matrix composites - A review, Rev. Adv. Mater. Sci. 38 (2014) 55–60.

[17] M. Shukla, S.K. Dhakad, P. Agarwal, M.K. Pradhan, Characteristic behaviour of aluminium metal matrix composites: A review, Mater. Today Proc. 5 (2018) 5830–5836. https://doi.org/10.1016/j.matpr.2017.12.180.

[18] P. Samal, P.R. Vundavilli, A. Meher, M.M. Mahapatra, Recent progress in aluminum metal matrix composites: A review on processing, mechanical and wear properties, J. Manuf. Process. 59 (2020) 131–152. https://doi.org/10.1016/j.jmapro.2020.09.010.

[19] C.R. Dandekar, Y.C. Shin, Modeling of machining of composite materials: A review, Int. J. Mach. Tools Manuf. 57 (2012) 102–121. https://doi.org/10.1016/j.ijmachtools.2012.01.006.

[20] O.O. Joseph, K.O. Babaremu, Agricultural waste as a reinforcement particulate for aluminum metal matrix composite (AMMCs): A review, Fibers 7 (2019). https://doi.org/10.3390/fib7040033.

[21] S.K. Tripathy, A.K. Senapati, A review on turning analysis of industrial waste reinforced aluminum metal matrix composite, Mater. Today Proc. 33 (2020) 5740–5745. https://doi.org/10.1016/j.matpr.2020.05.731.

[22] G. Hatti, G.J. Naveen, V. Koti, V.S. Uppin, S.V. Lingaraju, S. Janamatti, V. V. Hokrani, S.N. Pujar, Green metal matrix composites: A multi-faceted study on Al alloy composites with egg shell powder and silicon carbide as reinforcements, Metall. Res. Technol. 121 (2024). https://doi.org/10.1051/metal/2024086.

[23] P.S. Bains, S.S. Sidhu, H.S. Payal, Fabrication and Machining of Metal Matrix Composites: A Review, Mater. Manuf. Process. 31 (2016) 553–573. https://doi.org/10.1080/10426914.2015.1025976.

[24] A. Kar, A. Sharma, S. Kumar, A Critical Review on Recent Advancements in Aluminium-Based Metal Matrix Composites, Crystals 14 (2024). https://doi.org/10.3390/cryst14050412.

[25] K.C. Nayak, K.K. Rane, P.P. Date, T.S. Srivatsan, Synthesis of an Aluminum Alloy Metal Matrix Composite Using Powder Metallurgy: Role of Sintering Parameters, Appl. Sci. 12 (2022). https://doi.org/10.3390/app12178843.

[26] N.S. P Sharma, G Chauhan, Production of AMC by stir casting–an overview, Int. J. Contemp. Pract. 2 (n.d.) 23–46.

[27] X. Rong, D. Zhao, C. He, N. Zhao, Review: recent progress in aluminum matrix composites reinforced by in situ oxide ceramics, J. Mater. Sci. 59 (2024) 9657–9684. https://doi.org/10.1007/s10853-023-09120-z.

[28] M.K. Akbari, H.R. Baharvandi, O. Mirzaee, Nano-sized aluminum oxide reinforced commercial casting A356 alloy matrix: Evaluation of hardness, wear resistance and compressive strength focusing on particle distribution in aluminum matrix, Compos. Part B Eng. 52 (2013) 262–268. https://doi.org/10.1016/j.compositesb.2013.04.038.

[29] J. Zhu, W. Jiang, G. Li, F. Guan, Y. Yu, Z. Fan, Microstructure and mechanical properties of SiC_{np}/Al6082 aluminum matrix composites prepared by squeeze casting combined with stir casting, J. Mater. Process. Technol. 283 (2020). https://doi.org/10.1016/j.jmatprotec.2020.116699.

[30] M.S. Kumar, M. Vasumathi, S.R. Begum, S.M. Luminita, S. Vlase, C.I. Pruncu, Influence of B_4C and industrial waste fly ash reinforcement particles on the micro structural characteristics and mechanical behavior of aluminium (Al–Mg–Si-T6) hybrid metal matrix composite, J. Mater. Res. Technol. 15 (2021) 1201–1216. https://doi.org/10.1016/j.jmrt.2021.08.149.

[31] S.O. Akinwamide, O.J. Akinribide, P.A. Olubambi, Microstructural evolution, mechanical and nanoindentation studies of stir cast binary and ternary aluminium based composites, J. Alloys Compd. 850 (2021). https://doi.org/10.1016/j.jallcom.2020.156586.

[32] S. Sulaiman, M. Sayuti, R. Samin, Mechanical properties of the as-cast quartz particulate reinforced LM6 alloy matrix composites, J. Mater. Process. Technol. 201 (2008) 731–735. https://doi.org/10.1016/j.jmatprotec.2007.11.221.

[33] A.K. Gupta, T.K. Dan, P.K. Rohatgi, Aluminium alloy-silica sand composites: preparation and properties, J. Mater. Sci. 21 (1986) 3413–3419. https://doi.org/10.1007/bf00553778.

[34] Umesh, Suresh N, Sundaresh S, Fatigue Behavior of Fly ash reinforced in LM6 Aluminum Metal Matrix Composite, Int. J. Adv. Sci. Res. Eng. 2 (2016) 1–13. http://www.ijasre.net/uploads/1/2788_pdf.pdf.

[35] K.R. Kumar, K.M. Mohanasundaram, G. Arumaikkannu, R. Subramanian, Effect of particle size on mechanical properties and tribological behaviour of aluminium/fly ash composites, Sci. Eng. Compos. Mater. 19 (2012) 247–253. https://doi.org/10.1515/secm-2011-0139.

[36] T. Bera, S.K. Acharya, Utilization of Fly Ash Cenosphere as Reinforcement for Abrasive Wear Behaviour of LM6 Al Alloy Metal Matrix Composites, Iran. J. Sci. Technol. - Trans. Mech. Eng. 43 (2019) 273–280. https://doi.org/10.1007/s40997-017-0132-y.

[37] J. David Raja Selvam, D.S. Robinson Smart, I. Dinaharan, Microstructure and some mechanical properties of fly ash particulate reinforced AA6061 aluminum alloy composites prepared by compocasting, Mater. Des. 49 (2013) 28–34. https://doi.org/10.1016/j.matdes.2013.01.053.

[38] P. Shanmughasundaram, R. Subramanian, G. Prabhu, Some Studies on Aluminium – Fly Ash Composites Fabricated by Two Step Stir Casting Method Some Studies on Aluminium – Fly Ash Composites Fabricated by Two Step Stir Casting Method, Eur. J. Sci. Res. 63 (2011) 204–218.

[39] M. Kumar Ch, N. Rajendra Kumar, M. Thenarasu, Study on Mechanical Properties of LM 6 Aluminium Alloy Reinforced with Ground Granulated Blast Slag (GGBS) Particles, Mater. Today Proc. 24 (2020) 904–911. https://doi.org/10.1016/j.matpr.2020.04.401.

[40] Pankaj, Nishant, Hardness and Microstructure of Aluminum Metal Matrix Composites Reinforced With Industrial Waste Slag, 6 (2017) 85–90.

[41] M. Srikanth, S.V.R.R. Kishore, Deformation and Tribological studies of A356 Slag Reinforced Composites, Int. J. Latest Res. Eng. Technol. 1 (2015) 33–36.

[42] G. Narasaraju, D.L. Raju, Characterization of Hybrid Rice Husk and Fly ash-Reinforced Aluminium alloy (AlSi10Mg) Composites, Mater. Today Proc. 2 (2015) 3056–3064. https://doi.org/10.1016/j.matpr.2015.07.245.

[43] S.B.V. Siva, R.I. Ganguly, G. Srinivasarao, K.L. Sahoo, Machinability of aluminum metal matrix composite reinforced with in-situ ceramic composite developed from mines waste colliery shale, Mater. Manuf. Process. 28 (2013) 1082–1089. https://doi.org/10.1080/10426914.2013.811734.

[44] P. Muthu, Optimization of dry sliding wear behaviour of industrial wastes reinforced aluminium based metal matrix composites, Materwiss. Werksttech. 54 (2023) 327–334. https://doi.org/10.1002/mawe.202200172.

[45] R. Das, M.K. Mondal, S. Pramanik, Strengthening Behaviour and Microstructural Properties during the Compaction of Reduced Blast Furnace Flue Dust—Fly Ash—Iron Metal Matrix Composite Fines using Powder Metallurgy Route, Trans. Indian Inst. Met. 75 (2022) 2255–2263. https://doi.org/10.1007/s12666-022-02592-8.

[46] P.P. Kulkarni, B. Siddeswarappa, A study on microstructure and mechanical behaviour of AA6063 metal matrix composite reinforced with areca sheath ash (ASA) and rice husk ash (RHA), Mater. Today Proc. 52 (2022) 445–451. https://doi.org/10.1016/j.matpr.2021.09.104.

[47] I.P. Okokpujie, L.K. Tartibu, K. Babaremu, C. Akinfaye, A.T. Ogundipe, E.T. Akinlabi, Study of the corrosion, electrical, and mechanical properties of aluminium metal composite reinforced with coconut rice and eggshell for wind turbine blade development, Clean. Eng. Technol. 13 (2023). https://doi.org/10.1016/j.clet.2023.100627.

[48] A. Bhowmik, R. Kumar, A. Babbar, V. Romanovski, S. Roy, L. Patnaik, J.P. Kumar, A.H. Alawadi, Analysis of physical, mechanical and tribological behavior of Al7075-fly ash composite for lightweight applications, Int. J. Interact. Des. Manuf. (2023). https://doi.org/10.1007/s12008-023-01583-3.

[49] U.A. Dabade, S.S. Joshi, Analysis of chip formation mechanism in machining of Al/SiC_p metal matrix composites, J. Mater. Process. Technol. 209 (2009) 4704–4710. https://doi.org/10.1016/j.jmatprotec.2008.10.057.

[50] M.S. Zakaria, M. Mustapha, A.I. Azmi, A. Ahmad, M. Danish, S. Rubaiee, Machinability investigations of AZ31 magnesium alloy via submerged convective cooling in turning process, J. Mater. Res. Technol. 19 (2022) 3685–3698. https://doi.org/10.1016/j.jmrt.2022.06.127.

[51] S. Pradhan, S. Singh, C. Prakash, G. Królczyk, A. Pramanik, C.I. Pruncu, Investigation of machining characteristics of hard-to-machine Ti-6Al-4V-ELI alloy for biomedical applications, J. Mater. Res. Technol. 8 (2019) 4849–4862. https://doi.org/10.1016/j.jmrt.2019.08.033.

[52] K. Gobivel, K.S. Vijay Sekar, Machinability Studies on the Turning of Magnesium Metal Matrix Composites, Arch. Metall. Mater. 67 (2022) 939–948. https://doi.org/10.24425/amm.2022.139686.

[53] A. Das, M. Kamal, S.R. Das, S.K. Patel, A. Panda, M. Rafighi, B.B. Biswal, Comparative assessment between AlTiN and AlTiSiN coated carbide tools towards machinability improvement of AISI D6 steel in dry hard turning, Proc. Inst. Mech. Eng. Part C J. Mech. Eng. Sci. 236 (2022) 3174–3197. https://doi.org/10.1177/09544062211037373.

[54] V. Sharma, P. Kumar, J.P. Misra, Cutting force predictive modelling of hard turning operation using fuzzy logic, Mater. Today Proc. 26 (2019) 740–744. https://doi.org/10.1016/j.matpr.2020.01.018.

[55] S.R. Ruban, K.L. Dev Wins, J.D. Raja Selvam, R. S Rai, Influence of turning parameters on the machinability of Al6061/ZrB_2 & ZrC hybrid in-situ Aluminium Matrix Composite, Aust. J. Mech. Eng. (2021). https://doi.org/10.1080/14484846.2021.1963081.

[56] A. Pugazhenthi, I. Dinaharan, G. Kanagaraj, J.D.R. Selvam, Predicting the effect of machining parameters on turning characteristics of AA7075/TiB_2 in situ aluminum matrix composites using empirical relationships, J. Brazilian Soc. Mech. Sci. Eng. 40 (2018). https://doi.org/10.1007/s40430-018-1480-2.

[57] A. Pugazhenthi, G. Kanagaraj, I. Dinaharan, J. David Raja Selvam, Turning characteristics of in situ formed TiB_2 ceramic particulate reinforced AA7075 aluminum matrix composites using polycrystalline diamond cutting tool, Meas. J. Int. Meas. Confed. 121 (2018) 39–46. https://doi.org/10.1016/j.measurement.2018.02.039.

[58] C. Shoba, N. Ramanaiah, D. Nageswara Rao, Effect of reinforcement on the cutting forces while machining metal matrix composites–An experimental approach, Eng. Sci. Technol. an Int. J. 18 (2015) 658–663. https://doi.org/10.1016/j.jestch.2015.03.013.

[59] S. V. Sujith, R.S. Mulik, Surface Integrity and Flank Wear Response Under Pure Coconut Oil-Al_2O_3 Nano Minimum Quantity Lubrication Turning of Al-7079/ 7 wt%-TiC In Situ Metal Matrix Composites, J. Tribol. 144 (2022). https://doi.org/10.1115/1.4051863.

[60] A. Das, M.K. Gupta, S.R. Das, A. Panda, S.K. Patel, S. Padhan, Hard turning of AISI D6 steel with recently developed HSN2-TiAlxN and conventional TiCN coated carbide tools: comparative machinability investigation and sustainability assessment, J. Brazilian Soc. Mech. Sci. Eng. 44 (2022). https://doi.org/10.1007/s40430-022-03445-7.

[61] M. Nataraj, K. Balasubramanian, D. Palanisamy, Influence of Process Parameters on CNC Turning of Aluminium Hybrid Metal Matrix Composites, Mater. Today Proc. 5 (2018) 14499–14506. https://doi.org/10.1016/j.matpr.2018.03.037.

[62] N. Muthukrishnan, M. Murugan, K.P. Rao, An investigation on the machinability of Al-SiC metal matrix composites using pcd inserts, Int. J. Adv. Manuf. Technol. 38 (2008) 447–454. https://doi.org/10.1007/s00170-007-1111-z.

[63] Y. Wang, W. Liao, K. Yang, X. Teng, W. Chen, Simulation and experimental investigation on the cutting mechanism and surface generation in machining SiC_p /Al MMCs, Int. J. Adv. Manuf. Technol. 100 (2019) 1393–1404. https://doi.org/10.1007/s00170-018-2769-0.

[64] P. Suresh, K. Marimuthu, S. Ranganathan, T. Rajmohan, Optimization of machining parameters in turning of Al-SiC-Gr hybrid metal matrix composites using grey-fuzzy algorithm, Trans. Nonferrous Met. Soc. China (English Ed. 24 (2014) 2805–2814. https://doi.org/10.1016/S1003-6326(14)63412-9.

[65] I. Dinaharan, J. David Raja Selvam, J. Jose, R. Palanivel, Influence of Fly Ash Particles on Machining Characteristics of AA6061 Aluminum Matrix Composites Produced Using Semisolid Slurry Casting, Trans. Indian Inst. Met. (2023). https://doi.org/10.1007/s12666-022-02869-y.

[66] A.K. Sahoo, S. Pradhan, Modeling and optimization of Al/SiC_p MMC machining using Taguchi approach, Meas. J. Int. Meas. Confed. 46 (2013) 3064–3072. https://doi.org/10.1016/j.measurement.2013.06.001.

[67] R.M. Hooper, J.L. Henshall, A. Klopfer, Wear of polycrystalline diamond tools used in the cutting of metal matrix composites, Int. J. Refract. Met. Hard Mater. 17 (1999) 103–109. https://doi.org/10.1016/S0263-4368(98)00040-7.

[68] L. Iuliano, L. Settineri, A. Gatto, High-speed turning experiments on metal matrix composites, Compos. Part A Appl. Sci. Manuf. 29 (1998) 1501–1509. https://doi.org/10.1016/S1359-835X(98)00105-5.

[69] A. Kannan, R. Mohan, R. Viswanathan, N. Sivashankar, Experimental investigation on surface roughness, tool wear and cutting force in turning of hybrid (Al7075 + SiC + Gr) metal matrix composites, J. Mater. Res. Technol. 9 (2020) 16529–16540. https://doi.org/10.1016/j.jmrt.2020.11.074.

[70] A. Chauhan, J. Singh, S. Bala, Optimization of Reinforcement Parameters and Turning Conditions for Improving Surface Quality of Hybrid Al-SiC-Red Mud Composite for Automotive and Aerospace Components, Adv. Compos. Aerosp. Eng. Appl. (2022) 237–262. https://doi.org/10.1007/978-3-030-88192-4_12.

[71] P. Shanmughasundaram, R. Subramanian, Influence of graphite and machining parameters on the surface roughness of Al-fly ash/graphite hybrid composite: A Taguchi approach, J. Mech. Sci. Technol. 27 (2013) 2445–2455. https://doi.org/10.1007/s12206-013-0630-9.

[72] J. Udaya Prakash, A. Divya Sadhana, S. Jebarose Juliyana, S. Ananth, C. Sarala Rubi, Multi-objective optimisation of tribological parameters of AMCs (356/fly ash), Mater. Today Proc. 52 (2022) 1451–1455. https://doi.org/10.1016/j.matpr.2021.11.194.

[73] P. Saini, P.K. Singh, Characterization and optimization analysis on surface finish and energy consumption in turning of Al-4032/GMP MMC produced by stir casting, Proc. Inst. Mech. Eng. Part C J. Mech. Eng. Sci. 236 (2022) 11549–11563. https://doi.org/10.1177/09544062221110475.

[74] B.S. Silvestre, D.M. Ţîrcă, Innovations for sustainable development: Moving toward a sustainable future, J. Clean. Prod. 208 (2019) 325–332. https://doi.org/10.1016/j.jclepro.2018.09.244.

[75] H. Berns, W. Theisen, Ferrous materials: Steel and cast iron, Springer Berlin Heidelberg, Berlin, Heidelberg, 2008. https://doi.org/10.1007/978-3-540-71848-2.

[76] C.M. Hansson, Cast iron technology, Mater. Sci. Eng. A 114 (1989) 218. https://doi.org/10.1016/0921-5093(89)90868-X.

[77] Staff Report, Census of world casting production: Total casting tons dip in 2019, Mod. Cast. Am. Foundry Soc. 111 (2021) 28–30.

[78] India is the world's second largest producer of castings, Foundry Planet (n.d.). https://www.foundry-planet.com/d/india-ist-the-worlds-second-largest-producer-of-castings/. (accessed January 15, 2025).

[79] S. Chakravarty, P. Haldar, T. Nandi, G. Sutradhar, Cupola slag reutilization for sustainable waste management: review and economic analysis, Int. J. Environ. Sci. Technol. (2021). https://doi.org/10.1007/s13762-021-03574-x.

[80] F.I. Center, Profile of Indian Foundry Industry, Informatics Foundry Cent. (2018) 2–8. http://foundryinfo-india.org/profile_of_indian.aspx.

[81] D.A. Aderibigbe, A.E. Ojobo, Properties of cupola slag as a pozzolana and its effects on partial replacement of cement in a mortar, Conserv. Recycl. 5 (1982) 203–208. https://doi.org/10.1016/0361-3658(82)90048-0.

[82] G. Agarwal, R.F. Speyer, Devitrification hardening of cupola slag glass with CaO and SiO_2 additions, J. Non. Cryst. Solids 135 (1991) 95–104. https://doi.org/10.1016/0022-3093(91)90409-Y.

[83] G. Agarwal, K.S. Hong, M.R. Fletcher, R.F. Speyer, Crystallization behavior of cupola slag glass-ceramics, J. Non. Cryst. Solids 130 (1991) 187–197. https://doi.org/10.1016/0022-3093(91)90454-E.

[84] S.I. Pavlenko, V.I. Malyshkin, Fine grained cementless concrete containing slag from foundry, Exploit. Wastes Concr. (1999) 101–108.

[85] R. Balaraman, S.A. Ligoria, Utilization of cupola slag in concrete as fine and coarse aggregate, Int. J. Civ. Eng. Technol. 6 (2015) 6–14.

[86] J. Ladomerský, I. Janotka, E. Hroncová, I. Najdená, One-year properties of concrete with partial substitution of natural aggregate by cupola foundry slag, J. Clean. Prod. 131 (2016) 739–746. https://doi.org/10.1016/j.jclepro.2016.04.101.

[87] J.F. Lara-Sánchez, H. Lopez, M. Rodríguez-Reyes, J.A. Díaz-Guillen, J.R. Parga-Torres, Development of Ceramic Foams Using Cast Iron Slag as a Raw Material, Adv. Ceram. Sci. Eng. 5 (2016) 11. https://doi.org/10.14355/acse.2016.05.002.

[88] D. Baricova, A. Pribulova, P. Futas, Recycling possibilities of the slag from cupola furnace, Int. Multidiscip. Sci. GeoConference Surv. Geol. Min. Ecol. Manag. SGEM 18 (2018) 137–144. https://doi.org/10.5593/sgem2018/4.2/S18.018.

[89] A. Pribulova, D. Baricova, P. Futas, M. Pokusova, S. Eperjesi, Cupola Furnace Slag: Its Origin, Properties and Utilization, Int. J. Met. 13 (2019) 627–640. https://doi.org/10.1007/s40962-019-00314-3.

[90] V.K. Mistry, D.J. Varia, Green Concrete by Replacing Coarse Aggregate with Cupola Slag for Environmental Protection, Smart Innov. Syst. Technol. 161 (2020) 223–237. https://doi.org/10.1007/978-981-32-9578-0_20.

[91] S. Ndlovu, G.S. Simate, E. Matinde, Waste Production and Utilization in the Metal Extraction Industry, Waste Prod. Util. Met. Extr. Ind. (2017) 1–512. https://doi.org/10.1201/9781315153896.

[92] Y.H.M. Amran, R. Alyousef, H. Alabduljabbar, M. El-Zeadani, Clean production and properties of geopolymer concrete; A review, J. Clean. Prod. 251 (2020). https://doi.org/10.1016/j.jclepro.2019.119679.

[93] R. Anuwattana, K.J. Balkus, S. Asavapisit, P. Khummongkol, Conventional and microwave hydrothermal synthesis of zeolite ZSM-5 from the cupola slag, Microporous Mesoporous Mater. 111 (2008) 260–266. https://doi.org/10.1016/j.micromeso.2007.07.039.

[94] B. Deo, A. Overbosch, B. Snoeijer, D. Das, K. Srinivas, Control of slag formation, foaming, slopping, and chaos in BOF, Trans. Indian Inst. Met. 66 (2013) 543–554. https://doi.org/10.1007/s12666-013-0306-2.

[95] S. Ren, J. Zhang, L. Wu, W. Liu, Y. Bai, X. Xing, B. Su, D. Kong, Influence of B_2O_3 on Viscosity of High Ti-bearing Blast Furnace Slag, ISIJ Int. 52 (2012) 984–991. https://doi.org/10.2355/isijinternational.52.984.

[96] A.M. Rashad, A comprehensive overview about the influence of different additives on the properties of alkali-activated slag - A guide for Civil Engineer, Constr. Build. Mater. 47 (2013) 29–55. https://doi.org/10.1016/j.conbuildmat.2013.04.011.

[97] J.O. Afolayan, S.A. Alabi, Investigation on the Potentials of Cupola Furnace Slag in Concrete, Int. J. Integr. Eng. 5 (2013) 59–62.

[98] L.K. Deng, A., Hung, Y. T., & Wang, 4 Management, Minimization, and Recycling of Metal Casting Wastes, in: Waste Treat. Met. Manuf. Forming, Coating, Finish. Ind., CRC press, 2016: pp. 151–195.

[99] H.K. Eggleston, The Successful Utilization of Iron & Steel Slags., in: Second Miner. Waste Util. Symp., IIT Research Institute, Chicago, Illinois, 1970: pp. 15–22.

[100] W.W. Stroup, R.D. Stroup, J.H. Fallin, Cupola slag cement mixture and methods of making and using the same, 2003.

[101] F. Bellmann, J. Stark, Activation of blast furnace slag by a new method, Cem. Concr. Res. 39 (2009) 644–650. https://doi.org/10.1016/j.cemconres.2009.05.012.

[102] C. Fredericci, E.D. Zanotto, E.C. Ziemath, Crystallization mechanism and properties of a blast furnace slag glass, J. Non. Cryst. Solids 273 (2000) 64–75. https://doi.org/10.1016/S0022-3093(00)00145-9.

[103] E.F. Osborn, R.C. DeVries, K.H. Gee, H.M. Kraner, Optimum composition of blast furnace slag as deduced from liquidus data for the quaternary system CaO-MgO-Al_2O_3- SiO_2, Jom 6 (1954) 33–45. https://doi.org/10.1007/bf03397977.

[104] I.G. Richardson, G.W. Groves, Microstructure and microanalysis of hardened cement pastes involving ground granulated blast-furnace slag, J. Mater. Sci. 27 (1992) 6204–6212. https://doi.org/10.1007/BF01133772.

[105] I.G. Richardson, S. Li, Composition and structure of an 18-year-old 5M KOH-activated ground granulated blast-furnace slag paste, Constr. Build. Mater. 168 (2018) 404–411. https://doi.org/10.1016/j.conbuildmat.2018.02.034.

[106] G.K. Barbara, G.K. Ann, Fly ash characterization by SEM-EDS, Fuel 85 (2006) 2537–2544.

[107] M.H. Shehata, M.D.A. Thomas, R.F. Bleszynski, The effects of fly ash composition on the chemistry of pore solution in hydrated cement pastes, Cem. Concr. Res. 29 (1999) 1915–1920. https://doi.org/10.1016/S0008-8846(99)00190-8.

[108] A. Fernández-Jiménez, A. Palomo, Composition and microstructure of alkali activated fly ash binder: Effect of the activator, Cem. Concr. Res. 35 (2005) 1984–1992. https://doi.org/10.1016/j.cemconres.2005.03.003.

[109] F. Goodarzi, Characteristics and composition of fly ash from Canadian coal-fired power plants, Fuel 85 (2006) 1418–1427. https://doi.org/10.1016/j.fuel.2005.11.022.

[110] U. Kukier, C.F. Ishak, M.E. Sumner, W.P. Miller, Composition and element solubility of magnetic and non-magnetic fly ash fractions, Environ. Pollut. 123 (2003) 255–266. https://doi.org/10.1016/S0269-7491(02)00376-7.

[111] C. Jaturapitakkul, B. Roongreung, Cementing Material from Calcium Carbide Residue-Rice Husk Ash, J. Mater. Civ. Eng. 15 (2003) 470–475. https://doi.org/10.1061/(asce)0899-1561(2003)15:5(470).

[112] A.A. Raheem, M.A. Kareem, Chemical composition and physical characteristics of rice husk ash blended cement, Int. J. Eng. Res. Africa 32 (2017) 25–35. https://doi.org/10.4028/www.scientific.net/JERA.32.25.

[113] K. Ganesan, K. Rajagopal, K. Thangavel, Rice husk ash blended cement: Assessment of optimal level of replacement for strength and permeability properties of concrete, Constr. Build. Mater. 22 (2008) 1675–1683. https://doi.org/10.1016/j.conbuildmat.2007.06.011.

[114] S.O. Mitchell, Concrete science, Concr. Constr. - World Concr. 55 (2010) 18. https://doi.org/10.1016/b978-081551437-4.50004-7.

[115] L.J. Murdock, G.F. Blackledge, Concrete Materials and Practice, Concr. Mater. Pract. (1968) 226–251.

[116] B. Suhendro, Toward green concrete for better sustainable environment, Procedia Eng. 95 (2014) 305–320. https://doi.org/10.1016/j.proeng.2014.12.190.

[117] A. Rao, K.N. Jha, S. Misra, Use of aggregates from recycled construction and demolition waste in concrete, Resour. Conserv. Recycl. 50 (2007) 71–81. https://doi.org/10.1016/j.resconrec.2006.05.010.

[118] M. Limbachiya, M.S. Meddah, Y. Ouchagour, Use of recycled concrete aggregate in fly-ash concrete, Constr. Build. Mater. 27 (2012) 439–449. https://doi.org/10.1016/j.conbuildmat.2011.07.023.

[119] P. Lastra-González, M. Calzada-Pérez, D. Castro-Fresno, Á. Vega-Zamanillo, I. Indacoechea-Vega, Porous asphalt mixture with alternative aggregates and crumb-rubber modified binder at reduced temperature, Constr. Build. Mater. 150 (2017) 260–267. https://doi.org/10.1016/j.conbuildmat.2017.06.008.

[120] S.M. Cramer, P. Bakke, Potential use of cupola slag as road construction material, Am. Foundrymen's Soc. Inc.(United States), (1994) 113–122.

[121] R. Sikder, S. Chakravarty, D. Sau, P. Haldar, S. Mandal, T. Nandi, G. Sutradhar, Study of durability and mechanical properties for utilization of cupola slag as a coarse aggregate in M20 grade green concrete, J. Build. Eng. 87 (2024). https://doi.org/10.1016/j.jobe.2024.109101.

[122] C. Arum, G.O. Mark, Partial Replacement of Portland Cement by Granulated Cupola Slag – Sustainable Option for Concrete of Low Permeability, Civ. Environ. Res. 6 (2014) 17–26.

[123] R. Balaraman, N.S. Elangoval, Behaviour of cuplola slag in concrete as partial replacement with combination of fine and coarse aggregate., Taga J. Graph. Technol. 14 (2018).

[124] S.A. Alabi, J. Mahachi, Behaviour of ground cupola furnace slag blended concrete at elevated temperature, J. Mater. Eng. Struct. 7 (2020) 35–46.

[125] Y.E. Rodríguez-Mendoza, A.F. Fuentes, J.I. Escalante-García, Cementitious blends of portland cement with calcium sulphate, fly ash and cupola slag, Mater. Res. Soc. Symp. Proc. 1488 (2012) 9–15. https://doi.org/10.1557/opl.2012.1541.

[126] I. Sosa, C. Thomas, J.A. Polanco, J. Setién, P. Tamayo, High performance self-compacting concrete with electric arc furnace slag aggregate and cupola slag powder, Appl. Sci. 10 (2020). https://doi.org/10.3390/app10030773.

[127] C. Prakash, P. Senthil, N. Manikandan, D. Palanisamy, Investigations on machinability characteristics of Cast Aluminum Alloy based (LM 26+Graphite+Fly ash) Hybrid Metal Matrix Composites for automobile components, Mater. Manuf. Process. (2021). https://doi.org/10.1080/10426914.2021.1962531.

[128] O.G. Mark, A.N. Ede, O. Olofinnade, G. Bamigboye, C. Okeke, S.O. Oyebisi, C. Arum, Influence of Some Selected Supplementary Cementitious Materials on Workability and Compressive Strength of Concrete – A Review, IOP Conf. Ser. Mater. Sci. Eng. 640 (2019) 012071. https://doi.org/10.1088/1757-899X/640/1/012071.

[129] K. V. Mahendra, K. Radhakrishna, Fabrication of Al-4.5% Cu alloy with fly ash metal matrix composites and its characterization, Mater. Sci. Pol. 25 (2007) 57–68.

[130] P.K. Bannaravuri, A.K. Birru, Strengthening of Al-4.5%Cu alloy with the addition of Silicon Carbide and Bamboo Leaf Ash, Int. J. Struct. Integr. 10 (2019) 149–161. https://doi.org/10.1108/IJSI-03-2018-0018.

[131] Y. Zhang, W. Yu, X. Wang, Y. Xue, Trace Scandium addition on the strength and thermal stability of TiB_2 particles reinforced Al-4.5 Cu composites, J. Phys. Conf. Ser. 2133 (2021). https://doi.org/10.1088/1742-6596/2133/1/012018.

[132] C. Thomas, J. Sainz-Aja, I. Sosa, J. Setién, J.A. Polanco, A. Cimentada, Physical-mechanical properties of cupola slag cement paste, Appl. Sci. 11 (2021). https://doi.org/10.3390/app11157029.

[133] G. Upadhyay, K.K. Saxena, Role of Stir Casting in development of Aluminium Metal Matrix Composite (AMC): An Overview, IOP Conf. Ser. Mater. Sci. Eng. 1116 (2021) 012022. https://doi.org/10.1088/1757-899x/1116/1/012022.

[134] U.K. Annigeri, G.B. Veeresh Kumar, Method of stir casting of Aluminum metal matrix Composites: A review, Mater. Today Proc. 4 (2017) 1140–1146. https://doi.org/10.1016/j.matpr.2017.01.130.

[135] E. Sjölander, S. Seifeddine, The heat treatment of Al-Si-Cu-Mg casting alloys, J. Mater. Process. Technol. 210 (2010) 1249–1259. https://doi.org/10.1016/j.jmatprotec.2010.03.020.

[136] A. Manente, G. Timelli, Optimizing the Heat Treatment Process of Cast Aluminium Alloys, Recent Trends Process. Degrad. Alum. Alloy. (2011). https://doi.org/10.5772/21659.

[137] P.K. Rohatgi, B.F. Schultz, A. Daoud, W.W. Zhang, Tribological performance of A206 aluminum alloy containing silica sand particles, Tribol. Int. 43 (2010) 455–466. https://doi.org/10.1016/j.triboint.2009.07.010.

[138] A. Ramanathan, P.K. Krishnan, R. Muraliraja, A review on the production of metal matrix composites through stir casting – Furnace design, properties, challenges, and research opportunities, J. Manuf. Process. 42 (2019) 213–245. https://doi.org/10.1016/j.jmapro.2019.04.017.

[139] B.F. Schultz, J.B. Ferguson, P.K. Rohatgi, Microstructure and hardness of Al_2O_3 nanoparticle reinforced Al-Mg composites fabricated by reactive wetting and stir mixing, Mater. Sci. Eng. A 530 (2011) 87–97. https://doi.org/10.1016/j.msea.2011.09.042.

[140] S. Poria, G. Sutradhar, P. Sahoo, Wear and friction behavior of Al-TiB2-nano-Gr hybrid composites fabricated through ultrasonic cavitation assisted stir casting, Mater. Res. Express 5 (2018). https://doi.org/10.1088/2053-1591/aac0df.

[141] C.C. Nwaeju, F.O. Edoziuno, A.A. Adediran, T.J. Tuaweri, M. Saravana Kumar, Grain characteristics and mechanical properties of as-cast Cu-10%Al alloy: Effects of alloying additions, Results Eng. 12 (2021). https://doi.org/10.1016/j.rineng.2021.100295.

[142] A.A. Akinwande, O.A. Balogun, A.A. Adediran, O.S. Adesina, V. Romanovski, T.C. Jen, Experimental analysis, statistical modeling, and parametric optimization of quinary-(CoCrFeMnNi)100 –x/TiCx high-entropy-alloy (HEA) manufactured by laser additive manufacturing, Results Eng. 17 (2023). https://doi.org/10.1016/j.rineng.2022.100802.

[143] J. Hashim, L. Looney, M.S.J. Hashmi, Particle distribution in cast metal matrix composites - Part I, J. Mater. Process. Technol. 123 (2002) 251–257. https://doi.org/10.1016/S0924-0136(02)00098-5.

[144] H.X. Peng, Z. Fan, D.Z. Wang, In situ Al3Ti-Al_2O_3 intermetallic matrix composite: Synthesis, microstructure, and compressive behavior, J. Mater. Res. 15 (2000) 1943–1949. https://doi.org/10.1557/JMR.2000.0280.

[145] M.K. Sahu, R.K. Sahu, Synthesis, microstructure and hardness of Al 7075/ B_4C /Fly-ash composite using stir casting method, Mater. Today Proc. 27 (2019) 2401–2406. https://doi.org/10.1016/j.matpr.2019.09.150.

[146] S. Sachinkumar, S. Narendranath, D. Chakradhar, Studies on microstructure and mechanical characteristics of as cast AA6061/SiC/fly ash hybrid AMCs produced by stir casting, Mater. Today Proc. 20 (2020) A1–A5. https://doi.org/10.1016/j.matpr.2020.01.266.

[147] S. Banerjee, S. Poria, G. Sutradhar, P. Sahoo, Dry sliding tribological behavior of AZ31-WC nano-composites, J. Magnes. Alloy. 7 (2019) 315–327. https://doi.org/10.1016/j.jma.2018.11.005.

[148] M. Kok, Production and mechanical properties of Al_2O_3 particle-reinforced 2024 aluminium alloy composites, J. Mater. Process. Technol. 161 (2005) 381–387. https://doi.org/10.1016/j.jmatprotec.2004.07.068.

[149] K.S.S. Raja, V.K.B. Raja, K.R. Vignesh, S.N.R. Rao, Effect of Steel Slag on the Impact Strength of Aluminium Metal Matrix Composite, Appl. Mech. Mater. 766–767 (2015) 240–245. https://doi.org/10.4028/www.scientific.net/amm.766-767.240.

[150] I.N. Murthy, N.A. Babu, J.B. Rao, Comparative Studies on Microstructure and Mechanical Properties of Granulated Blast Furnace Slag and Fly Ash Reinforced AA 2024 Composites, J. Miner. Mater. Charact. Eng. 02 (2014) 319–333. https://doi.org/10.4236/jmmce.2014.24037.

[151] M. Rahimian, N. Ehsani, N. Parvin, H. reza Baharvandi, The effect of particle size, sintering temperature and sintering time on the properties of Al-Al_2O_3 composites, made by powder metallurgy, J. Mater. Process. Technol. 209 (2009) 5387–5393. https://doi.org/10.1016/j.jmatprotec.2009.04.007.

[152] R. Yang, Z. Zhang, Y. Zhao, G. Chen, Y. Guo, M. Liu, J. Zhang, Effect of multi-pass friction stir processing on microstructure and mechanical properties of Al3Ti/A356 composites, Mater. Charact. 106 (2015) 62–69. https://doi.org/10.1016/j.matchar.2015.05.019.

[153] P.K. Rohatgi, A. Daoud, B.F. Schultz, T. Puri, Microstructure and mechanical behavior of die casting AZ91D-Fly ash cenosphere composites, Compos. Part A Appl. Sci. Manuf. 40 (2009) 883–896. https://doi.org/10.1016/j.compositesa.2009.04.014.

[154] A.A. Hamid, P.K. Ghosh, S.C. Jain, S. Ray, The influence of porosity and particles content on dry sliding wear of cast in situ Al(Ti)-Al_2O_3(TiO_2) composite, Wear 265 (2008) 14–26. https://doi.org/10.1016/j.wear.2007.08.018.

[155] K.S. Sridhar Raja, V.K. Bupesh Raja, M. Gupta, Using anthropogenic waste (steel slag) to enhance mechanical and wear properties of a commercial aluminium alloy A356, Arch. Metall. Mater. 64 (2019) 279–284. https://doi.org/10.24425/amm.2019.126249.

[156] P. Poddar, V.C. Srivastava, P.K. De, K.L. Sahoo, Processing and mechanical properties of SiC reinforced cast magnesium matrix composites by stir casting process, Mater. Sci. Eng. A 460–461 (2007) 357–364. https://doi.org/10.1016/j.msea.2007.01.052.

[157] J.A.K. Gladston, N.M. Sheriff, I. Dinaharan, J.D. Raja Selvam, Production and characterization of rich husk ash particulate reinforced AA6061 aluminum alloy composites by compocasting, Trans. Nonferrous Met. Soc. China (English Ed. 25 (2015) 683–691. https://doi.org/10.1016/S1003-6326(15)63653-6.

[158] A. Mortensen, M.N. Gungor, J.A. Cornie, M.C. Flemings, Alloy Microstructures in Cast Metal Matrix Composites, Jom 38 (1986) 30–35. https://doi.org/10.1007/BF03257892.

[159] C. Tekmen, I. Ozdemir, U. Cocen, K. Onel, The mechanical response of Al-Si-Mg/SiC_p composite: Influence of porosity, Mater. Sci. Eng. A 360 (2003) 365–371. https://doi.org/10.1016/S0921-5093(03)00461-1.

[160] S.G. Kulkarni, J.V. Meghnani, A. Lal, Effect of Fly Ash Hybrid Reinforcement on Mechanical Property and Density of Aluminium 356 Alloy, Procedia Mater. Sci. 5 (2014) 746–754. https://doi.org/10.1016/j.mspro.2014.07.324.

[161] P. Saini, P.K. Singh, Studies on microstructural characteristics and mechanical properties of hybrid Al-4032 AMC reinforced with SiC and granite marble powder, Proc. Inst. Mech. Eng. Part C J. Mech. Eng. Sci. 236 (2022) 6192–6203. https://doi.org/10.1177/09544062211065342.

[162] G. Anbuchezhiyan, N.M. Mubarak, R.R. Karri, M. Khalid, A synergistic effect on enriching the Mg–Al–Zn alloy-based hybrid composite properties, Sci. Rep. 12 (2022). https://doi.org/10.1038/s41598-022-24427-8.

[163] J. Kumar, D. Singh, N.S. Kalsi, S. Sharma, M. Mia, J. Singh, M.A. Rahman, A.M. Khan, K.V. Rao, Investigation on the mechanical, tribological, morphological and machinability behavior of stir-casted Al/SiC/Mo reinforced MMCs, J. Mater. Res. Technol. 12 (2021) 930–946. https://doi.org/10.1016/j.jmrt.2021.03.034.

[164] S.P. Dwivedi, A. Saxena, S. Sharma, A.K. Srivastava, N.K. Maurya, Influence of SAC and eggshell addition in the physical, mechanical and thermal behaviour of Cr reinforced aluminium based composite, Int. J. Cast Met. Res. 34 (2021) 43–55. https://doi.org/10.1080/13640461.2021.1877943.

[165] C. Suryanarayana, D. Mukhopadhyay, S.N. Patankar, F.H. Froes, Grain size effects in nanocrystalline materials, J. Mater. Res. 7 (1992) 2114–2118. https://doi.org/10.1557/JMR.1992.2114.

[166] A.H. Idrisi, A.H.I. Mourad, Conventional stir casting versus ultrasonic assisted stir casting process: Mechanical and physical characteristics of AMCs, J. Alloys Compd. 805 (2019) 502–508. https://doi.org/10.1016/j.jallcom.2019.07.076.

[167] F. Saba, F. Zhang, S. Liu, T. Liu, Reinforcement size dependence of mechanical properties and strengthening mechanisms in diamond reinforced titanium metal matrix composites, Compos. Part B Eng. 167 (2019) 7–19. https://doi.org/10.1016/j.compositesb.2018.12.014.

[168] H. N., Hall-Petch relation and boundary strengthening, Scr. Mater. (2004) 801. https://www.sciencedirect.com/science/article/pii/S1359646204003434.

[169] S. Gopalakrishnan, N. Murugan, Production and wear characterisation of AA 6061 matrix titanium carbide particulate reinforced composite by enhanced stir casting method, Compos. Part B Eng. 43 (2012) 302–308. https://doi.org/10.1016/j.compositesb.2011.08.049.

[170] T. Satish Kumar, S. Shalini, K.K. Kumar, R. Thavamani, R. Subramanian, Bagasse Ash Reinforced A356 Alloy Composite: Synthesis and Characterization, Mater. Today Proc. 5 (2018) 7123–7130. https://doi.org/10.1016/j.matpr.2017.11.377.

[171] M. Meignanamoorthy, M. Ravichandran, Synthesis of metal matrix composites via powder metallurgy route: A review, Mech. Mech. Eng. 22 (2018) 65–75. https://doi.org/10.2478/mme-2018-0007.

[172] S. V. Bobylev, A.G. Sheinerman, Effect of crack bridging on the toughening of ceramic/graphene composites, Rev. Adv. Mater. Sci. 57 (2018) 54–62. https://doi.org/10.1515/rams-2018-0047.

[173] A.H.I. Mourad, J.V. Christy, P.K. Krishnan, M.S. Mozumder, Production of novel recycled hybrid metal matrix composites using optimized stir squeeze casting technique, J. Manuf. Process. 88 (2023) 45–58. https://doi.org/10.1016/j.jmapro.2023.01.040.

[174] A. Mandal, J.D. Barma, G. Majumdar, Effect of Tool Pin Geometries on Weld Quality of Al/Cu Dissimilar Friction Stir Welding, J. Inst. Eng. Ser. D 105 (2024) 211–225. https://doi.org/10.1007/s40033-023-00472-z.

[175] J. Ma, X. Ge, S.I. Chang, S. Lei, Assessment of cutting energy consumption and energy efficiency in machining of 4140 steel, Int. J. Adv. Manuf. Technol. 74 (2014) 1701–1708. https://doi.org/10.1007/s00170-014-6101-3.

[176] M. Pul, S. Yağmur, Examination of the effect of B_4C and GNP reinforcements on machinability in the machining of Al 6061 matrix B_4C/GNP reinforced hybrid composites, J. Brazilian Soc. Mech. Sci. Eng. 44 (2022) 469. https://doi.org/10.1007/s40430-022-03776-5.

[177] V.A. Balogun, P.T. Mativenga, Modelling of direct energy requirements in mechanical machining processes, J. Clean. Prod. 41 (2013) 179–186. https://doi.org/10.1016/j.jclepro.2012.10.015.

[178] J. Suthar, K.M. Patel, Processing issues, machining, and applications of aluminum metal matrix composites, Mater. Manuf. Process. 33 (2018) 499–527. https://doi.org/10.1080/10426914.2017.1401713.

[179] I. Dinaharan, K. Kalaiselvan, N. Murugan, Influence of rice husk ash particles on microstructure and tensile behavior of AA6061 aluminum matrix composites produced using friction stir processing, Compos. Commun. 3 (2017) 42–46. https://doi.org/10.1016/j.coco.2017.02.001.

[180] N.H. Ononiwu, C.G. Ozoegwu, N. Madushele, E.T. Akinlabi, Machinability studies and optimization of aa 6082/fly ash/carbonized eggshell matrix composite, Rev. Des Compos. Des Mater. Av. 31 (2021) 207–216. https://doi.org/10.18280/rcma.310404.

[181] C. Ramesh Kumar, V. JaiGanesh, R.R.R. Malarvannan, Optimization of drilling parameters in hybrid (Al6061/SiC/B_4C/talc) composites by grey relational analysis, J. Brazilian Soc. Mech. Sci. Eng. 41 (2019) 155. https://doi.org/10.1007/s40430-019-1661-7.

[182] Y. Kaynak, H.E. Karaca, R.D. Noebe, I.S. Jawahir, Tool-wear analysis in cryogenic machining of NiTi shape memory alloys: A comparison of tool-wear performance with dry and MQL machining, Wear 306 (2013) 51–63. https://doi.org/10.1016/j.wear.2013.05.011.

[183] Y.F. Ge, J.H. Xu, Y.C. Fu, High speed machining of particulate reinforced metal matrix composites with PCD tools, Adv. Mater. Res. 188 (2011) 392–397. https://doi.org/10.4028/www.scientific.net/AMR.188.392.

[184] A.H. Idrisi, A. Hamid Ismail Mourad, Wear performance analysis of Aluminum matrix composites using Artificial neural network, 2019 Adv. Sci. Eng. Technol. Int. Conf. ASET 2019 (2019). https://doi.org/10.1109/ICASET.2019.8714330.

[185] A. Pramanik, L.C. Zhang, J.A. Arsecularatne, An FEM investigation into the behavior of metal matrix composites: Tool-particle interaction during orthogonal cutting, Int. J. Mach. Tools Manuf. 47 (2007) 1497–1506. https://doi.org/10.1016/j.ijmachtools.2006.12.004.

[186] M.J. Bermingham, J. Kirsch, S. Sun, S. Palanisamy, M.S. Dargusch, New observations on tool life, cutting forces and chip morphology in cryogenic machining Ti-6Al-4V, Int. J. Mach. Tools Manuf. 51 (2011) 500–511. https://doi.org/10.1016/j.ijmachtools.2011.02.009.

[187] Ravi Sekhar, T.P. Singh, Mechanisms in turning of metal matrix composites: a review, J. Mater. Res. Technol. 4 (2015) 197–207.

[188] Y. Zhu, H.A. Kishawy, Influence of alumina particles on the mechanics of machining metal matrix composites, Int. J. Mach. Tools Manuf. 45 (2005) 389–398. https://doi.org/10.1016/j.ijmachtools.2004.09.013.

[189] R. M'Saoubi, D. Axinte, S.L. Soo, C. Nobel, H. Attia, G. Kappmeyer, S. Engin, W.M. Sim, High performance cutting of advanced aerospace alloys and composite materials, CIRP Ann. - Manuf. Technol. 64 (2015) 557–580. https://doi.org/10.1016/j.cirp.2015.05.002.

[190] Ü.A. Usca, S. Şap, M. Uzun, M. Kuntoğlu, E. Salur, A. Karabiber, D.Y. Pimenov, K. Giasin, S. Wojciechowski, Estimation, optimization and analysis based investigation of the energy consumption in machinability of ceramic-based metal matrix composite materials, J. Mater. Res. Technol. 17 (2022) 2987–2998. https://doi.org/10.1016/j.jmrt.2022.02.055.

[191] S. Poria, P. Sahoo, G. Sutradhar, Tribological Characterization of Stir-cast Aluminium-TiB2 Metal Matrix Composites, Silicon 8 (2016) 591–599. https://doi.org/10.1007/s12633-016-9437-5.

[192] Y. Han, X. Liu, X. Bian, In situ TiB2 particulate reinforced near eutectic Al-Si alloy composites, Compos. - Part A Appl. Sci. Manuf. 33 (2002) 439–444. https://doi.org/10.1016/S1359-835X(01)00124-5.

[193] A.R. Eivani, H. Ahmed, J. Zhou, J. Duszczyk, Evolution of grain boundary phases during the homogenization of AA7020 aluminum alloy, Metall. Mater. Trans. A Phys. Metall. Mater. Sci. 40 (2009) 717–728. https://doi.org/10.1007/s11661-008-9741-9.

[194] A. Mussatto, I.U.I. Ahad, R.T. Mousavian, Y. Delaure, D. Brabazon, Advanced production routes for metal matrix composites, Eng. Reports 3 (2021). https://doi.org/10.1002/eng2.12330.

[195] R. Ekici, M. Kemal Apalak, M. Yildirim, F. Nair, Effects of random particle dispersion and size on the indentation behavior of SiC particle reinforced metal matrix composites, Mater. Des. 31 (2010) 2818–2833. https://doi.org/10.1016/j.matdes.2010.01.001.

[196] S. Ozden, R. Ekici, F. Nair, Investigation of impact behaviour of aluminium based SiC particle reinforced metal-matrix composites, Compos. Part A Appl. Sci. Manuf. 38 (2007) 484–494. https://doi.org/10.1016/j.compositesa.2006.02.026.

[197] N.V.R. Maganti, R.R. Potturi, Investigation on Mechanical and Machinability Properties of Aluminium Metal Matrix Composite Reinforced with Titanium Oxide (TiO_2) and Graphite (Gr) Particles, Trends Sci. 20 (2023). https://doi.org/10.48048/tis.2023.5682.

[198] M.A. Alam, H.B. Ya, M. Azeem, M. Mustapha, M. Yusuf, F. Masood, R.V. Marode, S.M. Sapuan, A.H. Ansari, Advancements in aluminum matrix composites reinforced with carbides and graphene: A comprehensive review, Nanotechnol. Rev. 12 (2023). https://doi.org/10.1515/ntrev-2023-0111.

[199] A.M. Razzaq, D.L. Majid, U.M. Basheer, H.S.S. Aljibori, Research summary on the processing, mechanical and tribological properties of aluminium matrix composites as effected by fly ash reinforcement, Crystals 11 (2021). https://doi.org/10.3390/cryst11101212.

[200] M. Sharma, V. Singhal, A. Gupta, O.P. Pandey, V.K. Dwivedi, Microstructural, Mechanical and Wear Characteristics of Industrial Waste (Brass Slag) Reinforced LM30 Alloy-Based Composite, Silicon 16 (2024) 133–146. https://doi.org/10.1007/s12633-023-02665-3.

[201] A. Wąsik, B. Leszczyńska-Madej, M. Madej, M. Goły, Effect of Heat Treatment on Microstructure of Al4Cu-SiC Composites Consolidated by Powder Metallurgy Technique, J. Mater. Eng. Perform. 29 (2020) 1841–1848. https://doi.org/10.1007/s11665-020-04685-1.

[202] C. Sun, R. Shen, M. Song, Effects of sintering and extrusion on the microstructures and mechanical properties of a SiC/Al-Cu composite, J. Mater. Eng. Perform. 21 (2012) 373–381. https://doi.org/10.1007/s11665-011-9940-1.

[203] A. Wazeer, A. Mukherjee, A. Das, B. Sengupta, G. Mandal, A. Sinha, Mechanical Properties of Aluminium Metal Matrix Composites: Advancements, Opportunities and Perspective, in: 2024: pp. 145–160. https://doi.org/10.1007/978-981-99-5982-2_9.

[204] M.I. Abd El Aal, H.H. El-Fahhar, A.Y. Mohamed, E.A. Gadallah, The Mechanical Properties of Aluminum Metal Matrix Composites Processed by High-Pressure Torsion and Powder Metallurgy, Materials (Basel). 15 (2022). https://doi.org/10.3390/ma15248827.

[205] P.A. Rometsch, Y. Zhang, S. Knight, Heat treatment of 7xxx series aluminium alloys - Some recent developments, Trans. Nonferrous Met. Soc. China (English Ed. 24 (2014) 2003–2017. https://doi.org/10.1016/S1003-6326(14)63306-9.

[206] R.J. Arsenault, L. Wang, C.R. Feng, Strengthening of composites due to microstructural changes in the matrix, Acta Metall. Mater. 39 (1991) 47–57. https://doi.org/10.1016/0956-7151(91)90327-W.

[207] H. Hanizam, M.S. Salleh, M.Z. Omar, A.B. Sulong, Effects of mechanical stirring and short heat treatment on thixoformed of carbon nanotube aluminium alloy composite, J. Alloys Compd. 788 (2019) 83–90. https://doi.org/10.1016/j.jallcom.2019.02.217.

[208] M. Saravana Kumar, Assessment on morphological and mechanical properties of silicon nitride and goat dung ash reinforced Al-Fe-Si alloy hybrid composites, Mater. Today Commun. 31 (2022). https://doi.org/10.1016/j.mtcomm.2022.103716.

[209] A.K. Sharma, R. Bhandari, A. Aherwar, R. Rimašauskiene, C. Pinca-Bretotean, A study of advancement in application opportunities of aluminum metal matrix composites, Mater. Today Proc. 26 (2020) 2419–2424. https://doi.org/10.1016/j.matpr.2020.02.516.

[210] J. Eliasson, R. Sandstrom, Applications of aluminium matrix composites, Key Eng. Mater. 104–107 (1995) 3–36. https://doi.org/10.4028/www.scientific.net/kem.104-107.3.

[211] S.P.F.C. Jaspers, J.H. Dautzenberg, Material behaviour in metal cutting: Strains, strain rates and temperatures in chip formation, J. Mater. Process. Technol. 121 (2002) 123–135. https://doi.org/10.1016/S0924-0136(01)01227-4.

[212] S.J. James, A.R. Annamalai, Machinability study of developed composite AA6061-ZrO_2 and analysis of influence of MQL, Metals (Basel). 8 (2018). https://doi.org/10.3390/met8070472.

[213] M. Kuttolamadom, S. Hamzehlouia, L. Mears, Effect of machining feed on surface roughness in cutting 6061 aluminum, SAE Tech. Pap. (2010) 108–119. https://doi.org/10.4271/2010-01-0218.

[214] D.Y. Pimenov, M. Kiran, N. Khanna, G. Pintaude, M.C. Vasco, L.R.R. da Silva, K. Giasin, Review of improvement of machinability and surface integrity in machining on aluminum alloys, Int. J. Adv. Manuf. Technol. 129 (2023) 4743–4779. https://doi.org/10.1007/s00170-023-12630-4.

[215] A. Thirumoorthy, T. V. Arjunan, M. Arulraj, R. Kumaravelan, T.C.R. Dinesh, Parametric optimisation of high speed turning operation of hybrid aluminium composites using Taguchi-based grey relational analysis, Int. J. Comput. Mater. Sci. Surf. Eng. 9 (2020) 261–281. https://doi.org/10.1504/IJCMSSE.2020.112733.

[216] P. Bansal, L. Upadhyay, Experimental investigations to study tool wear during turning of alumina reinforced aluminium composite, Procedia Eng. 51 (2013) 818–827. https://doi.org/10.1016/j.proeng.2013.01.117.

[217] S.P. Sahoo, S. Datta, Dry Machining Performance of AA7075-T6 Alloy Using Uncoated Carbide and MT-CVD TiCN-Al_2O_3-Coated Carbide Inserts, Arab. J. Sci. Eng. 45 (2020) 9777–9791. https://doi.org/10.1007/s13369-020-04947-z.

[218] S. Basavarajappa, G. Chandramohan, J.P. Davim, M. Prabu, K. Mukund, M. Ashwin, M. Prasannakumar, Drilling of hybrid aluminium matrix composites, Int. J. Adv. Manuf. Technol. 35 (2008) 1244–1250. https://doi.org/10.1007/s00170-006-0804-z.

[219] R.K. Bhushan, Optimization of cutting parameters for minimizing power consumption and maximizing tool life during machining of Al alloy SiC particle composites, J. Clean. Prod. 39 (2013) 242–254. https://doi.org/10.1016/j.jclepro.2012.08.008.

[220] I. Korkut, M. Kasap, I. Ciftci, U. Seker, Determination of optimum cutting parameters during machining of AISI 304 austenitic stainless steel, Mater. Des. 25 (2004) 303–305. https://doi.org/10.1016/j.matdes.2003.10.011.

[221] N. Radhika, R. Subramaniam, S.B. Senapathi, Machining parameter optimisation of an aluminium hybrid metal matrix composite by statistical modelling, Ind. Lubr. Tribol. 65 (2013) 425–435. https://doi.org/10.1108/ILT-01-2011-0008.

[222] R. Bertolini, G. Andrea, N. Tamil Alagan, S. Bruschi, Tool wear reduction in ultrasonic vibration-assisted turning of SiC-reinforced metal-matrix composite, Wear 523 (2023). https://doi.org/10.1016/j.wear.2023.204785.

[223] G. Kiswanto, D.L. Zariatin, T.J. Ko, The effect of spindle speed, feed-rate and machining time to the surface roughness and burr formation of Aluminum Alloy 1100 in micro-milling operation, J. Manuf. Process. 16 (2014) 435–450. https://doi.org/10.1016/j.jmapro.2014.05.003.

[224] R. Fernández Gutiérrez, F. Sket, E. Maire, F. Wilde, E. Boller, G. Requena, Effect of solution heat treatment on microstructure and damage accumulation in cast Al-Cu alloys, J. Alloys Compd. 697 (2017) 341–352. https://doi.org/10.1016/j.jallcom.2016.11.280.

Soumyabrata Chakravarty
25/10/25